Università degli Studi di Palermo

AREA RICERCA E TRASFERIMENTO TECNOLOGICO
SETTORE DOTTORATI E CONTRATTI PER LA RICERCA
U. O. DOTTORATI DI RICERCA

Corso di Dottorato di Ricerca in
Energy – Low Carbon Energetics and Innovative Nuclear Systems
Dipartimento di Ingegneria
Settore Scientifico Disciplinare ING-IND/19

ANALYSIS AND DEVELOPMENT OF UNCERTAINTY QUANTIFICATION METHODOLOGIES FOR THE DETERMINISTIC SAFETY ANALYSIS OF SEVERE ACCIDENT PROGRESSIONS IN FISSION NUCLEAR POWER PLANTS

IL DOTTORE
GIUSEPPE AGNELLO

LA COORDINATRICE
CH.MA PROF.SSA E. RIVA SANSEVERINO

IL TUTOR
CH.MO PROF. P. A. DI MAIO

I CO-TUTOR
DR. ING. F. MASCARI
CH.MO PROF. P. CHIOVARO

CICLO XXXVI
ANNO CONSEGUIMENTO TITOLO 2024

To my grandfather Vincenzo.

To my uncle Pietro.

Contents

List of figures

List of tables

Acronyms

ADS	Automatic Depressurization System
AOO	Anticipated Operational Occurrence
ASTEC	Accident Source Term Evaluation Code
BAF	Bottom of Active Fuel
BEMUSE	Best Estimate Methods plus Uncertainty and Sensitivity Evaluation
BEPU	Best Estimate Plus Uncertainty
CAV	Cavity MELCOR package
CDF	Cumulative Distribution Function
CEA	Commissariat à l'Energie Atomique
CESAM	Code for European Severe Accident Management
CIEMAT	Centro de Investigaciones Energétican, Medioambientales y Technólogicas
CL	Cold Leg
COR	Core MELCOR package
CRP	Cooperative Research Project
CSARP	Cooperative Severe Accident Research Program
CSNI	Committee on the Safety of Nuclear Installation
CV	Control Volume
CVH	Control Volume Hydrodynamic MELCOR package
DAKOTA	Design Analysis Kit for Optimization and Terascale Application
DBA	Design Basis Accident
DC	Downcomer
DCH	Direct Containment Heating
DEC	Design Extended Conditions
DiD	Deference-in-Depth
DOE	Department Of Energy
DSA	Deterministic Safety Analysis
DVI	Direct Vessel Injection
DW	Drywell
EBT	Emergency Boration Tanks
EDF	Électricité de France

EHRS	Emergency Heat Removal System
ENEA	Agenzia nazionale per le nuove tecnologie, l'energia e lo sviluppo economico sostenibile
EPRI	Electric Power Research Institute
FASTNET	FAST Nuclear Emergency Tools
FL	Flow Path MELCOR package
FOM	Figure of Merit
FP	Fission Product
FRS	Fuel Rod Simulator
FWI	Fast Water Injection
GRS	Gesellschaft für Anlagen- und Reaktorsicherheit
GUI	Graphic User Interface
HL	Hot Leg
HS	Heat Structure MELCOR package
HX	Heat eXchangers
IAEA	International Atomic Energy Agency
ICE	Ingress of Coolant Event
iPWR	integral Pressurized Water Reactor
IRSN	Institut de Radioprotection et de Sûreté Nucléaire
ISP	International Standard Problem
IVMR	In Vessel Melt Retention
JAERI	Japan Atomic Energy Research Institute
JRC	Joint Research Centre
KIT	Karlsruhe Institute of Technology
LGMS	Long-Term Gravity Make-up System
LH	Lower Head
LOCA	Loss Of Coolant Accident
LP	Lower Plenum
LWR	Light Water Reactors
MAAP	Modular Analysis Accident Program
MCCI	Molten Core Concrete Interaction

MP	Material Properties MELCOR package
MUSA	Management and Uncertainty of Severe Accident
NEA	Nuclear Energy Agency
NPP	Nuclear Power Plant
OECD	Organization for Economic Co-operation and Development
PCS	Primary Cooling System
PDF	Probability Density Function
PhW	Phenomenological Window
PIE	Postulated Initiating Event
PREMIUM	Post-BEMUSE Reflood Model input Uncertainty Methods
PRZ	Pressurizer
PSA	Probabilistic Safety Analysis
PSS	Pressure Suppression System
PWR	Pressurized Water Reactor
QT	Quench Tank
R&D	Research and Development
RAVEN	Risk Analysis Virtual Environment
RC	Reactor Cavity
RCP	Reactor Coolant Pump
RCS	Reactor Coolant System
RELAP	Reactor Excursion and Leak Analysis Program
RI-DC	Riser-Downcomer valves
RN	Radionuclide MELCOR package
RPV	Reactor Pressure Vessel
RWST	Refueling Water Storage Tank
SA	Severe Accident
SAM	Severe Accident Management
SAMG	Severe Accident Management Guidance
SASPAM-SA	Safety Analysis of SMR with Passive Mitigation Strategies – Severe Accident
SBO	Station Black-Out

SCDAPSIM	Severe Core Damage Analysis Package SIMulator
SCS	Secondary Cooling System
SEBIM	Safety Valves of Pressure Compensator
SFP	Spent Fuel Pool
SG	Steam Generator
SMR	Small Modular Reactor
SNAP	Symbolic Nuclear Analysis Package
SNL	Sandia National Laboratories
SOARCA	State-Of-the-Art Reactor Consequence Analysis
SOT	Start Of the Transient
TAF	Top of Active Fuel
TMI-2	Three Miles Island Unit-2
TRACE	TRAC/RELAP Advanced Computational Engine
UP	Upper Plenum
USNRC	United States Nuclear Regulatory Commission
UT	Uncertainty Tool
V&V	Verification and Validation
WP	Working Package

Nomenclature

g	Probability Density Function
K	Reaction rate
L	Lower tolerance limit
n	Code run
N	Number of code runs
p	Number of FOMs
P	Number of parallel system code runs
r	Simple correlation coefficient
T	Temperature
U	Upper tolerance limit
x	Input variable
y	Output variable
y	Value of the FOM of each code run
β	Confidence level
γ	Probability content
ρ	Simple rank correlation coefficient

Summary

Deterministic safety analyses (DSAs) are conducted to simulate the response of a nuclear system during normal and transient conditions to evaluate its safety in terms of fulfilment of acceptance criteria. Among the accidental scenarios evaluated for the performance of DSAs, particular attention is placed by the international scientific community on the study of Severe Accidents (SAs), which are characterized by specific conditions (e.g. postulated failure of part or all the safety systems) that lead to reactor core meltdown. In those countries where nuclear energy is included in the national energy mix, such scenarios are crucial in the development of SA management programmes.

To simulate the broad spectrum of phenomena characterizing such scenarios, specific computational tools, called SA integral codes, are used. Considering the level of maturity reached by these codes, the international scientific community involved in SAs has been focused on assessing the state-of-the-art definition and consolidation for the quantification of the codes' uncertainties employing the Best Estimate Plus Uncertainty (BEPU) approach.

Given the knowledge gathered from uncertainty quantification in the thermal-hydraulics field, several uncertainty methodologies have been established. Among them, the "probabilistic method to propagate input uncertainty" is commonly used by the international scientific nuclear community and the present work aims to highlight research needs related to the application of this method on the development of DSAs in the SA domain following a BEPU approach.

After presenting the development of the main computational environments by using the SA integral code MELCOR, developed by SNL for the USNRC, the uncertainty methodology has been first tested against experimental data of the internationally recognized test Phebus FPT1, to investigate the code uncertainty on aerosol physics, and QUENCH-06, to study the code uncertainties on hydrogen generation. Then, the uncertainty methodology has been applied and tested to full plant application, in particular on a generic Pressurized Water Reactor (PWR) and a generic integral PWR (iPWR).

The activities have been carried out during the three years of the PhD program in "Energy", curriculum "Low carbon energetics and innovative nuclear systems", XXXVI cycle, in close collaboration with the ENEA FSN-SICNUC, in the framework of the projects HORIZON 2020 MUSA, the IAEA CRP and the Horizon Euratom SASPAM-SA.

Introduction

Reducing greenhouse gas emissions, in general, represents one of the most demanding and necessary challenges facing humanity. In this view, nuclear energy plays a pivotal role since CO_2 emissions per kWh of electricity produced by Nuclear Power Plants (NPPs) are minimal considering the whole life cycle of the plant and its related auxiliary activities. Every industrial complex, such as a power plant, chemical facility, etc., is intrinsically subjected to risk and several safety measures have to be considered since the conceptual project. More in detail, a NPP contains radioactive materials, carefully shielded, and produced in the reactor core during the operational irradiation phase. Potential leaks of radioactive materials to the environment have to be avoided or limited below the minimum level reasonably obtained, adopting the "ALARA" principle (As Low As Reasonably Achievable).

During the licensing phase of a NPP, safety analyses are carried out to demonstrate that the release of radioactive materials does not exceed thresholds imposed by the nuclear authority. In this regard, Deterministic Safety Analyses (DSAs) permit to analytically evaluate and characterize the physical phenomena occurring in NPPs during postulated operational and accidental transients. Specific computational tools, also called system codes, are used to predict the overall response (e.g. thermal-hydraulics) of a nuclear reactor.

State-of-the-art thermal-hydraulics system codes have reached a high level of maturity; however, there are still certain sources of uncertainty in their use, which may influence their results. Since such codes are used during the licencing process of NPP, the estimation of the uncertainties is suggested by the safety standards of the IAEA. Then, several methodologies based on the Best Estimate Plus Uncertainty (BEPU) approach have been developed to conduct uncertainty quantification in the thermal-hydraulic field and, among them, the "probabilistic method to propagate input uncertainty" is nowadays largely adopted.

Afterwards to "Three Miles Island Unit-2" (TMI-2) (1979) and "Fukushima Daiichi" (2011), the nuclear research community has been more focused towards several aspects of nuclear safety aimed at developing Severe Accident (SA) mitigation strategies. In this view, DSAs in the SA domain are conducted using state-of-the-art computational tools, called SA integral codes, which permit the simulation of the complex and mutual multi-physics phenomena occurring during a SA sequence. Nowadays, the definition of the state-of-the-art methodologies for uncertainty quantification in the SA domain using state-of-the-art SA integral codes represents one of the open key points for which the international scientific

community involved in SAs focused its attention, in view of developing reliable SA management strategies.

Within this framework, the activities carried out during the three years of the XXXVI Cycle of the PhD program in “Energy”, curriculum “Low Carbon Energetics and Innovative Nuclear Systems”, aimed at reviewing the uncertainty methodologies consolidated over the past decades, identifying the research needs to be highlighted by the international scientific community involved in the Research and Development (R&D) activities on SAs, and at developing, applying and testing the uncertainty methodology to different SA applications. The activities have been carried out in close collaboration with the ENEA FSN-SICNUC laboratory within the framework of international projects, such as the HORIZON 2020 MUSA project, the IAEA CRP project and the Horizon Euratom SASPAM-SA project.

The work here discussed presents the role of DSAs in nuclear safety, particularly focusing on DSAs in the SA domain and their pivotal role and introduces the BEPU approach, particularly focusing on the methodologies defined in the past to conduct the uncertainty quantification analyses. Among them, the “probabilistic method to propagate input uncertainty” has been here analysed, highlighting the statistical principles on which it is based.

Subsequently, the present work focused on analysing the reasons for the international scientific community to study the applicability of the BEPU approach to investigate the uncertainties in the results of SA integral codes during transients with partial or total core melting. In particular, the main challenges concerning the application of the BEPU approach on SA integral codes are highlighted, making special reference to the development of solid computational environments that allow flexibility to the user and at the same time the correct application of the methodology. Specifically, this thesis work analyses the computational environments developed during the three years of PhD program for the development of uncertainty analyses with the SA integral code MELCOR, developed by SNL for USNRC. The development of such computational environments has played a pivotal role in the PhD program and it has taken place through intensive collaboration with various international research organizations within the major international research projects on uncertainty analyses in the SA domain. The research activity has also made it possible to define a well-defined procedure for the development of uncertainty analysis, seeking to propose tools that can allow the most complete investigation of the uncertainties that characterize the SA integral code used.

To test the computational environments and the uncertainty methodology in the SA domain, the uncertainty analysis of the internationally recognized Phebus FPT1 and QUENCH-06 experimental tests has been developed. These activities have been carried out respectively along the MUSA and the IAEA CRP projects. Along the Phebus FPT1 uncertainty application, conducted employing the coupling between MELCOR and the Uncertainty Tool (UT) DAKOTA using Python, the uncertainty of MELCOR code on aerosol physics have been investigated and the parameters affecting the aerosols particles interactions, aerosol dynamics and aerosol removal process have been considered as uncertain input parameters. Instead, during the uncertainty analysis of the QUENCH-06 test, the interest has been directed toward studying the uncertainties of the MELCOR code on hydrogen generation from zircalloy oxidation processes, characterizing the in-vessel phase of a SA sequence. The present uncertainty application has also played a pivotal role in the development and testing of the computational environment developed in Python that enables the entire performance of uncertainty analysis with MELCOR code. Uncertain input parameters related to the boundary conditions of the experimental facility and to the hydrogen generation kinetics have been considered.

After testing the methodology against experimental data, in the framework of the MUSA project, the uncertainty quantification analysis of a generic Pressurized Water Reactor (PWR) during a SA sequence has been developed. A Station Black-Out (SBO) has been selected as a Postulated Initiating Event (PIE) considering the unavailability of all safety systems. The analysis's purpose was to assess the MELCOR code's uncertainty regarding the prediction of aerosol behaviour within the reactor containment during a SA on a full plant scale. For this reason, the same uncertainty input parameters of the previous Phebus FPT1 exercise have been considered. This analysis allowed for an in-depth study of the methodology in a SA plant scenario.

State-of-the-art SA integral codes reached a high maturity. As a result, the research community working in SAs begin to explore their application to Small Modular Reactors (SMRs). Investigating the applicability of the knowledge related to Light Water Reactors (LWRs) and analyzing the transfer of such know-how for the future realization of integral PWRs (iPWRs) is the main goal of the SASPAM-SA project.

In this framework, during the PhD program, several activities have been carried out to evaluate phenomena occurring in a generic iPWR during a postulated transient scenario. In this regard, thermal-hydraulic characterization is crucial considering the specific features characterizing iPWRs such as the adoption of passive safety systems.

A MELCOR input deck of a generic iPWR has been developed without using proprietary data and adopting only public data. The results of the input deck have been compared to the results obtained with the ASTEC code. Then, the uncertainty methodology has been applied considering two postulated scenarios: a mitigated (DBA) and un-mitigated (SA) Loss Of Coolant Accident (LOCA). Along with the uncertainty analysis in the DBA scenario, the uncertainty of the code related to thermal-hydraulic phenomena has been investigated, also considering uncertain input parameters related to the passive systems adopted by this advanced reactor design. In the SA scenario, the unavailability of all passive safety systems has been postulated to study the code response and the related uncertainty on hydrogen generation. In this regard, the main uncertain input parameters identified in the literature that influence hydrogen production in LWRs have been selected.

1 DETERMINISTIC SAFETY ANALYSES AND THE BEPU APPROACH

1.1 Introduction

Safety analyses are carried out to analytically demonstrate that the release of radioactive materials does not exceed thresholds imposed by the nuclear authority during nominal and postulated transient conditions. This chapter aims to generally introduce the DSAs, especially focusing on the DSA in the SA domain, presenting their fundamentals and a general description of a SA sequence. After a general introduction to computational tools used to conduct DSAs, the chapters focused on the reason for the development of the BEPU approach. Then, the main uncertainty methodologies developed during the last decades are presented, with special reference to the "probabilistic method to propagate input uncertainty".

1.2 Fundamentals on deterministic safety analyses

Safety analyses are performed during the *licencing phase* of a NPP and are included in the safety report [1]. They assess and demonstrate the safe operation of the reactor after a PIE [2]. According to [3], a PIE consists of a postulated event, such as equipment/human failures or natural catastrophes, capable of leading to an operational or accidental condition.

Specific acceptance criteria are adopted to evaluate the results of safety analyses. They are defined by the regulatory body and consist of specified thresholds of functional indicators (e.g. cladding temperature, containment pressure, etc.) giving information about the performance of the systems (e.g. structures, components, etc.) in performing their design purpose [3].

DSAs and Probabilistic Safety Analyses (PSAs) are the two complementary methods used to conduct safety analyses. DSAs provide information to PSAs on the failure (e.g. single failure, multiple failure, etc.) of physical barriers which separate the environment from radioactive materials following the *Defence-in-Depth* (DiD) concept [4]. Furthermore, the PSA fault trees are powerful instruments used to verify the hypotheses carried out for DSAs.

In general, DSAs analytically predict the physical response of a NPP during accidental transient progressions due to PIEs. They evaluate whether the acceptance criteria are met and therefore assess the effectiveness of the plant systems, considering also operator actions, in keeping radioactive materials releases within acceptable limits under different plant states [5].

For this reason, DSAs are carried out considering different plant states, characterized by a different probability of occurrence and, according to IAEA nuclear safety standard code, divided in [6]:

- **Normal operation**.
- **Anticipated Operational Occurrence**
- **Design Basis Accident**
- **Design Extended Conditions**

Normal operation refers to operation within specified operational limits and conditions [3]. It includes phases such as the reactor start-up and the steady-state power generation. Moreover, condition-based and preventive maintenance, as well as any modifications to power generation based on requested electrical loads and any shutdowns (e.g. hot, cold, or refuelling) are considered normal operations. During normal operation plant state, a NPP is required to work without early release of radioactive material and unexpected fluctuation in reactivity.

An Anticipated Operational Occurrence (AOO) is defined as a deviation from normal plant operation. Although this event is predicted to happen at least once in a plant's lifetime, considering proper design choices, it does not cause safety systems damage and does not lead to accidental conditions [3].

A Design Basis Accident (DBA) is a hypothetical event leading to accident conditions considered in the design of the plant, by applying a defined conservative approach and requirements, with acceptable limitations on radioactive material releases [3].

Design Extended Conditions (DECs) denote specific accident conditions which are beyond the DBA. These analyses are carried out during the design process to check the quantity of radioactive materials released to the environment against acceptable limits [3]. DECs are characterized by the postulated failure of a certain number of safety systems and comprise sequences without significant fuel degradation (DEC-A) and sequences leading to the core meltdown (DEC-B), typically called SAs. In Table 1.1, the plant states discussed above are presented.

During the performance of DSAs, the phenomenological response of a NPP along a transient is typically evaluated considering the time evolution and spatial distribution of typical variables such as thermal power, pressures, temperatures, flow rates, concentration of radionuclides, fuel integrity and quantification of Fission Products (FPs) releases to the environment.

Table 1.1 Plant states according to the IAEA Nuclear Safety Standard Code [6].

Operational states		Accident conditions		
			DEC	
Normal Operation	AOO	DBA	Without significant fuel degradation (DEC-A)	With core melting (DEC-B)

1.3 Deterministic safety analysis in severe accident domain

1.3.1 Scope of severe accident analyses

A SA event is characterized by the core meltdown, followed by the release of FPs which could reach the environment, becoming a public health risk. In this framework, according to the IAEA Safety Requirements [6], DSAs in SA conditions are considered for the design of NPPs to further improve the safety of a NPP increasing its capability to withstand accidents beyond a DBA without unacceptable radiological consequences. Extended conditions are chosen on deterministic and probabilistic assessments as well as based on engineering judgment.

The interest in SA mitigation strategies has increased subsequently the Fukushima Daiichi accident and several worldwide R&D activities on DSAs in the SA domain have been carried out. These research campaigns aim to support SA Management (SAM) programmes (for the prevention and mitigation of SAs) and SAM Guidance (SAMG) (for the mitigation of SAs) development. Moreover, DSAs in the SA domain are conducted to support PSA, to assess the source term and in the framework of equipment qualification programmes as well as to improve knowledge about specific phenomena occurring in these events [7].

Since this work aims to consider accidental sequences in the SA domain, the next section generally discusses the main phenomenology of a SA sequence. A description of the present state-of-the-art knowledge about SA in LWR is presented in [8].

1.3.2 Severe accident phenomenology general description

A SA occurs when the reactor core is placed under certain conditions leading to partial or total meltdown, involving a wide range of interactive phenomena [9]. It could be caused by several accidental scenarios (discussed in 1.3.2.1) which are characterized by a first phase mainly driven by thermal-hydraulic phenomena causing the loss of core cooling, with the subsequent increase of the fuel temperature due to the decay heat. During this phase,

degradation phenomena occur such as the oxidation of the cladding surrounding fuel pellets. Fuel releases FPs which are in the form of gases and aerosols. They are transported along the Primary Cooling System (PCS) and then to the containment.

If no actions are taken to restore core cooling, the core melts and relocates within the LP. After the Lower Head (LH) failure, several phenomena involving the molten core and the containment occur such as the Molten Core Concrete Interactions (MCCIs) and Direct Containment Heating (DCH). The next section 1.3.2.2 generally introduces the *in-vessel* phase and section 1.3.2.3 discusses the *ex-vessel* of a SA sequence.

Figure 1.1 presents the key phenomena which characterize a NPP during a generic SA sequence.

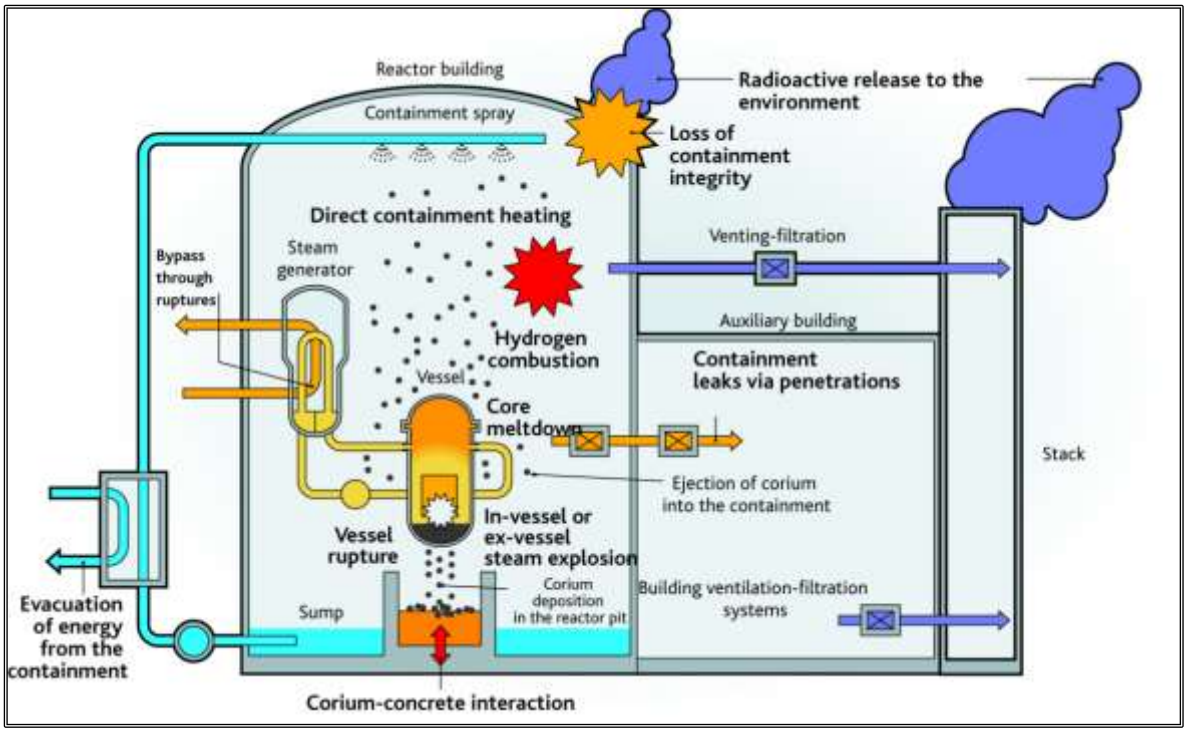

Figure 1.1 Scheme of the main phenomena of a SA [10].

1.3.2.1 Accidental scenarios leading to severe accidents

Based on PSA, it is possible to define several accidental scenarios which could lead to a SA if not mitigated with safety systems:

- **LOCA**: it is caused by the break of a pipe of the RCS. The PSA considers several scenarios concerning the reactor's initial conditions and the dimension of the break.
- **LOCA with containment bypass**: it is determined by a break of a component connected to a loop of RCS but placed outside the containment.

- **Steam-line break accidents**: these occur due to a break in the feedwater line of a Steam Generator (SG), a break in the steam line or a stuck-open dump valve on the secondary system.
- **Steam Generator Tube Rupture accidents**: these are determined by significant leakages of one or multiple SG tubes or a break of secondary lines.
- **Accidents with total loss of heat sink or associated systems**: such scenarios are characterized by the loss of the heat sink (e.g. unavailability of cooling water pumped from a river or a sea near the plant) and lead directly to the failure of cooling systems used to discharge heat to the environment.
- **Accidents with total loss of the steam generator feedwater supply**: caused by equipment failure loading to a simultaneous ability of the feedwater and the emergency feedwater.
- **SBO**: caused by loss of offsite than onsite power.
- **Loss of onsite power**: it is a type of transient determined by the loss of voltage of one or multiple low-voltage switchboards.
- **Anticipated Transient Without SCRAM**: it is a transient caused by the failure of an automatic trip after the insertion of control rods. It results in an internal initiating event, which should result in an automatic trip.
- **RCS transients**: they are caused by inadvertent operation of the safety injection system, uniform dilution with gradual drop of the boron concentration, non-uniform dilution, failure of the chemical and volume control system or uncontrolled control rods withdrawal.

1.3.2.2 In-vessel phenomena

Table 1.2 presents the main phenomena and time intervals characterizing the early and late sub-phases of the in-vessel phase. Regardless of reactor type or transient investigated, thermal-hydraulic phenomena drive the beginning of the transient[1]. Generally, such phenomena characterize the PCS and the Secondary Cooling System (SCS) of the reactor and concern the choked flow at the break (e.g. during a LOCA) and natural circulation (first single-phase and later two-phase), as well as the heat transfer phenomena between the

[1] It should be noted that this first phase also contains the phenomenology characterizing neutronics, as indicated in Table 1.2. However, it is highlighted that neutronics is exhausted in a very short time scale when compared to the time scale of the entire transient.

partially uncovered core and the primary coolant and, then, between the primary coolant and the secondary coolant within the SGs.

Table 1.2 Sub-phases of the In-Vessel phase [11].

In-Vessel Phases	Characterizing Phenomena	Time interval
Early phase	Thermal-hydraulic and neutronic transient	From the start of the transient to core heat-up
	Core uncover and heat-up	From core heat-up to core temperature up to 1500 K
	Oxidation, melting, relocation and slumping	From core temperature up to 1500 K to core slumping
Late phase	LH heating and RPV failure	From the formation of corium pool in the LP to RPV failure.

These phenomena lead to the decrease of coolant mass in the PCS and, due to coolant evaporation, the collapsed core coolant level decreases causing the core uncover when the level drops below the Top of Active Fuel (TAF). The period between the Start Of the Transient (SOT) and core uncover varies from a very short time to a very long time, depending on the type of reactor and transient.

The low heat transfer between the fuel rods and the steam and the decay power cause the increase of fuel rods temperature (*core heat-up*). Once the onset temperature for the zircalloy oxidation reactions with steam is reached (about 1300 K), the hydrogen generation starts. The zircalloy oxidation is a high exothermic reaction and, if the coolant is not able to absorb heat generated by oxidation, the zircalloy temperature increases. When the zircalloy temperature reaches 1500 K, defined as *reaction runaway* onset, the oxidation reaction rate increases considerably.

The amount of hydrogen produced at this stage is determined by the state of core degradation and thus the area available for oxidation reactions. Hydrogen is released into the PCS and then into the containment, where it could ignite, causing a deflagration and, eventually, a detonation. For this reason, the mass of hydrogen is considered a pivotal Figures of Merit (FOMs) which is analysed during DSAs in the SA domain.

High temperatures can also cause the phenomena of ballooning of the fuel cladding and then, the rupture which causes an initial release of FPs. In addition, the natural circulation established between the Upper Plenum (UP) and the reactor core could be reduced by ballooning. It causes a low heat transfer and thus a faster core heat-up.

The melting of materials with the lowest melting temperatures (e.g. structural materials, control rods etc.) determines the loss of core geometry. In this regard, core degradation is characterized by eutectic reactions which cause the melting of eutectic mixtures (e.g. eutectic mixtures of Ag-In-Cd and Zr) at temperatures below the melting point of the materials composing the mixture. The melted materials flow downward to the core, and, due to the lower temperatures, tend to solidify creating obstructions to the reactor coolant flow, accelerating the core heat-up and, then, the degradation of the cladding and fuel. In this regard, it is important to note that fuel can melt at temperatures below its melting point. UO_2 forms with ZrO_2 an eutectic mixture with a melting temperature below the melting temperature of UO_2. The ceramic melted materials, after the solidification, can form obstructions within the core at higher elevations than those generated by the solid metallic materials solidified, mainly due to the higher freezing temperature (about 2800 K). Then, pools of molten material can be formed within the ceramic crust. The loss of the core geometry results in the relocation of the melted core in the Lower Plenum (LP), a phenomenon called *slumping*. It corresponds to the beginning of the *late phase* of the in-vessel phase of a SA sequence.

The late phase is characterized by physical and chemical phenomena occurring in the molten core within the LP in the form of an eutectic mixture called *corium*. characterize the *late phase*. Corium imposes both a thermal and mechanical load on the LH and can cause its failure. Furthermore, the failure of the LH depends on the boundary conditions on it (e.g. Reactor Cavity -RC- flooded with water). In general, the actual comprehension of the phenomena characterizing the late phase is mainly based on the analysis of the damaged core of TMI-2, schematically represented in Figure 1.2 [8].

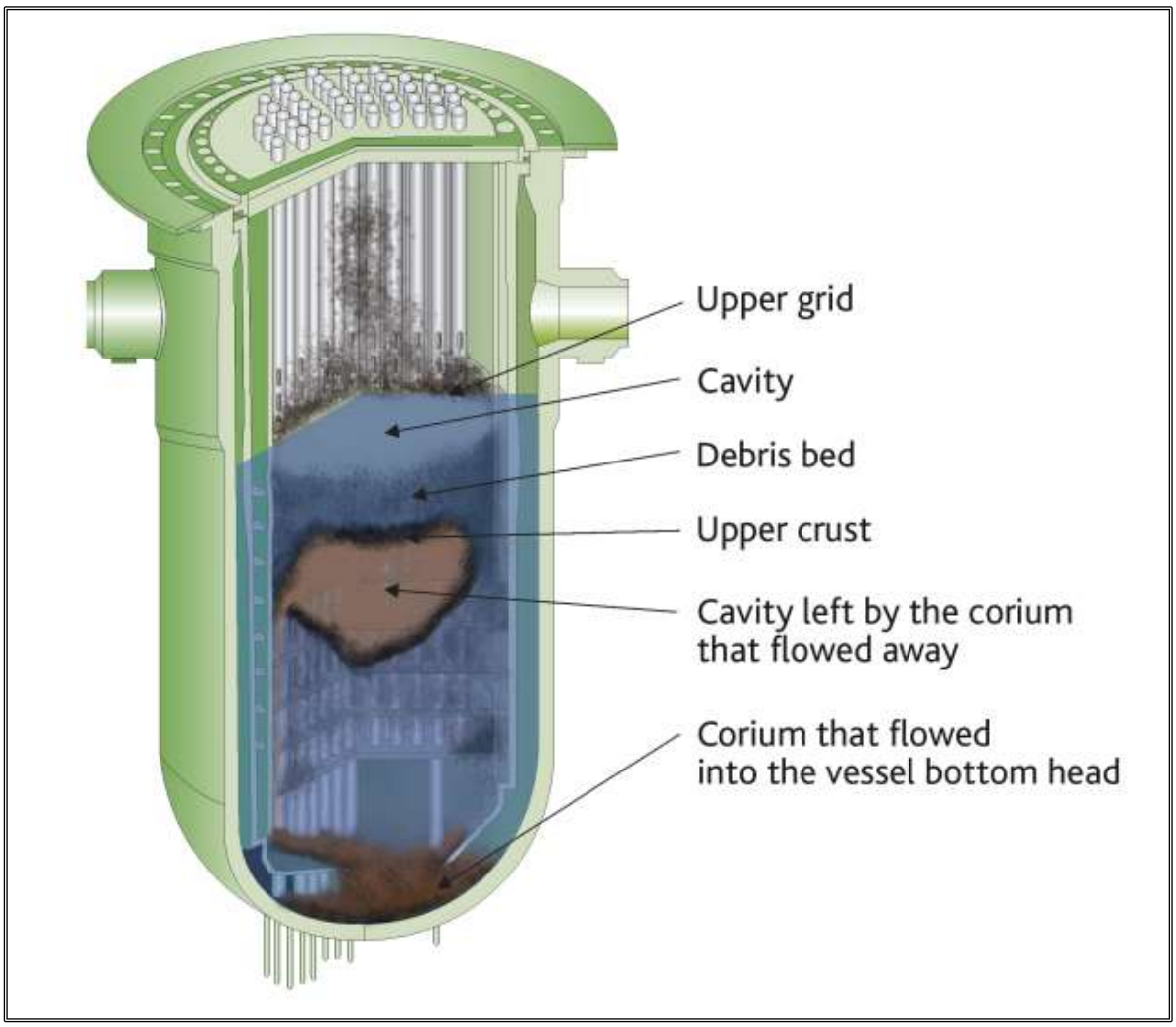

Figure 1.2 Final state of the highly degraded core of the TMI-2 [8].

The OECD/NEA/CSNI validation matrixes developed for Integral and Separate Effect Test Facilities offer comprehensive details on the thermal-hydraulic phenomena that characterize a transient sequence preceding the onset of core degradation [12] [13] [14]. Moreover, in [15] [16] [17] [18] the relevant thermal hydraulic phenomena characterizing advanced reactor designs[2] are investigated in detail. The internationally in-vessel core degradation code validation matrix [11], developed in the framework of the OECD/NEA/CSNI, contains more specific information about all the processes and phenomena that characterize a SA sequence related to in-vessel core degradation phenomena. Further details regarding accident-postulated source terms for LWRs are

[2] Advanced designs comprise two categories:

- *Evolutionary designs*: they are developed starting from the projects of existing facilities, but present improvements based on the know-how acquired from the operational experience over the years as well as the adoption of new technologies and the introduction of innovative features.
- *Innovative designs*: they are significantly different from existing projects and requires further testing and verification activities, possibly considering, previously the commercial use, the building of a demonstration or prototype plant.

available in [19]. Furthermore, an additional description of significant in-vessel phenomena is present in [20].

1.3.2.3 Ex-vessel phenomena

As a consequence of the LH failure, corium flows into the RC, starting the ex-vessel phase. If the failure of the LH takes place when the pressure of the PCS is still high, the corium is ejected into the containment with high velocity, causing a fast increase in the containment temperature and a massive release of radioactive material in the form of aerosol to the atmosphere. This phenomenon is called high-pressure melt ejection.

During scenarios characterized by low pressure, if the RC contains no water inside, the corium relocates into the RC driven by gravity and the maximum quantity of corium relocated in the RC depends on the physical state of the corium before the relocation and on the boundaries of mass flow.

Instead, if the RC is filled with water, the corium interacts with the water leading to steam production which contributes to the increase of containment pressure. The corium ejection into the water of the RC may break apart and create a coolable debris bed. In this regard, the cooling of the corium by flooding is highlighted as an accident management measure. It has been determined that several processes, including bulk cooling, water infiltration into the corium top crust, etc., contribute to the cooling of the corium.

Considering both the case of a wet or dry RC, if the degree of corium fragmentation is insufficient, the melt begins to ablate the concrete of the RC in many hours or even days depending on the composition and thickness of the RC. Along this phase, characterized by MCCIs, non-condensable gases and steam are released within the containment, causing a risk of deflagration of combustible gases (a detailed overview of MCCIs is reported in [21]).

To reduce the special concentration of flammable gas mixtures and, then, the risk of rapid burn, igniters and passive autocatalytic recombiners are located within the containment.

FPs and gases are distributed within the containment according to chemical and physical behaviour. Volatile gases spread within the containment due to the airflow conditions. Aerosols may be carried out by air currents until they settle and agglomerate (a detailed description of aerosol behaviour is listed in [22]). For this reason, condensing steam/water films wash off from structures deposited aerosols and relocate them to the containment sump and additional spray systems remove aerosols from the atmosphere of the containment.

Finally, the source term is influenced by the containment failure (e.g. over-pressurization) and the release path to the environment (e.g. release by filtered or unfiltered venting path, etc.).

Ex-vessel phase and its related phenomena are described in detail in [23] concerning a SA sequence in a LWR.

1.4 Computational tools for deterministic safety analyses

1.4.1 Role of system codes in nuclear safety

Qualified and validated computational system codes simulate the response of a NPP during the plant states defined by the IAEA Nuclear Standard Safety Code previously presented in Table 1.1. System codes are software written in a specific programming language and permit the user to model and evaluate different aspects such as thermal-hydraulics, reactor kinetics, etc. of a complex system.

At the beginning of their use in nuclear safety, system codes were characterized by simplified models and conservative assumptions. The need to study more deeply the main phenomena, in particular referring to thermal-hydraulic phenomena, occurring in a NPP during possible transients, coupled with the increasing computational resources, has led to the development of advanced computational system codes, also referred to as *best estimate system codes*. They are characterized by advanced models which, combined with realistic assumptions, permit the development of reliable predictions of the NPP response. System codes solve energy, mass and momentum conservation equations, independently for the liquid and vapour phases. Moreover, concerning mass conservation, the system code considers the non-condensable gases mass conservation equations The models used by the codes are based on a one-dimensional approach; however, for some plant components such as the RPV, some codes permit solving a system of 3-D equations.

To use them for DSAs, the results of a system code have to be properly qualified, and the code has to be validated by undergoing the Verification and Validation (V&V) procedure, described in detail in [24]. After the V&V, the *qualified frozen code* is distributed to the code user community to simulate the behaviour of a full-scale NPP. The potential code limitations and validation range must be documented, typically within the code documentation. The tool can be also adopted to support experimental tests and for extrapolation of experimental results to full-scale reactors.

Other requirements for the proper use of a system code are the qualification of the user and the qualification of the code *input deck*, also called *nodalization*. The nodalization represents an interface between the real system to be simulated and the system code in which the user inserts specific information to simulate the geometry, boundary conditions, initial conditions, and the control logic of the system. A qualified nodalization reproduces the

geometrical characteristics of the facility as well as the thermal-hydraulics parameters unless an acceptable error. In general, considering a generic system to be reproduced, a nodalization is considered *qualified* when there is correspondence with its geometric feature, and it can reproduce its steady-state and transient thermal-hydraulic behaviour [25].

1.4.2 Severe accident integral codes

To simulate unmitigated transient progressions with expected partial or total core melting, specific computational codes are used. They are programmed with specific integrated advanced models for a thorough, self-consistent investigation of the complex response of a NPP which is characterized by mutual different interactions as well as interrelated phenomena/processes (discussed briefly in 1.3.2) [26].

Such computational tools are also called *SA integral codes*. They are relatively fast running to permit the simulation of a sufficient number of different case simulations and parametric simulations. As specified previously, these tools are pivotal in supporting PSA and developing SAM programmes.

Nowadays, the main state-of-the-art SA integral codes are:

- ASTEC (Accident Source Term Evaluation Code) [27], developed IRSN.
- MAAP (Modular Analysis Accident Program) [28], programmed by EPRI.
- MELCOR [29] [30], developed by SNL for USNRC.
- AC^2 [31], managed by GRS.
- RELAP/SCDAPSIM (Reactor Excursion and Leak Analysis Program/Severe Core Damage Analysis Package SIMulator) [32] [33], developed by the Innovative Systems Software as part of the international SCDAP Development and Training Program.

In the research activities presented in this work, the SA integral code MELCOR has been used. A general description of the MELCOR code is presented in APPENDIX A.

1.5 The Best Estimate Plus Uncertainty approach

As previously discussed in 1.2, the main objective of a DSA is to analytically simulate the transient response of a NPP under postulated conditions in view of demonstrating the fulfilment of safety requirements expected by the regulatory body. Generally, it means the assessment of adequate margins between the values of critical parameters for safety (e.g. maximum cladding temperature, containment pressure, etc.) and corresponding acceptance criteria.

In the early 1970s, DSAs were conducted by adopting a *conservative approach* to consider the computational uncertainties due to the limited modelling capabilities characterizing the early system codes adopted in nuclear safety and the limited knowledge about specific phenomena. As mentioned in [34], the best estimate system codes store all the know-how gained from experimental research campaigns over the last decades and are the state-of-the-art instruments to conduct DSAs. Critical plant parameters for safety, calculated using a best estimate system code, are the best estimate of the real operating conditions of the plant. Nonetheless, there are still sources of uncertainties which influence the application of these tools and their results. For this reason, the IAEA safety analysis standards require the uncertainty quantification of the results adopting the also-called *BEPU approach*. The goal of the conservative approach is to compare the acceptance criterion with parameters calculated considering unfavourable effects on safety to consider uncertainties. On the other hand, the BEPU approach is based on comparing an *uncertainty band* (referring to the upper/lower limit of that band) to the acceptance criterion, as presented in Figure 1.3.

Therefore, by adopting the BEPU approach, the uncertainty quantification of the results plays a pivotal role in carrying out a DSA. Generally, the uncertainty quantification goal is to calculate the uncertainty band of code results and to characterize the influence of uncertain input parameters and the combination of them to the results. Uncertainty of the code results is analysed by estimating the uncertainty band of significative FOMs from a safety point perspective (e.g. maximum cladding temperature, containment pressure, etc.). A general overview of the BEPU approach features and applications in thermal-hydraulics is presented in [35].

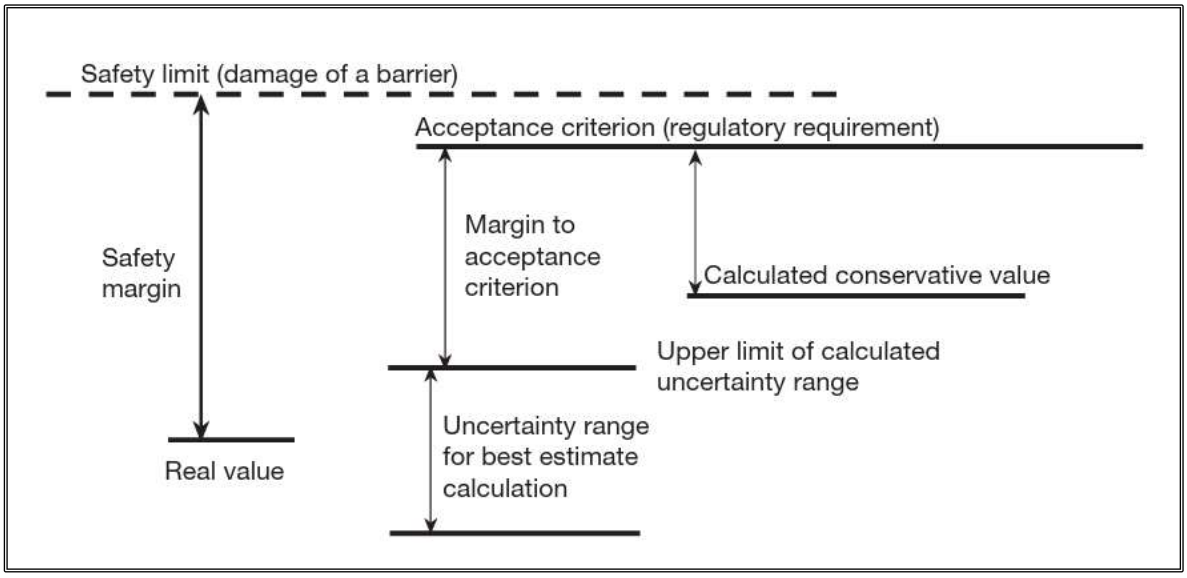

Figure 1.3 Safety margins concept [34].

1.5.1 Origins of uncertainty and characterization

The source of uncertainty characterizing DSAs can be listed, in general, in five different categories [34]:

- *Code uncertainties*: related to approximation in field equations (e.g. assumption of fully developed flows, material properties, etc.).
- *Representation uncertainties*: related to the effects of the discretization of the system in finite volumes (also noted as *nodalization effects*).
- *Scaling issue*: uncertainties arising from the validation of the code by comparison with data from scaled-down experimental plants.
- *Plant uncertainties*: related to the boundary and initial conditions of the facility under investigation.
- *User effect*: uncertainties associated with the choices of the user.

1.5.2 Methodologies for the uncertainty quantification

In the field of thermal hydraulics, during the last decades, several uncertainty methodologies have been developed. As presented in Figure 1.4, in general, they are divided into two macro methods: *methods for propagation of input uncertainty* and the *method for the extrapolation of output uncertainty* [34].

1.5.2.1 Methods for the propagation of input uncertainty

According to them, the FOMs' uncertainty band is evaluated by examining several code runs, characterized by different sets of selected parameters of the input deck, called *uncertain input parameters*. They are defined by a Probability Density Function (PDF) and a range of variation. These methods are divided into *probabilistic* and *deterministic*.

The probabilistic method is based on statistical approaches to correlate the input uncertainty, identified by selected uncertain input parameters, to output uncertainty, expressed by the uncertainty of selected significative FOMs. Despite the choice of the system code adopted, the method is defined by fundamental steps that can be identified in [34] and [36].

After selecting the FOMs to be investigated, the application of the methodology starts with the choice of the uncertain input parameters which is based on their contribution to the general output uncertainty of the FOMs. In this regard, the input deck is characterized by many parameters. Since some parameters, such as geometrical dimensions, are typically known with negligible uncertainty, it would be practically irrelevant to examine the

uncertainties of all the parameters characterizing a code input deck and it might be almost unachievable [37].

Following this method, a PDF characterizes each uncertain input parameter and it is usually selected based on previous analyses, available experimental data and engineering judgment [38]. Recently, novel approaches to derive PDFs from experimental data and computer simulations are under investigation such as the inverse uncertainty quantification [39].

A number N of sets of values of uncertain input parameters are defined by performing a Monte Carlo random sampling and are used to define N input deck used to start N code runs. Each code run *n* returns an y_n value of the FOM (e.g. maximum cladding temperature during a LOCA); then in general, considering N code runs, a set of $(y_1, \ldots, y_N)$ values of the FOM can be identified.

Two random functions $L = L(y_1, \ldots, y_N)$ and $U = U(y_1, \ldots, y_N)$, defined as *tolerance limits*, can be considered such that [40]:

$$P\left\{\int_L^U g(y)\,dy > \gamma\right\} = \beta \tag{1}$$

where $g(y)$ is the PDF of the FOM, γ is defined as *probability content* and the term $\int_L^U g(y)\,dy$ represents the fraction of the distribution included inside the *tolerance interval*, defined by $L = L(y_1, \ldots, y_N)$ and $U = U(y_1, \ldots, y_N)$.

The minimum amount of code runs N can be calculated using Wilks' formula, presented in [41] [42], which takes into account the number of FOMs examined *p*, their probability content γ and the confidence level β.

If the study is conducted applying the condition defined in (1) only considering L or U, N is calculated through Wilks' formula for the *one-sided tolerance interval*:

$$\beta = 1 - \gamma^N \tag{2}$$

For example, for the one-sided tolerance interval, considering a probability content γ and a confidence level β of 0.95, the minimum code runs N requested are 59. It means that the upper limit (or lower limit) of the values $(y_1, \ldots, y_N)$ of the FOM calculated by the code are contained within the 0.95 percentile (or 0.05 percentile) of the correspondent theoretical PDF of the FOM with a confidence level of 0.95.

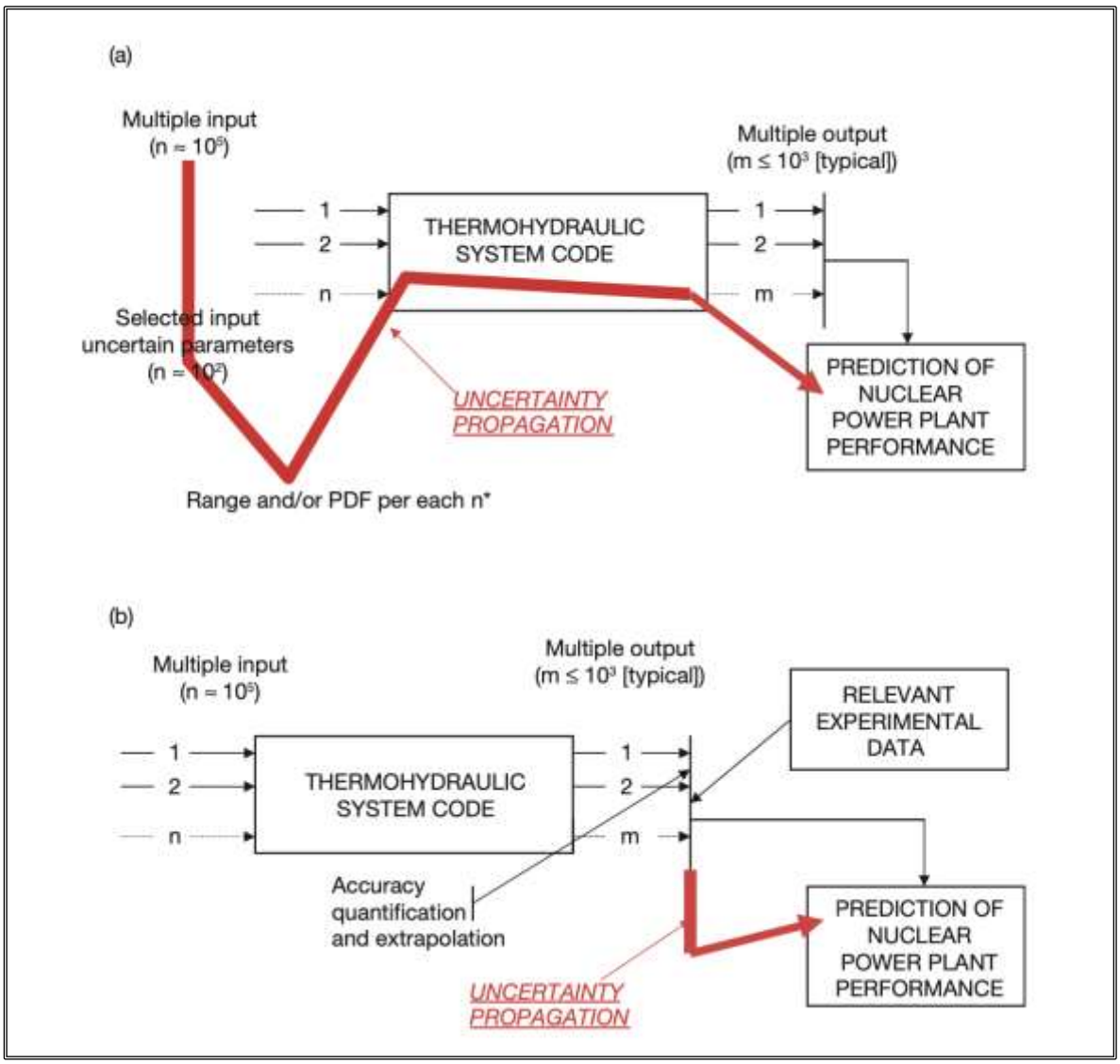

Figure 1.4 Method to conduct uncertainty quantification: (a) methods for propagation of input uncertainty, (b) method for extrapolation of output uncertainty [34].

In case the study is conducted considering the entire tolerance interval, Wilks' formula for the *two-sided tolerance interval* can be used:

$$\beta = 1 - \gamma^{N} - (N-1)(1-\gamma)\gamma^{N-1} \tag{3}$$

For example, for the two-sided tolerance interval, considering a probability content γ and a confidence level β of 0.95, the minimum code runs N requested are 93. It means that the upper and the lower limits of the values $(y_1, \ldots, y_N)$ of the FOM calculated by the code will be contained within the 0.05 and 0.95 percentile of the correspondent theoretical PDF of the FOM with a confidence level of 0.95.

Usually, multiple FOMs *p* are investigated. If FOMs are statistically independent, Wilks's formula could be used [40]. Instead, if the *p* FOMs are statistically dependent, N is calculated

using Wald's formula [43] respectively for the one-sided tolerance interval (4) and for the two-sided tolerance interval (5):

$$\beta = \sum_{j=0}^{N-p} \binom{N}{j} \alpha^j (1-\alpha)^{N-j} \tag{4}$$

$$\beta = \sum_{j=0}^{N-2p} \binom{N}{j} \alpha^j (1-\alpha)^{N-j} \tag{5}$$

As specified above, the number of FOMs analysed *p*, the target probability γ and the confidence level β are the only factors that affect the number of code runs N. Therefore, N is independent of the number of uncertain input parameters. In this regard, more details on the statistical aspects can be found in [40].

The N code outputs are combined to evaluate the FOMs' uncertainty band and to calculate statistical parameters which permit to characterisation of the uncertainties of the code such as the *mean*, *median*, *standard deviation*, and *coefficient of variation*[3].

Furthermore, a statistical correlation analysis involving the FOMs, and the uncertain input parameters is typically carried out. According to past activities developed in the framework of uncertainty quantification in DSAs [44] [45], the *simple* and *simple rank correlation coefficients* are computed [46] [47].

An indication of the magnitude of linear correlation between an input variable, denoted with x, and an output variable, denoted with y, is provided by the simple correlation coefficient, denoted with r. The value of this coefficient is between -1 and 1. A *negative* correlation is indicated by $r < 0$, which implies that a linear increase in x results in a linear decrease in y. Instead, a *positive* correlation, indicated by $r > 0$, indicates that a linear increase in x results in a linear increase in y. The simple correlation coefficient can be computed by *Pearson's correlation* as [47]:

$$r = \frac{\sum_{i=1}^{N}(x_i - \bar{x})(y_i - \bar{y})}{\sqrt{\sum_{i=1}^{N}(x_i - \bar{x})^2 \sum_{i=1}^{N}(y_i - \bar{y})^2}} \tag{6}$$

The simple rank correlation coefficient, indicated with ρ, is representative of the degree of monotonous correlation between x and y. It is computed through *Spearman's correlation* which is analytically equivalent to Pearson's correlation but calculated using ranked values

[3] The coefficient of variation is defined as the ratio between the standard deviation and the mean value.

in ascending order. It is adopted when x and y are characterized by a significant magnitude difference.

As indicated in [47] concerning ρ, the statistical correlation is significant if the coefficient is greater than 0.5 (or less than -0.5) or moderate if it is between 0.2 and 0.5 (or -0.2 and -0.5). Finally, if the coefficient is between 0 and 0.2 (or between 0 and -0.2) the correlation is low. The same thresholds are usually adopted for the simple correlation coefficient r. An example of the application of the BEPU approach adopting the probabilistic method in the thermal-hydraulics field can be found in [44]. In this application, the uncertainty quantification of the thermal-hydraulic system code TRACE [48] [49] [50] during a LBLOCA in a generic PWR-900 has been conducted. The methodology has been applied also to investigate the uncertainties of the system codes in simulating typical phenomena related to passive safety systems. In this regard, in [37] an uncertainty application conducted with the thermal-hydraulic codes RELAP5/MOD3.3 [51] and RELAP5-3D [52] codes have been carried out comparing the uncertainty outcomes with experimental data results. Several activities have been carried out to study the uncertainties of thermal-hydraulics system codes related to two-phase thermohydraulic phenomena typical of an Ingress of Coolant Event (ICE), considered as one of the possible PIEs in fusion machines, such as ITER. Several studies have been conducted through the use of the TRACE code, with the development of a nodalization of the integrated ICE facility in JAERI, adopting a BEPU approach and the probabilistic method and reported in [45] and [53].

On the other hand, the deterministic method has the same characteristics as the probabilistic one, previously explained, except for the definition of the uncertain input parameters. Following the deterministic method, uncertain input parameters are defined only by uniform PDFs or a range of variations derived from experimental data. In general, following the deterministic approach, every insight about the uncertainty of the code is deterministic and not probabilistic [34].

1.5.2.2 Method for extrapolation of output uncertainty

The Uncertainty Method based upon Accuracy Extrapolation, which is the method for extrapolating output uncertainty, relies on directly scaling data from a readily available database. It computes code uncertainties by extrapolating accuracy assessed from integral experiments to full-scale NPP [54]. The estimation of the accuracy of code results is obtained by using the Fast Fourier Transform Based Method [55]. This method has the advantage of

not requiring uncertainty range information for code input parameters but requires relevant experimental data obtained in properly scaled facilities, not always available [56].

2 UNCERTAINTY QUANTIFICATION IN THE SEVERE ACCIDENT DOMAIN

2.1 Introduction

Considering the need of the research community in the estimation of uncertainty using the state-of-the-art SA integral codes, given the development of SAM and SAM guidelines, this chapter aims to analyse the applicability of the BEPU approach to DSAs in the SA domain. In particular, this chapter focuses on the main challenges of applying the BEPU approach in SA and aims to present solid computational approaches to conduct uncertainty analysis. Then, the present chapter explores the computational environments developed along the PhD program to carry out uncertainty quantification analyses with the MELCOR code. Specifically, the coupling between MELCOR and UT DAKOTA is described as well as the development of a Python uncertainty tool conducted along the PhD program.

2.2 Role of uncertainty quantification in severe accident domain

To simulate the NPP response under a postulated unmitigated transient, SA integral codes are used. These tools are developed by embedding specific models representing the current knowledge on multiphysics phenomena occurring in these scenarios. Models and correlations are set by the user during the development of the input deck.

Even though several experimental campaigns in the field of SA phenomena have been performed (e.g. [11] [57] [58] [59] [22]) and a valuable assessment database has been provided because of the SA integral codes validation process [24], the international scientific community involved in SAs has highlighted the need to investigate some uncertainties that are still present in the use of these codes [60] [61] [62]. The analysis of the state-of-the-art related to DSAs in the SAs domain highlights the need to identify, contextualize, and reduce sources of uncertainty mostly related to different models (e.g. core degradation models) that influence SA integral code calculations. Consequently, it presupposes a focus on what are the typical phenomena and processes that have not been experimentally studied adopting prototypical geometries and prototype materials [62].

Since the SA integral codes have reached a high level of maturity, the application of the BEPU approach in the SA domain is currently a pivotal topic of nuclear safety, considering also the key role of SA integral codes in the development of SAMs and SAMGs. In this regard, many works have been carried out by USNRC in the framework of the State-Of-The-

Art Reactor Consequence Analysis (SOARCA) project. One of the aims of this project was to evaluate the realistic outcomes in terms of source term evaluation during SA due to postulated scenarios. Two uncertainty analyses have been conducted, respectively referred to a Boiling Water Reactor in the Peach Bottom Atomic Power Station [63] and a PWR in the Surry Power Station [64]. The Sequoyah uncertainty analysis [65] [66] has been conducted using the same uncertainty methodology and lessons learned from these two applications to develop insights into the overall sensitivity of results to uncertainty in selected modelling inputs. A set of regression analyses have been applied to evaluate the probability of early containment failure and the ensuing consequences.

Nowadays, the research community involved in SAs has focused its interest on defining a harmonized methodology for the uncertainty quantification of SA integral codes. A great experience has been carried out in nuclear engineering in developing uncertainty quantification analyses with thermal-hydraulic best estimate system code, as presented in 1.5.2.1, and performed along several international projects over the years. Two of the most internationally recognized projects in this field were the BEMUSE project (Best Estimate Methods plus Uncertainty and Sensitivity Evaluation) [67] [68] [69] and the PREMIUM project (Post-BEMUSE Reflood Model input Uncertainty Methods) [70] [71].

Nowadays, several international projects, such as the MUSA project [72] and the IAEA CRP [73] [74] [75] [76], have been carried out to review and consolidate the state-of-the-art uncertainty methodology in the SA domain. A more detailed description of these two international projects is presented in APPENDIX B and APPENDIX C.

2.3 Main challenges

In the context of developing uncertainty analyses for the DSAs in the SA domain, the direct application of the BEPU approach is expected to be more challenging. In this regard, several aspects have been highlighted by the international scientific community as key open issues that characterize uncertainty analyses in the SA domain. These include the identification and characterization of the uncertain input parameters to be used during the analysis, the development of a solid computational interface between the SA integral code and an UT, and the handling of failed code executions.

The work presented here, conducted along the PhD program within the framework of international projects, such as the previously mentioned MUSA project [72] [77] and the IAEA CRP [73], aimed to establish a harmonized and consistent procedure for applying the

BEPU approach in the SA domain, addressing the main needs of the international scientific community.

2.3.1 Identification of uncertain input parameters

The identification of uncertain input parameters is the first step that guides the uncertainty analysis and plays a pivotal role. Uncertain input parameters should be related to the main phenomena which directly affect the FOMs evaluated during the uncertainty analysis. In this regard, before characterizing and identifying the sources of uncertainty, an assessment of the transient and the plant is required to identify the related phenomena.

Furthermore, the range of variation of uncertain input parameters may influence their statistical correlation with the FOMs. As a result, careful consideration and the use of references or engineering judgments should be used when defining PDFs. Generally, experimental data, analytical data and expert judgment are required.

Particular combinations of parameters can generally influence the trend of the selected FOMs, and combinations that may lead to physically unacceptable results must be investigated separately, conducting separate sensitivity analyses leading to a deeper understanding of such combinations.

Finally, the identification of uncertain input parameters can be assisted by the use of established Phenomena Identification and Ranking Table techniques.

2.3.2 Development of a solid computational environment

As previously defined, the application of methodologies for uncertainty analysis, in particular for those based on the propagation of input uncertainties, presupposes the analysis of an N number of code runs (typically equal to several tens of calculations), subsequently analysed by a UT dedicated to the statistical analysis of FOMs. For many years, initiatives have been conducted from an international perspective to develop UTs, such as DAKOTA [78] [79] and RAVEN [80] and others, for the quantification of uncertainties.

To perform a full uncertainty analysis, a computational environment which manages the direct coupling process between a simulation code and a UT is necessary. It coordinates the *pre-processing phase* (sampling, generation of input decks, code runs) and the *post-processing phase* (statistical analysis and statistical correlation analysis).

Extensive experience in developing computational environments using best-estimate thermal-hydraulic system codes has already been acquired within the nuclear community. The development of computational environments for uncertainty analyses has played a central role within the research community engaged in this topic. The main goal is to develop

tools which ensure flexibility and robustness to the analysis and allow the user to study uncertainties of SA integral codes through the calculation of requested statistical parameters and correlation coefficients. This aspect plays a pivotal role in DSAs in the SA domain since these analyses are characterized by several output data and typically require a higher computational time than thermal-hydraulic analyses.

2.3.3 Management of failed code runs

The potential failure of some code runs could compromise the statistical robustness of the analysis. Since this point is critical for the adoption of the BEPU, it is necessary to identify the best strategy for the treatment of these cases without compromising the statistical validity of the analysis. In fact, during simulations of accidental transients and even more, particularly in the simulation of unmitigated accidental transients with SA integral codes, it is possible to encounter failed cases, identified as runs finished before the final time set by the user. Failed runs, as analysed in [77], can affect the empirical PDF of the FOM, calculated as an outcome of the uncertainty analysis. For this reason, several approaches have been investigated and adopted. The first approach used relies on the increase in the amount of code runs than the minimum calculated using Wilks' formula (see 1.5.2.1). A second approach is based on the replacement of failed cases with new cases characterized by a different set of uncertain input parameter values. Further approaches consist of working on the input deck or restarting the failed code runs by decreasing the timestep in the time region of the transient close to the time of calculation failure or making small changes to the input parameters (e.g. changing the third or fourth decimal place). If a parameter does not allow the uncertainty analysis to succeed because it causes a high number of failures, one approach is to remove the uncertain input parameters causing the failures and consider them in the results. Finally, an additional strategy, presented in [71], consists of increasing the Wilks' order to allow discarding higher FOMs' values, assuming the failed cases would give the higher FOMs' magnitudes.

2.4 Computational environments/architectures for the uncertainty quantification in severe accident domain

A pivotal objective of the work carried out during the three years of the PhD program is represented by the development of computational environments to conduct full uncertainty quantification analyses with SA integral codes (using the MELCOR code) considering the research needs highlighted by the international scientific community involved in SAs.

The study and the development of a computational environment for conducting uncertainty analysis in the SA domain started with the investigation of the coupling between the SA integral code MELCOR and the UT DAKOTA using the Symbolic Nuclear Analysis Package (SNAP), state-of-the-art Graphic User Interface (GUI) for USNRC codes [81] [82] [83] [84]. A certain degree of experience has been gained within the SNAP environment coupling the TRACE code with DAKOTA, as reported in [44] [53]. This environment architecture has been also used to investigate the use of the TRACE code for PSA studies, with the application of the Reliability Evaluation of Passive Safety System methodology [85]. Considering the limitation in performing uncertainty analysis with the MELCOR code, highlighted in detail in the next section 2.4.1.2, the implementation of Python capabilities in SNAP, using the PyPost module, has been investigated [83].

Then, considering the needs underlined during the MUSA project [77], the coupling of the MELCOR code with the DAKOTA software using a Python environment/architecture has been developed and tested. A detailed presentation of this approach is given in the next section 2.4.1.3. As specified in that section, this computational environment, while very powerful, is characterized by limitations for its use in the DSAs in the SA domain that have led to the development of an independent tool, written entirely in Python, allowing the entire uncertainty analysis, both in its pre-processing and post-processing phases. A detailed description of this tool, developed from the experience gained along the investigation of the previous computational environments, is presented in section 2.4.2.

2.4.1 The coupling between MELCOR and DAKOTA

2.4.1.1 The DAKOTA software

DAKOTA (Design Analysis Kit for Optimization and Terascale Application) is an UT capable of performing uncertainty analyses, sensitivity analyses, parameter estimation, optimization, parametric analyses and employs meta-algorithms to develop hybrid optimization, surrogate-base optimization, and optimization under uncertainty or mixed aleatory/epistemic uncertainty quantification.

To conduct an uncertainty analysis, it is first used to generate a set of code input decks, previously sampling the uncertain input parameters using a sampling technique chosen by the user. Then, it assesses the main statistical parameters characterizing the FOMs after the code runs and the extraction of code run outputs. In this regard, the UT calculates the simple and partial correlation coefficients as well as the simple rank and partial rank.

2.4.1.2 Coupling between MELCOR and DAKOTA in a SNAP environment/architecture

Since DAKOTA is provided as a plug-in inside SNAP, it is possible to couple USNRC codes to it and perform uncertainty analysis. In this regard, following the procedure described in detail in [83], it is possible to develop the coupling between DAKOTA and MELCOR shown schematically in Figure 2.1.

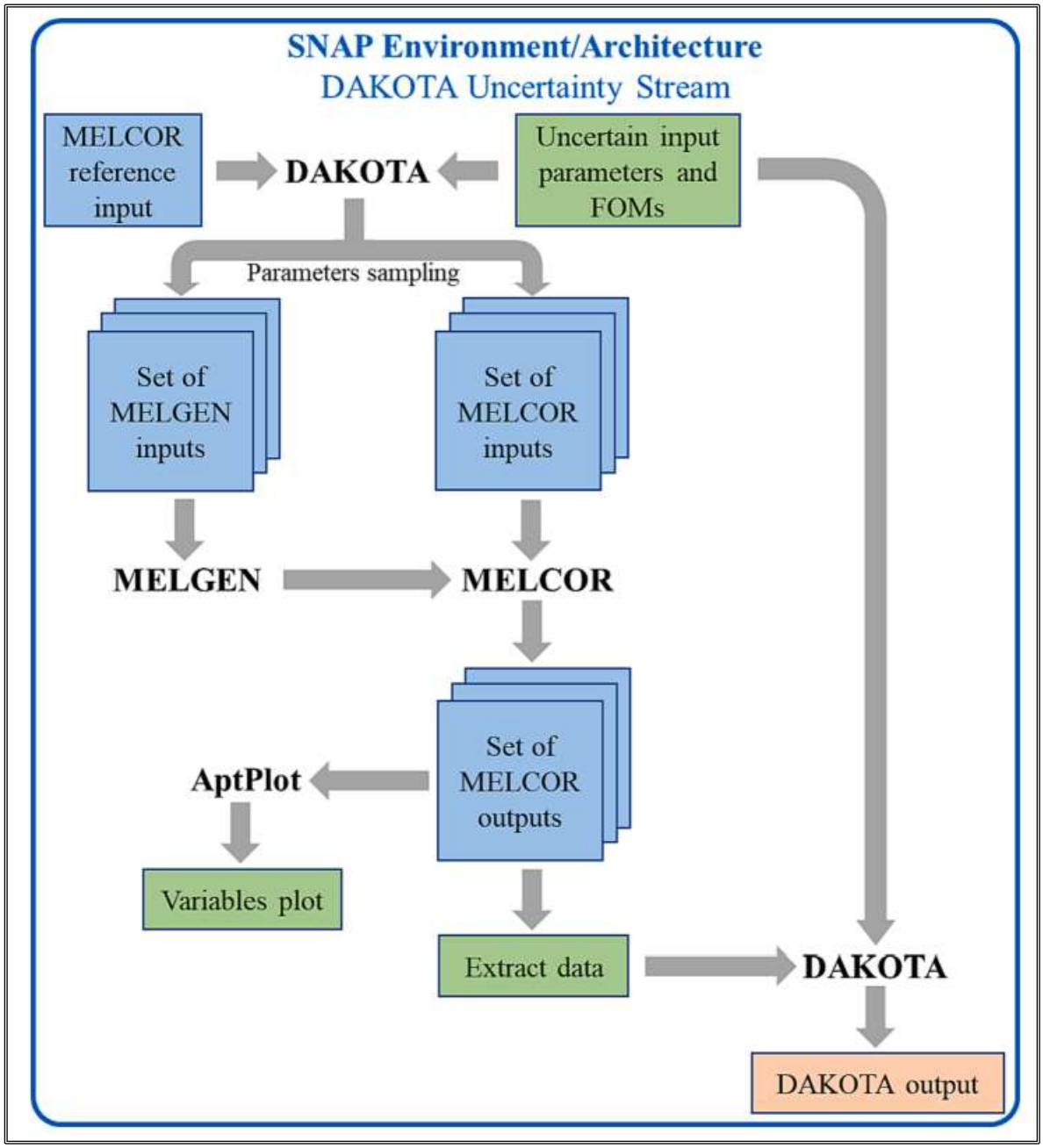

Figure 2.1 Workflow of the coupling between MELCOR and DAKOTA in the SNAP environment/architecture [83].

After the definition of uncertain input parameters (e.g. PDF type, range of variation), DAKOTA enables the user to select a sampling method (Monte Carlo or Latin Hypercube stratified sampling method) as well as the FOMs to be investigated.

It is also possible to customize the final report, printed by SNAP, which includes the computed statistical outcomes of the FOMs (median, mean, maximum, minimum, standard deviation, coefficient of variation). Furthermore, the plots of the Cumulative Distribution Function (CDF) and PDF of the FOM are given.

At the present stage, as underlined by the research community working on the MUSA project [77], this coupling approach presents some limitations regarding the impossibility of completing the uncertainty analysis if one or multiple MELCOR runs fail. If a calculation fails, the extraction of the FOMs data is precluded and the DAKOTA toolkit does not finalize the final report.

To overcome it, SNAP has been updated considering an advanced stream option directed by using Python. Using this feature, it is possible to replace the failed runs, using a specified number of replacement samples. In general, Python runs the MELCOR input decks modified considering the sampled uncertain input parameter values evaluated by DAKOTA. Then, it permits to calculation of the FOMs value for each run and, using the *PyPost* module developed by AptPlot, it permits to plotting of the dispersion band of the FOMs. Finally, it generates the final report reporting the statistical calculations and the statistical correlation coefficients.

2.4.1.3 Coupling between MELCOR and DAKOTA in a Python environment/architecture

The coupling between MELCOR and DAKOTA using Python, shown in Figure 2.2 with its workflow, has been developed in the framework of the MUSA project to fully explore the potential of the DAKOTA software [77].

Using the DAKOTA GUI, the main features of the uncertainty analysis are set through the DAKOTA input file, which is divided into three sections: *sampling*, *interface* and *responses*.

The sampling section is related to the definition of the sampling method, number of samples and the definition of uncertain input parameters in terms of PDF type, mean value, upper and lower limits, standard deviation, etc.

The interface section manages the direct coupling between DAKOTA and MELCOR runs. A Python script, also called *driver* script, permits substituting through the ad-hoc DAKOTA module *dprepro* the values obtained by the sampling of the uncertain input

parameters in a template input, prepared by the user. The template input contains strings, identifiable by DAKOTA, instead of the numeric values of the parameters to be replaced. Then, it manages the code runs and extracts the FOMs channels from the MELCOR output file through the AptBatch executable [86]. Concerning the possible failures of code runs, the driver script permits not to consider the failed code runs for the statistical analysis which is performed by DAKOTA. Some difficulties related to setting the driver script have been encountered, related to the return of the code output to DAKOTA to perform the statistical analysis. Advanced Python knowledge is needed to complete this procedure since it is based on the management of several scripts.

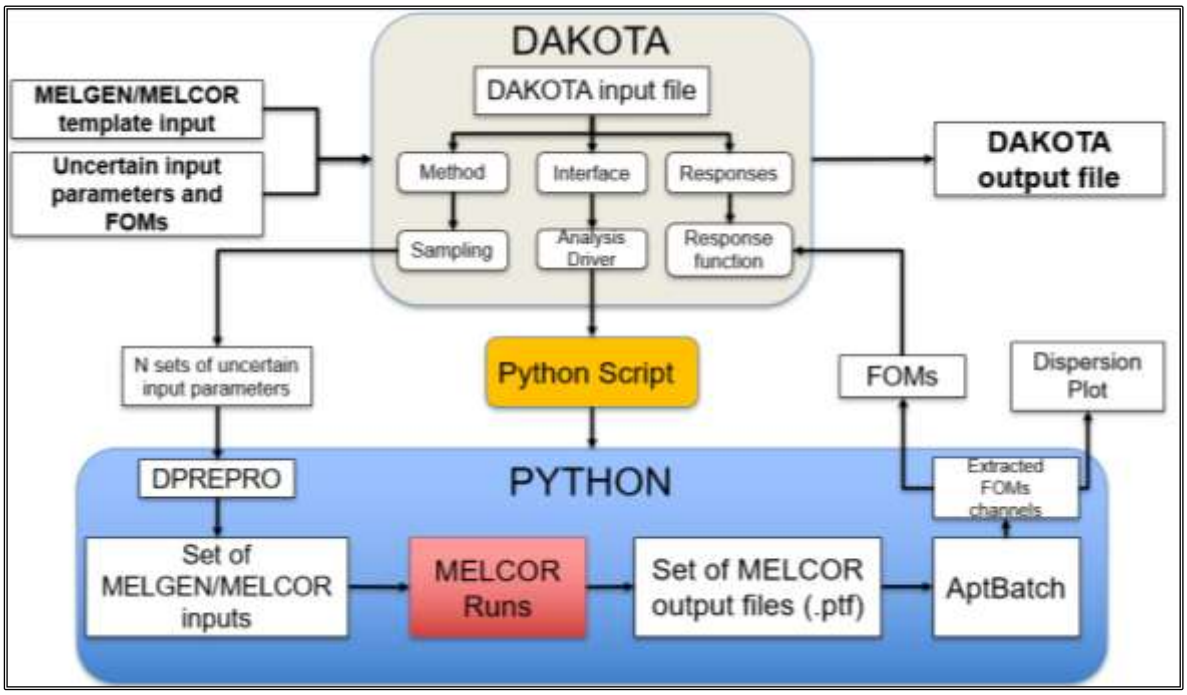

Figure 2.2 Workflow of the coupling between MELCOR and DAKOTA in a Python environment/architecture.

Finally, the response section manages the calculation of the FOM statistical parameters reported in the DAKOTA output file. In this regard, some limitations on the DAKOTA output file have been underlined. The limitations are related to the calculation of statistical parameters and correlation coefficients at each time step and the management of the results directly by the DAKOTA output file. The calculation of statistical parameters and correlation coefficients along the transient is possible but considering only specific timings selected by the user and not all the time-step, which could be useful to study the variation of statistical correlation along the transient. Furthermore, the DAKOTA output file seems to be not user-friendly for developing automatic post-processing of the data.

Considering these limitations and, using the Python post-processing capability, an external in-house script has been developed to conduct the post-processing phase and the calculation of statistical parameters.

2.4.2 Development of a Python uncertainty tool

Starting from the experience gained along the MUSA project and leading to the development of the previous coupling procedure between MELCOR and DAKOTA using Python (as presented in 2.4.1.3), a full UT, written in Python, has been developed. A general scheme of the tool is presented in Figure 2.3.

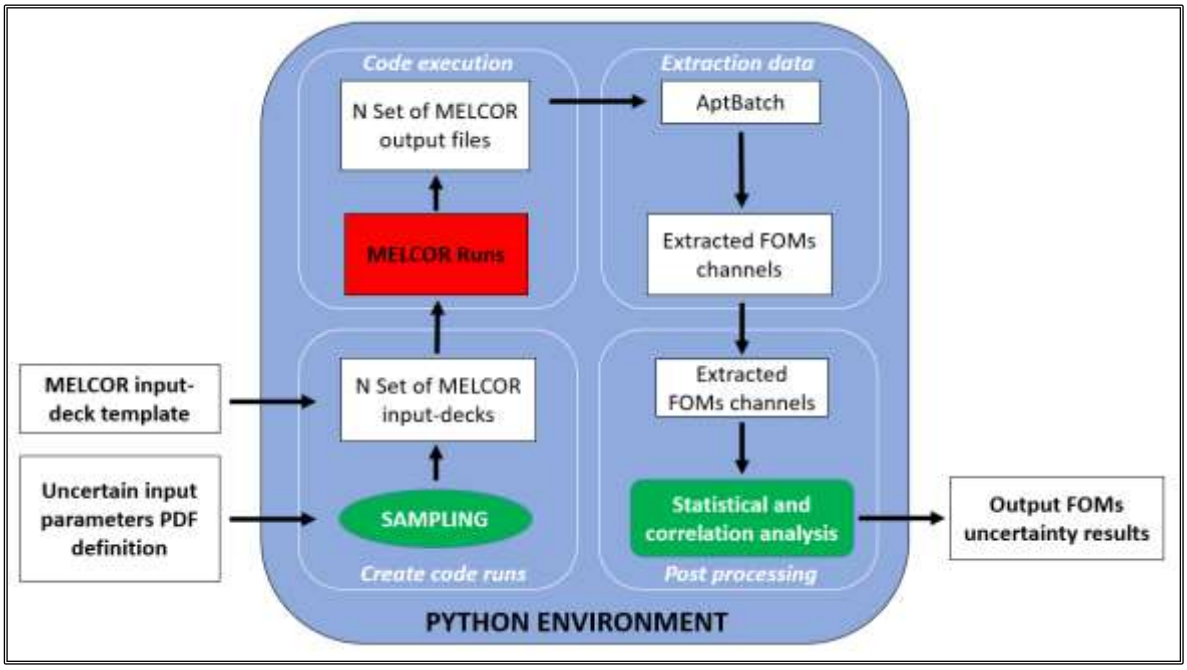

Figure 2.3 Workflow of the uncertainty in-house tool for MELCOR in a Python Environment/Architecture.

The tool permits to conducting of a full uncertainty quantification analysis and customising the analysis on the user's goals. As presented in the following, the tool consists of four independent scripts.

In the *create code runs* script, the user specifies the number of code runs N and the uncertain input parameters. Using the *numpy* library, the tool samples the uncertain input parameters from their specified PDFs to create the N sets of uncertain input parameters to be replaced in the input-deck template. In a similar way to what was done in the previous computational environment, the input-deck template is prepared beforehand by inserting a string instead of the value of the input parameters that can be recognized by the Python tool and replaced with the corresponding sampled value. Once the N input decks have been

created, the script generates N folders in which there are, in addition to the code input deck, the commands necessary for the code execution, the commands necessary for the execution of the AptBatch executable and the related script in which the desired channels to be extracted are defined. Furthermore, using the *pandas* library, the tool creates an Excel file in which all the N sets of values of the sampled input parameters are printed.

The *code execution* script starts the code runs. Through the *ProcessPoolExecutor* Python function, it allows the execution of a number P of parallel runs, which are defined by the user and which, generally, are chosen based on the processors characterizing the CPU of the machine used to perform the analysis.

The *extraction data* script manages the FOMs channels extraction by AptBatch executable from the N code runs output files. In a very similar way to the previous script, the user can set the number of parallel processes to be divided into.

The *post processing* script, starting from the extracted FOMs channels, computes the statistical parameters and develops the post-processing. Using the Pandas library, it calculates the mean, median, upper and lower bounds, empirical PDF and CDF, standard deviation and coefficients of variation of the FOMs. Moreover, the script permits the development of the statistical correlation analysis by computing the simple and simple rank coefficient using Pearson and Spearman's correlation. In addition, to study the evolution of the main statistical parameters as well as to graphically analyse the uncertainty band of the code on the FOMs variables along the transient, the script computes the statistical parameters and the statistical correlation coefficients at each timestep. Using the *matplotlib* library permits to development and manage the desired plots for the uncertainty analysis and through the Pandas library to print in Excel all the calculated data.

In general, the development of an independent tool allows more flexibility than using external software. As discussed in the previous section, it requires managing several scripts to interface the UT to the code. On the other hand, the development of an independent tool could present programming challenges (e.g. debugging, etc.). In addition, it is highlighted that the use of an open-source language such as Python allows the continuous update and customization of the tool according to the user's needs taking into account the breadth of Python user's community and the amount of public information about Python libraries' capability.

3 APPLICATION OF THE UNCERTAINTY METHODOLOGY AGAINST EXPERIMENTAL DATA IN SEVERE ACCIDENT DOMAIN

3.1 Introduction

The present chapter aims to give a first insight into the application of the uncertainty methodology based on the application of the "probabilistic method to propagate input uncertainty" to SAs. In this view, the methodology has been tested against the Phebus FPT1 and QUENCH-06 experimental tests.

The uncertainty analysis of the Phebus FPT1 has been carried out employing the coupling between MELCOR and DAKOTA within the Python environment/architecture, described in detail in 2.4.1.3. The uncertainties of the MELCOR code on aerosol physics within the containment of the experimental facility have been investigated.

Then, to study the uncertainties related to hydrogen generation from zircalloy oxidation, the uncertainty analysis of the QUENCH-06 test has been carried out using the uncertainty tool developed in Python for the MELCOR code and presented in 2.4.2.

3.2 Uncertainty quantification of the Phebus FPT1 test

The integral Phebus FPT1 test [87], conducted in the framework of the Phebus Programme [88], represents a milestone for the current knowledge on cladding oxidation phenomena and fuel rod degradation, effects of control rod materials on fuel degradation, FPs chemistry and transport and iodine chemistry within the containment, as discussed in [89] [90] [91] [92]. The Phebus FPT1 has been also adopted for the International Standard Problem of the OECD/NEA [93] [94] [95]. Previous analyses on the Phebus FPT1 conducted with the MELCOR code can be found in [96] and [97] concerning core degradation mechanism simulation and in [98] concerning the study of MELCOR response on radioactive materials releases from the test bundle.

The uncertainty application of the Phebus FPT1 test has been carried out in collaboration with ENEA along the MUSA project [77]. This uncertainty application aims to test the methodology estimating the uncertainties of the MELCOR code on aerosol physics. The FOM selected for the presented study is the maximum value of aerosol mass in suspension in the containment atmosphere of the test facility. Then, the uncertain input parameters chosen for the uncertainty application are the aerosol miscellaneous constants. In MELCOR,

they are user-defined coefficients governing the aerosol dynamics, removal process and particle interactions.

3.2.1 The Phebus program and the FPT1 test

The Phebus FP program was launched in 1998 by IPSN (France), now IRSN, in cooperation with the European Commission and EDF. The research program was performed closely with the CEA operating the experimental Phebus reactor. It involved five in-pile integral tests intending to study nuclear fuel degradation as well as iodine chemistry in the RCS and containment, aerosol physics, hydrogen production, molten pool formation, release, and transport of FPs.

The Phebus test fuel bundle, placed in a middle cell of the Phebus reactor, replicated the core of a full-scale reactor. It was made up of ten fuel rods, similar to PWR fuel rods, and an additional absorber rod. Furthermore, it was enclosed by a zirconia shroud which was inserted into an in-pile tube kept cool by pressurized water.

The cooling circuit of the experimental facility consisted of three parts: a Hot Leg (HL), a SG, which consists of one inverted U-Tube, and a Cold Leg (CL). A tank with a volume of 10 m^3 simulated the containment, considering a ratio of 5000:1 to a full-scale PWR 900 MWe. A sump held the condensed water that was gathered from the condensation of steam on specific cooled structures. In Figure 3.1 a schematic view of the Phebus FP test setup is presented [8].

Among the tests of the research program, the FPT1 [87] has been mainly devoted to investigating the degradation of a fuel bundle. The Phebus FPT1 test fuel bundle consisted of two fresh and eight irradiated fuel rods and a control rod made of silver, indium, and cadmium.

The test was divided into four phases:

I. **Degradation phase**: it involved the degradation of the test fuel bundle and lasted for around five hours. It was divided into two parts: the *thermal calibration period*, which endured for about 7900 seconds, and the temperature transient causing the bundle degradation. The second part was divided into four periods: *pre-oxidation*, *oxidation*, *heat-up* and *cooling period*. During the first period, the fuel bundle was heated, causing the onset of the zircalloy oxidation reaction and the beginning of hydrogen generation. The oxidation phase was characterized by an initial rump of the steam mass flow rate and bundle power, followed by a steady mass flow rate with an increase in the temperature and zircalloy oxidation

runaway. After 14500 s after the start of the test, a second power ramp began the heat-up phase, causing the heating up of the fuel rods and the bundle material to liquefy. The cooling period started when the system was set to shut down at around 17000 s after the start of the test.

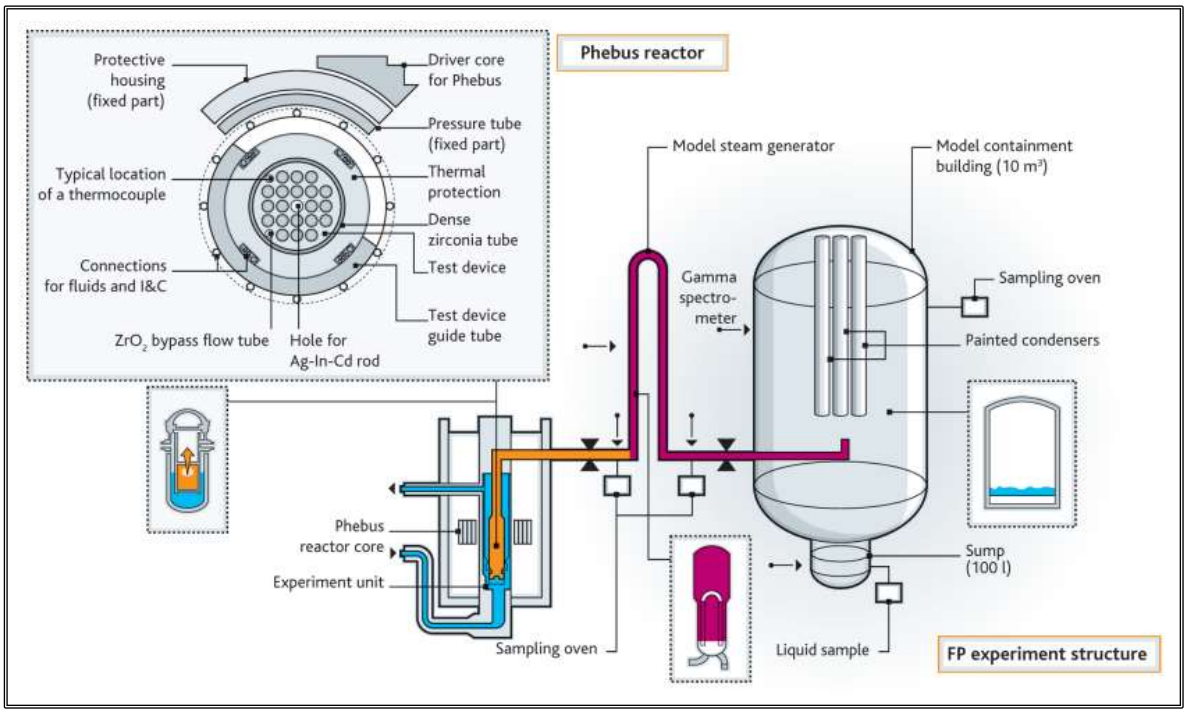

Figure 3.1 Schematic view of the Phebus FP test setup [8].

II. **Aerosol phase**: it was dedicated to the study of aerosol physics and deposition processes on the inner surfaces of the containment. It started at about 18000 s after the start of the test with the isolation of the containment from the CL.

III. **Washing phase**: it was devoted to washing out the aerosol deposited in the containment floor into the sump water. It began about 64 hours after the start of the test.

IV. **Chemistry phase**: it was characterized by the temperature increase of the containment atmosphere and conditions were kept constant for 18 h to permit to study of the iodine chemistry in the sump.

3.2.2 Description of the nodalization

To develop the reference case because of the uncertainty quantification results, the MELCOR nodalization of the Phebus FPT1 test has been built up starting from the input deck developed by USNRC [99]. Italy is a member of USNRC's CSARP [100], hence ENEA has requested permission (accepted by USNRC) to use the Phebus FPT1 input deck within the framework of the MUSA project [72].

The model, shown in Figure 3.2, consists of 31 Control Volumes (CVs), 68 Heat Structures (HS) and 29 flow paths.

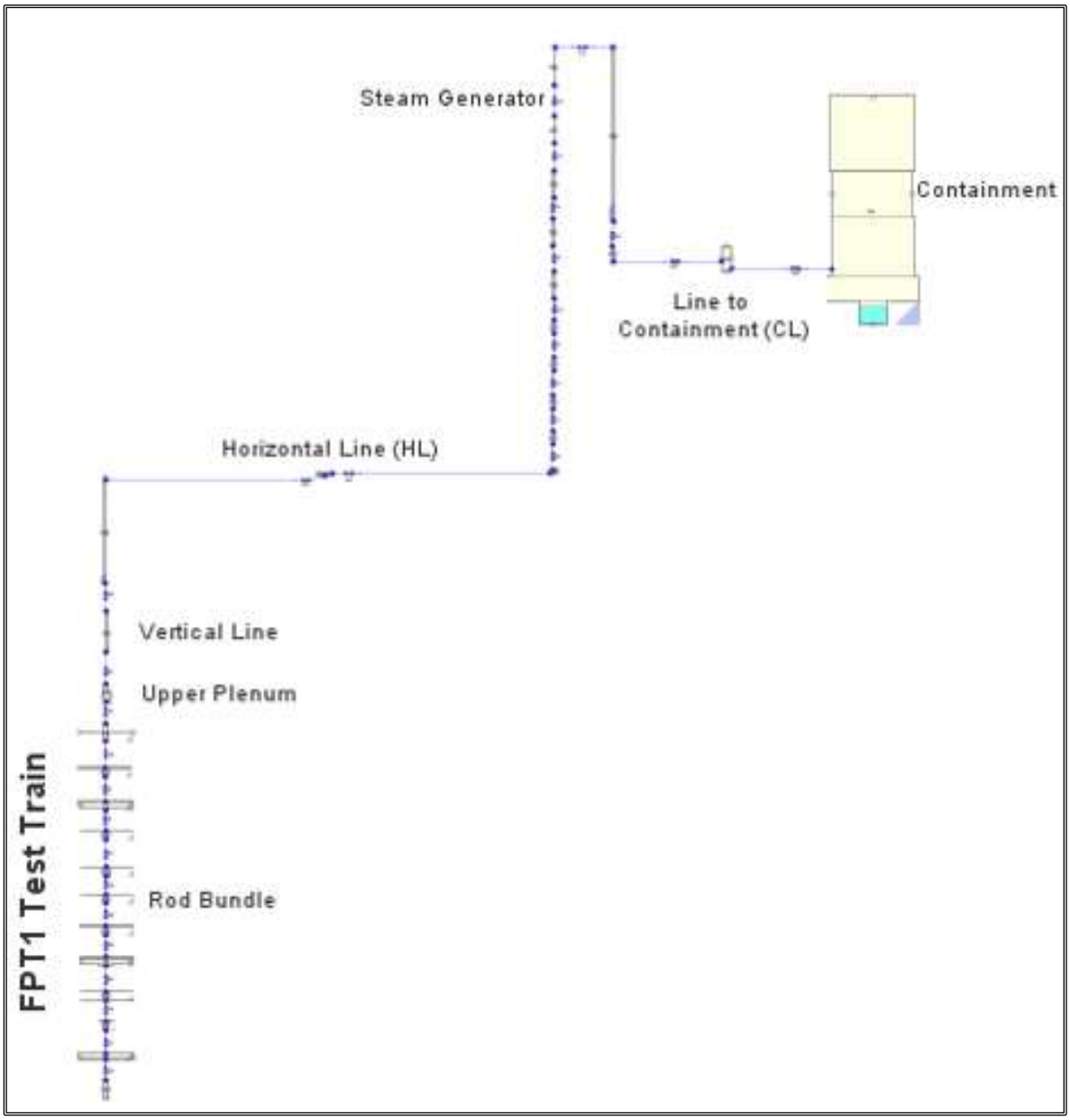

Figure 3.2 SNAP visualization of the Phebus FPT1 CVH and FL nodalization.

The vertical line is divided using three CVs: one for the upper plenum, one for the lower line and one for the upper vertical line. Two CVs have been used to model the horizontal line between the vertical line and the SG's inlet. Two CVs on the descending side and nine CVs on the ascending side have been considered. The containment, which is modelled by a single CV, is connected to the SG outlet through a single CV.

The hydraulic model of the fuel bundle consists of eleven CVs while, to simulate core degradation phenomena, it is modelled employing the MELCOR COR package. The COR nodalization has been subdivided into 31 axial and 2 radial regions. To simulate the FPs

transport and aerosol physics, the MELCOR RN package has been activated. To carry out the analyses (reference case and uncertainty analysis) described in this chapter, the MELCOR 2.2 v18019 has been used.

3.2.3 Description of the reference case

The reference case has been carried out by simulating the entire *degradation phase* and the beginning of the *aerosol phase*. Then, a total simulation time of 29000 s has been considered for the reference case.

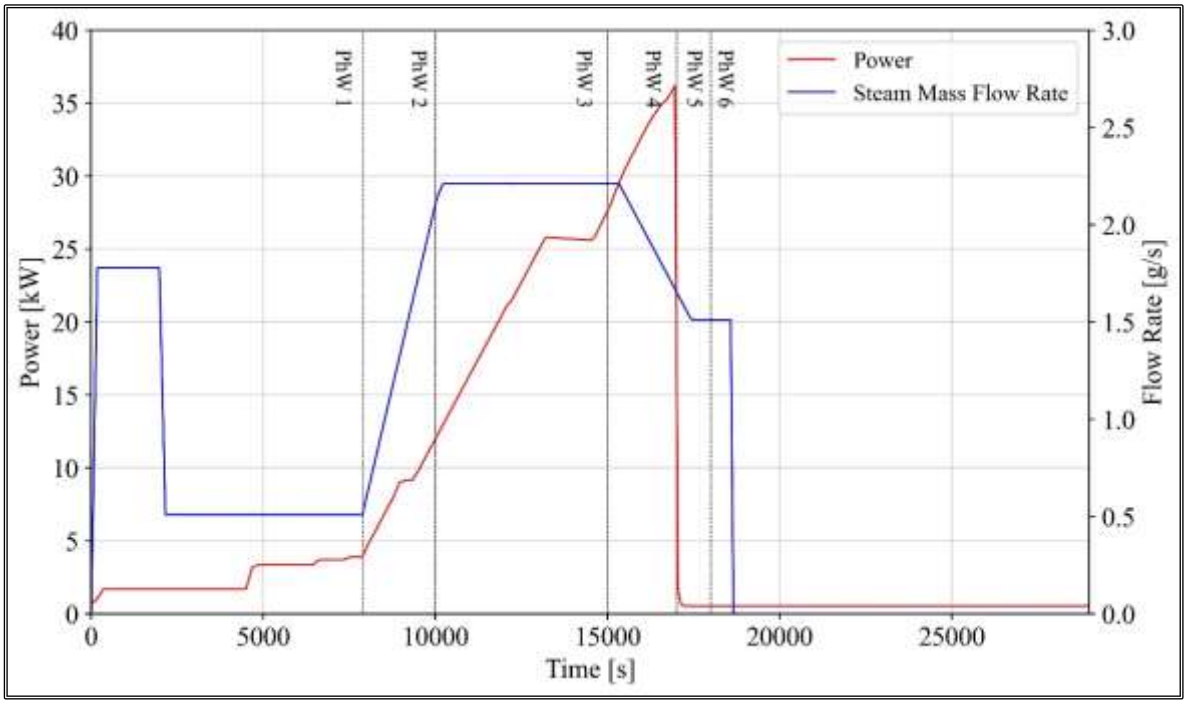

Figure 3.3 Power and steam mass flow rate during the reference case.

A total of six Phenomenological Windows (PhWs) have been identified, respectively for:

I. **Thermal-calibration period** - PhW 1
II. **Pre-oxidation period** - PhW 2
III. **Oxidation period** - PhW 3
IV. **Heat-up period** - PhW 4
V. **Cooling period** - PhW 5
VI. **Beginning of aerosol phase** - PhW 6.

The applied boundary conditions in terms of steam flow rate and power of the bundle are presented in Figure 3.3.

During the pre-oxidation phase of the test, due to the linear increase of the power, the code predicts the start of the degradation of the fuel bundle and the release of iodine and

caesium from the bundle, leading to a small increase in the amount of aerosol mass suspended in the containment atmosphere. Figure 3.4 compares the code prediction on the aerosol mass suspended in the containment atmosphere with the experimental data.

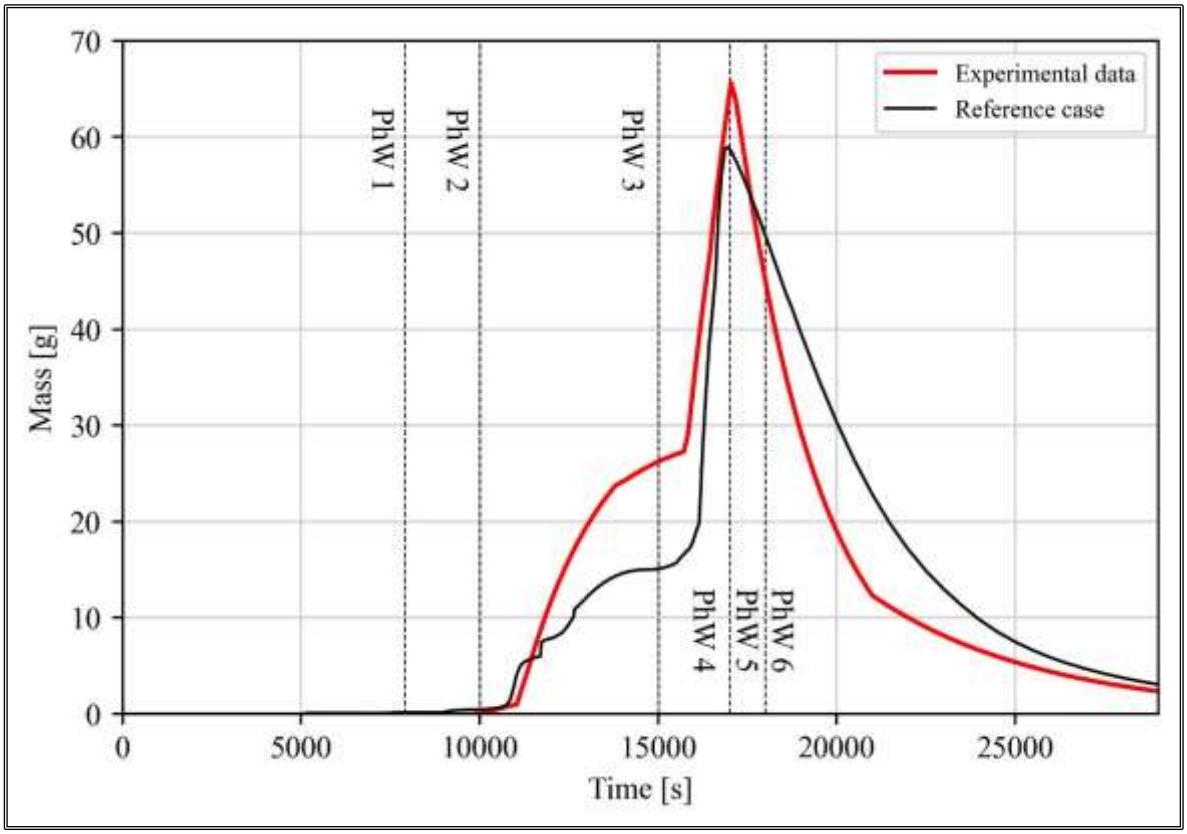

Figure 3.4 Aerosol suspended mass in the containment atmosphere during the reference case [89].

The subsequent oxidation phase is defined by a constant steam mass flow rate a linear increase and then a plateau of the power. These conditions determine the runaway of cladding oxidation and the heat-up of the bundle, leading to the increase of release rate of FPs into the containment and, consequently, the increase of the amount of the suspended aerosol mass in the containment atmosphere.

The linear rise of the power and the fall of steam mass flow rate drive the bundle test to the final degradation stage during the heat-up phase. At the end of this phase, at about 17000 seconds after the start of the test, the aerosol mass in the containment reaches the maximum value. The code predicts a maximum value of the aerosol mass suspended in the containment atmosphere of about 59 g, with a discrepancy of about 5 g from the experimental value.

At about 17000 s, following the system shutdown, a constant mass flow rate of steam is pumped into the bundle. Then, the isolation of the containment occurs at about 18600 s after

the start of the tests, initiating the aerosol phase of the test characterized by the deposition of the aerosols into the inner containment surfaces (fallout).

3.2.4 Hypotheses of the uncertainty analysis

The objective of the uncertainty application is to carry out a full uncertainty analysis testing the uncertainty methodology in the SA domain [77]. Furthermore, the analysis permits to give some insights into the uncertainties of the MELCOR code related to aerosol physics.

In the MELCOR code, aerosol physics and in general all the phenomena related to aerosol phenomenology are based on MAEROS, included in the RN package. The RN package is described in detail in APPENDIX A. Considering the complexity characterizing the aerosol phenomenology during a SA sequence, MELCOR implements simplified models based on constant parameters [30]. Among them, some parameters affect aerosols particle-particle interaction:

- *Agglomeration shape factor* (GAMMA): it models the effect of non-spherical shape upon aerosol collision cross sections. A value greater than 1 indicates that the particle has a higher propensity to aggregate than a spherical particle.
- *Sticking coefficient* (STICK): it represents the agglomeration probability of two colliding particles.
- *Turbulence dissipation rate* (TURBDS): it is the turbulence kinetic energy transferred into heat.

Other parameters influence the aerosol dynamics:

- *Dynamic shape factor* (CHI): it models the effect of non-spherical shape upon aerosol-atmosphere drag forces. A value greater than 1 indicates that the particle has a higher deviation of motion than a spherical particle.
- *Slip coefficient* (SLIP): it represents the momentum exchange between gas molecules and moving particles.
- *Ratio of the gas-to-particle thermal conductivities* (TKGOP).

Then, other parameters influence the aerosol removal processes:

- *Thermal accommodation coefficient* (FTHERM): fraction of thermal energy transferred from a particle to the surface on which it is depositing.

- *Diffusion boundary layer thickness* (DELDIFF): boundary layer for Brownian diffusion of aerosols and determines the concentration gradient driving diffusion.

The parameters described above are also called *aerosol miscellaneous constants* in the MELCOR code and for the uncertainty application against Phebus FPT1 experimental data have been selected as uncertain input parameters. Table 1.1 shows the uncertain input parameters' PDF with the distribution type and range of variation.

Table 3.1 Uncertain input parameters [29] [30] [99] [101] [102].

Uncertain input parameter	**Unit**	**Distribution type**	**Mean**	**Distribution characteristics**	
CHI	[-]	Beta	1	α	1
				β	1.5
				min	1
				max	5
GAMMA	[-]	Beta	1	α	1
				β	1.5
				min	1
				max	5
FSLIP	[-]	Beta	1.257	α	4
				β	4
				min	1.2
				max	1.3
STICK	[-]	Beta	1	α	2.5
				β	1
				min	0.5
				max	1
TURBDS	[m^2/s^3]	Uniform	0.001	min	0.00075
				max	0.00125
TKGOP	[-]	Log-Uniform	0.05	min	0.006
				max	0.06
FTHERM	[-]	Uniform	2.25	min	2
				max	2.5
DELDIF	[m]	Uniform	1.00E-05	min	0.000005
				max	0.0002

To analyse the code uncertainty related to the maximum aerosol mass suspended in the containment atmosphere, an approach based on estimating the two-sided tolerance interval (see 1.5.2.1) has been adopted. According to equation (5), a minimum of 93 code runs are needed for the two-sided tolerance interval and a probability γ and confidence level β equal to 0.95. Following the first strategy defined in 2.3.3, an amount of 130 code runs have been started.

3.2.5 Results of the uncertainty analysis

Among the 130 runs of the code, a total number of 10 failed runs were identified. To analyse the nature of the failure of these runs, an approach based on the analysis of the phase space of the normalized parameters has been adopted. It permits the identification of potential threshold values of uncertain input parameters leading to a region characterized by total code run failures. From the evaluation of the normalized uncertain input parameters phase space, presented in Figure 3.5, the distribution of failed runs seems to be random, i.e. there are no threshold limits of the sampled input parameters where there are only failed runs.

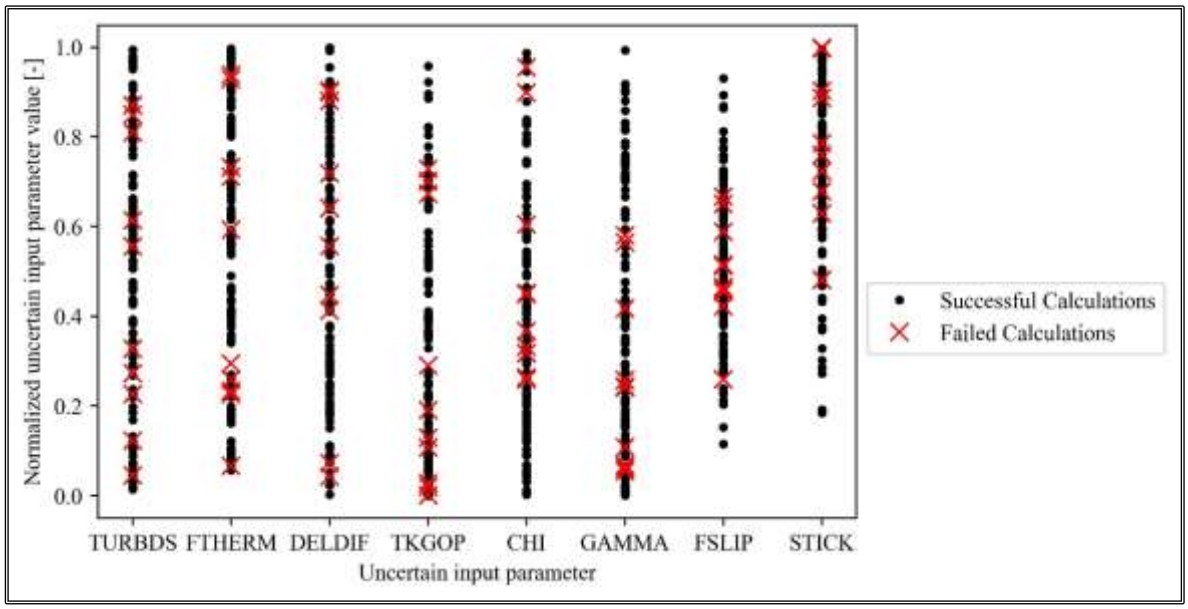

Figure 3.5 Normalized uncertain input parameters phase space.

The uncertainty analysis of Phebus FPT1 has been carried out through the calculation of the statistical parameters of interest characterizing the FOM such as the mean, the median, the lower and upper bounds, the standard deviation, and the coefficient of variation. They are presented in Table 3.2.

Table 3.2 Statistical parameters of the FOM.

Statistical parameter	Unit	Value
Mean	[g]	67.14
Median	[g]	66.94
Lower bound	[g]	20.71
Upper bound	[g]	134.74
Standard deviation	[g]	25.60
Coefficient of variation	[-]	0.38

Downstream of the propagation of the input uncertainties, the uncertainty band of the FOM is calculated by the computational environment and it is equal to 114 g. The reference calculation value of 59 g is within the uncertainty band calculated by the statistical analysis.

In addition, the reference value is close to the mean and the median values, both of which are about 67 g, as shown in Table 3.2. The empirical CDF and PDF of the FOM have been also evaluated to characterize the code uncertainty and are shown in Figure 3.6 and Figure 3.7 where they are compared to the experimental value, the reference calculation, including the mean and median values, previously discussed. Through Python, the PDF kernel density estimation has been calculated to estimate the shape of the PDF of the FOM.

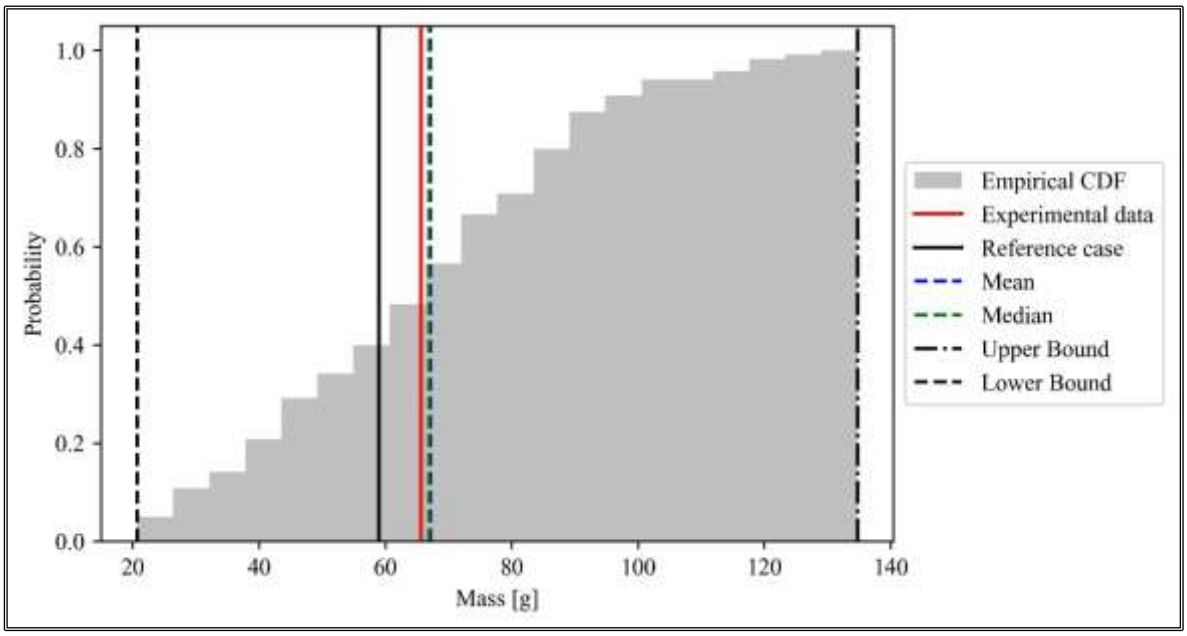

Figure 3.6 Empirical CDF of the FOM [89].

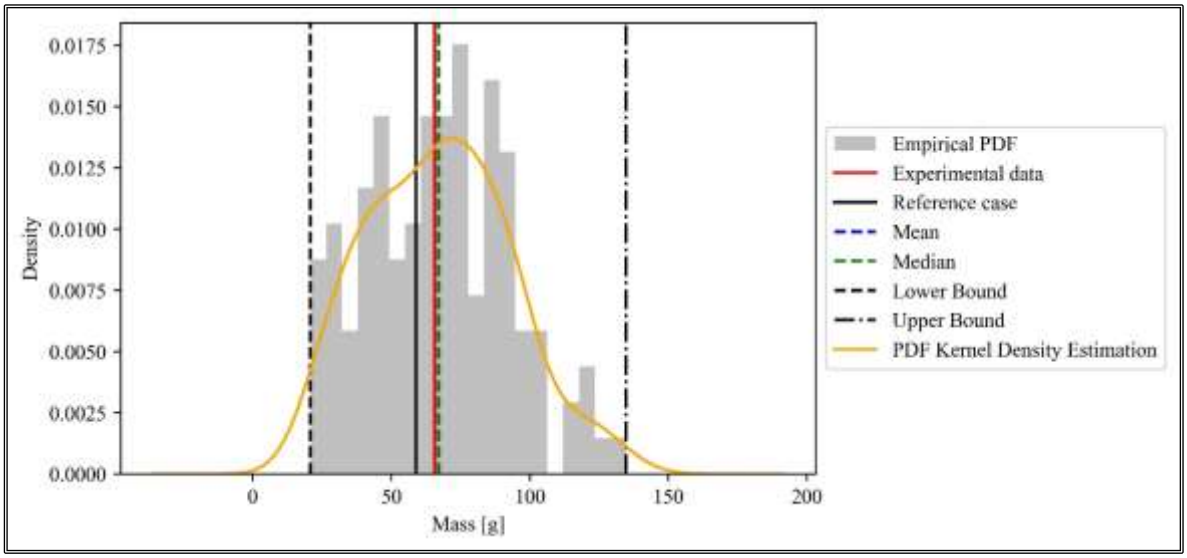

Figure 3.7 Empirical PDF of the FOM [89].

Simple and simple rank correlation coefficients have been calculated using respectively Pearson and Spearman's correlations, presented in 1.5.2.1. From the statistical correlation analysis, a moderate statistical correlation with the CHI uncertain parameter (positive correlation), representing the aerosol dynamic shape factor, has been encountered. In addition, a significant correlation (negative correlation) with the GAMMA parameter, representing the aerosol agglomeration shape factor, has been underlined. The other input uncertainty parameters have a low correlation with the FOM selected for analysis. The simple and simple rank correlation coefficients for each uncertain input parameter are reported in Figure 3.8 and Figure 3.9.

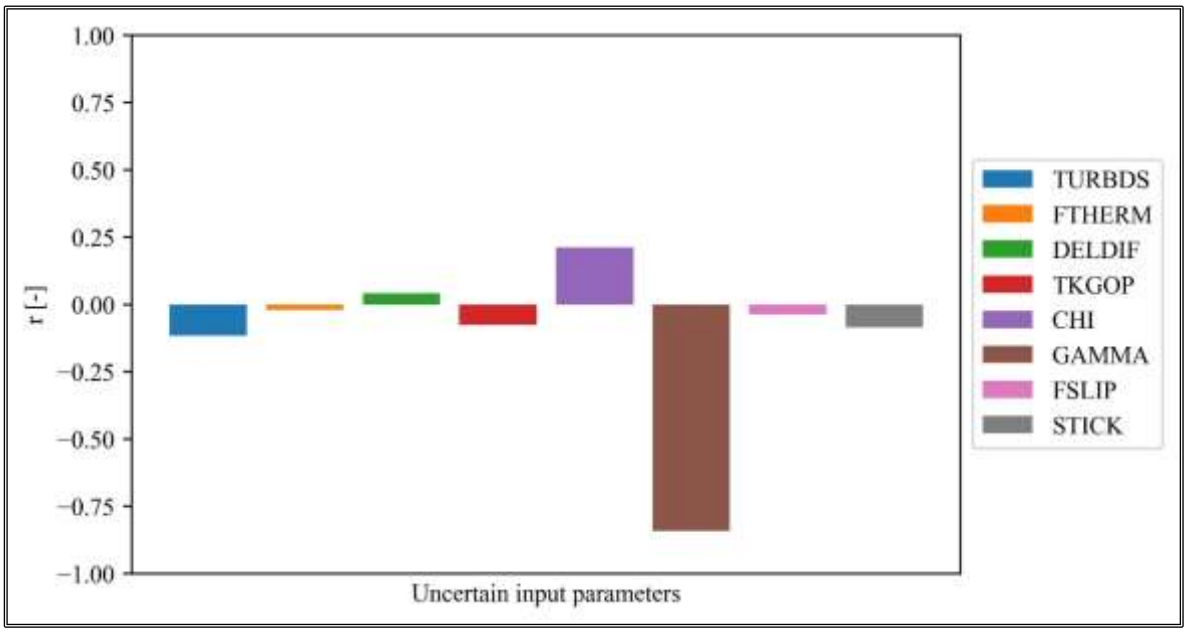

Figure 3.8 Simple correlation coefficient.

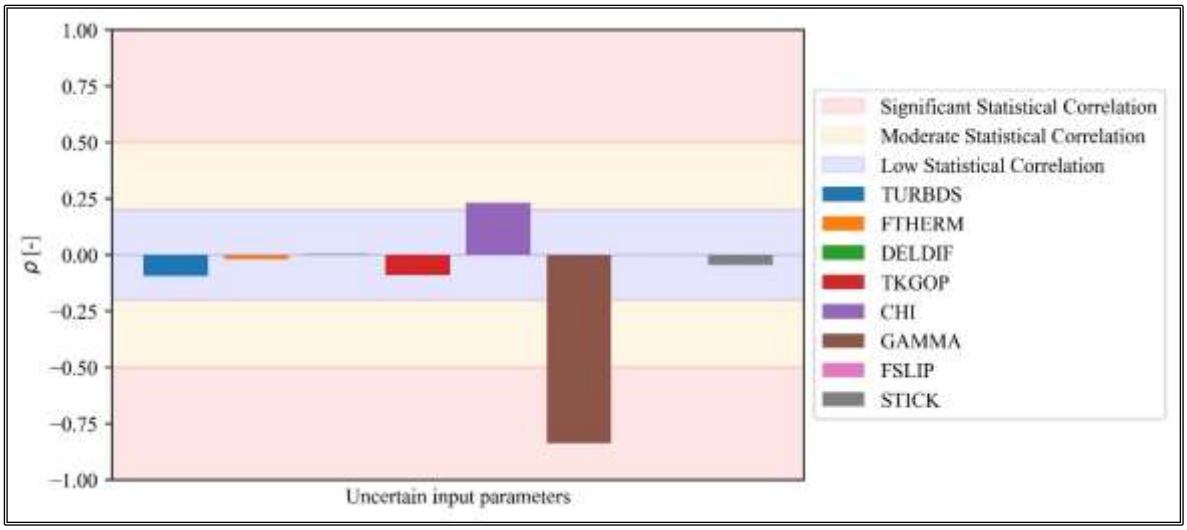

Figure 3.9 Simple rank correlation coefficient.

The meaning of the correlation coefficients calculated above can be assessed through scatter plots, which represent the distribution and relationship between the FOM, and the value of a given uncertain input parameter. From Figure 3.10 to Figure 3.17 the scatter plots representing the FOM values for each uncertain input parameter are shown. Furthermore, the statistical correlation has been also highlighted using the linear regression technique and the calculation of a trend curve, which has been considered in the scatter plots by a red line.

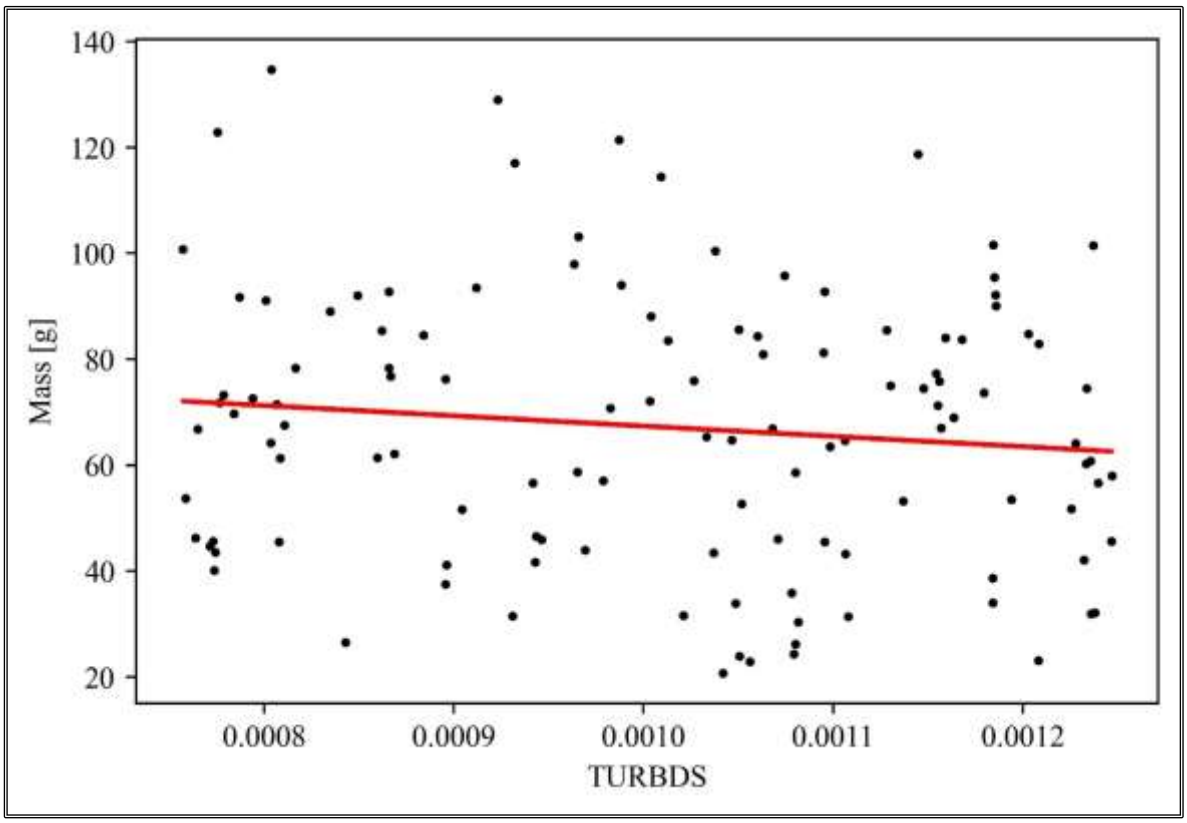

Figure 3.10 Scatter plot of FOM and TURBDS values.

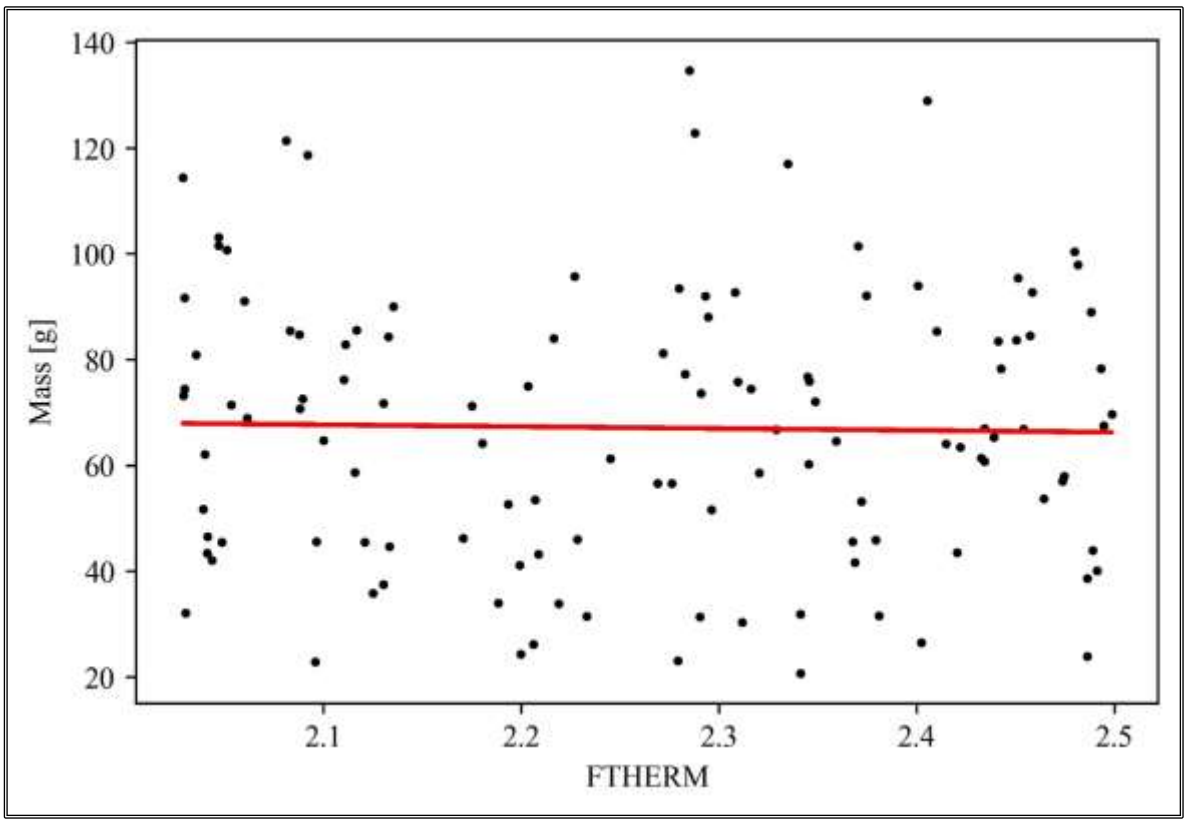

Figure 3.11 Scatter plot of FOM and FTHERM values.

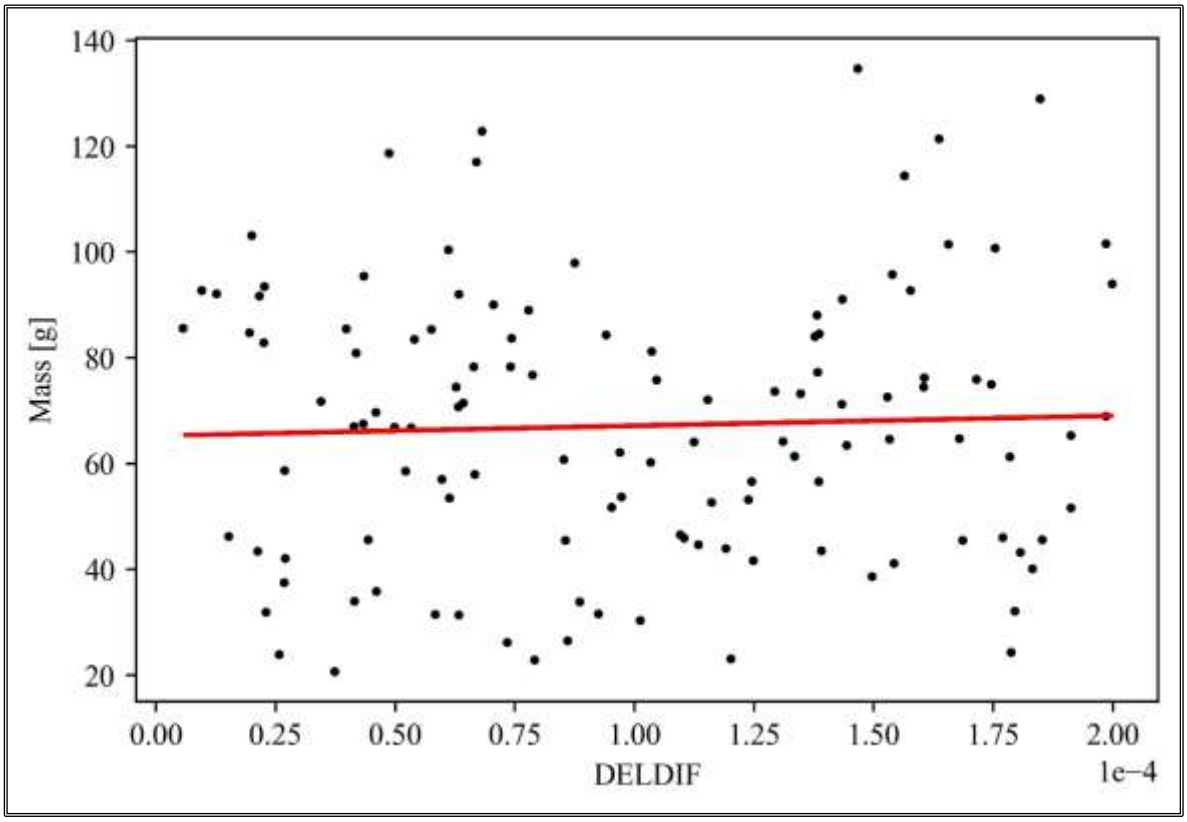

Figure 3.12 Scatter plot of FOM and DELDIF values.

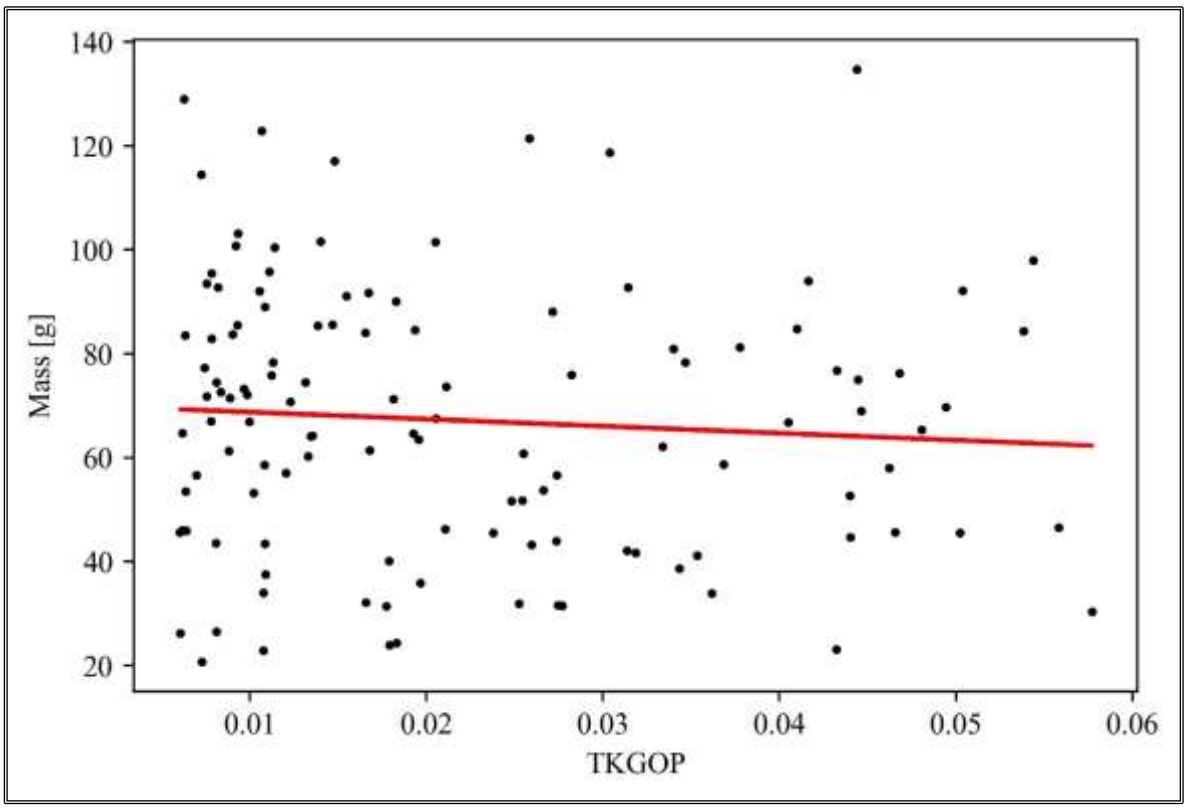

Figure 3.13 Scatter plot of FOM and TKGOP values.

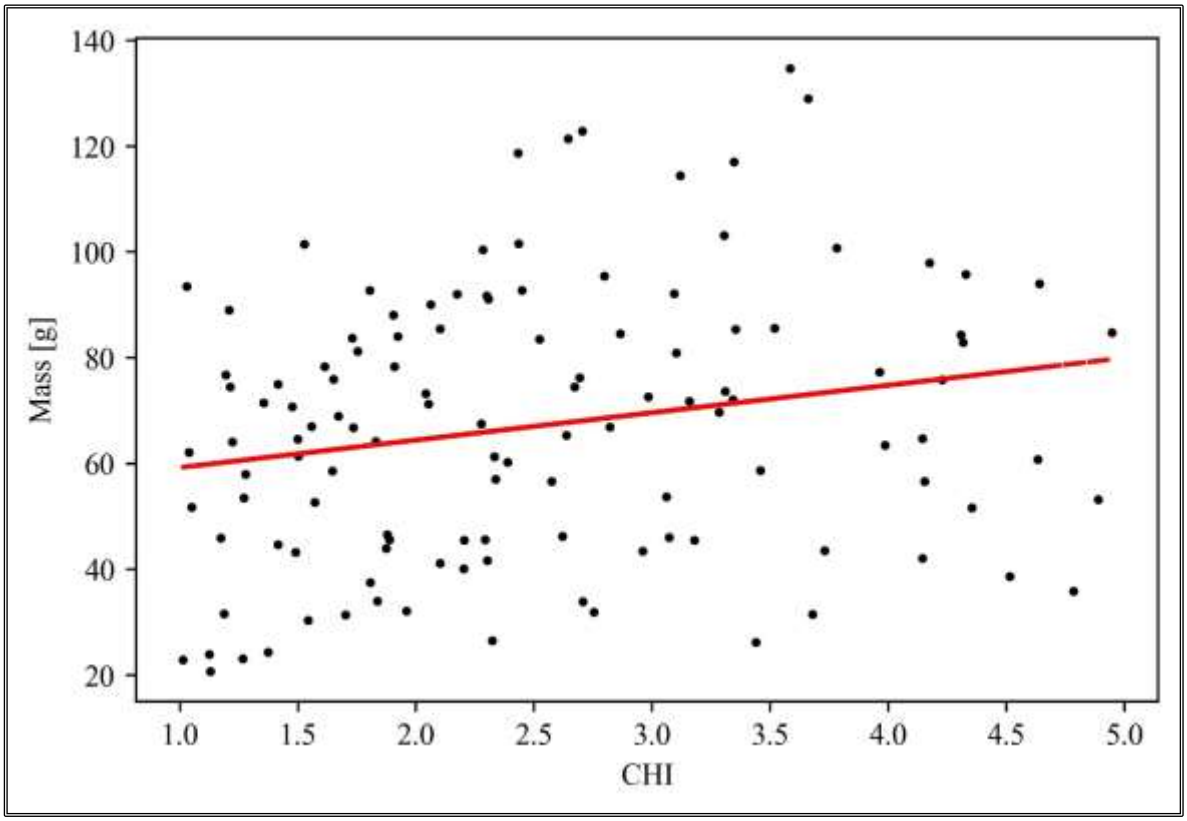

Figure 3.14 Scatter plot of FOM and CHI values.

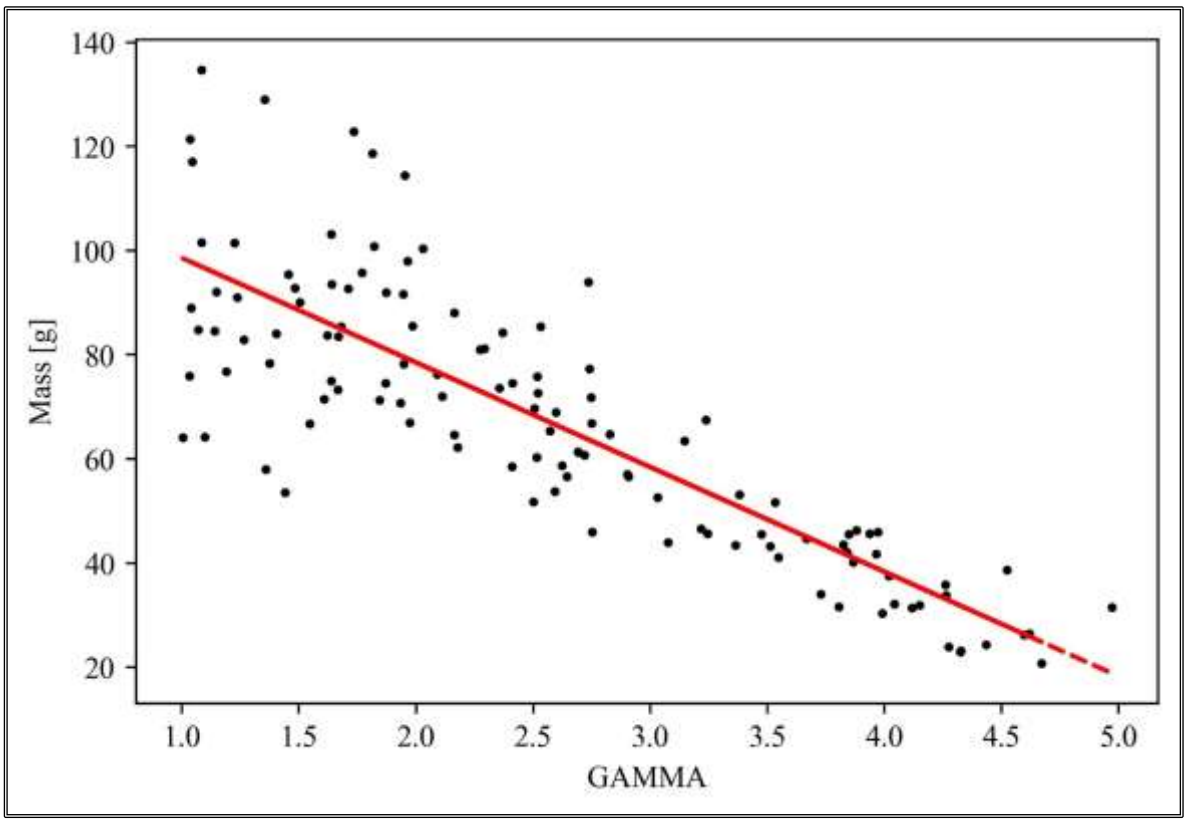

Figure 3.15 Scatter plot of FOM and GAMMA values.

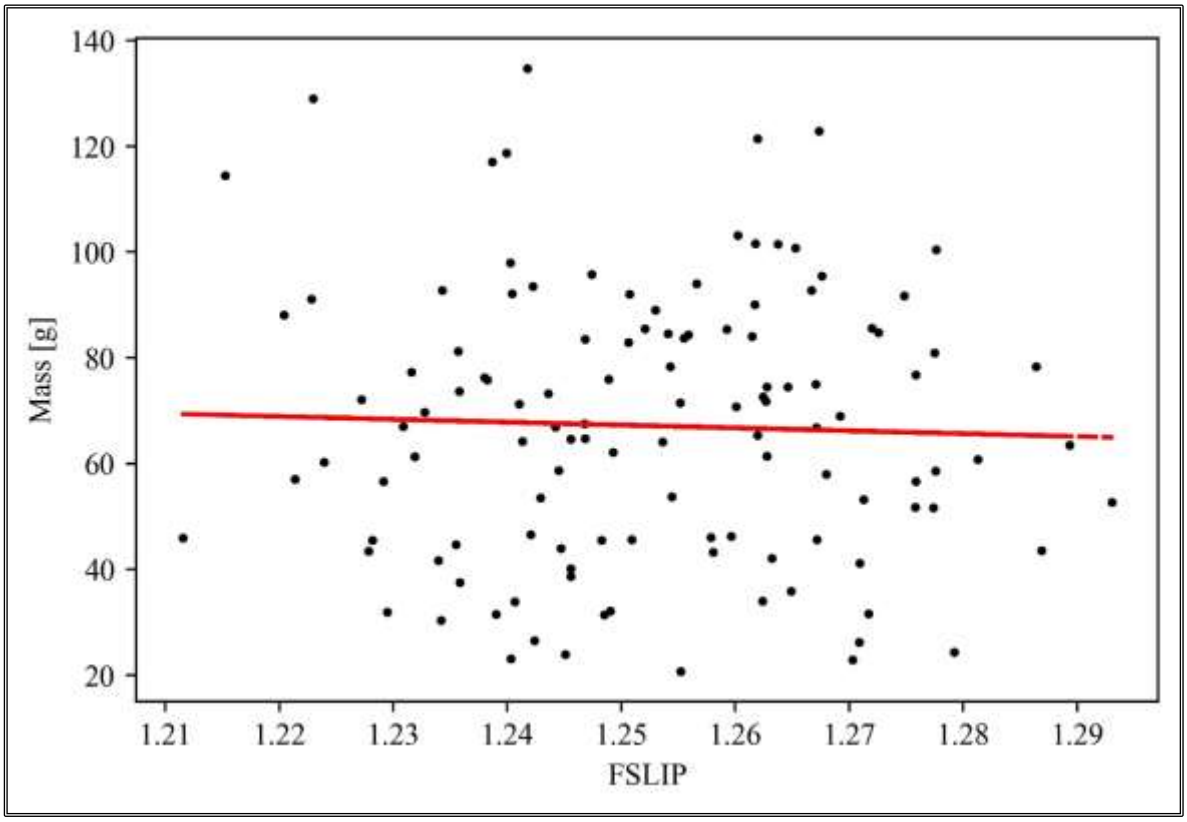

Figure 3.16 Scatter plot of FOM and FSLIP values.

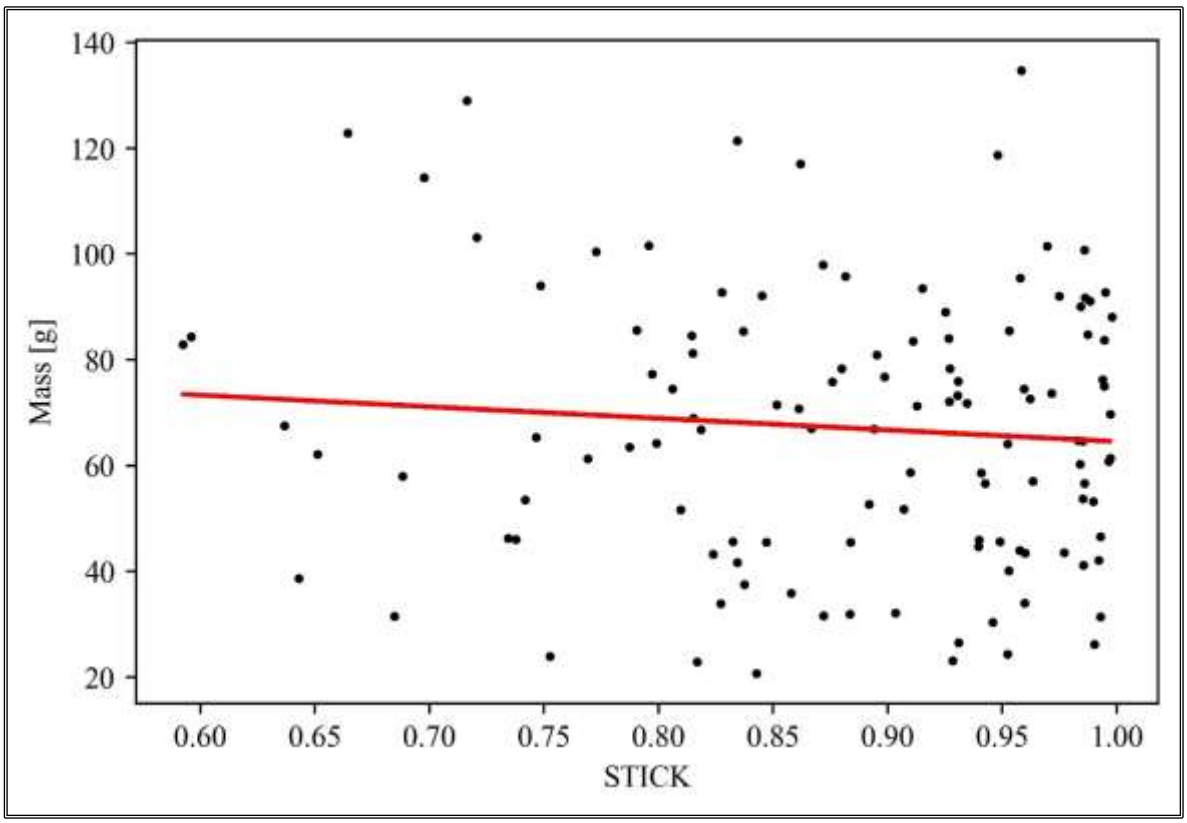

Figure 3.17 Scatter plot of FOM and STICK values.

To characterize the uncertainty band of the code during all the simulated PhWs, the values of aerosol suspended mass in the containment atmosphere at each time-step have been compared to the temporal experimental values and the reference case. As shown in Figure 3.18, the experimental data and the reference case are within the uncertainty band during all the simulated PhWs. As presented in this figure, the main statistical parameters have been computed at each time step of the calculation and compared with the experimental data. In this regard, a good agreement between the mean and the median value is underlined.

The uncertainty bandwidth increases during the oxidation period (PhW 3) starting 10000 s after the beginning of the test. Figure 3.19, presenting the standard deviation calculation at each time-step, highlights this behaviour: it increases throughout the oxidation period and reaches its maximum value of roughly 30 g during the heat-up period, at around 16000 s after the beginning of the test. Finally, the coefficient of variation reaches a constant value of about 1.4 at the end of the simulated test.

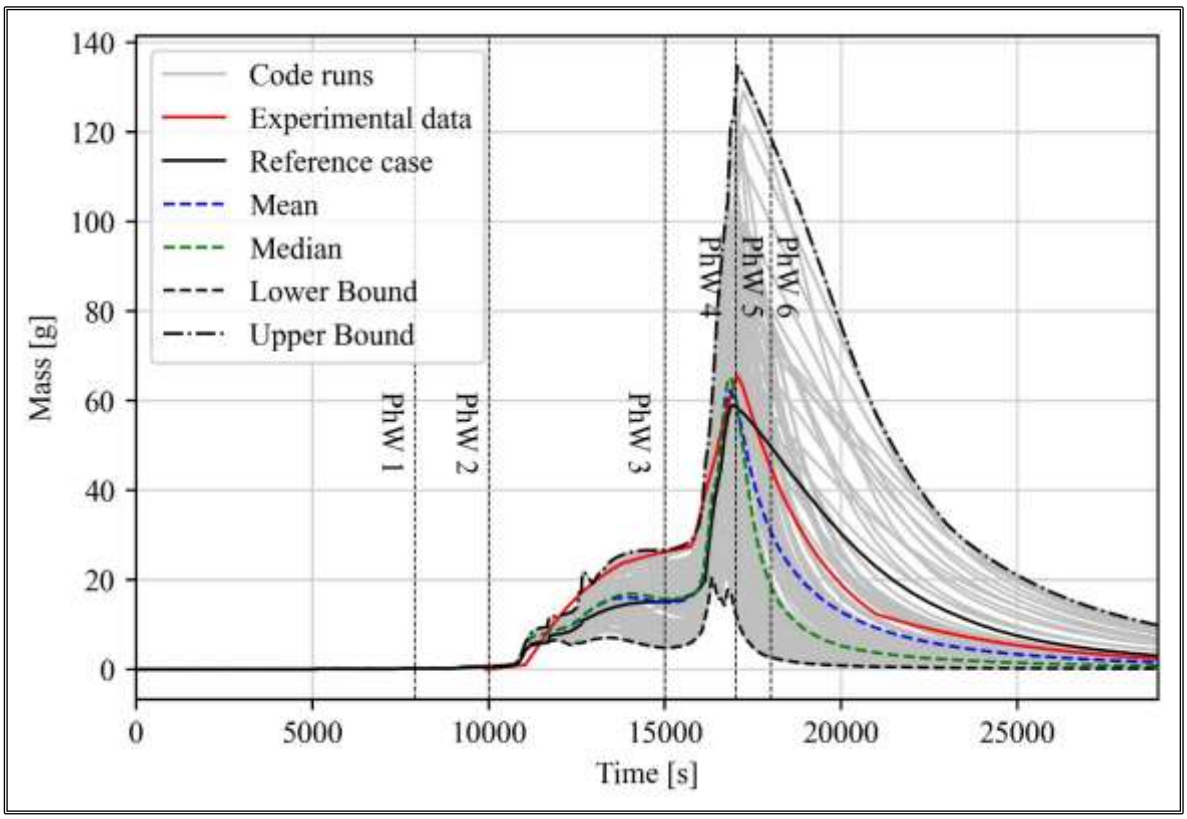

Figure 3.18 Aerosol mass suspended in the containment atmosphere uncertainty band [89].

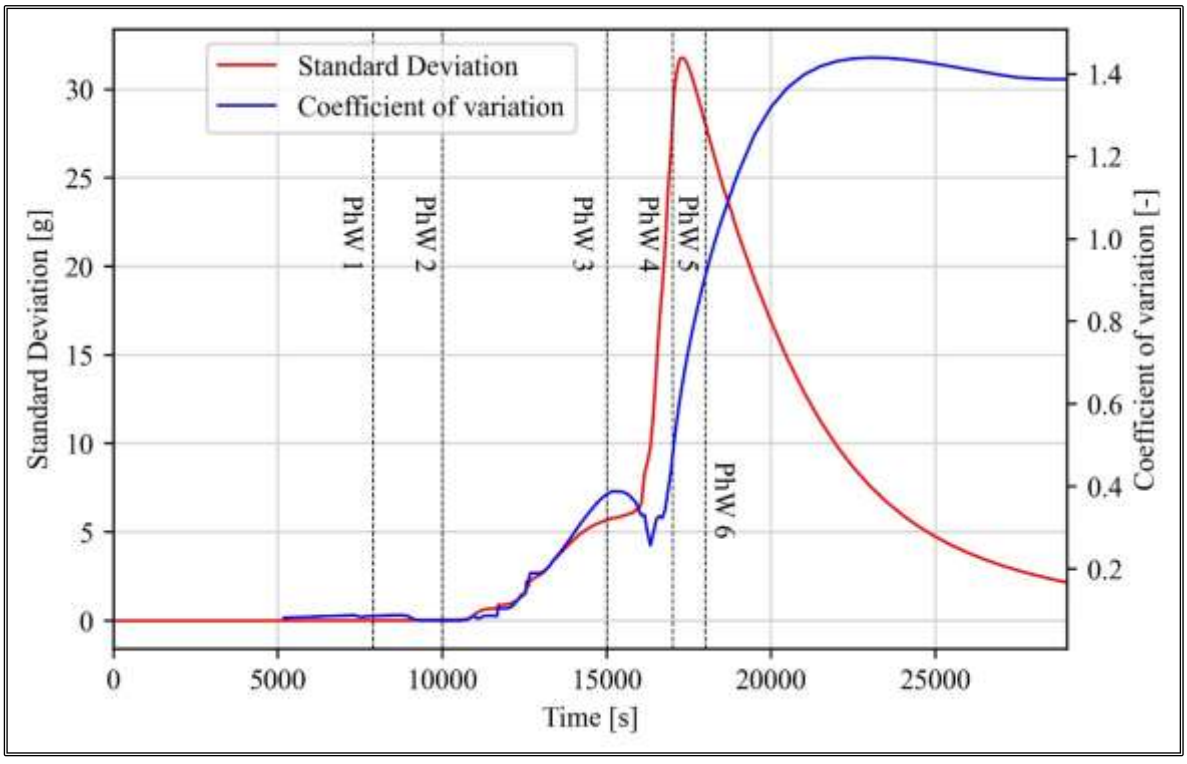

Figure 3.19 Standard deviation and coefficient of variation.

The simple and simple rank correlation coefficients have been also calculated starting from the beginning of the oxidation period since the uncertainty band before that time is absent. They are shown in Figure 3.20 and Figure 3.21.

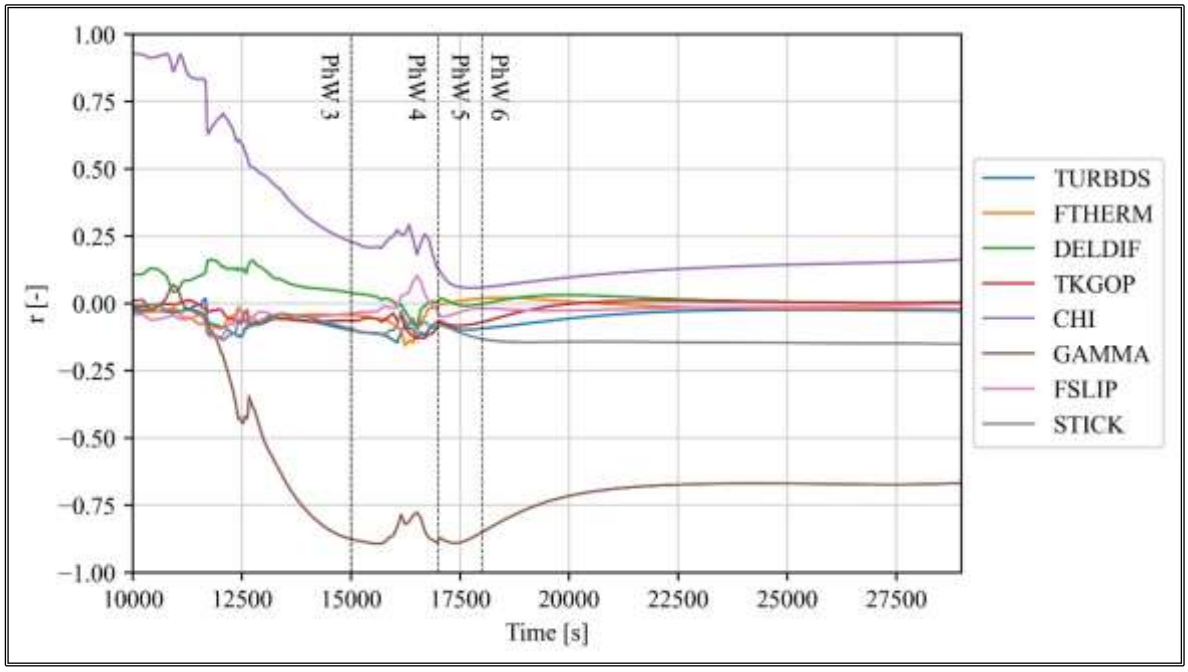

Figure 3.20 Simple correlation coefficient along the simulated phases.

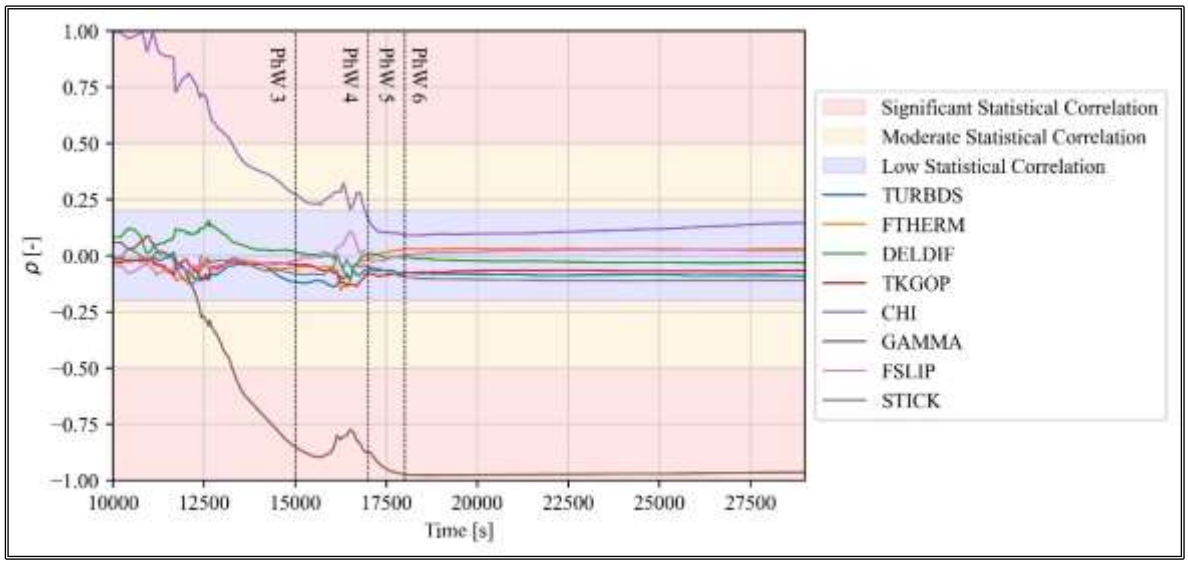

Figure 3.21 Simple rank correlation coefficient along the simulated phases.

The CHI parameter presents a statistical correlation up to the middle of the oxidation period (positive correlation). Subsequently, it presents a moderate statistical correlation and then, a low statistical correlation during the heat-up and cooling periods of the test. Instead, the GAMMA parameter presents a low statistical correlation at the beginning of the

oxidation period and then, the correlation changes from low to moderate and then to significant (negative correlation). Instead, the other uncertain input parameters present a low statistical correlation along the simulated test.

3.3 Uncertainty quantification of the QUENCH-06 test

QUENCH refers to scaled-down separate effect test experiments conducted at KIT in Germany to simulate, by a heated bundle representing an uncovered hot reactor core, the termination of accidental transients in LWRs by injection of water [103] (*quenching*) and then, to evaluate the hydrogen mass generation from zircalloy oxidation reactions. The results of these experimental campaigns provide a large and reliable dataset used for the SA integral codes validation against the models for zircalloy oxidation which represents the most important process for hydrogen production during a SA sequence (see 1.3.2).

Among the experiments which are part of the QUENCH experimental campaign, the QUENCH-06 experiment was considered by OECD/NEA/CSNI as ISP n°42 [103] [104]. A previous analysis conducted with the MELCOR code on QUENCH-06 can be found in [105], focusing on the accuracy of the code in simulating the phenomena along the different phases of the test. Furthermore, an application conducted with the ASTEC code, including the uncertainty analysis conducted with the coupling of the SA code with the UT RAVEN, is presented in [106].

The present uncertainty application has been conducted within the framework of the IAEA CRP [75] [107] and aims to investigate the uncertainties of the MELCOR code related to hydrogen generation. In this regard, the total hydrogen cumulative mass production has been considered as FOM. The outputs of the analysis have given some first key insights about the statistical correlation between boundary conditions and oxidation kinetics parameters and hydrogen generation.

Moreover, the QUENCH-06 uncertainty analysis represents a key point in the research activity presented in this manuscript as it allowed to test and develop the in-house tool in Python, described in 2.4.2.

3.3.1 The QUENCH-06 test facility

The QUENCH-06 test facility represented schematically in Figure 3.22, consists mainly of a test bundle which includes 21 full-scale fuel rods. They are divided into one unheated central rod, surrounded by 20 Fuel Rod Simulators (FRSs) heated by electric tungsten heaters, and distributed along two concentric rings. FRSs are surrounded by a hollowed pellet stack of ZrO_2 and permitted to simulate the thermal behaviour of nuclear fuel rods and

shielded by a Zircalloy-4 cladding. Then, the test bundle is insulated by an annular ZrO_2 fibre sponge and a double-walled stainless steel cooling jacket.

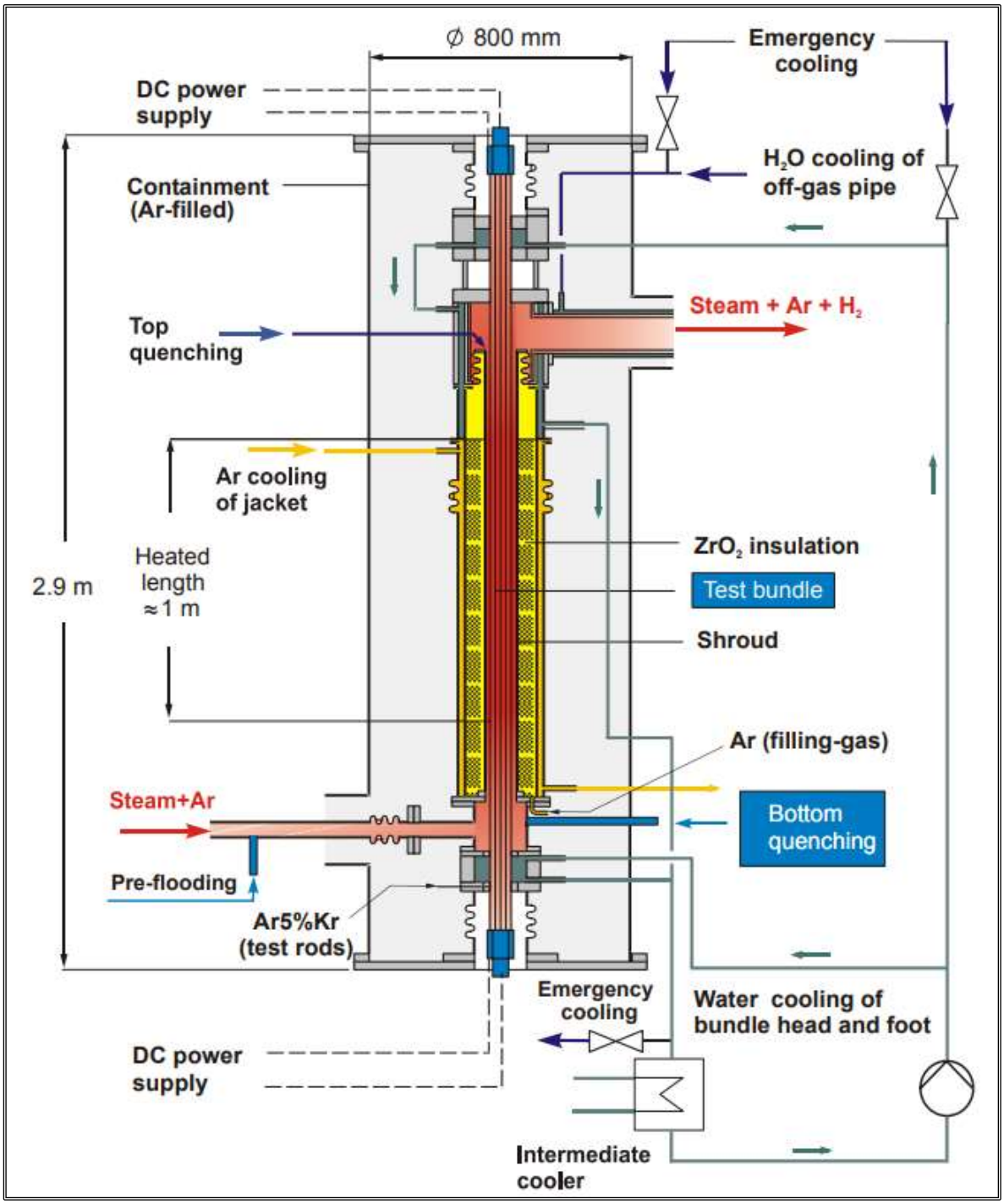

Figure 3.22 Schematic view of the QUENCH-06 test facility [104].

The experimental apparatus is then completed by systems for supplying water, steam, and argon as well as monitoring instruments for pressure, temperature and mass flow rate. The water supply system is composed of a water loop connected to the LP of the test fuel bundle, providing superheated steam and subcooled water, and a Fast Water Injection (FWI) tank

injecting a larger water mass flow rate into the test fuel bundle to simulate the fast core flooding.

The QUENCH-06 experimental test was divided into three PhWs:

I. **Pre-oxidation phase** – PhW 1: the test bundle is heated to 873 K from room temperature in an atmosphere of 3 g/s of superheated steam, with a pressure of 2 bar and temperature of 640 K, and 3 g/s of upward flowing argon gas, with a bundle power at 4 kW. Subsequently, without altering the total mass flow rate and composition of the flowing mixture, the bundle power is gradually ramped up to 11 kW once the test section reaches thermal equilibrium. Then, the power is maintained constant for the next 4046 s, bringing the maximum axial zircalloy cladding outer surface temperature to 1473 K. During this PhW, the zircalloy oxidation reaction kinetics is slowly determining a limited hydrogen production.

II. **Heat-up phase** – PhW 2: the test bundle power is increased by 6 W/s to start a transient phase with temperature, zircalloy cladding oxidation reaction rate and massive hydrogen production.

III. **Quenching phase** – PhW3: the quenching phase begins with the removal of steam injection and the redirection of argon gas flow rate to the bundle head when the minimum temperature of the three-rod thermocouples and the central rod thermocouple, located at the end of the active region, exceeds 1873 K. The FWI injects four liters of subcooled water into the test section to pre-fill pipes and LP and, subsequently after 30 s, the bundle power is decreased to 4 kW to simulate the decay power. To remove the decay heat and interrupt the zircalloy oxidation reactions, the water circuit supplies 42 g/s of water for 255 seconds concurrently with the bundle power reduction. Then, the bundle power is reset to zero once the quenching injection is turned off.

3.3.2 Description of the nodalization

The QUENCH-06 MELCOR input deck has been developed by ENEA in collaboration with Politecnico di Milano and KIT [108]. A general scheme of the CVH and FL MELCOR nodalization is presented in Figure 3.23. The LP of QUENCH-06, the lower molybdenum electrode zone, the active region, and the entire upper plenum, containing the off-gas pipe, have been all included in the MELCOR input deck. The test bundle and the insulation up to the inner cooling jacket made of stainless steel have been radially modelled.

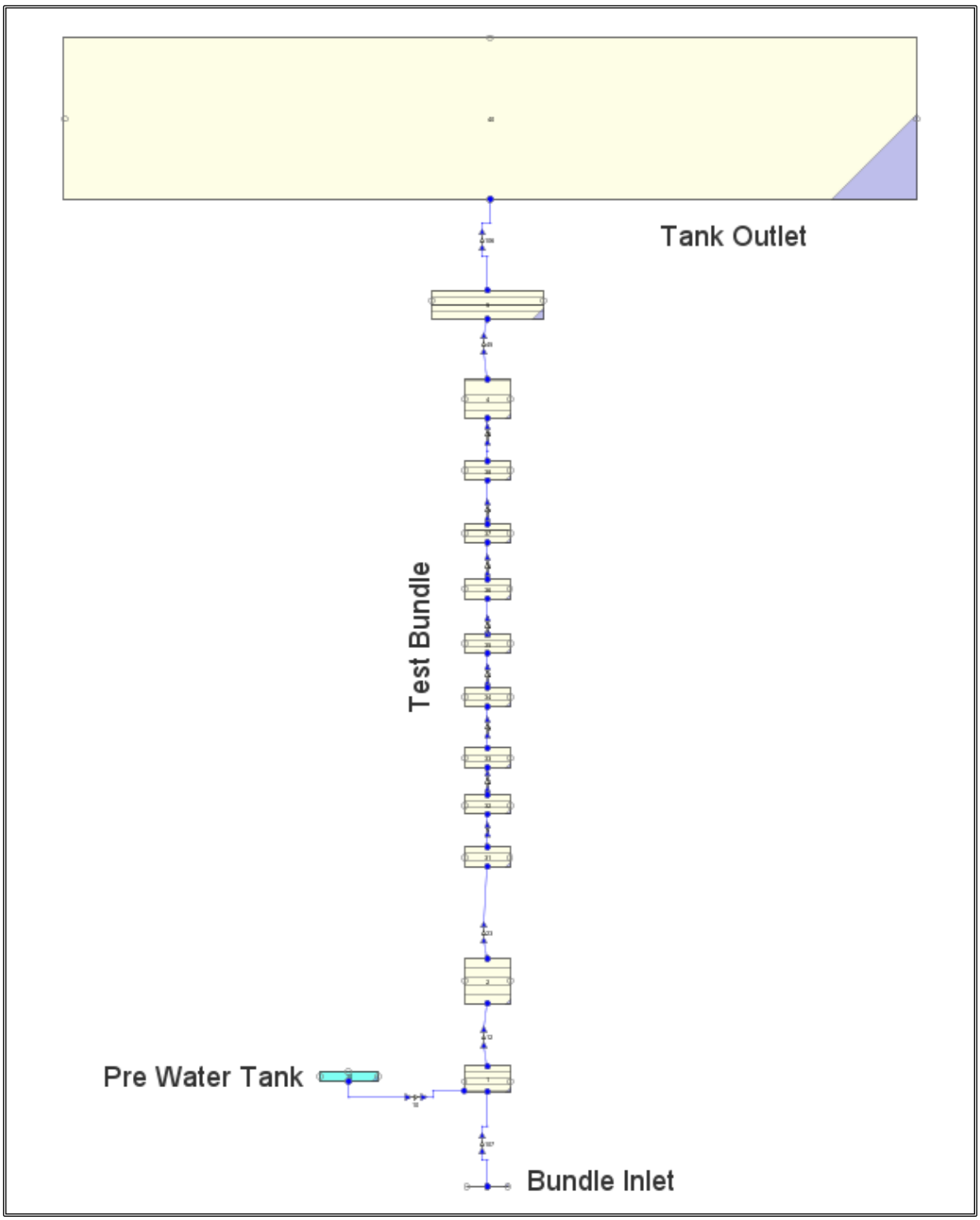

Figure 3.23 SNAP visualization of the QUENCH-06 CVH and FL nodalization.

The QUENCH-06 test section's thermal-hydraulics are modelled using the CVH and FL MELCOR packages. To model the available volume to the fluid in the bundle test and the surrounding regions, 12 active CVs, connected by 12 FL junctions, are used. Additionally, 10 additional CVH CVs have been used to model the FWI system, mass sink (as off-gas pipe), etc. Rod structures, grid spacers and the zircalloy shroud have been modelled with the

MELCOR COR package to simulate oxidation and degradation phenomena. In this regard, the COR nodalization is divided into 42 axial levels and 4 rings. To carry out the analyses (reference case and uncertainty analysis) described in this chapter, the MELCOR 2.2 v18019 has been used.

3.3.3 Description of the reference case

The QUENCH-06 input deck has been developed in view to simulate the three PhWs described in 3.3.1. A sensitivity on zircalloy-steam oxidation correlations has been developed in [107] and [108]. Since the present uncertainty application is focused on investigating the uncertainties of the code on hydrogen cumulative mass generation, the input deck adopting the Cathcart-Pawel [109] correlations for zircalloy temperature between 1100 K and 1800 K and the Volchek-Schanz [110] correlations for zircalloy temperature above 1800 K have been selected considering the outcomes obtained in [108], highlighting a higher accuracy of the results with experimental data concerning the hydrogen cumulative mass produced.

In Figure 3.24 the three PhW are shown with the different boundary conditions in terms of power and mass flow rates and Figure 3.25 presents the hydrogen cumulative mass production predicted by the code and compared with the experimental data.

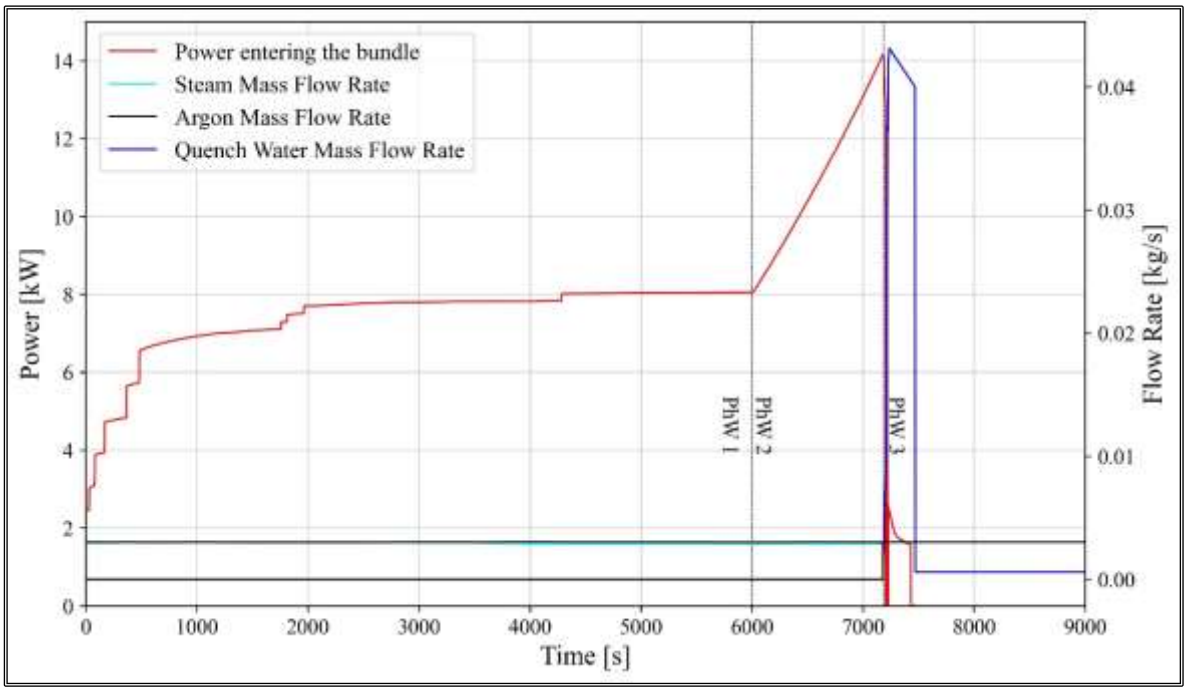

Figure 3.24 Power and mass flow rates during the reference case.

Hydrogen generation begins when the zircalloy structures are exposed to high-temperature steam: from the results of the code, the onset of the zircalloy oxidation reaction is predicted at about 750 seconds after the beginning of the test.

During the beginning of the heat-up phase, at about 6000 s after the start of the test, the bundle power is rapidly ramped up. It determines the increase in rods temperature and then an increase in the hydrogen generation rate. During this phase, the code estimates a slightly more hydrogen cumulative mass than the experimental data.

Then, after the end of the quenching phase, the final hydrogen mass production is about 0.032 kg, showing a slight underestimation compared to the experimental data.

3.3.4 Hypotheses of the uncertainty analysis

As specified above, the present uncertainty application against the QUENCH-06 test has been focused on investigating the code uncertainty on hydrogen production related to zircalloy oxidation reactions. Table 3.3 presents the uncertain input parameters adopted for the present uncertainty application. They are related to boundary conditions (provided by KIT) and kinetics parameters, K1 and K2, of the zircalloy oxidation reaction. These latter characterize the reaction rate for zircalloy oxidation, as follows:

$$K(T) = K1 * e^{-\frac{K2}{T}} \tag{7}$$

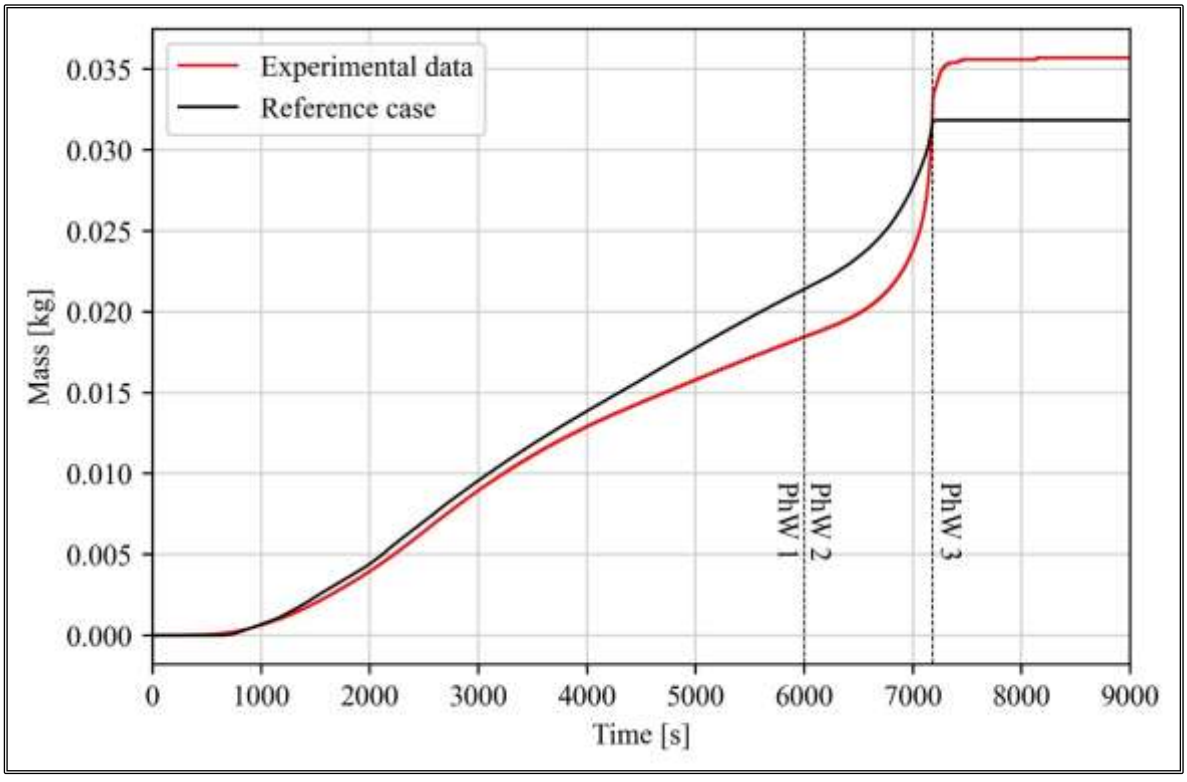

Figure 3.25 Hydrogen cumulative mass production during the reference case [103].

To calculate the minimum runs needed, the approach adopted for the uncertainty application against the Phebus FPT1 and discussed in 3.2 has been chosen. However, a different strategy has been chosen for the management of failed code runs: despite what has been done in 3.2.4, possible failed code runs are replaced with new cases with a new set of sampled uncertain input parameters values, as specified in [77].

3.3.5 Results of the uncertainty analysis

The uncertainty analysis has been developed following the same steps previously discussed concerning the Phebus FPT1 uncertainty application. Then, the mean, median, lower, and upper bound, standard deviation and coefficient of variation have been computed and shown in Table 3.4.

Table 3.3 Uncertain input parameters [109].

Uncertain input parameter	Unit	Distribution type	Mean	Distribution characteristics	
Steam flow rate	[-] (multiplier)	Normal	1	min	0.98
				max	1.02
Argon flow rate	[-] (multiplier)	Normal	1	min	0.98
				max	1.02
Quench flow rate	[-] (multiplier)	Normal	1	min	0.98
				max	1.02
Steam temperature	[-] (multiplier)	Normal	1	min	0.98
				max	1.02
Argon temperature	[-] (multiplier)	Normal	1	min	0.98
				max	1.02
Quench temperature	[-] (multiplier)	Normal	1	min	0.98
				max	1.02
Outlet pressure	[Pa]	Normal	200000	min	180000
				max	220000
K1	[kg^2(Zr)/m^4-s]	Normal	294.2	min	256.54
				max	331.85
K2	[K]	Normal	20100	min	19768.35
				max	20431.65

Table 3.4 Statistical parameters of the FOM.

Statistical parameter	Unit	Value
Mean	[g]	30.51
Median	[g]	30.59
Lower bound	[g]	22.25
Upper bound	[g]	39.19
Standard deviation	[g]	3.46
Coefficient of variation	[-]	0.11

The uncertainty band calculated using the uncertainty analysis is about 17 g. The reference calculated data of 32 g is within the uncertainty band and it is close to the mean and median. Following the methodology, the empirical CDF and the PDF of the FOM, shown in Figure 3.26 and Figure 3.27, have been evaluated and compared with experimental data, reference case, mean, median and upper and lower bound.

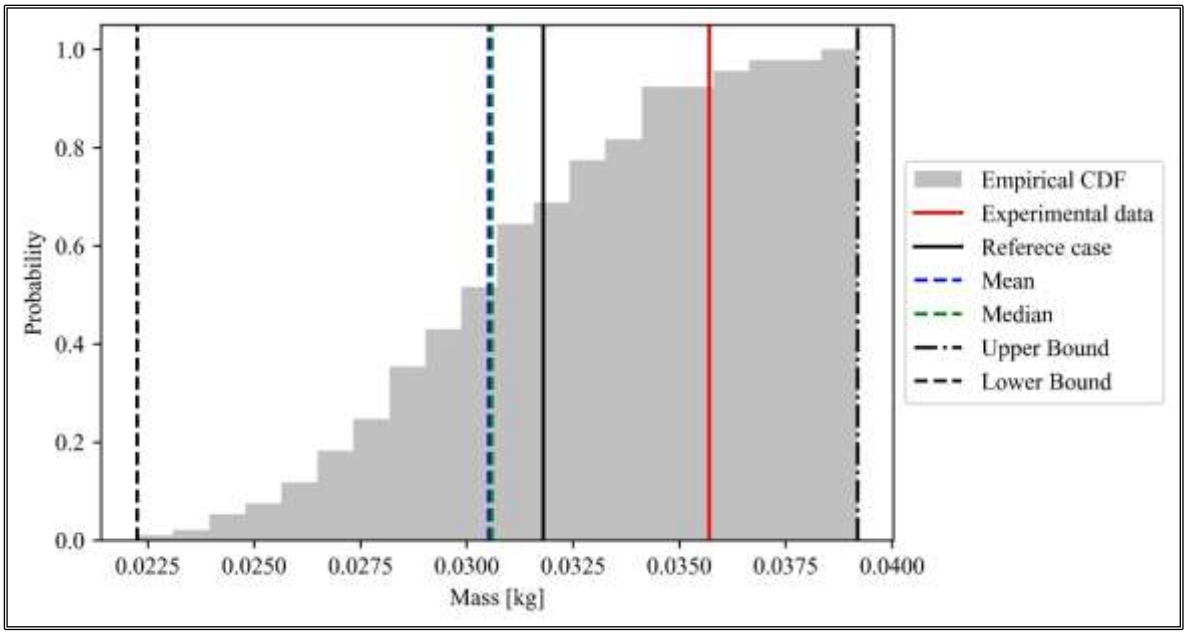

Figure 3.26 Empirical CDF of the FOM [103].

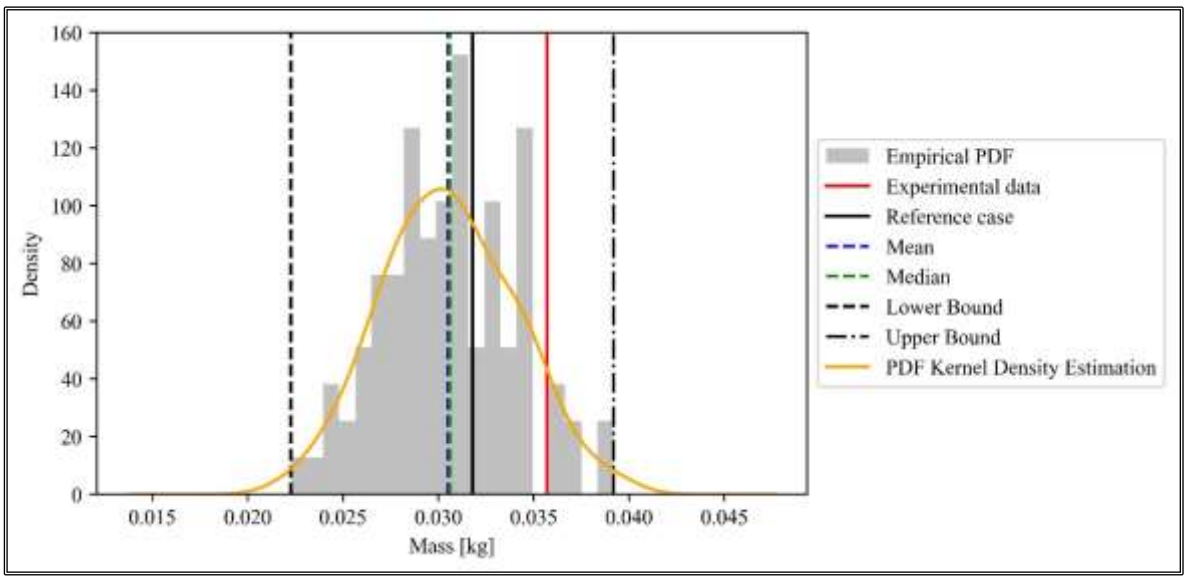

Figure 3.27 Empirical PDF of the FOM [103].

The simple and simple rank correlation coefficients have been calculated employing Person and Spearman's correlation, available in the Pandas Python library. The statistical correlation analysis has been fundamental to investigate and identify which of the uncertain

input parameters, between those related to boundary conditions and those related to the reaction kinetics of zircalloy oxidation, present a statistically relevant correlation to the hydrogen cumulative mass generation, which is a key parameter for the analysis of SA.

As presented in Figure 3.28 and Figure 3.29, the uncertain input parameters related to boundary conditions which present a moderate statistical correlation with the FOM are the steam flow rate (negative correlation), the steam temperature (positive correlation) and the outlet pressure (negative correlation). The other parameters related to the boundary conditions of the experiment present a low statistical correlation.

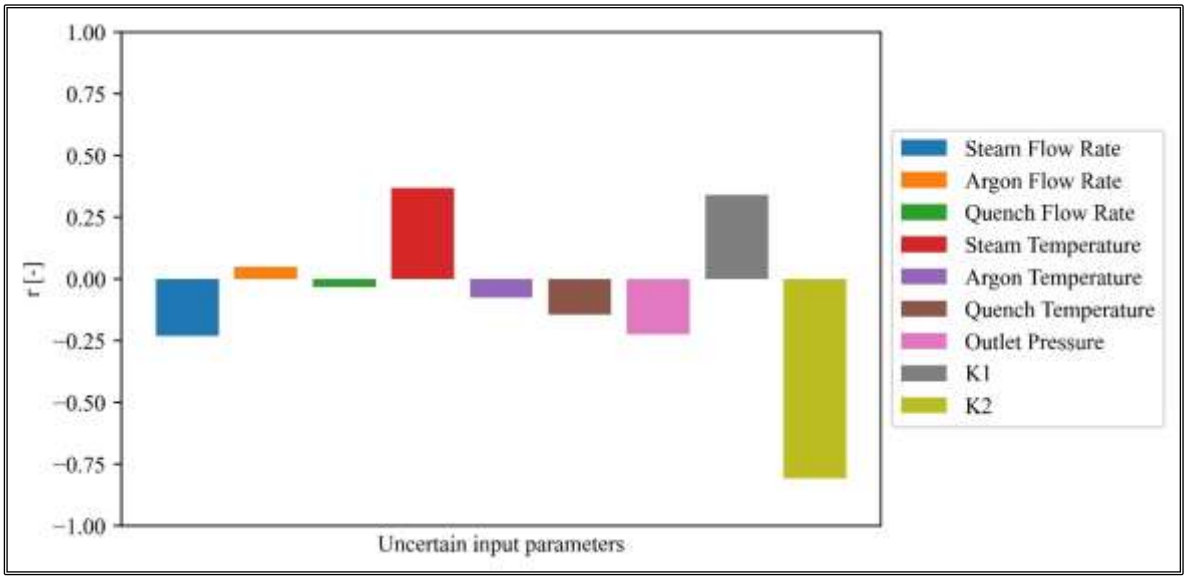

Figure 3.28 Simple correlation coefficient.

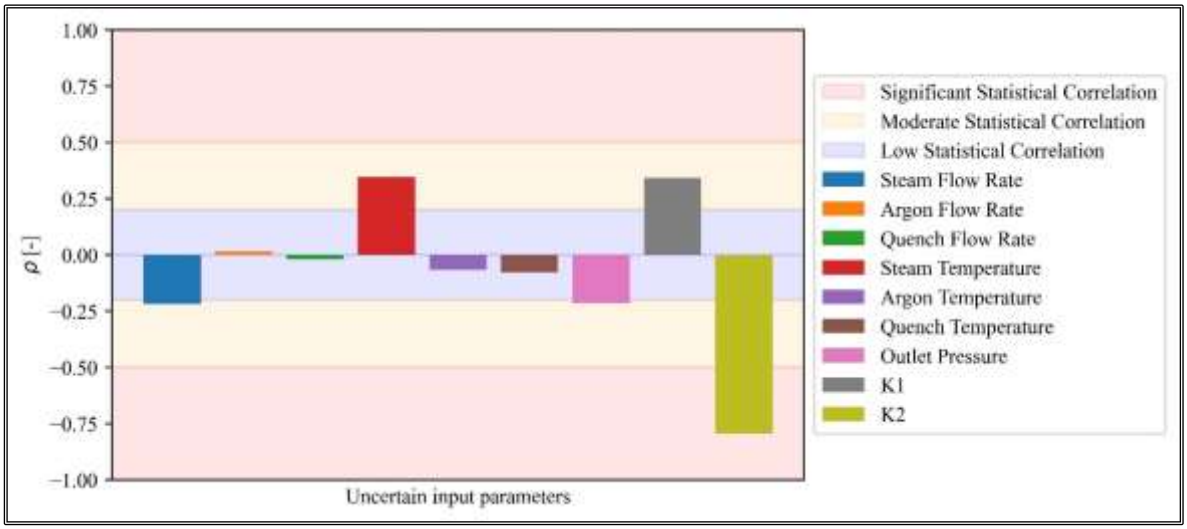

Figure 3.29 Simple rank correlation coefficient.

On the other hand, among the parameters related to the oxidation kinetics of zircalloy, the K1 parameter has a moderate statistical correlation (positive correlation) while the K2 parameter has a significant statistical correlation (negative correlation).

From Figure 3.30 to Figure 3.38 the scatter plots representing the FOM values for each sampled uncertain input parameter are shown as well as the trend curve obtained by linear regression technique.

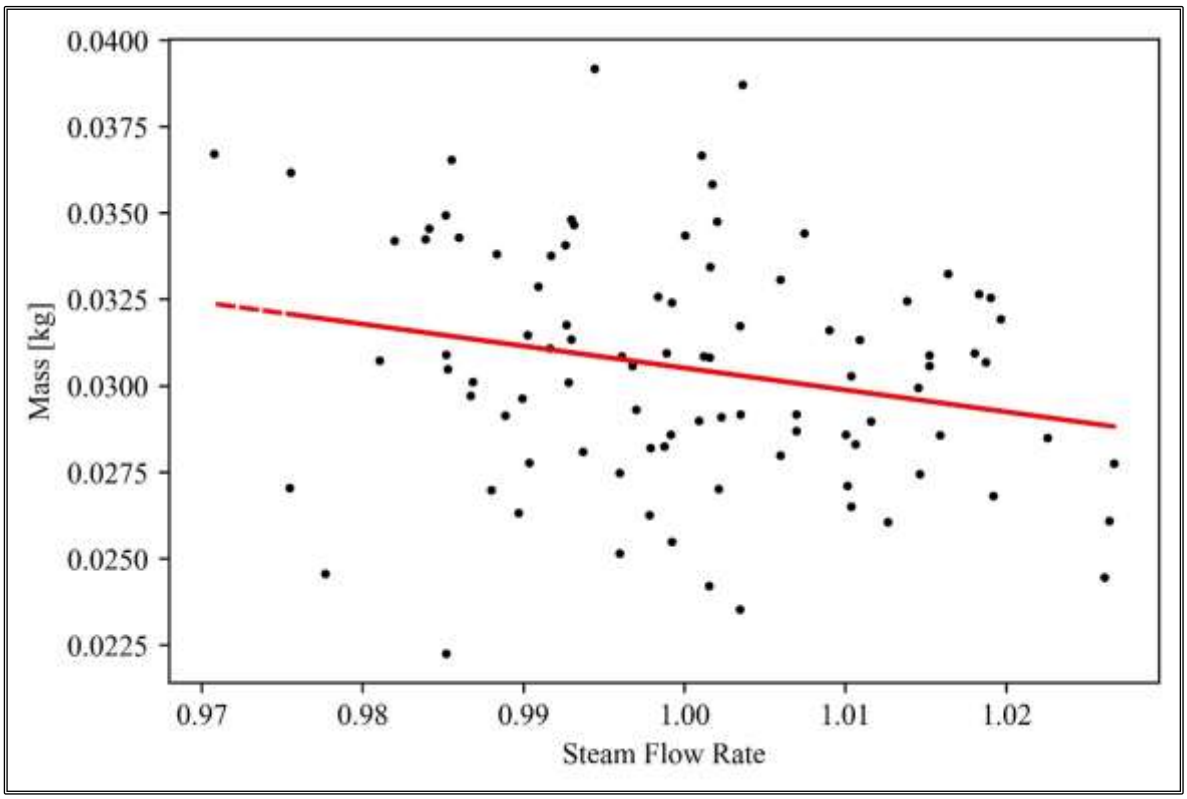

Figure 3.30 Scatter plot of FOM and steam flow rate values.

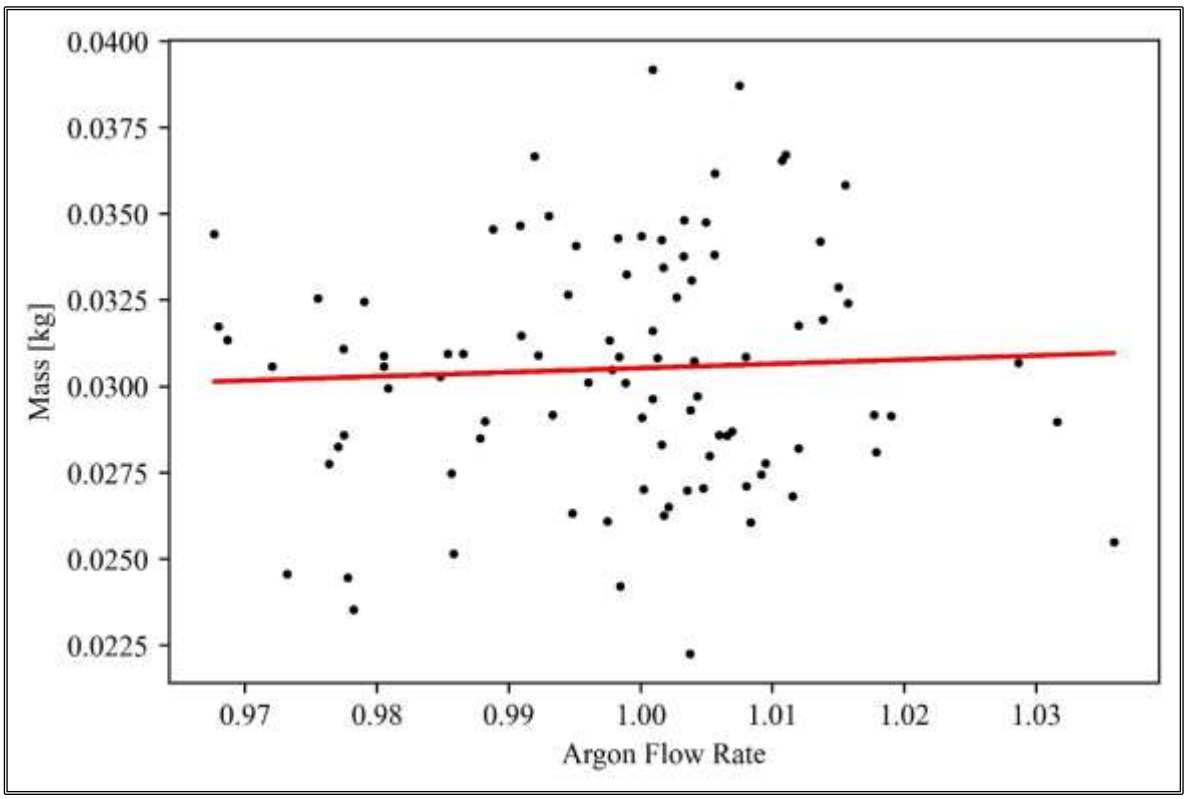

Figure 3.31 Scatter plot of FOM and argon flow rate values.

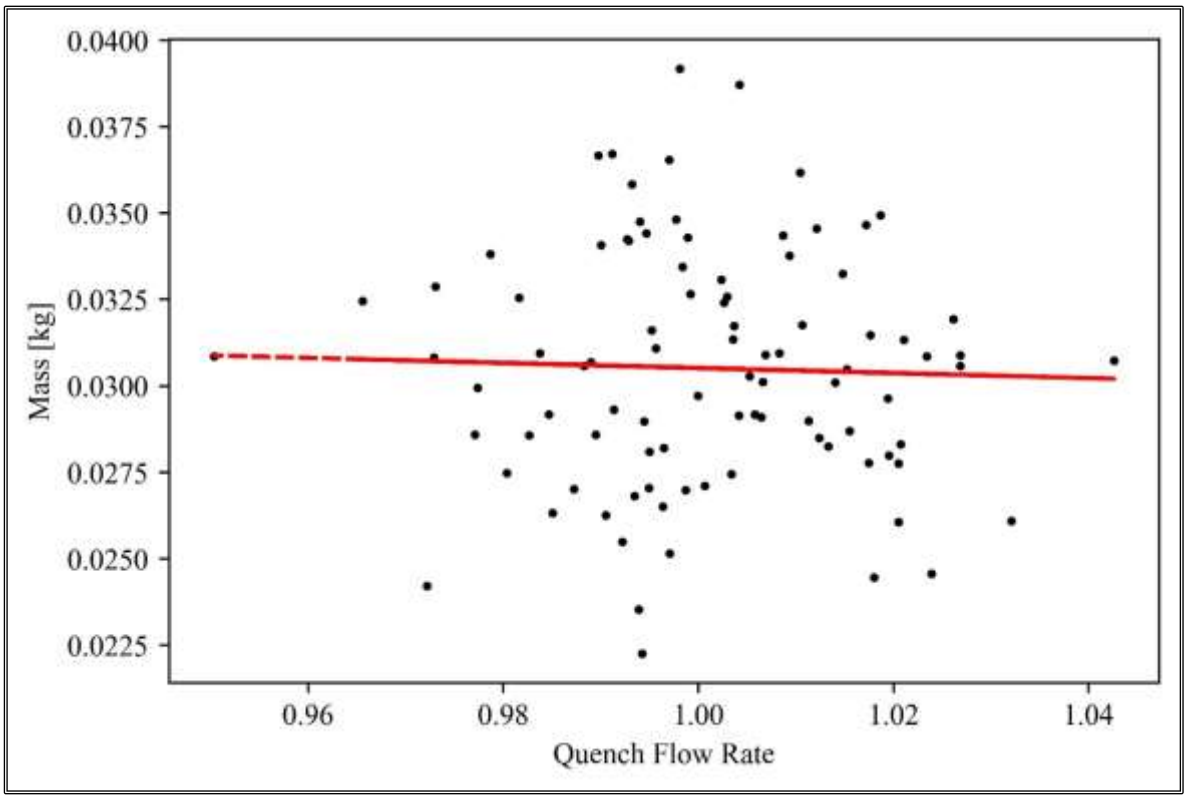

Figure 3.32 Scatter plot of FOM and quench flow rate values.

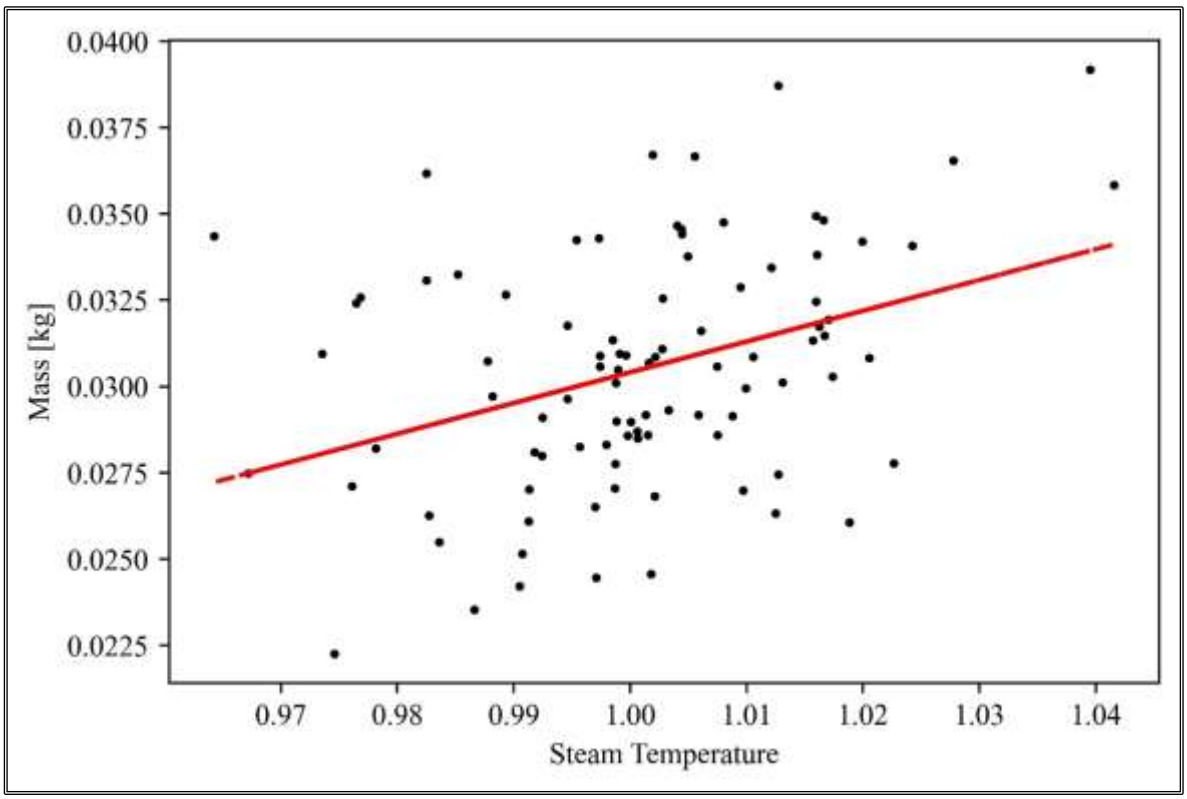

Figure 3.33 Scatter plot of FOM and steam temperature values.

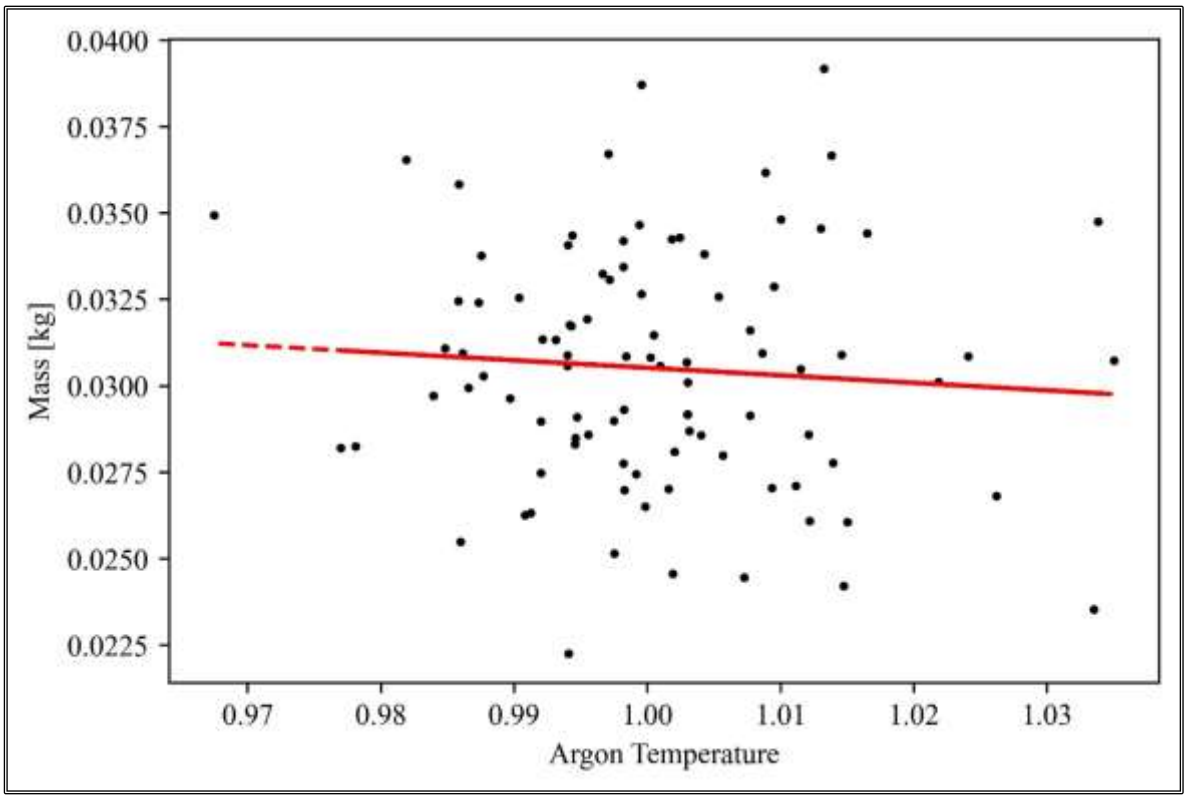

Figure 3.34 Scatter plot of FOM and argon temperature values.

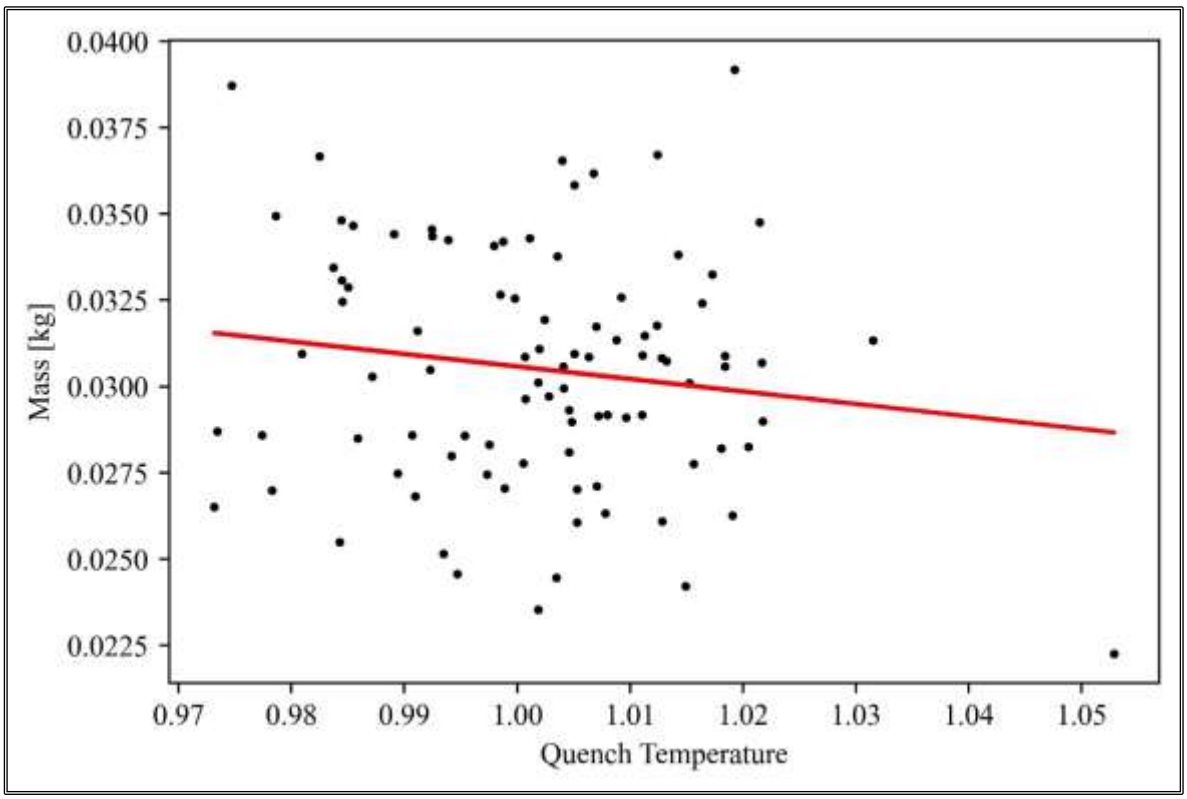

Figure 3.35 Scatter plot of FOM and quench temperature values.

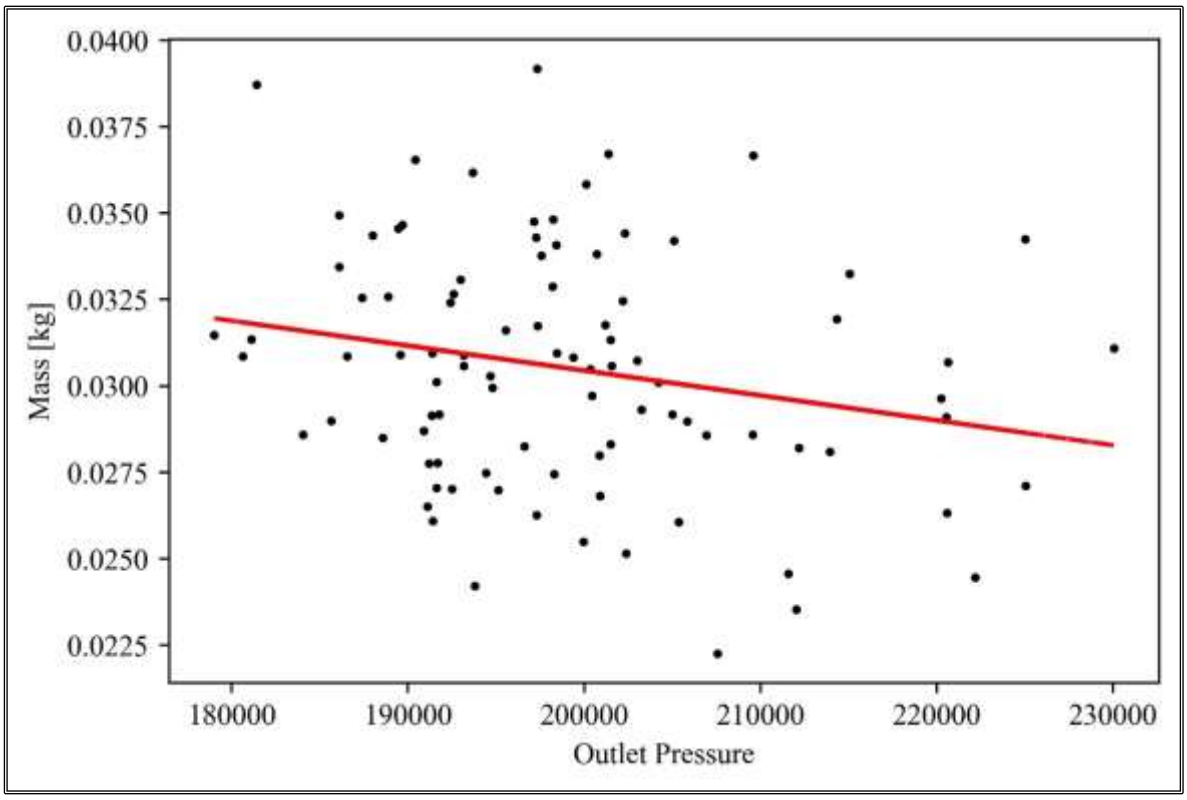

Figure 3.36 Scatter plot of FOM and outlet pressure values.

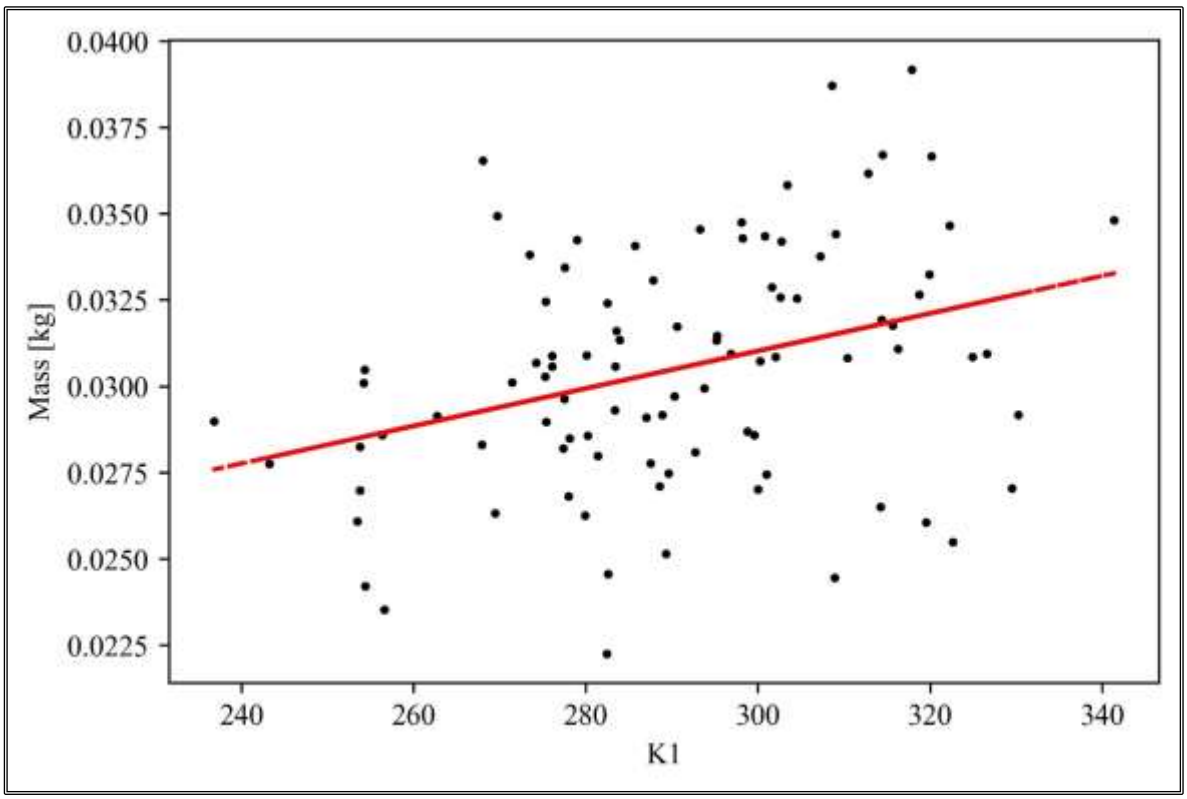

Figure 3.37 Scatter plot of FOM and K1 values.

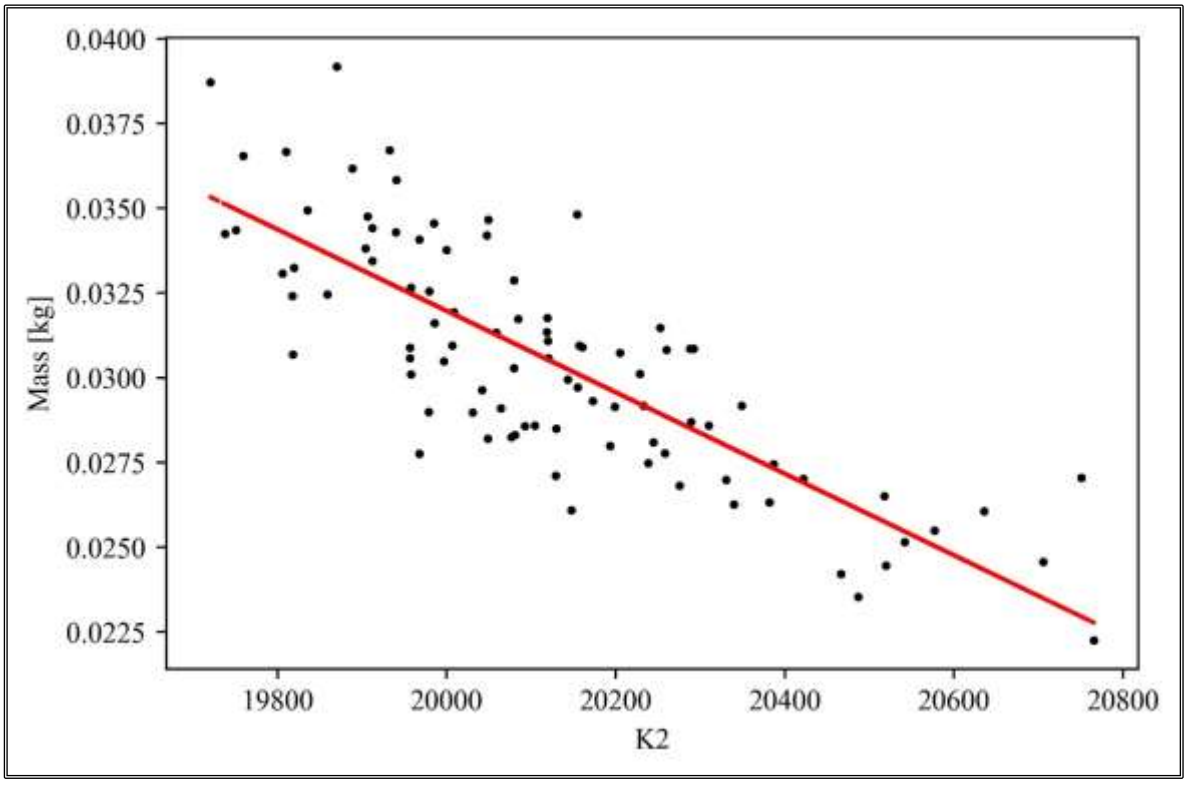

Figure 3.38 Scatter plot of FOM and K2 values.

To study the uncertainties of code on hydrogen production along the three PhWs defined previously, the uncertainty band of the hydrogen cumulative mass production has been evaluated at each time step, as well as the other statistical parameters, as shown in Figure 3.39. Both experimental data and reference case fall into the uncertainty band during all the simulated phases of the test. The uncertainty band increases along the transient, reaching a value of about 0.0169 kg after the beginning of the quenching phase. This behaviour can be evaluated by considering the trend of the standard deviation at each time step, shown in Figure 3.40. The standard deviation increases during the test up to 0.0035 kg. Then, the coefficient of variation decreases fast to a value next to 0.10. A qualitative good agreement is observed by comparing the mean and median values with the experimental data during the pre-oxidation phase and the heat-up phase. To investigate the statistical correlation between uncertain input parameters and the hydrogen cumulative mass during the PhWs, the statistical correlation coefficients have been calculated at each time step. The simple and simple rank correlation coefficients are presented in Figure 3.41 and Figure 3.42. As can be analysed from these figures, the outlet pressure and the K2 parameters present a significant statistical correlation (negative correlation) during the pre-oxidation phase. The K2 parameter presents a significant statistical correlation also for the other phases of the test (negative correlation). The steam temperature and the argon temperature present a moderate statistical correlation (positive correlation) during all the PhWs as well as the steam flow rate (negative correlation).

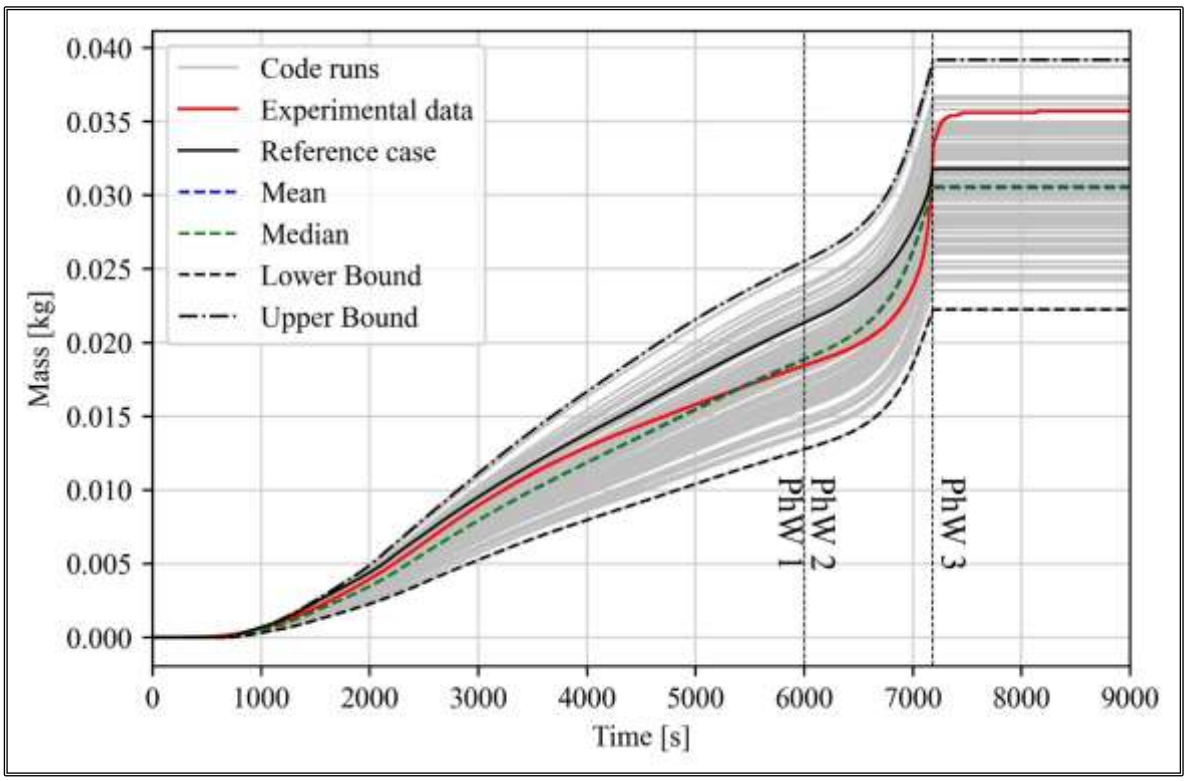

Figure 3.39 Hydrogen cumulative mass uncertainty band [103].

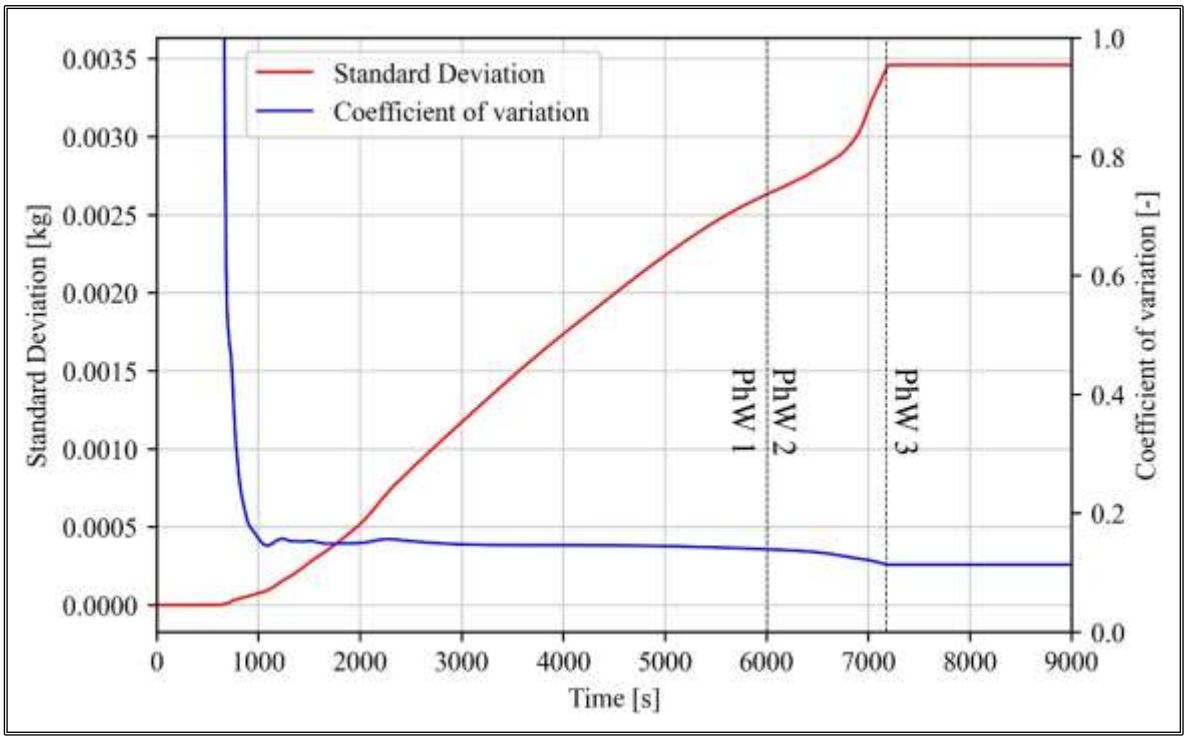

Figure 3.40 Standard deviation and coefficient of variation.

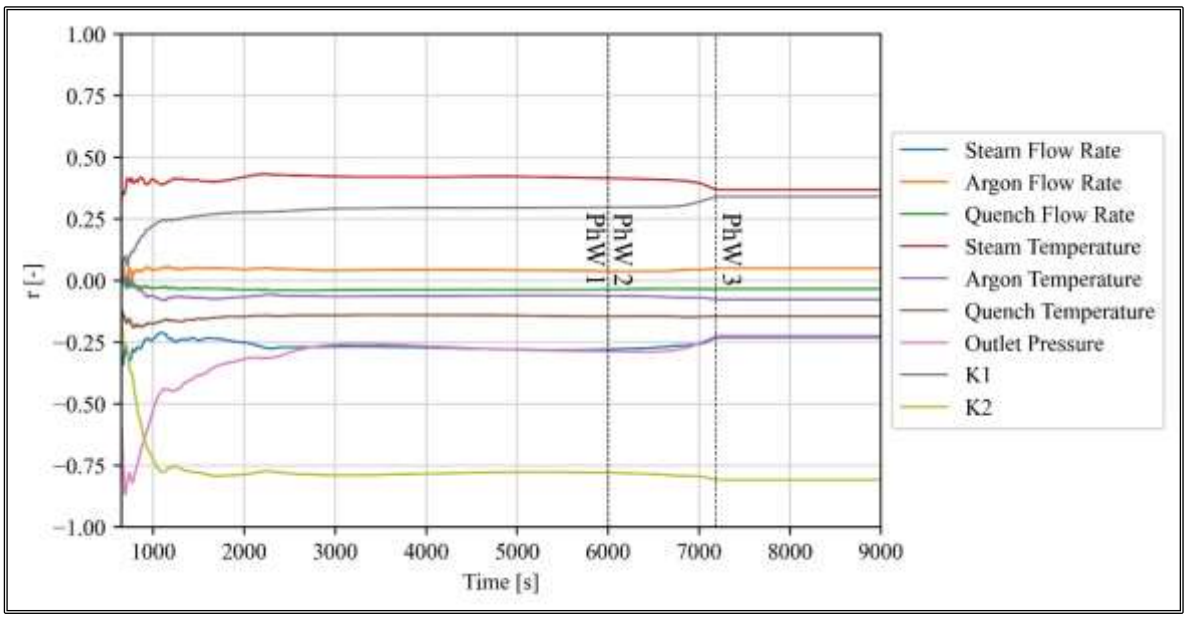

Figure 3.41 Simple correlation coefficient along the simulated phases.

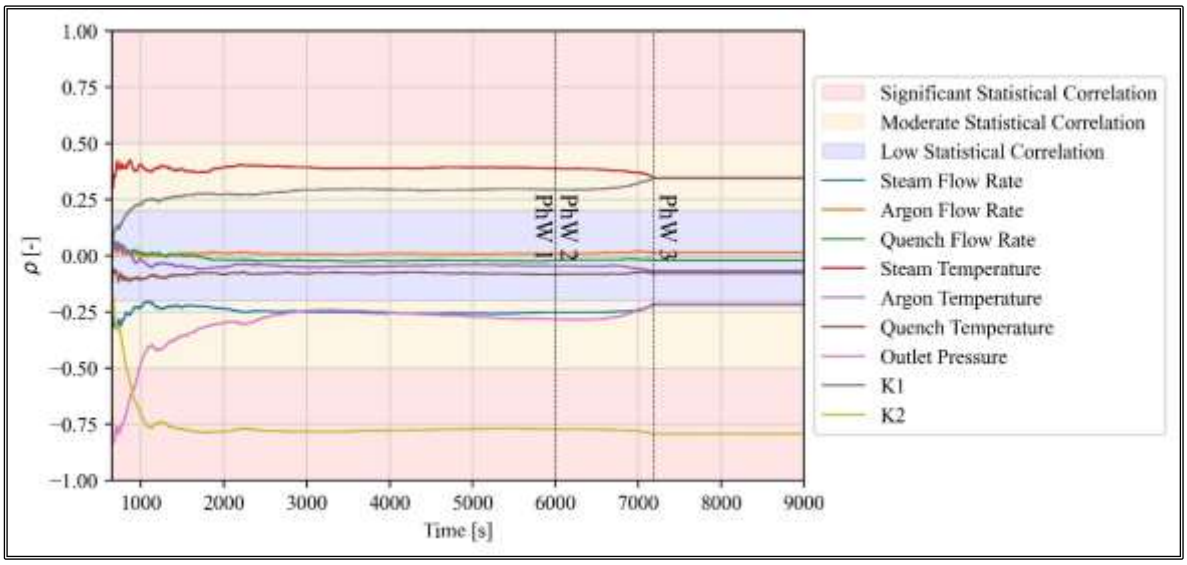

Figure 3.42 Simple rank correlation coefficient along the simulated phases.

4 APPLICATION OF THE UNCERTAINTY METHODOLOGY TO A SEVERE ACCIDENT SEQUENCE IN A GENERIC PWR-900

4.1 Introduction

In Chapter 3, the uncertainty methodology has been tested against experimental data. Furthermore, the computational computing environments have been tested and developed to carry out uncertainty quantification analyses with the MELCOR code.

The present chapter, gathering the key outcomes in terms of applying the methodology and developing the computational environment, focuses on the application of the uncertainty methodology to a SA accidental transient in a generic PWR characterized by an electric output of 900 MWe. The transient evaluated is a SBO with the postulated unavailability of all safety systems. After describing the transient sequence and the main hypotheses of the case study, the MELCOR input deck and the reference case are presented as well as the uncertainty analysis results. The main goal of this uncertainty application, conducted using the coupling between MELCOR and DAKOTA in a Python environment/architecture described in 2.4.1.3, is to investigate the uncertainty of the code on the aerosol suspended mass in the containment in a plant scale, considering the aerosol miscellaneous constant, previously described in 3.2.4, as uncertain input parameters. The analysis has been conducted in the framework of the MUSA project [111].

4.2 Description of an unmitigated Station Black-Out

The transient examined in this chapter is a SBO in a generic PWR characterized by three primary loops (as presented in Figure 4.1) and by an electric output of 900 MWe. The loss of off-site alternating current power in conjunction with the assumed failure of every diesel emergency generator constitutes the PIE. The Reactor Coolant Pump (RCP) seal injection, the level control of the Pressurizer (PRZ), the motor-driven auxiliary feedwater system, and the high and low-pressure injection systems are considered not available.

At the SOT, the reactor SCRAM and SGs' isolation (as a result of the closure of primary feedwater and steam valves) take place. SGs become the only heat sink available for the PCS coolant along the first part of the transient. In this regard, the heat loss to the containment is not significant. When the pressure set-point is achieved, the secondary side relief valves open as a result of the SCS pressure rising due to the heat transmitted by the PCS. The opening of these valves causes oscillations of the secondary pressure. On the PCS side, a

single-phase natural circulation is sustained by the pump' coast-down. During the SGs relief valves cycling phase, a PCS decrease takes place with a consequence steady-state condition till the SCS water inventory can remove core decay heat.

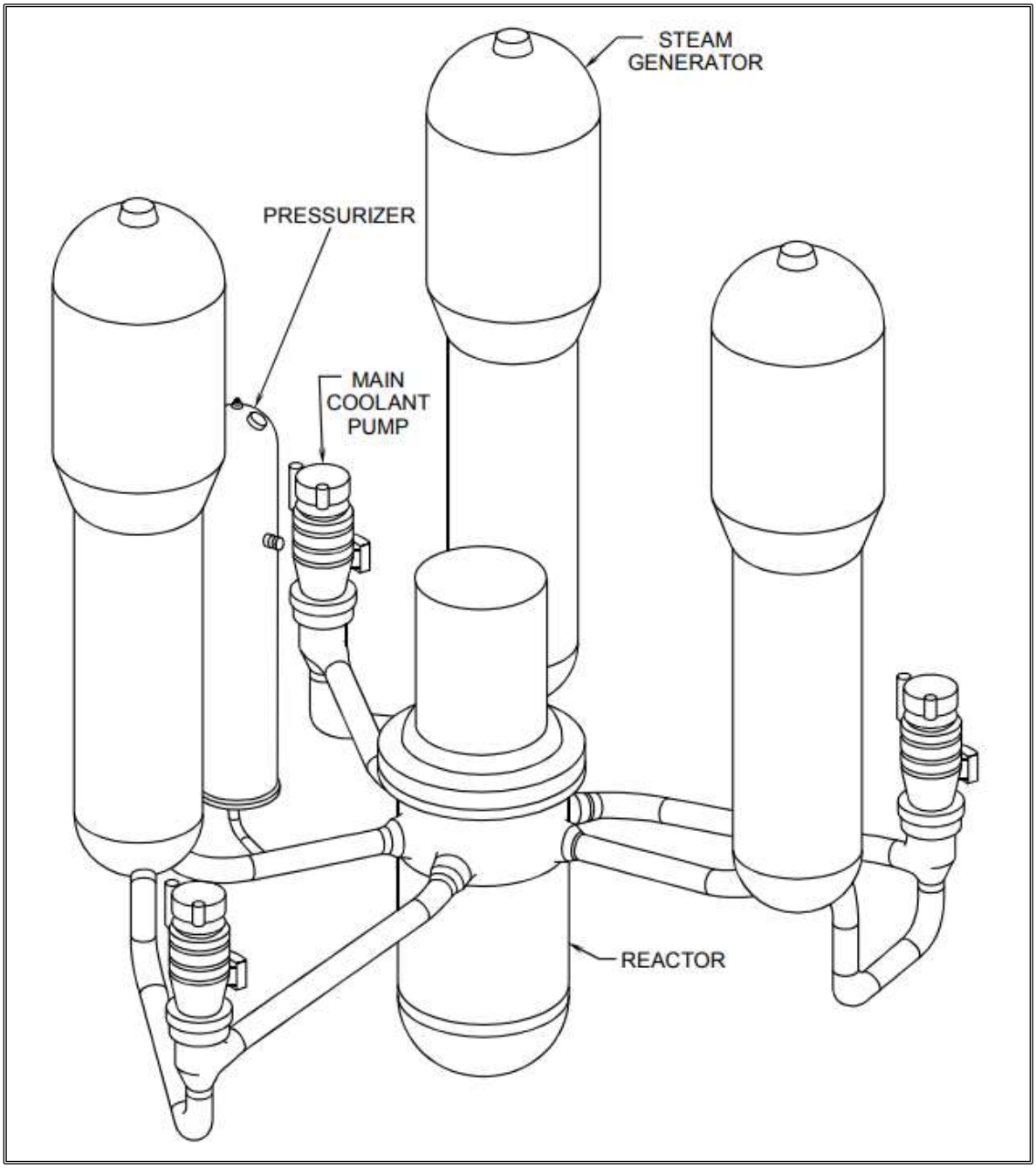

Figure 4.1 General view of the PCS of a generic PWR-900 [112].

As a result of the decrease in water inventory in SGs, the capacity of the SCS to absorb the power from the PCS decreases. The PCS pressure increase is limited by the opening of the Safety Valves of Pressure Compensator (SEBIM) valves when the coolant temperature at the core outlet reaches a fixed set point. The opening of these valves causes the loss of coolant from PCS.

The TAF starts to uncover, causing the fuel heat-up and the onset of the oxidation reactions between the zircalloy and the steam. Considering that the oxidation reactions between zircalloy and steam are exothermic, the heat generated from them is added to the core decay heat, determining the production of hot steam in the core. The fuel temperature increases as a result of the decrease in heat transfer between coolant and fuel rods. The oxidation reactions of zircalloy due to high temperatures and contact with steam, as discussed in 1.3.2, lead to the production of hydrogen.

Along the sequence, the core loses its initial geometry and starts to relocate into the LP. The slumping causes the evaporation of the amount of liquid in the LP, causing a PCS pressure spike. The thermo-mechanical load of the corium to the LH causes its rupture, initiating the ex-vessel phase of the SA sequence.

For the development of the reference case, additional hypotheses have been postulated as the independent failure of the accumulators, the non-occurrence of thermal degradation phenomena induced by primary structures (e.g. the possible rupture of SGs tubes has not been considered) and the independent failure of the turbine-driven auxiliary feedwater pump (no auxiliary feedwater). In addition, a postulated leakage of 0.1%Vol day at primary containment vessel design pressure has been considered.

4.3 Description of the nodalization

Developed based on the information reported in [113] [114] and from the ASTEC input decks provided by IRSN within the framework of the CESAM project [115], the MELCOR nodalization of the generic PWR-900 allows the investigation of thermal-hydraulic and core degradation phenomena occurring in such facility. The model has been used and updated within the framework of international projects, such as the FASTNET [116], IVMR [117] and MUSA projects [72].

Furthermore, the PWR-900 MELCOR nodalization has been adopted to develop multiple SA research activities, reported in [118] [119] [120] [121], as well as code-to-code benchmarks, detailed described in [60] [122] [123].

The nodalization has been developed using SNAP, separately modelling the three loops. Each one is composed of the HL, one SG (primary and secondary side), the loop seal, one pump, and the CL. Only one CV has been used to model the loop seal. Two equivalent hydraulic regions have been used to model the U-tubes: one region corresponds to the ascending side and the other to the descending side. Separate CVs have been created for the SG inlet and outlet channels to and from U-Tubes CVs. An HS connects the riser to the

matching secondary side to the ascending side of the U-Tube. As a result, an extra HS connects the U-Tubes' descending side to the matching secondary side's riser. The three regions of the SG's secondary side (riser, downcomer and cavity) are modelled with three different volumes. In Figure 4.2 the SNAP view of the CVH and FL nodalization of one loop is shown.

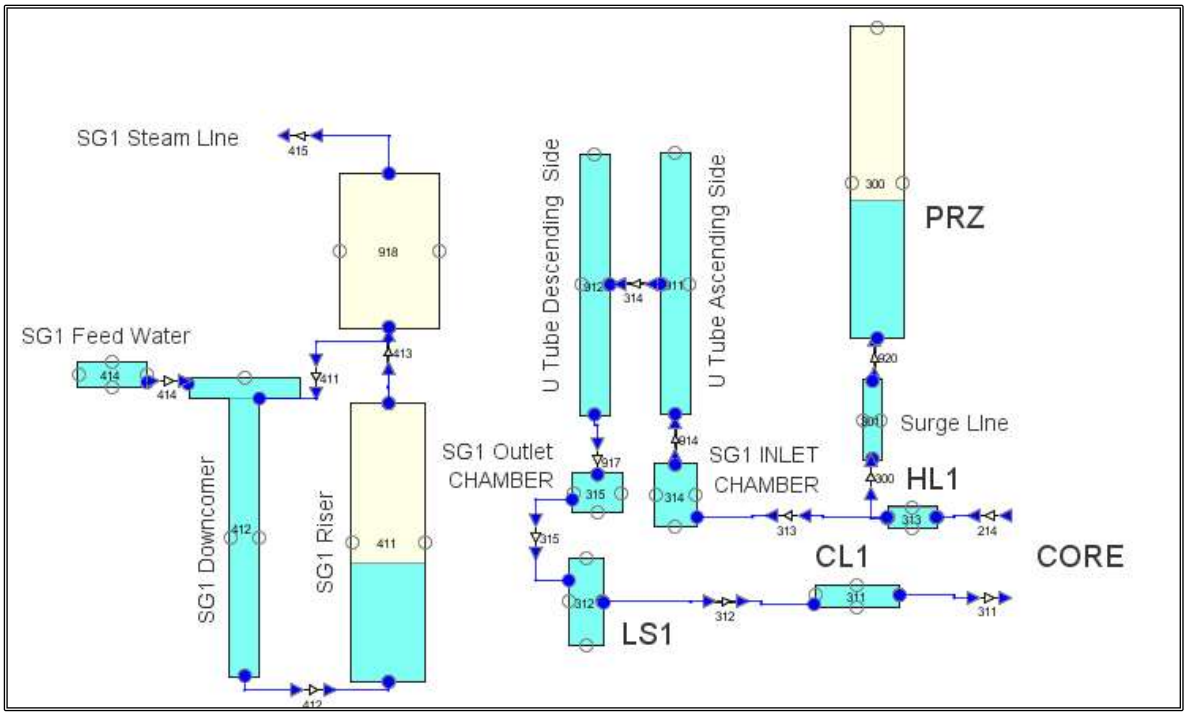

Figure 4.2 SNAP visualization of one loop of the generic PWR-900 CVH and FL nodalization.

The PRZ has been modelled with only one equivalent CV and the surge line with another CV. The RPV has been modelled with different CVs for the thermal-hydraulic simulation of its different regions: the LP, the reactor core, the core by-pass, UP and Downcomer (DC). A general SNAP view of the CVH and FL nodalization of the RCS is shown in Figure 4.3.

The core has been modelled by a single hydraulic CV, coupled with the correspondent COR nodalization. This latter consists of 17 axial levels and 6 radial rings, as shown in Figure 4.4. More in detail, the core region has been modelled with 5 radial rings. Ten axial levels have been used to model the core and seven axial levels for the LP. All the masses in terms of steel, zircalloy, poison and fuel have been considered. The hemisphere-type LH consists of 10 nodes and 13 rings. Activated models include the in-vessel falling debris quench model, the LH failure model, the silver release model, and the candling heat transfer model. The containment has been modelled with one equivalent CV coupled with several HSs. A different CV, coupled with the CAV package, models the RC. In Figure 4.5 a general

SNAP view of the CVH and FL nodalization is presented. To carry out the analyses (reference case and uncertainty analysis) described in this chapter, the MELCOR 2.2 v18019 has been used.

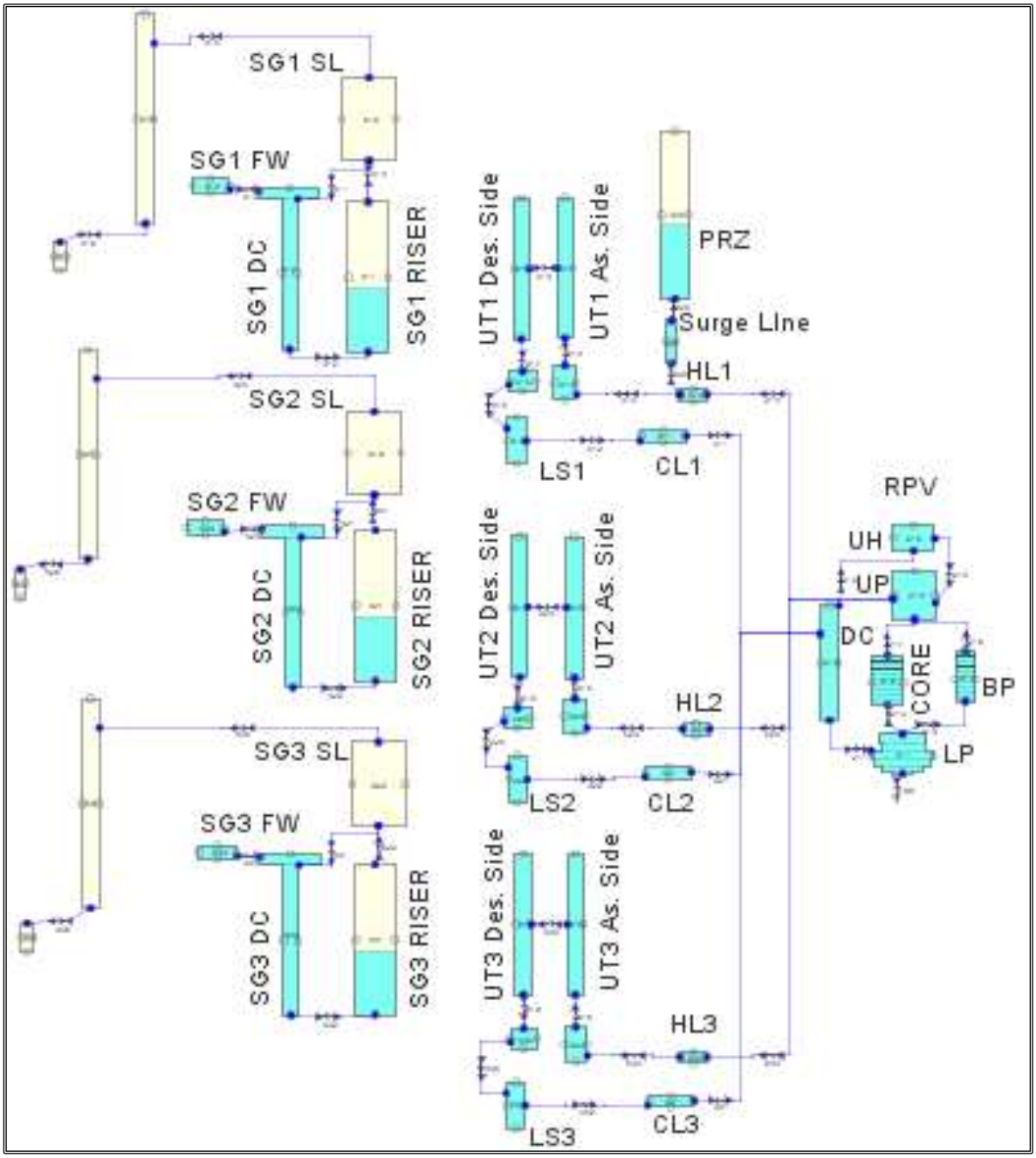

Figure 4.3 SNAP visualization of the RCS of the generic PWR-900 CVH and FL nodalization.

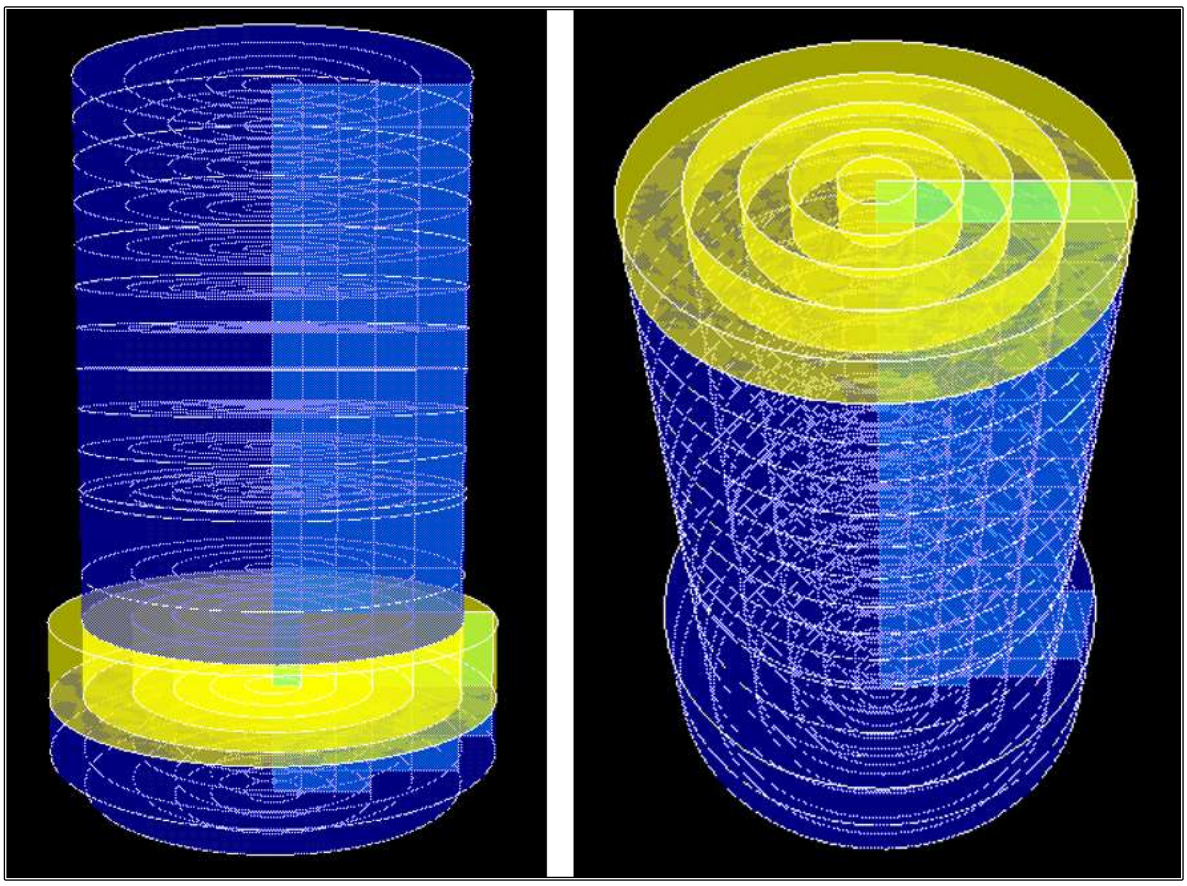

Figure 4.4 SNAP visualization of the reactor core and LP of the generic PWR-900 COR nodalization.

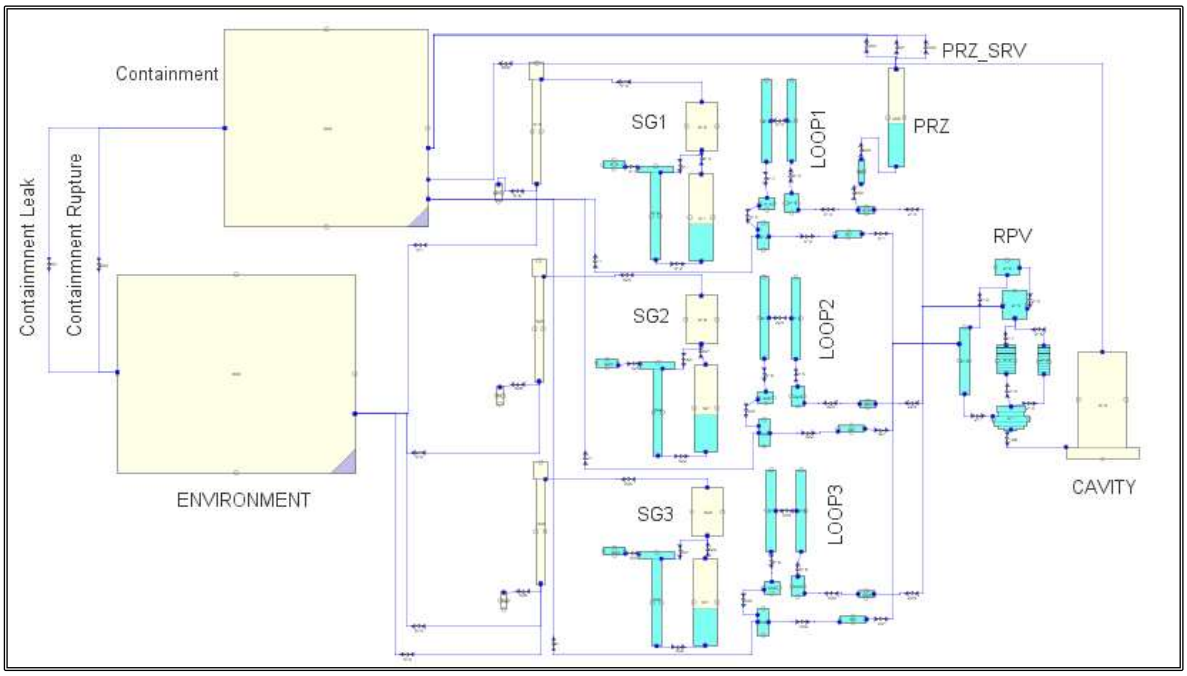

Figure 4.5 SNAP visualization of the generic PWR-900 CVH and FL nodalization.

4.4 Steady-state analysis

Previously to the transient analysis, a steady-state study was carried out by comparing the main thermal-hydraulic parameters with the results obtained with the ASTEC input deck. The comparison, presented in Table 4.1, shows a discrepancy of less than 2% between the codes.

Table 4.1 Main thermal-hydraulic parameters during the steady-state.

Parameter	Unit	ASTEC	MELCOR	Discrepancy [%][4]
PRZ pressure	[Pa]	15.516E6	15.478E6	0.24
PRZ level	[%]	50	50	0.00
CL mass flow rate	[kg/s]	4736	4736	0.00
Core mass flow rate	[kg/s]	13928	13926	0.01
Upper head mass flow rate	[kg/s]	275	275	0.00
Primary mass	[kg]	185000	185014	0.01
Inlet core temperature	[K]	560	560	0.00
Outlet core temperature	[K]	594.5	594.6	0.02
Separator pressure	[Pa]	5.8E6	5.8E6	0.00
SG water mass	[kg]	44385	44385	0.00
SG steam mass	[kg]	2725	2677	1.76
SG feedwater flow rate	[kg/s]	512	512	0.00
SG recirculation ratio	[-]	4.15	4.15	0.00

4.5 Description of the reference case

Following the description of the transient in 4.2 and the definition of the phases of a SA (see 1.3.2.2), the sequence can be divided into five PhWs [60]:

I. **Thermal-hydraulic phase** - PhW 1: it spans from the SOT to core heat-up, and contains the SCRAM, pumps-coast down, the single-phase natural circulation inside the PCS, the cycling of SGs safety valves, the beginning of the two-phase natural circulation inside the PCS and the start of SEBIM cycling.

II. **Core uncover and heat-up phase** - PhW 2: it evolves from the fuel heat-up to core temperature up to 1500 K and involves the TAF uncover and the onset of zircalloy oxidation reactions.

III. **Oxidation, melting, relocation and slumping phase** - PhW 3: it spans from the core fuel at 1500 K to core slumping and it is characterized by the SEBIM suck opening and the Bottom of Active Fuel (BAF) uncover, the total melting of the

[4] In Table 4.1 the discrepancy has been calculated as the percentage difference between the parameters evaluated by the codes.

fuel, the runaway of the zircalloy oxidation reactions and the massive production of hydrogen.

IV. **LH heating and RPV failure phase** - PhW 4: it starts from the slumping into the LP and ends with LH failure. It involves the heating of the molten core into the LP and the formation of molten material pools.

V. **Ex-Vessel phase** - PhW 5: it characterizes the transient from the failure of LH onwards and involves the transport of FPs to the containment and relocation of the molten core into the RC.

As described in 4.2, the loss of offsite alternating current power causes the SOT. The core power is switched from fission to decay power due to the SCRAM. The SCS acts as the only heat sink for the PCS. For this reason, the SGs pressure begins to increase as shown in Figure 4.6. The SCS pressure is limited by the relief valves which are turned on when the SCS pressure reaches the set point, predicted by the code at about 48 seconds after the SOT. It determines the beginning of the cycling phase of the safety valves of the SGs. During this phase, after the initial drop, the code correctly predicts the quasi-steady-state period of about 3000 s.

When the SCS water inventory decreases, its heat removal capability decreases as well leading to an increase of PCS pressure predicted by the code at about 3700 s after the SOT, as shown in Figure 4.6. The pressure increase of the PCS is stopped by the SEBIM valves' opening, occurring at about 4000 s after the SOT. The cycling phase of the SEBIM valves causes a decrease in the PCS coolant inventory, as shown in Figure 4.7. The loss of primary coolant determines the uncovering of the TAF, occurring at about 6000 s after the SOT, as shown in Figure 4.8.

Due to the core uncovering, the reactor core starts to heat-up. The cladding temperature increases considerably at about 7500 s after the SOT, as shown in Figure 4.9 where the maximum cladding temperature is presented. At about 8600 s the cladding temperature reaches the onset value for zircalloy reaction oxidations. Then, the hydrogen generation starts as presented in Figure 4.10. As a consequence of zircalloy oxidation, the code correctly predicts the decrease of zircalloy mass in the core and the ZrO_2 mass increase, as shown in Figure 4.11. The runaway of zircalloy oxidation occurs at about 9150 s and causes an increase in the cladding temperature and hydrogen generation rate. Considering all hydrogen production mechanisms, the code predicts a total of 350 kg of hydrogen in the reference case.

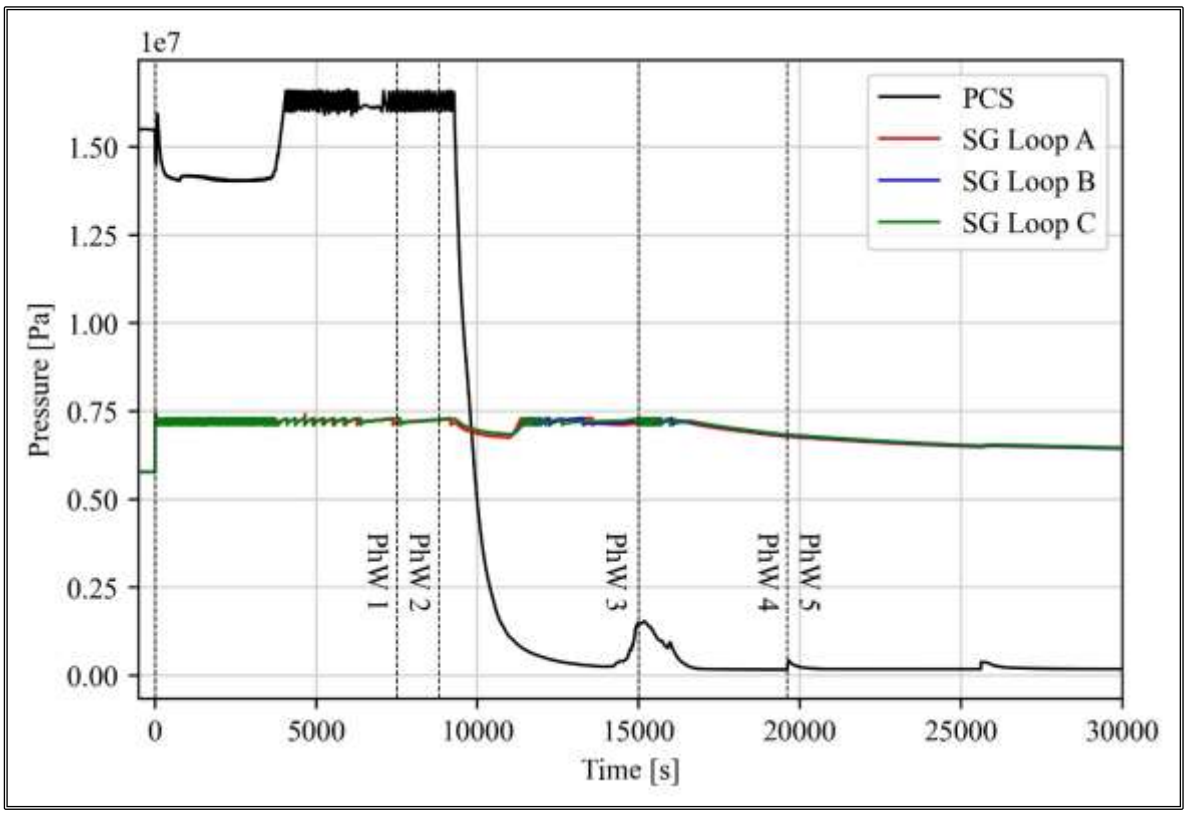

Figure 4.6 PCS and SCS pressure during the reference case.

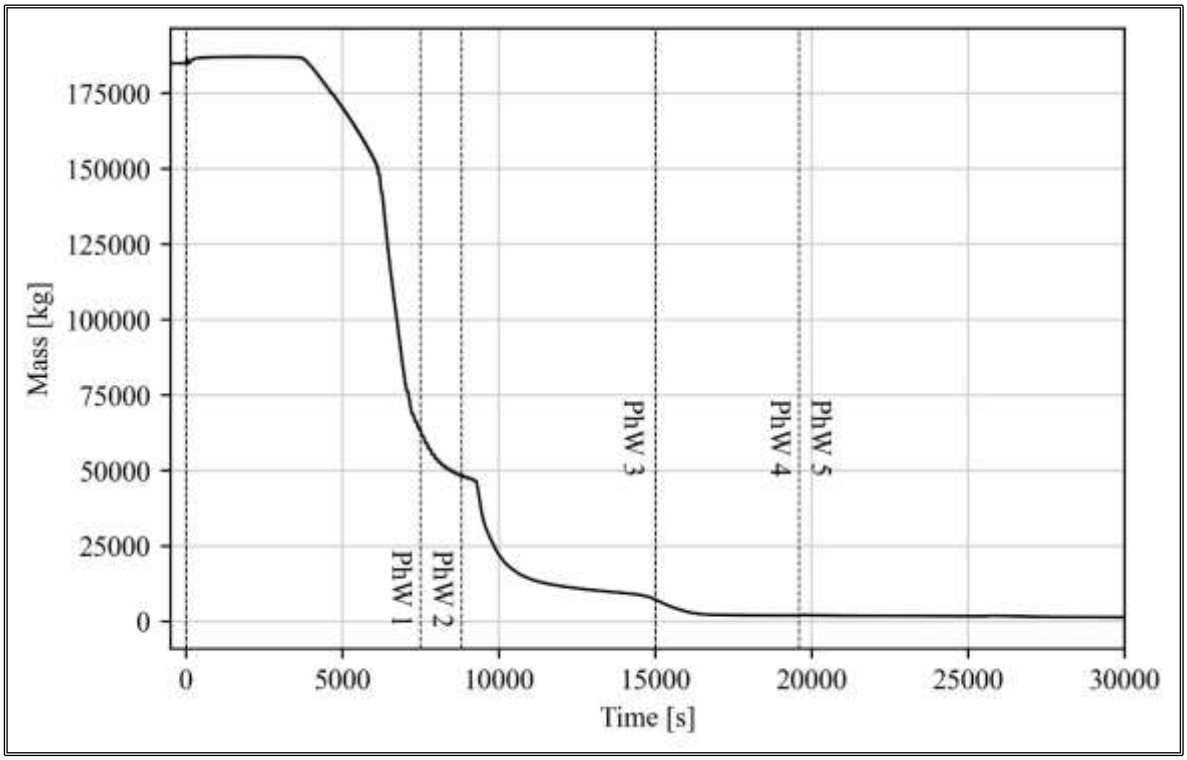

Figure 4.7 PCS water inventory during the reference case.

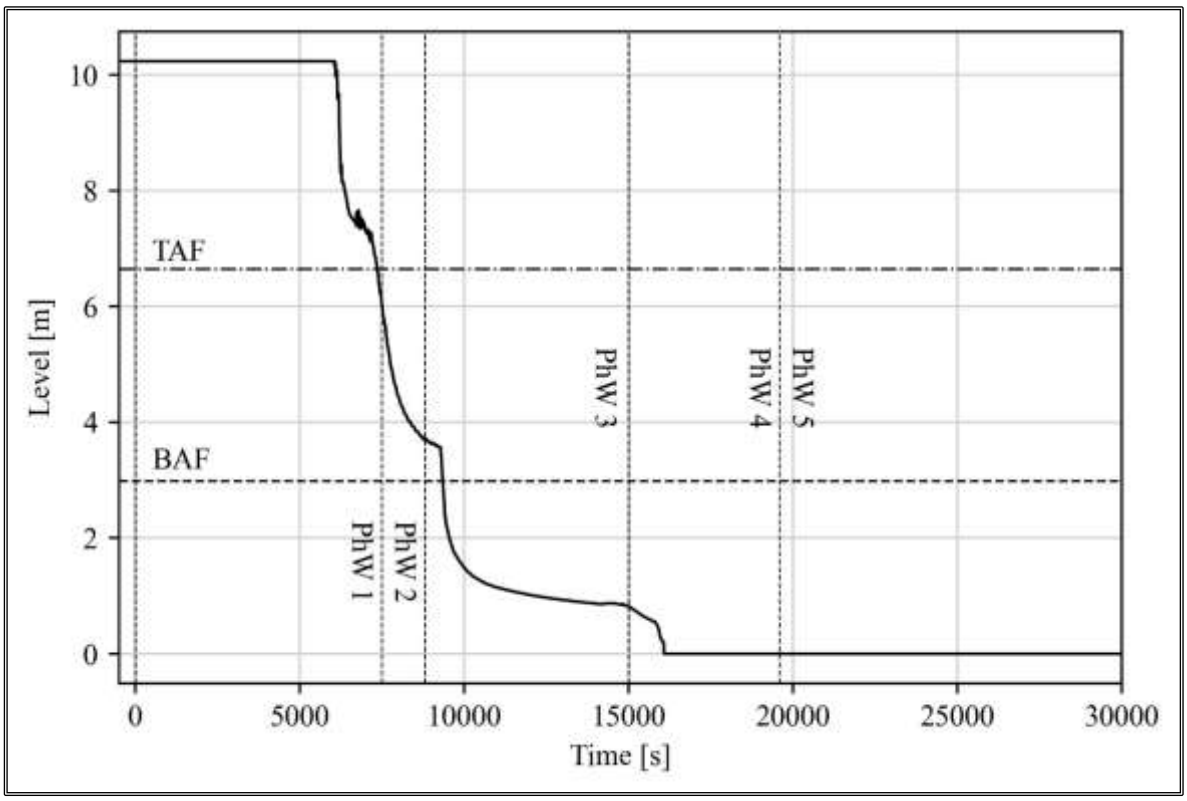

Figure 4.8 Collapsed coolant level into the RPV during the reference case.

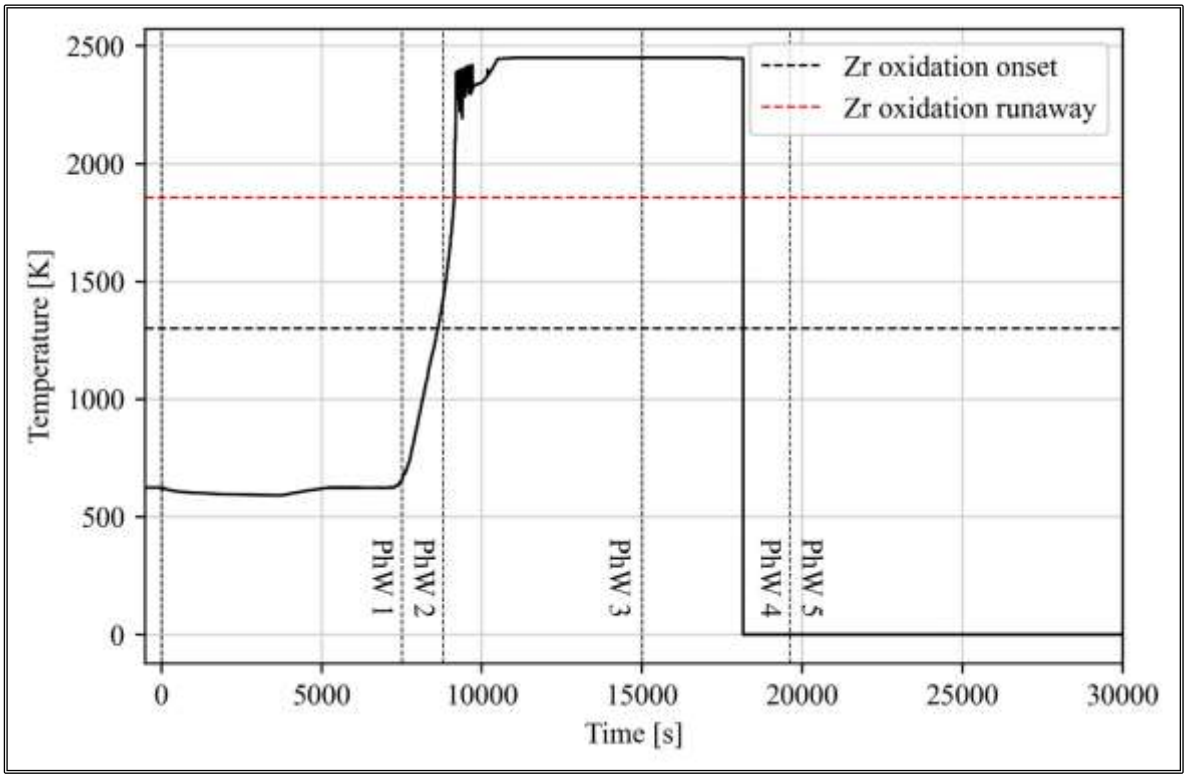

Figure 4.9 Maximum cladding temperature during the reference case.

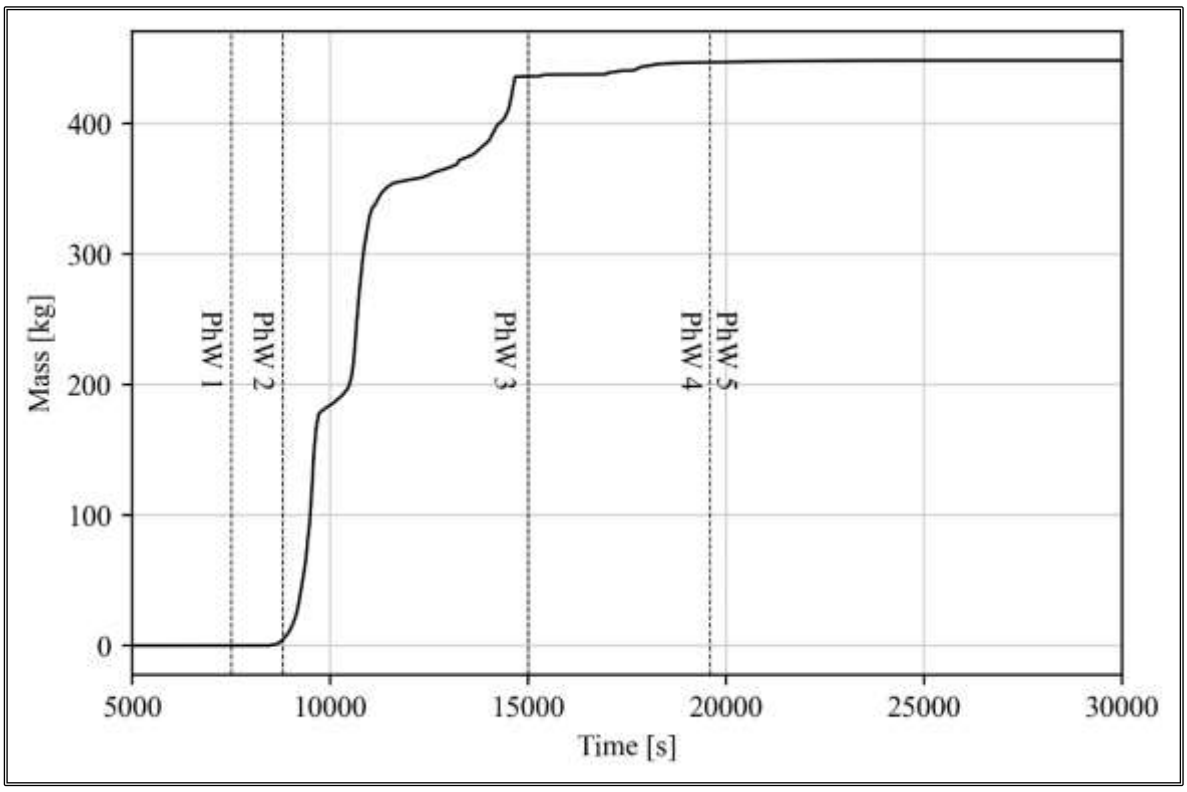

Figure 4.10 Cumulative hydrogen production during the reference case.

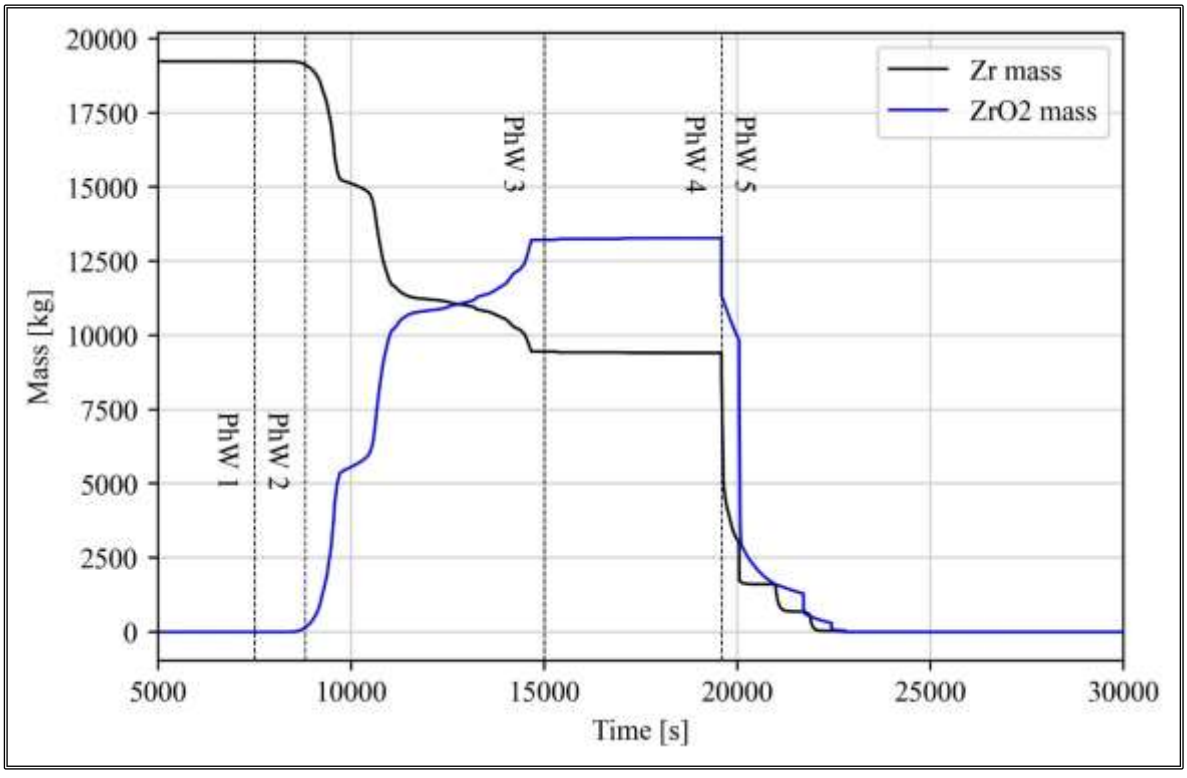

Figure 4.11 Mass of Zr and ZrO_2 during the reference case.

At about 9300 s after the SOT, the core outlet temperature reaches the pressure set point for the stuck opening of the SEBIM valves. It is shown in Figure 4.12 where the core inlet and outlet fluid temperatures are presented, for both the liquid and vapour phases. As a result, the primary pressure decreases drastically, as expected, and it is shown in Figure 4.6. Due to the loss of primary coolant, the collapsed core coolant level reaches the BAF at about 9400 s, accelerating core heat-up and degradation mechanisms.

The loss of core geometry takes place and the melted core materials start their relocation in the LP. The code predicts the slumping of the core at about 15000 seconds. Steam production occurs due to the evaporation of the liquid in the LP in contact with the corium. As also shown in Figure 4.8, the collapsed coolant level decreases to 0 subsequently to the start of the slumping. Furthermore, the steam production is underlined by the PCS pressure peak shown in Figure 4.6. Then, the steam production determines an additional hydrogen generation. The thermal and mechanical loads of the corium on the LH cause its failure, which is predicted by the code at about 19600 s after the SOT.

Due to the core melting and relocation within the LP, FPs are released in the form of gas and aerosols. Regarding the FPs in the form of aerosols, they remain in suspension in the containment atmosphere as shown in Figure 4.13 where the aerosol suspended mass in the containment atmosphere is presented. Degradation phases influence the FPs release from fuel and the rate of deposition of the containment surfaces, influencing the trend of the parameter. After the LH failure, the code predicts a rapid increase of the aerosol suspended mass in the containment atmosphere, reaching a maximum value of about 1300 kg at 22000 s. In Figure 4.14 the release of caesium from the containment to the environment is presented.

In Figure 4.15 the phases of the different core degradation simulated by the code are presented by showing the animation developed with SNAP. In addition, the animation reports the thermal field calculated by the code on the LH. In Table 4.2 and Table 4.3 are reported the colour map specifications respectively for the LH and core materials. Moreover, in Table 4.4 the main events characterizing the simulated transient are presented.

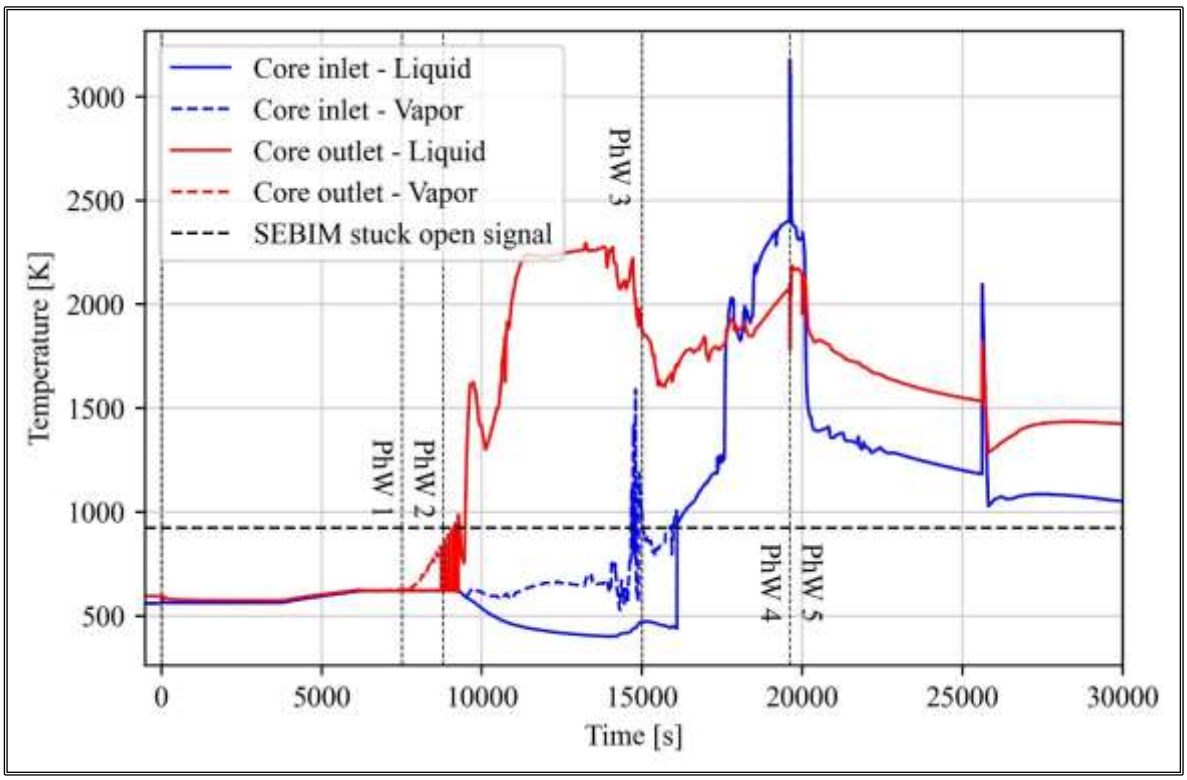

Figure 4.12 Core inlet and outlet fluid temperatures during the reference case.

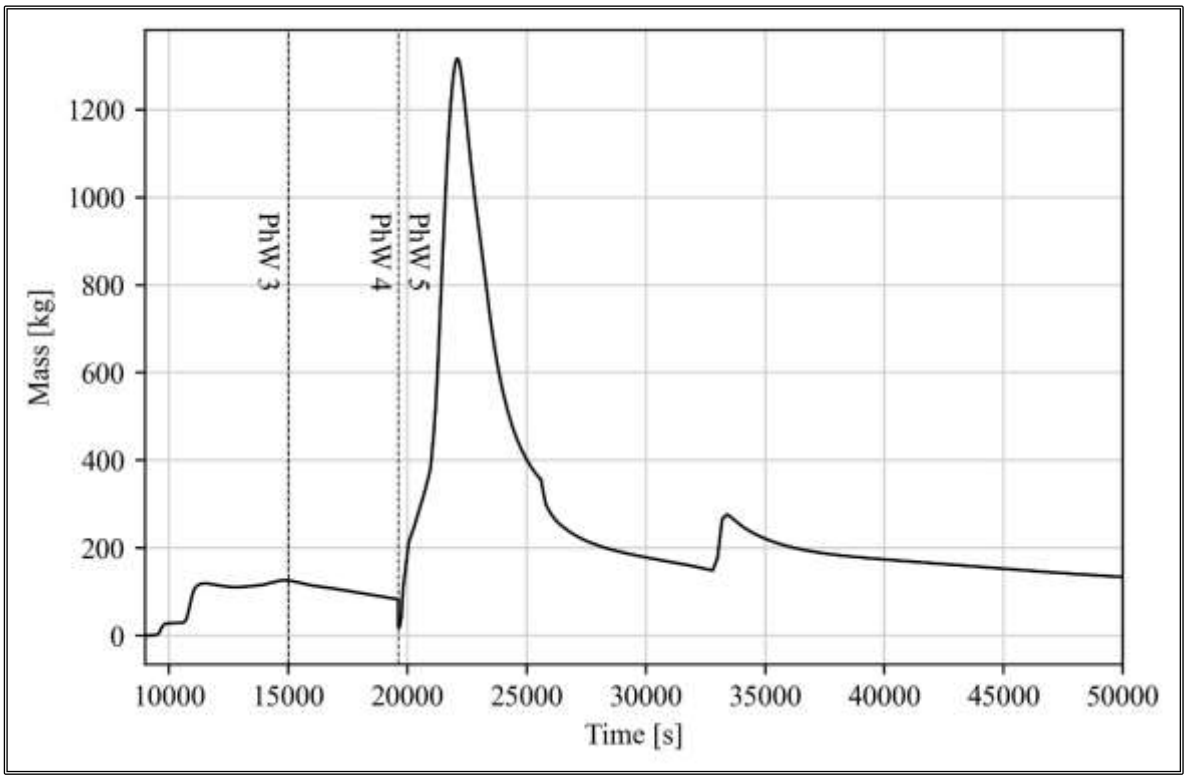

Figure 4.13 Aerosol suspended mass in the containment atmosphere during the reference case.

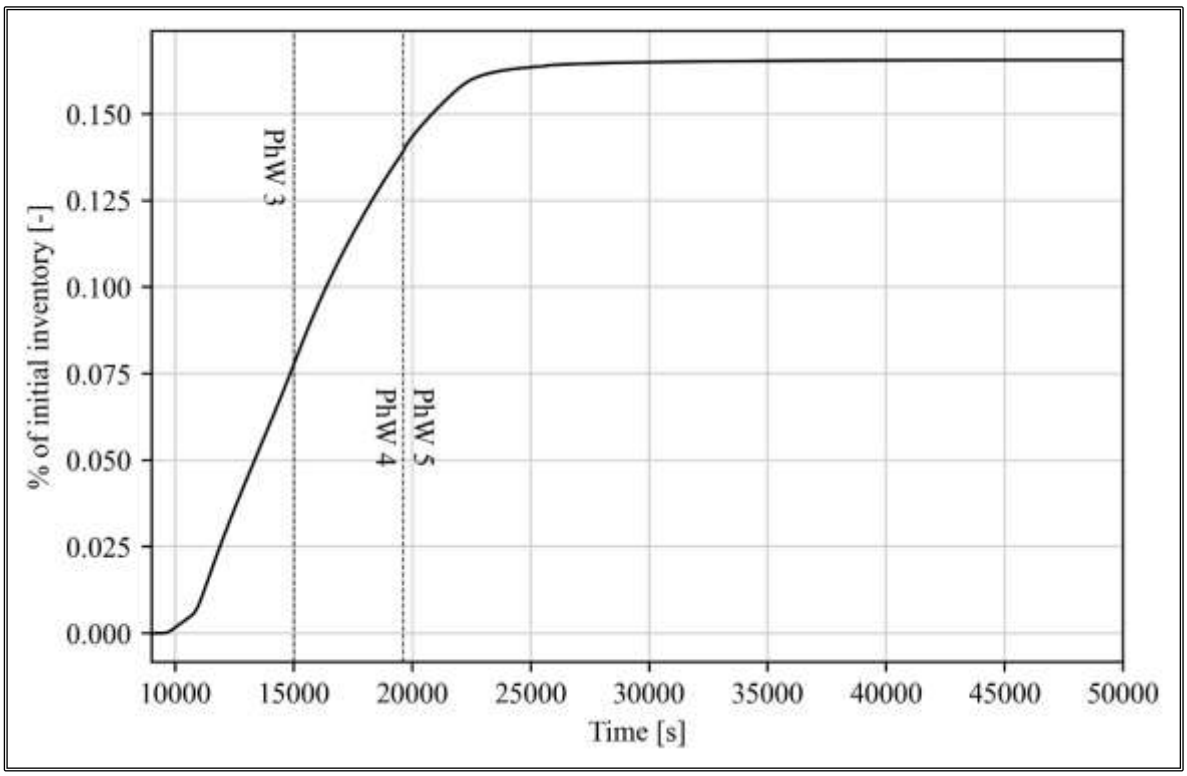

Figure 4.14 Caesium released to the environment during the reference case.

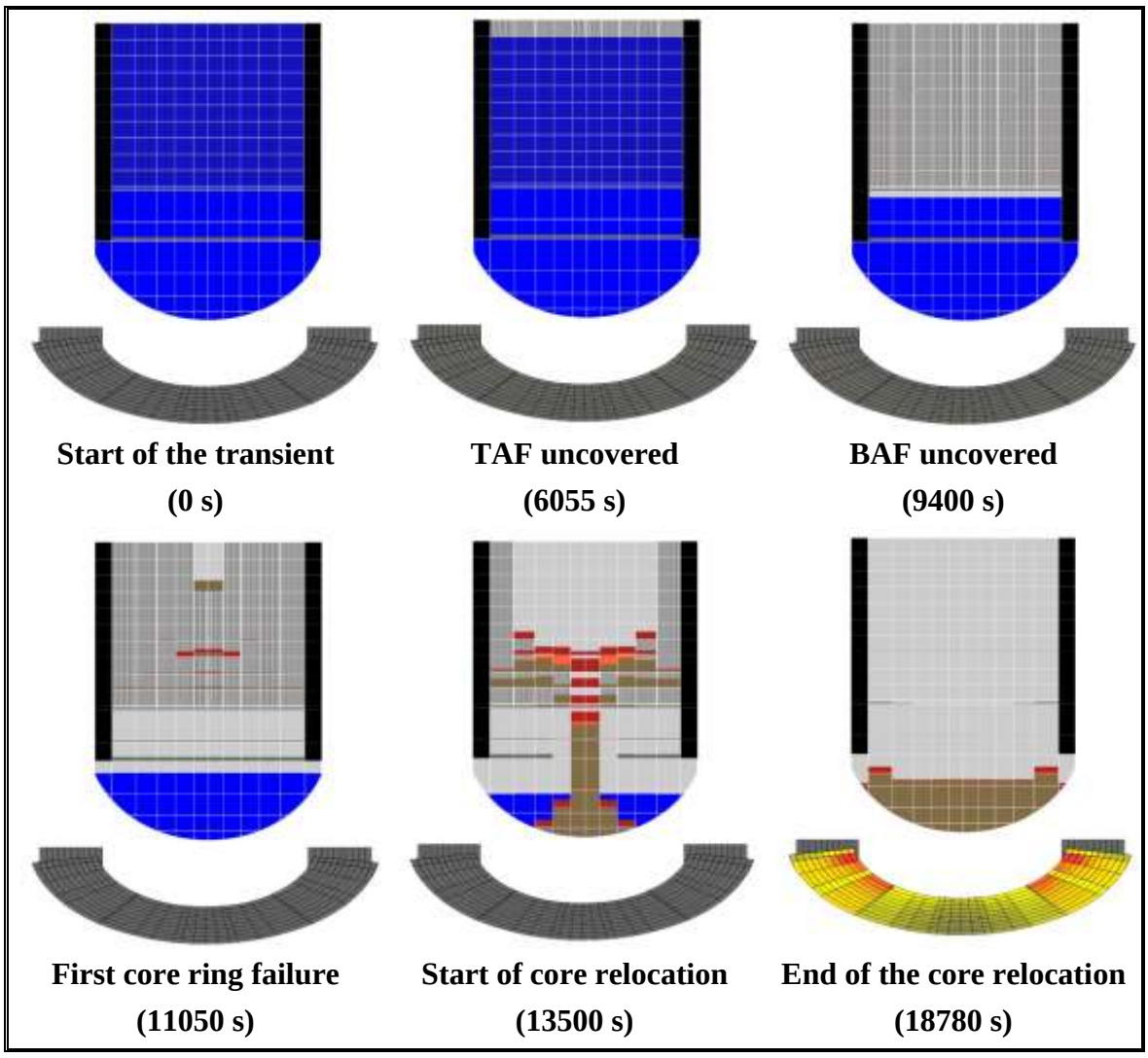

Figure 4.15 SNAP animation of the core degradation and thermal field of LH during the reference case.

Table 4.2 Colour map specifications for the LH.

LH colour map			
Start value (K)	End value (K)	Start colour	End colour
600	1000		
1000	1400		
1400	1800		

Table 4.3 Colour map specifications for core materials.

Core materials colour map			
Intact fuel		Void	
Structure			
Water			
Particulate debris			
Molten pool 1			
Molten pool 2			

Table 4.4 Table of the main events.

Event	Time [s]
SOT	0
SGs cycling inception	48
SEBIM valves cycling inception	4060
TAF uncovered	6055
Start of H2 generation	8320
SEBIM stuck open	9270
BAF uncovered	9400
Start of the core relocation	13500
End of the core relocation	18780
Failure of the LH	19595

4.6 Uncertainty quantification analysis

4.6.1 Hypotheses of the uncertainty analysis

The present full-plant uncertainty analysis aims to apply the uncertainty methodology to a full-scale plant. Furthermore, the uncertainty analysis investigates the uncertainties of the code on the aerosol physics in a full-scale accidental sequence.

In this view, following the hypotheses considered in the uncertainty application against the Phebus FPT1, the FOM considered for the full plant uncertainty quantification analysis is the maximum value of aerosol suspended mass in the containment atmosphere and the aerosol miscellaneous constants, previously presented in Table 3.1, have been chosen as uncertain input parameters.

Considering the two-sided tolerance interval, for a probability content γ and confidence level β of 0.95, a minimum of 93 runs is needed according to Wilks Formula (1.5.2.1). However, considering potential code failures, 130 code runs have been started.

4.6.2 Results

Along the running of the code runs, 14 failed runs have been encountered, underling a failure rate of code runs of about 10%. It is in line with what was observed in the Phebus FPT1 uncertainty application. Following as done in 3.2.5, the normalized uncertain input parameters phase space has been analysed and presented in Figure 4.16 to characterize the failed code runs. They seem to be random, as also underlined during the Phebus FPT1 uncertainty application, and they have not been considered for the statistical analysis.

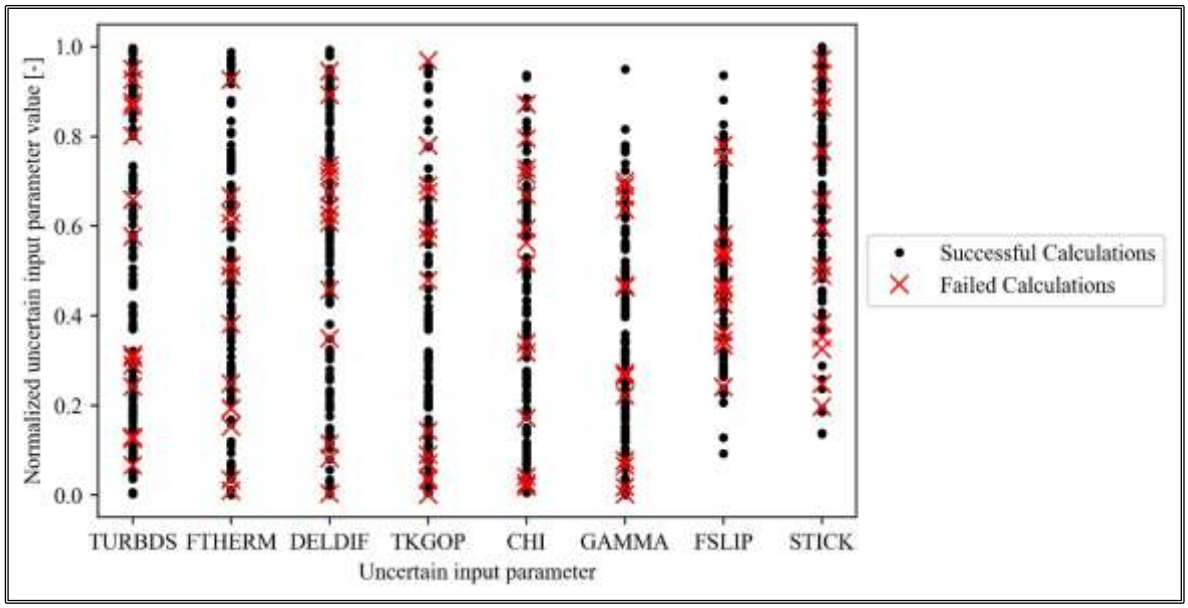

Figure 4.16 Normalized uncertain input parameters phase space.

The mean, median, lower bound, upper bound, standard deviation, and coefficient of variation of the FOM have been calculated and presented in Table 4.5.

It is to be noted that the uncertainty band calculated by the code is 1424.72 kg. The reference calculation is within the uncertainty band, as shown in Figure 4.17 and Figure 4.18. Moreover, these figures show the empirical CDF and PDF of the FOM are reported.

Table 4.5 Statistical parameters of the FOM.

Statistical parameter	Unit	Value
Mean	[kg]	667.45
Median	[kg]	594.82
Lower bound	[kg]	315.86
Upper bound	[kg]	1740.59
Standard deviation	[kg]	269.28
Coefficient of variation	[-]	0.40

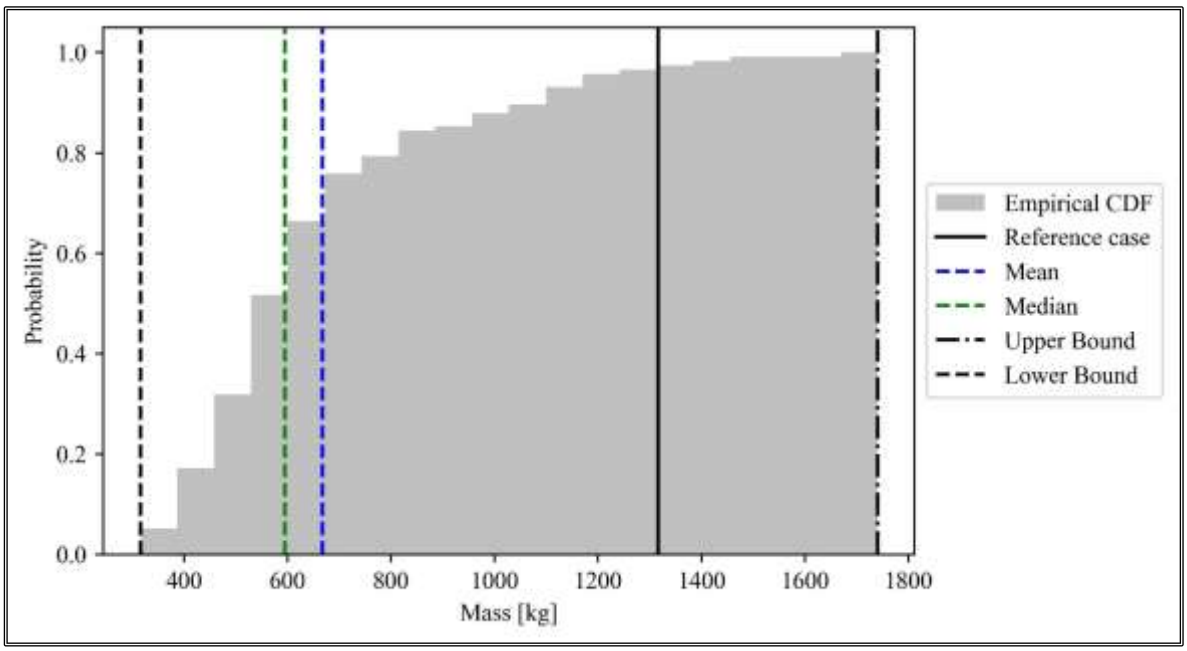

Figure 4.17 Empirical CDF of the FOM.

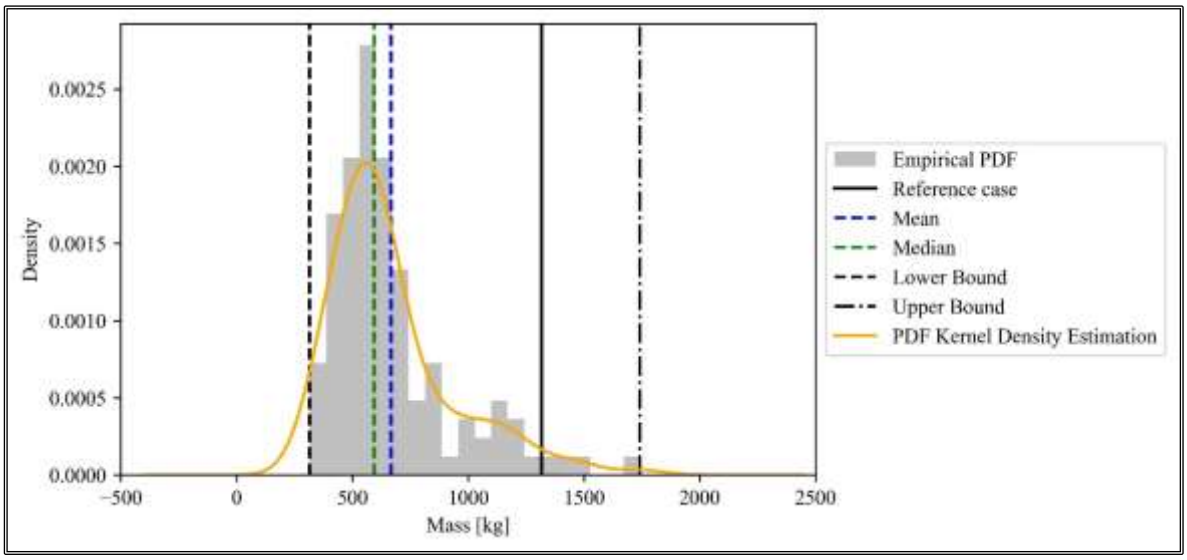

Figure 4.18 Empirical PDF of the FOM.

The uncertainty band has been compared with the uncertainty band obtained during the uncertainty application of the Phebus FPT1 and discussed in 3.2.5. In this regard, to better compare the uncertainty bands, 93 runs were considered randomly among the successful runs for both uncertainty analyses.

Then, the FOM values have been normalized on their mean value, using a similar approach discussed in [124]. Figure 4.19 presents the comparison between the PDFs obtained from the two uncertainty applications. It is underlined that, in normalized terms, the uncertainty band is qualitatively comparable. In addition, it should also be noted that the

values of the reference cases are as close to the mean value in the application of Phebus FPT1 as they are in the application of the PWR-900.

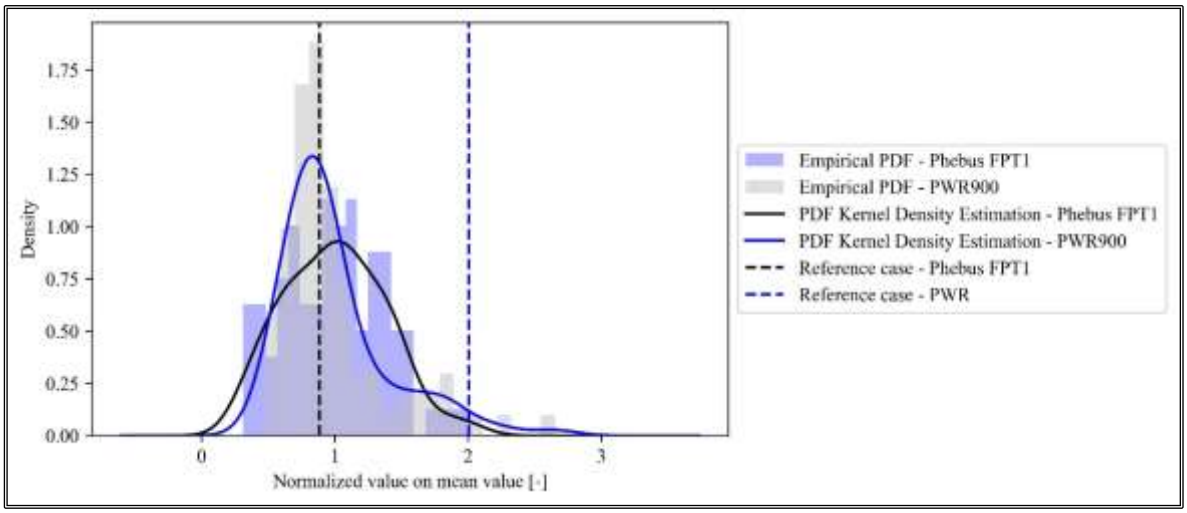

Figure 4.19 Comparison of the FOM PDF with Phebus FPT1 uncertainty application.

The simple and simple rank correlation coefficients have been calculated. As shown in Figure 4.20 and Figure 4.21, even in the present full plant uncertainty application, GAMMA presents a significant statistical correlation (negative correlation) with the FOM. Instead, the CHI parameter presents a low statistical correlation (positive correlation) with the FOM.

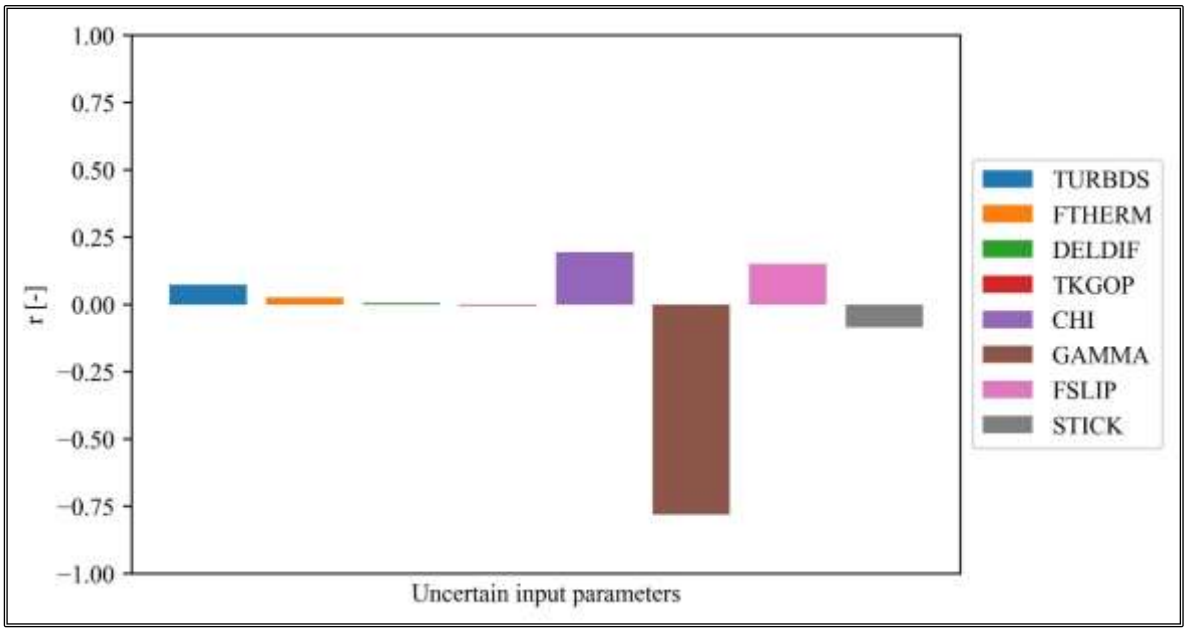

Figure 4.20 Simple correlation coefficient.

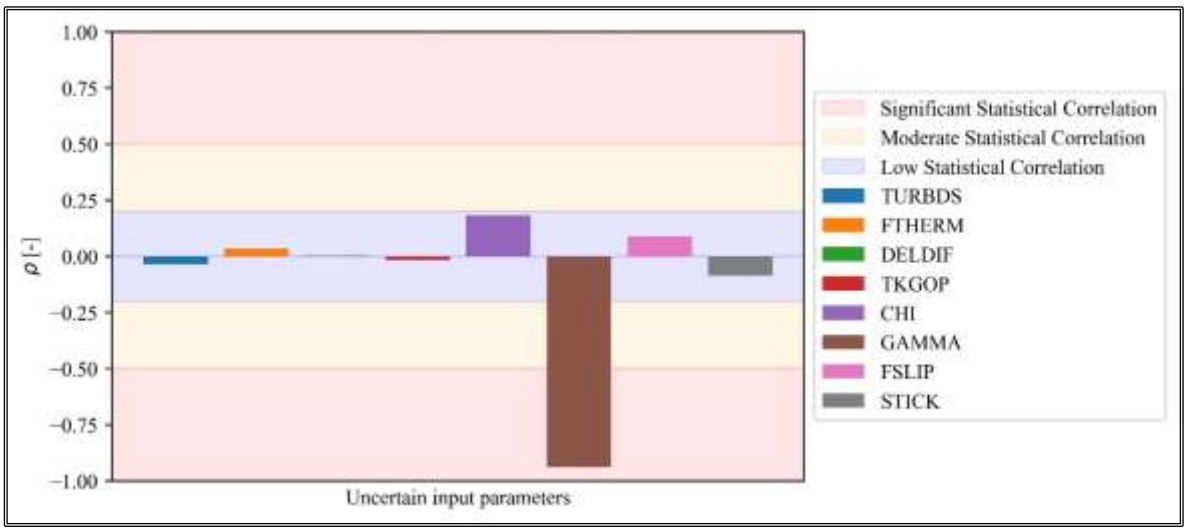

Figure 4.21 Simple rank correlation coefficient.

The statistical correlation between the FOM, CHI and GAMMA parameters has been analysed considering the normalized values of the FOM on the mean value and comparing them with the ones obtained along the Phebus FPT1 uncertainty application, following the same approach adopted above. In Figure 4.22 and Figure 4.23, the scatter plots and the trend curves have been presented to visualize the statistical correlation similarity.

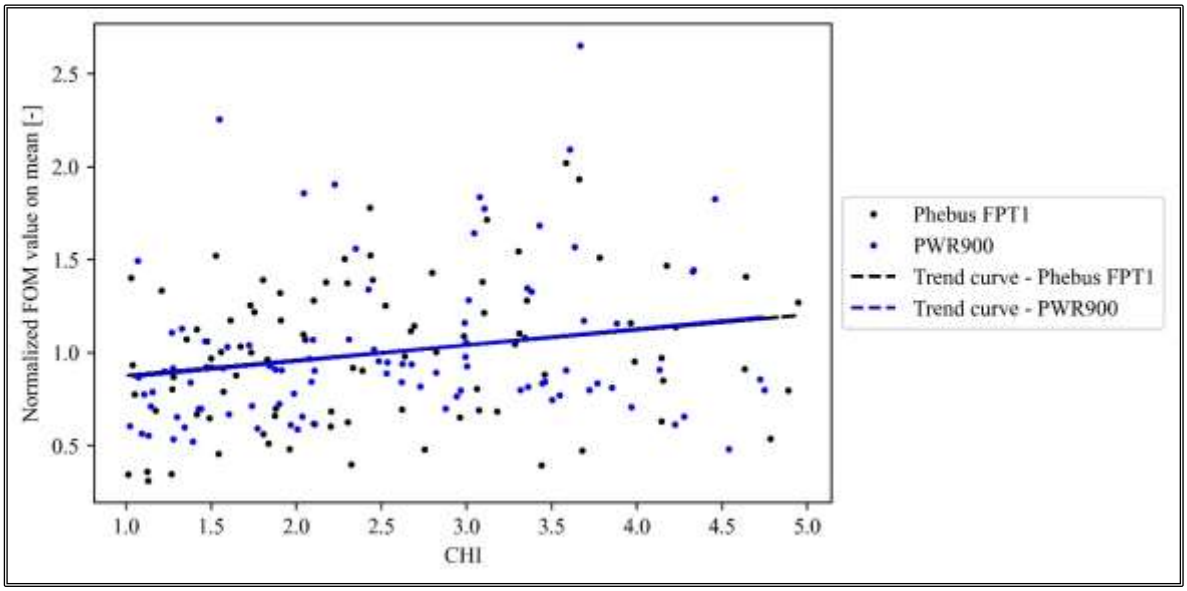

Figure 4.22 Scatter plots of the normalized FOM and CHI values and comparison with Phebus FPT1 uncertainty application.

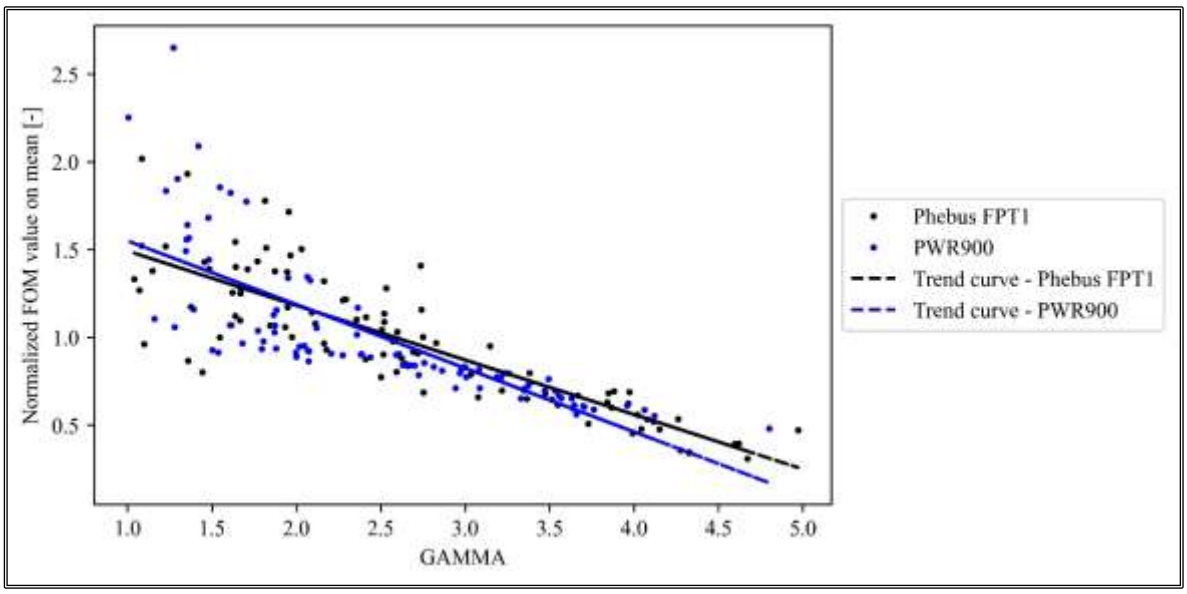

Figure 4.23 Scatter plots of the normalized FOM and GAMMA values and comparison with Phebus FPT1 uncertainty application.

To have some insight into the uncertainty band and the main statistical parameters evolution along the transient, the uncertainty band of the aerosol suspended mass in the containment atmosphere has been evaluated along the transient, as shown in Figure 4.24. The uncertainty band begins to increase after about 11000 s after the SOT and it remains almost constant and equal to about 250 kg until about 19000 s. After the failure of the LH, the uncertainty band starts to increase considerably. Then, along the fallout, the uncertainty band is significantly reduced to about 300 kg. The trend of the uncertainty band can be analysed by the trend of the standard deviation and the coefficient of variation, calculated at each time step, and presented in Figure 4.25. The standard deviation presents a maximum value of about 300 kg at 23000 s after the SOT. Furthermore, the coefficient of variation presents a value between 0.80 and 0.50 along the simulated transient. It is underlined that the trend of the uncertainty band is qualitatively similar to the trend observed in the previous Phebus FPT1 uncertainty application.

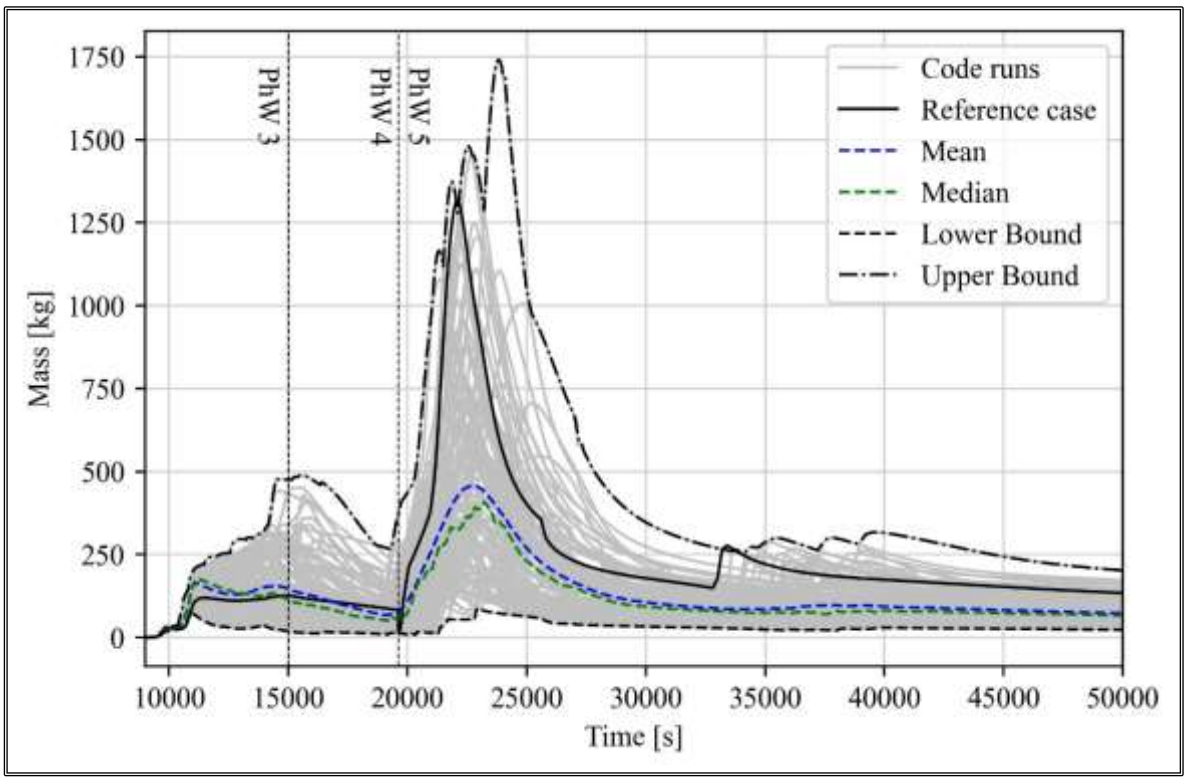

Figure 4.24 Aerosol mass suspended in the containment atmosphere uncertainty band.

In this regard, to better compare them, concerning the phase with the maximum spread, Figure 4.26 presents the comparison between the normalized uncertainty bands. The normalization has been obtained by normalizing the values on the maximum value of the mean during the transient. On the other hand, a time-normalized scale has been considered. The timescale refers to the time when the mean reaches its maximum value: the value zero corresponds to the value at which both mean values reach their maximum value.

Finally, the statistical correlation analysis has been conducted at each time step to study the statistical correlation between the aerosol mass suspended in the containment atmosphere and the uncertain input parameters in a full plant application. It has been underlined that the CHI parameter presents a significant statistical correlation before the LH failure (positive correlation), at the beginning of the release of FPs from the core. Instead, after the release of aerosol to the containment, GAMMA presents a significant statistical correlation with the aerosol suspended mass in the containment atmosphere (negative correlation). Figure 4.27 and Figure 4.28 present the simple and simple rank correlation coefficients calculated using Pearson and Spearman's correlations. The trends of correlation coefficients are confirmed as analysed in the Phebus FPT1 uncertainty application concerning GAMMA. On the other hand, there is a slightly lower statistical correlation for CHI than the experimental application.

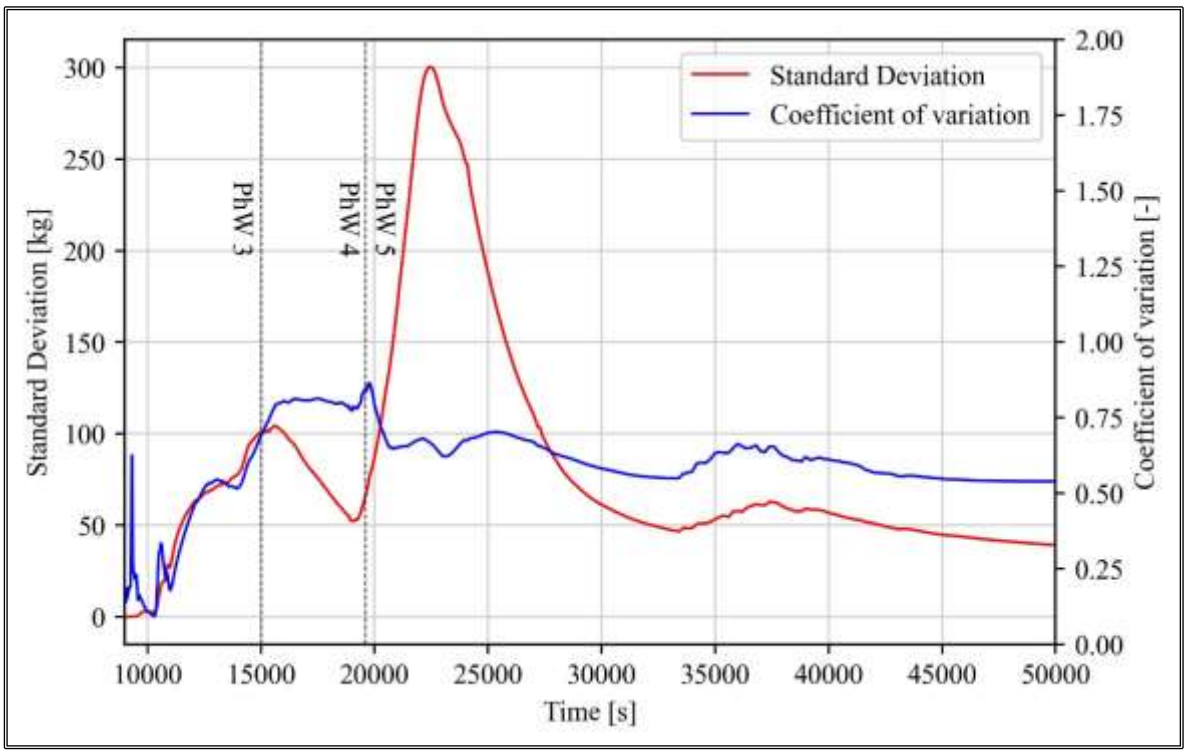

Figure 4.25 Standard deviation and coefficient of variation of the aerosol suspended mass in the containment atmosphere.

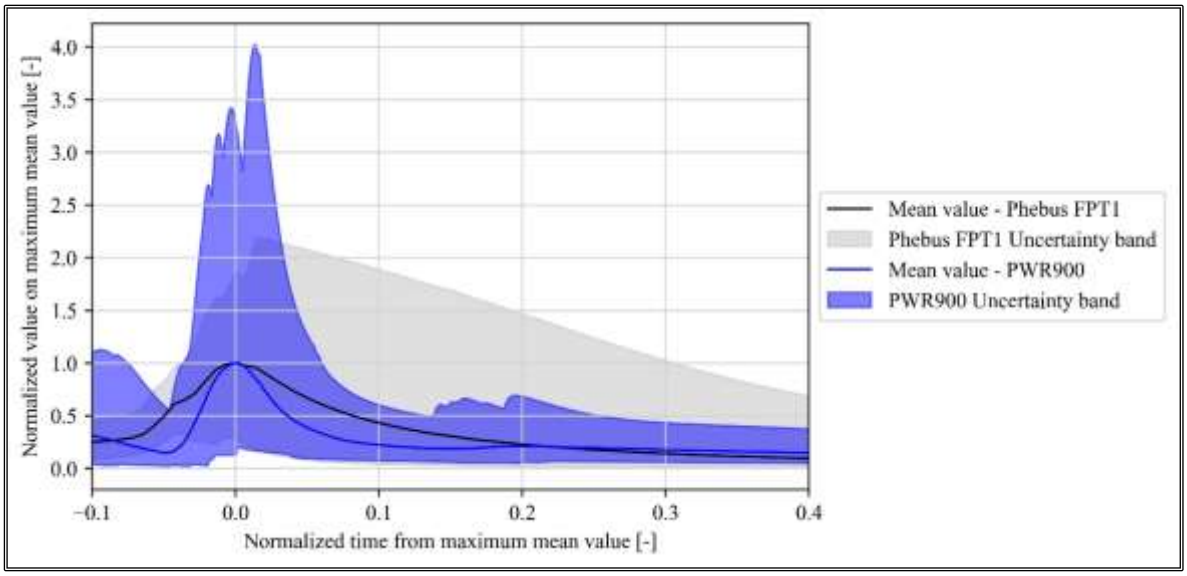

Figure 4.26 Comparison between the normalized uncertainty band obtained for the Phebus FPT1 and the PWR-900 uncertainty applications.

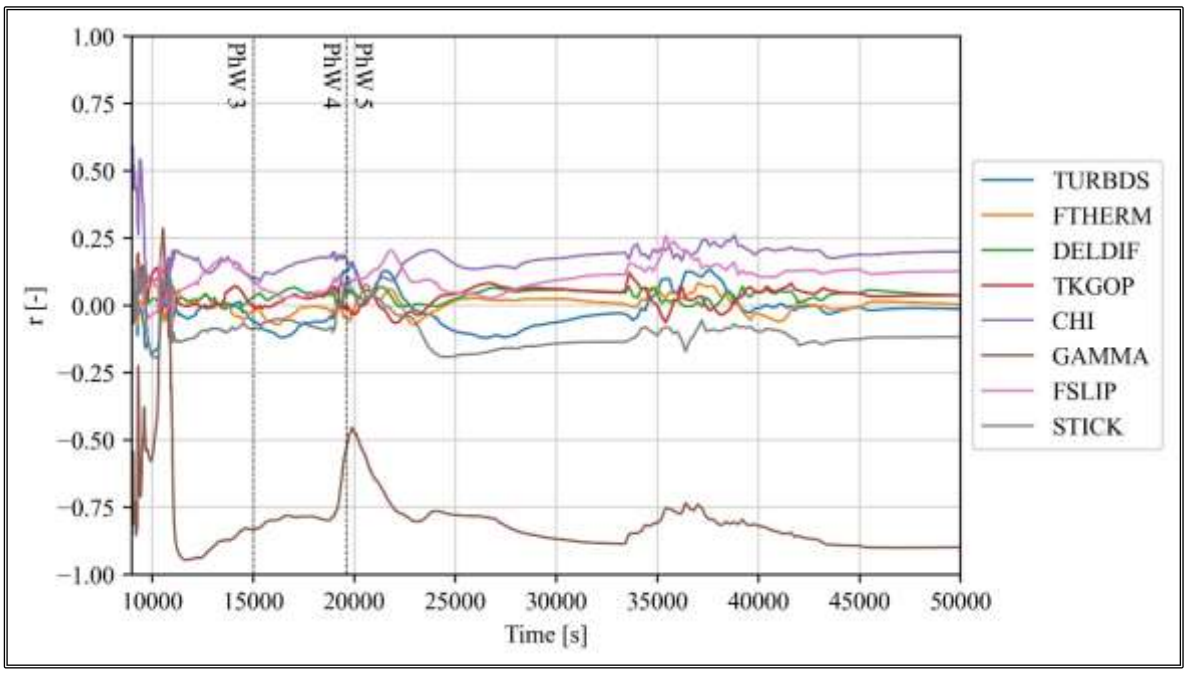

Figure 4.27 Simple correlation coefficient calculated along the transient.

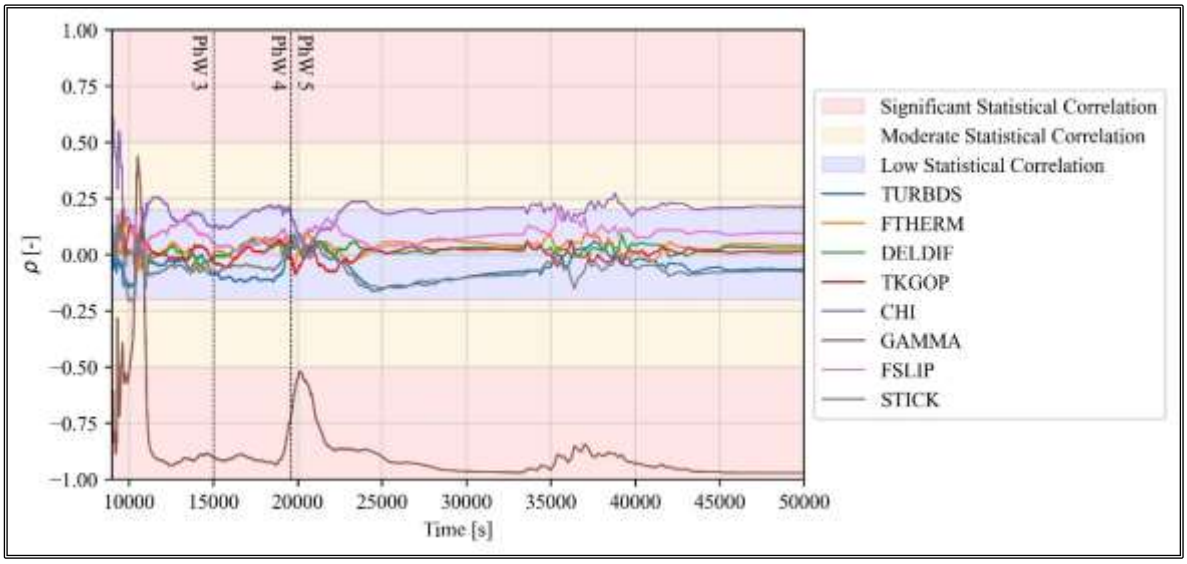

Figure 4.28 Simple rank correlation coefficient calculated along the transient.

5 DEVELOPMENT OF A GENERIC SMR MELCOR NODALIZATION AND UNCERTAINTY QUANTIFICATION APPLICATION

5.1 Introduction

In view of the possible licensing needs of SMR, the international scientific community is focusing on investigating the applicability of SA integral codes in simulating SMR response during postulated transients. Among SMR designs, the iPWR concept, starting from the technology characterizing LWR, is characterized by the adoption of passive safety systems and an integral configuration.

Within this framework, this chapter aims to give an overview of the development of a generic iPWR MELCOR nodalization and, after comparing its results with the ones obtained with the SA integral code ASTEC (study carried out with ASTEC V3.1, IRSN all rights reserved [2024]) during a mitigated sequence, the uncertainty methodology has been applied both during a DBA and a SA sequence.

5.2 Description of the generic iPWR design

Nowadays, the international nuclear community involved in SAs is focused on investigating the applicability of SA integral codes to light water SMR, particularly regarding iPWR. The iPWR concept starts from the well-proven and tested LWR technology with operational experience and includes design features to increase its inherent safety.

Some iPWR designs are characterized by the adoption of an integral RPV containing all the RCS components and the use of passive safety systems. Then, in view of their licensing process, the state-of-the-art SA integral codes should be capable of simulating their advanced features and related phenomenology. Within this context, the Horizon Euratom SASPAM-SA project [125] [126], led by ENEA (Italy), is intended to assess the capability of globally recognized computational tools in characterizing the performance of the most promising iPWR designs during unmitigated scenarios and estimate radiological impact both on- and off-site[5]. More information about this project can be found in APPENDIX D.

[5] Advanced designs, such as iPWRs, are in general characterized by common features with the current operating large-LWR and by other specific features typical of their inherent evolutionary designs, providing safety advantages that reinforce the first three levels of the DiD principle. However, even if a plant is designed with advanced inherent features (through the reinforcement of the 1,2,3 DiD levels) allowing a reduction of the Core Damage Frequency, independent features for preventing and mitigating a SA sequence have to be included in its design (DiD level 4) together with the offsite emergency response (DiD level 5). Therefore, some scenarios

The generic iPWR design, here analysed, is characterized by a thermal power of 1000 MWth with an electrical output of 300 MWe and adopts a dry containment and the use of different passive safety systems. Then, the design features an integral RPV containing all the RCS components such as the PRZ, compact SGs and the RCPs. Figure 5.1 shows a generic view of the RPV and its main components [127].

The primary coolant first flows through the core and then crosses the riser region (surrounded by the extended core barrel). At the top of the riser, it is directed radially into the upper annular plenum, which houses the RCPs suction region. The coolant is pumped by RCPs to the corresponding SG module. The SGs are characterized by the adoption of compact SGs as helical-coil tubes SGs. After flowing through the SG modules, the primary coolant flows downward the downcomer region, surrounding the core, to the LP. Finally, it returns to flow up to the reactor core.

The RPV is contained in a steel containment which is composed of the Drywell (DW) and the RC.

The passive mitigation strategy of an iPWR is based on several passive systems. To assess in a wider way the codes' capability, the following passive systems have been selected:

- *Natural circulation in the RPV*: during potential accidental conditions, following the primary pump trip, the flow in the RPV is driven by natural circulation. In case of a LOCA with subsequent RPV level reduction, natural circulation may be hindered when the level reduces below the upper connection between the riser outlet and the downcomer inlet. Therefore, additional connections may be present between the RPV riser and downcomer at a lower elevation to enable natural circulation at reduced RPV level.
- *Passive decay heat removal*: this system removes the core power during accidental scenarios. It operates in natural circulation and it is connected to the secondary side of the SGs. A pool where submerged Heat eXchangers (HXs) are placed constitutes the heat sink.

that could lead to SA need to be postulated and deterministically studied. More detailed information's are reported in [149]. Therefore, it is necessary to assess the capability of internationally recognized SA code to describe the behaviour of the most promising iPWR designs during SA scenarios and to predict the resulting radiological impact on- and off-site.

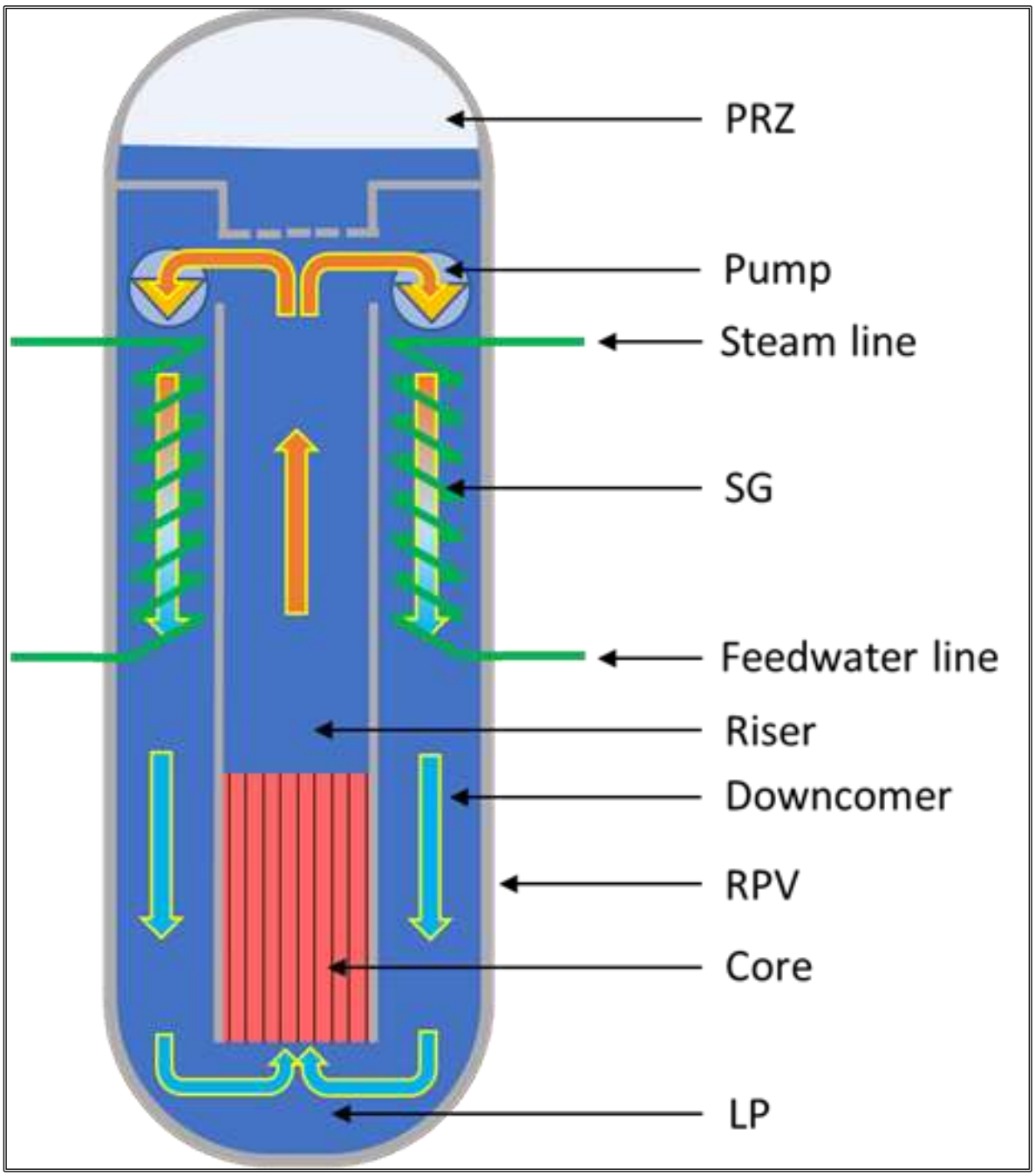

Figure 5.1 View of the RPV of the generic iPWR [128].

- *Primary automatic depressurization*: this system is devoted to the depressurization of the RPV in an automatic way to reduce the primary pressure and enable the passive safety injection.
- *Passive high-pressure safety injection*: the high-pressure safety injection reintegrates the primary coolant in case of a LOCA by injecting borated water. It is composed of a tank connected both at the top and at the bottom with the RPV. When the system is activated, natural circulation occurs between the RPV and the tank.

- *Passive low-pressure safety injection*: this system is devoted to water injection at low pressure, and it is driven by gravity. It is composed of elevated tanks which inject water into the RPV.
- *Containment pressure suppression*: this system mitigates the containment pressurization by suppressing the steam in a large water pool. The steam is directed to the water pool by proper connections between the containment DW and the water pool.
- *Flooding of the RC*: the flooding of the RC enables the external cooling of the LH, which may be fundamental for IVMR in the case of a SA.

Except for the heat sink of the decay heat removal system, all the passive systems considered in the passive mitigation strategy are supposed to be placed within the DW. A scheme of the iPWR layout, with the considered safety functions, is presented in Figure 5.2 [129].

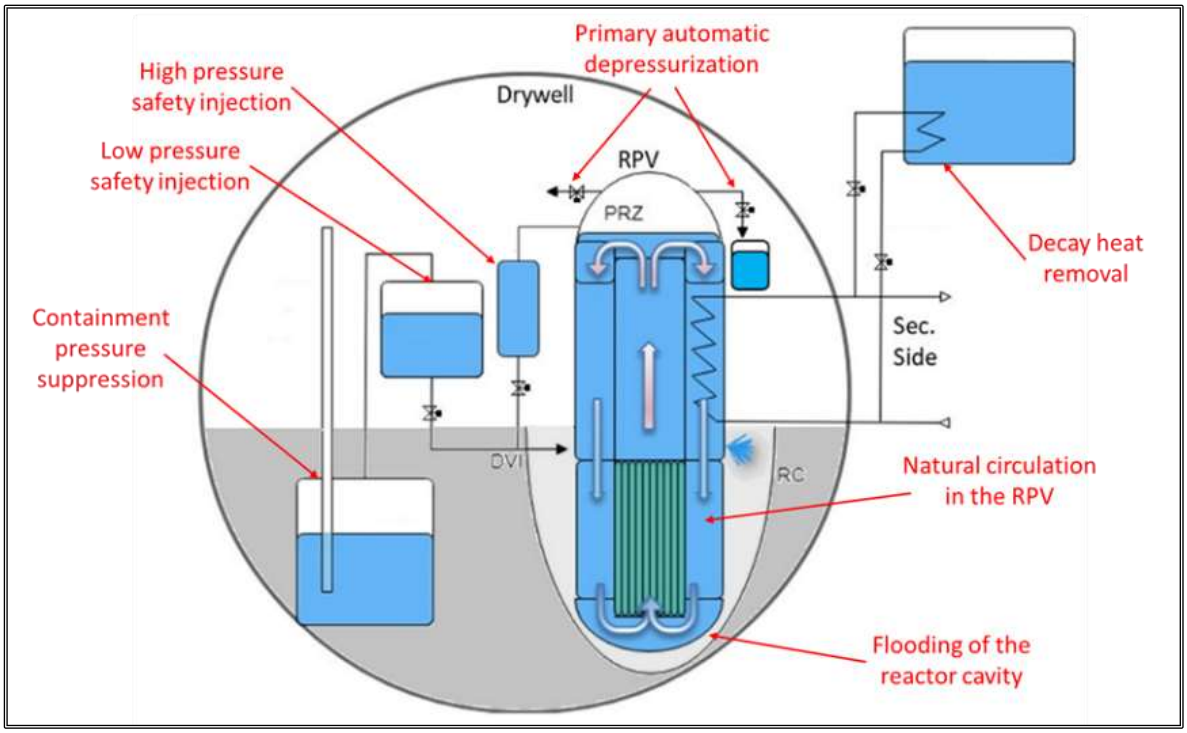

Figure 5.2 Scheme of the generic iPWR design with the passive safety systems [128].

Considering the iPWR main features described above, a generic International Reactor Innovative and Secure (IRIS) [127] iPWR design has been considered as a reference to develop the MELCOR input deck. Table 5.1 presents safety functions characterizing the iPWR design and the corresponding passive safety system. This concept design has been analysed through different activities conducted with integral SA codes. In [129] the capabilities of the ASTEC code in analysing the main thermal-hydraulic phenomena

occurring in this reactor design have been investigated. Furthermore, the study presented in [130] aims to give insights into the capability of the ASTEC code to predict SA phenomena considering the unavailability of the different passive safety systems.

Table 5.1 Passive safety systems of the generic iPWR.

Safety function	Passive safety system
Natural circulation in the RPV	Riser-Downcomer (RI-DC) valves
Decay heat removal	Emergency Heat Removal System (EHRS) and Refueling Water Storage Tanks (RWSTs)
Primary automatic depressurization	Automatic Depressurization System (ADS)
High-pressure safety injection	Emergency Boration Tanks (EBTs)
Low-pressure safety injection	Long-Term Gravity Make-up System (LGMS)
Containment pressure suppression	Pressure Suppression System (PSS)
Flooding of the RC	PSS-vent lines

5.3 Description of a mitigated LOCA in a generic iPWR

The reference scenario considered for the analyses here presented is LOCA transient. The sequence is here described according to what is presented in [131] [132] [133] referring to IRIS design. The PIE is the double-ended guillotine break of one of the two Direct Vessel Injection (DVI) lines. It results in the loss of primary coolant with the single and two-phase blowdown and the consequent RPV depressurization and containment pressurization. A steam-gas mixture moves from the DW to the PSS through the PSS-vent lines, increasing the pressure of PSS and LGMS which is connected to PSS. The RC is gradually filled with the primary coolant flowing from the break and with the steam condensed on the metal internal surface of the DW.

Once the containment high-pressure set-point is achieved, the S-signal initiates the reactor SCRAM which shifts from fission power to decay power, isolates the secondary side of SGs and opens two of the four EHRS loops[6]. Isolation of SGs secondary side determines the increase of secondary pressure. Natural circulation in the EHRS systems begins and permits the heat transfer to RWSTs and consequently the cooling of the RPV and the RPV depressurization.

The low level of the coolant in the PRZ triggers the RCPs to coast down and the opening of the RI-DC check valves. The LM-signal (LOCA Mitigation) is triggered when the PRZ pressure reaches the low-pressure set-point. It determines the opening of the ADS Stage-1,

[6] For the present analyses, because of the nodalization structure (only one equivalent EHRS loop), the logic is simplified and only one actuation of EHRS is considered.

the beginning of the injection from EBTs and the opening of the two remaining EHRS system loops.

The ADS Stage-1 allows the steam dump from the PRZ to the Quench Tank (QT), contributing to the RPV depressurization and accelerating the equalization between primary and DW pressures. The EBTs discharge borated cold water within the RPV through the DVI lines by gravity. Whereas the intact DVI line injects water into the RPV, the broken one discharges water into the RC.

At the primary and DW pressure equalization, the low RPV-DW differential pressure signal activates the injection from LGMS tanks. The LGMS tank of the intact line discharges water into the RPV by the intact DVI line while the LGMS tank of the broken line discharges water into the RC.

Because of the steam condensation in the DW walls and the heat removed by the EHRS, the pressure of DW decreases below the PSS pressure. Consequently, the water inside the PSSs is forced upward through the PSS vent pipes, until filling the RC after dropping from the top end of the PSS vent pipes. The head of the head inside the PSS vent pipes maintains a differential pressure between the LGMSs (equal pressure of PSSs) and RPV (equal pressure of RPV) throughout the depressurization phase, improving the LGMS water injection. Steam circulation between the RPV and DW is enabled by the ADS Stage-2 valves opening upon reaching the LGMS low water mass signal. The water in the RC keeps the core filled during the long-term cooling phase. The heat losses through the DW metal walls to the environment and the power extracted by the EHRS allow the cooling down of the core.

5.4 Description of the nodalization

The generic iPWR MELCOR nodalization, developed in the framework of the EU-SASPAM-SA project using MELCOR code version v2023, combines a trade-off between the computational time and a detailed prediction of the transient thermal-hydraulic and core degradation phenomenology. It has been developed without using proprietary data and by determining the main geometrical data from scaling the available data of the SPES-3 experimental facility [131] [134] as well as by engineering evaluation from available public data. The two lines of the passive systems have been modelled separately. Each line includes the EBT, the PSS, the PSS-vent and the LGMS systems. The RPV has been modelled in different hydraulic regions, including the LP, the reactor core, the core by-pass, the riser, the UP, the SGs and the downcomer and they have been modelled using the CVH and FL

MELCOR packages coupled with the HS package. The SNAP view of the MELCOR CVH and FL nodalization is shown in Figure 5.3.

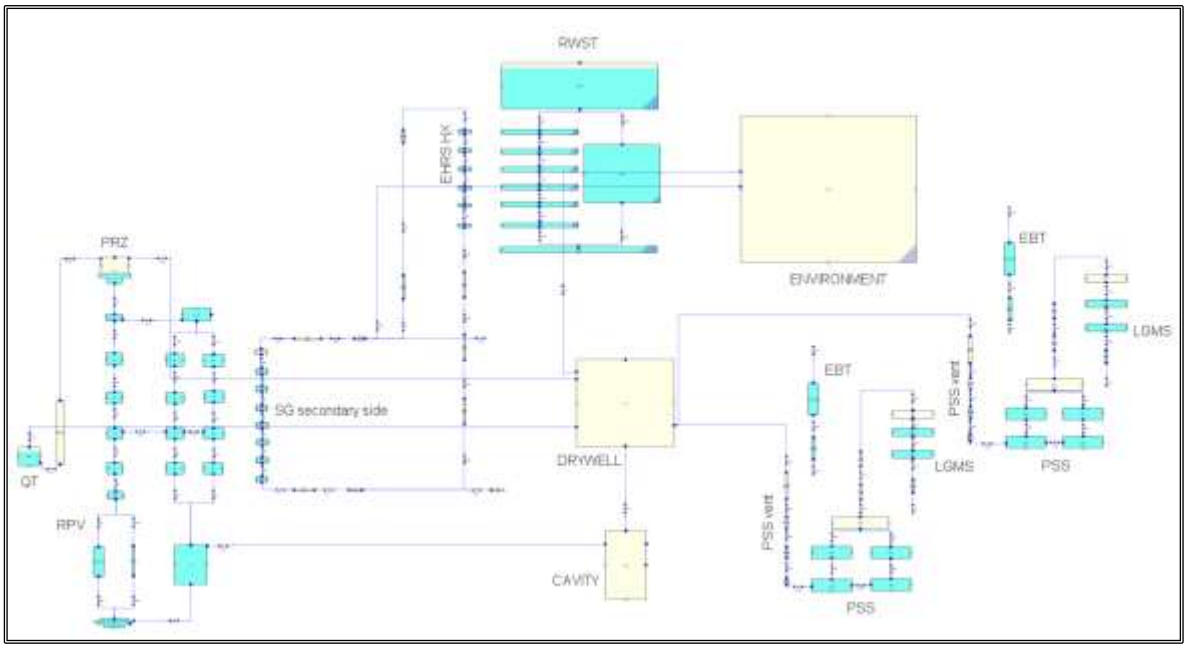

Figure 5.3 SNAP view of the MELCOR CVH and FL nodalization.

To simplify the model, the eight SGs have been modelled as an equivalent one, with four CVH CVs on the primary side and eight CVs on the secondary side. The reactor core has been modelled by a single hydraulic CVH CV coupled with the correspondent COR package nodalization. The COR package nodalization, shown in Figure 5.4, is characterized by sixteen axial levels and six radial rings. The containment region has been modelled with one CVH CV for the DW region, thermally coupled with the CV representing the environment, and one CV for the RC, coupled with the CAV MELCOR package.

5.5 Code-to-code benchmark with ASTEC code

Thermal-hydraulic characterization during nominal and transient conditions represents a crucial point since phenomena are specific and related to new system components or reactor configuration[7] [135]. More research is needed to validate advanced SMR and passive

[7] Passive systems are an advanced solution aimed at increasing the inherent safety of the plant (e.g., there is no need of pumps). On the other hand, the following points are highlighted:

a) Passive safety systems require extensive investigation for assessing the functional failure related to the thermal-hydraulic phenomena driving the operation of the systems and assess the related uncertainties.
b) An active initiation of the passive safety systems may still need.
c) Passive safety systems are characterized by very limited operational experience.

systems than was done for conventional reactors since these reactors feature novel characteristics and a different ranking of phenomena than the current generation of reactors. Several experimental facilities have been built [136] [24] and several experimental campaigns such as PERSEO [137] and OSU-MASLWR [138] have been conducted to achieve this goal.

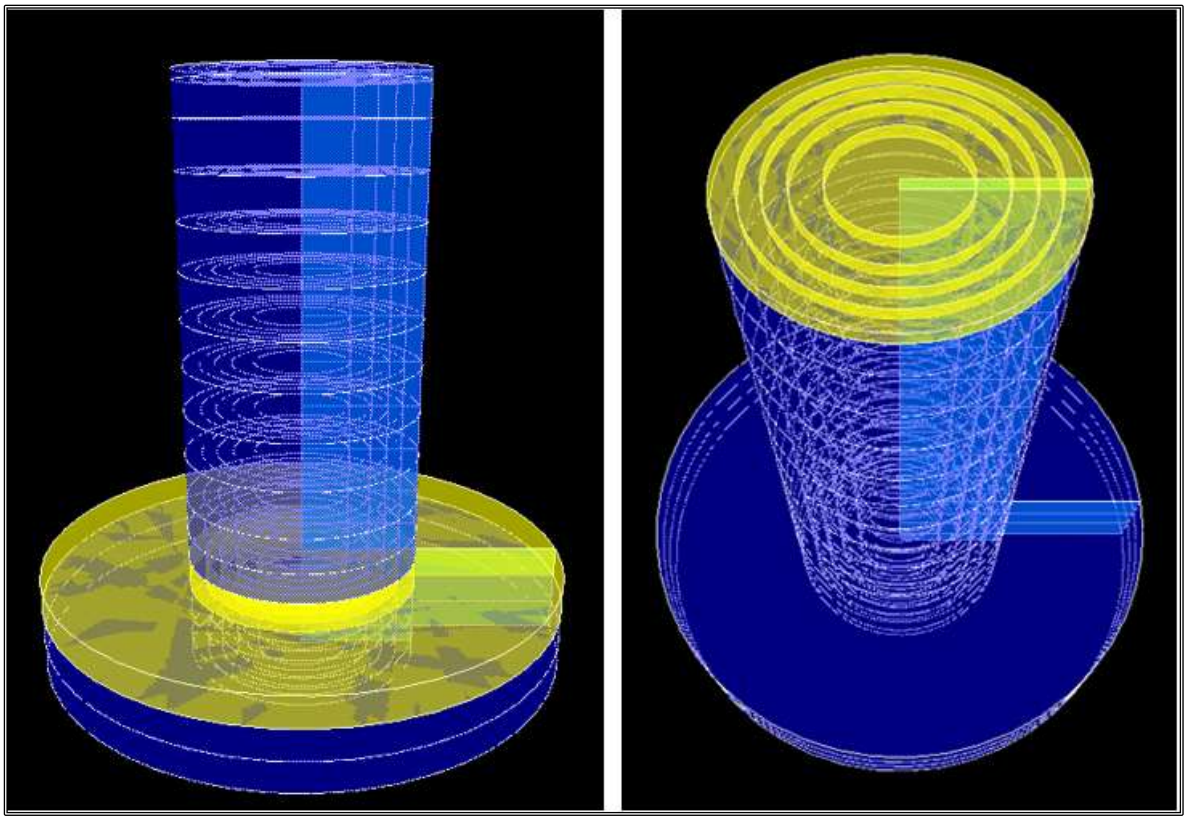

Figure 5.4 SNAP view of the MELCOR COR nodalization.

Employing experimental facilities is essential to creating an experimental database that will help validate the codes. Validation activities against the experimental database for SMR are reported in [139] [140] [141] and [142]. For the same reason, validation of integral SA codes is also necessary in addition to specific thermal-hydraulic system codes. In this regard, to investigate the capabilities of the MELCOR input deck in simulating the main thermal-hydraulic phenomena described in 5.3, the results obtained have been compared with the

Considering this, the impact of the operation of passive systems on postulated SA progression is a novel topic and needs to be assessed. Furthermore, the specific assessment of the code capability to simulate passive systems phenomenology is crucial. In this regard, in fact, in light water SMR, the evolution of SA sequences depends on the postulated partial or total not operation of passive systems (e.g. postulate the failure of passive system valve activation). Therefore, it is necessary to investigate the capability of SA codes to predict the main thermal-hydraulic phenomena involved in the passive mitigation strategy of LW-SMR in order to adequately apply them for the design of accident management's strategy (in-vessel phase of a SA is only dominated by thermal-hydraulic phenomena).

results obtained with ASTEC code, in a code-to-code benchmark activity. The ASTEC input deck of the generic iPWR has been widely used in previous activities described in [129] [130] [143]. Furthermore, the activity aims to gain first insights about the possible differences in predicting iPWR typical phenomena ASTEC and MELCOR codes.

5.5.1 Description of the generic ASTEC nodalization

The ASTEC nodalization has been developed by ENEA using the code version ASTEC v3.1. The ASTEC module CESAR has been used to model the thermal-hydraulic phenomena characterizing the RCS. It has been used for a detailed nodalization of the upper part of the RPV, the secondary system (steam line, feedline and SGs), and most of the passive safety systems (i.e., DVIs, EBTs, PSS, LGMS, EHRS). Figure 5.5 shows a generic scheme of the CESAR nodalization.

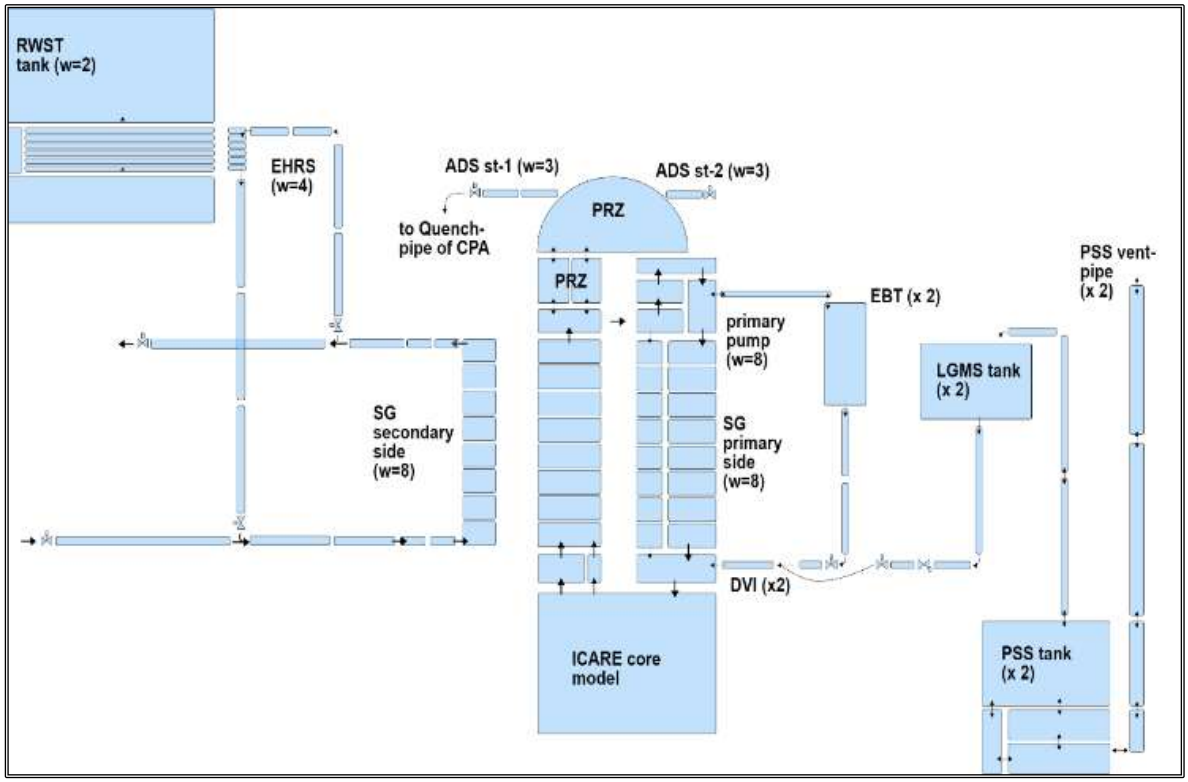

Figure 5.5 CESAR nodalization of the generic iPWR [129].

A 6-channel (4 core channels, 1 bypass channel and 1 downcomer channel) core model has been developed with ICARE module, for the bottom RPV and the core nodalization. The core internals have been realized as 2D components by employing the ICARE dedicated structures. Furthermore, the models for the simulation of in-vessel core degradation phenomena are activated. The CPA module of ASTEC, usually in charge of containment thermal-hydraulic modelling, has been used to model the DW of the containment. Moreover, CPA modules have been adopted to model the QT suppression system. The RC has been

modelled with CESAR and thermally coupled with the external vessel structure of ICARE, as schematically described in Figure 5.6.

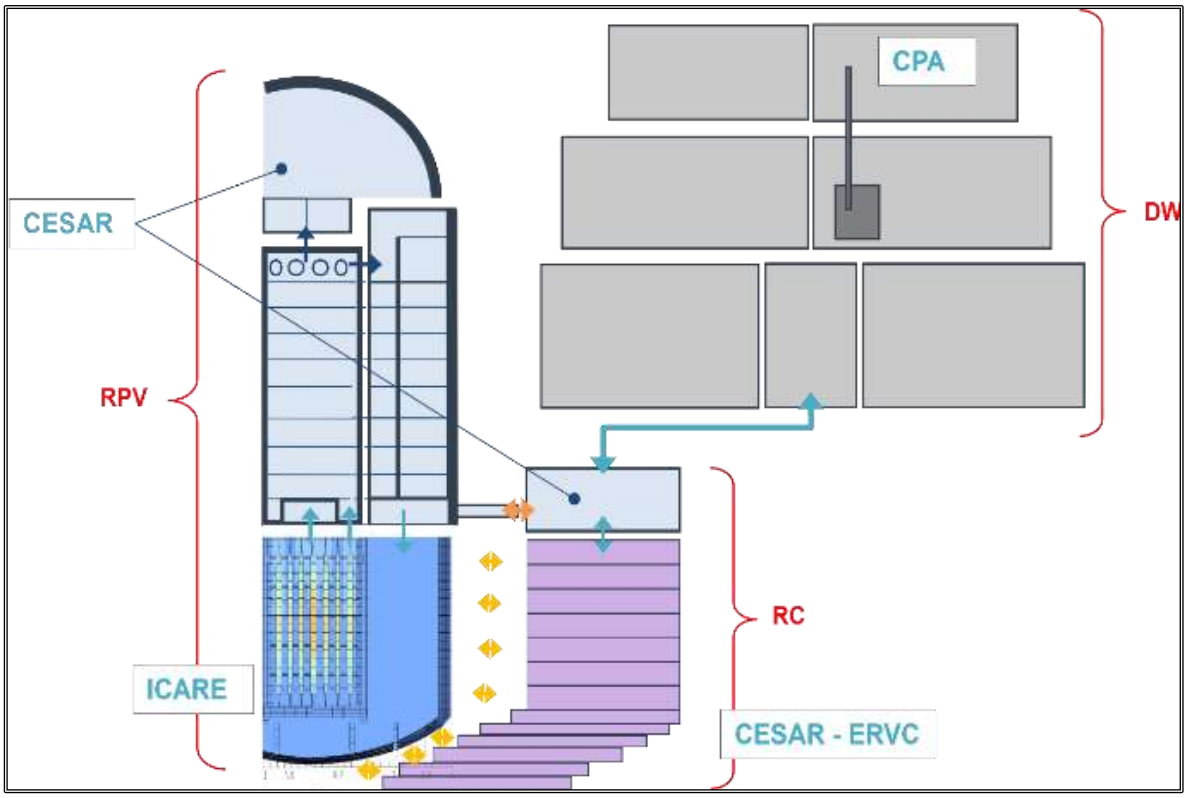

Figure 5.6 ASTEC CESAR nodalization coupling with external vessel structures [129].

5.5.1 Steady-state analysis

To reach the initial conditions before the transient, a steady-state analysis has been conducted. The main thermal-hydraulic parameters are presented in Table 5.2 and Table 5.3 for MELCOR and ASTEC respectively.

Table 5.2 MELCOR main thermal-hydraulic parameters during the steady-state.

Parameter	Unit	Reference	MELCOR	MELCOR discrepancy [%][8]
PRZ pressure	[Pa]	15.5E6	15.5E6	0.00
Primary flow rate	[kg/s]	4700	4732	0.68
Core bypass flow rate	[kg/s]	199.8	204	2.10
Inlet core temperature	[K]	566	570	0.71
Outlet core temperature	[K]	603	605	0.33
Core power	[MW]	1000	1000	0.00
SG outlet pressure	[Pa]	5.83E6	5.87E6	0.69
SG inlet temperature	[K]	497	497	0.00
SG outlet temperature	[K]	590	593	0.51
Total SG mass flow rate	[kg/s]	502.8	500.4	0.48

[8] In Table 5.2 and Table 5.3 the discrepancy has been calculated as the percentage difference between the parameters evaluated by, respectively, the MELCOR and ASTEC code and the reference case.

Table 5.3 ASTEC main thermal-hydraulic parameters during the steady-state.

Parameter	Unit	Reference	ASTEC	ASTEC discrepancy [%]
PRZ pressure	[Pa]	15.5E6	15.5E6	0.00
Primary flow rate	[kg/s]	4700	4699	0.02
Core bypass flow rate	[kg/s]	199.8	205	2.42
Inlet core temperature	[K]	566	570	0.65
Outlet core temperature	[K]	603	605	0.29
Core power	[MW]	1000	1000	0.00
SG outlet pressure	[Pa]	5.83E6	5.80E6	0.51
SG inlet temperature	[K]	497	497	0.01
SG outlet temperature	[K]	590	590	0.01
Total SG mass flow rate	[kg/s]	502.8	513	2.00

Steady-state parameters have been compared with reference steady-state values [129], taken from the SPES-3 facility design [134] [131] [144] (when necessary these values were multiplied by the facility scaling factor, i.e. 1/100). The codes present a discrepancy of less than 3% compared to the reference steady-state values. Moreover, to best characterize the results of the codes during the steady state, the comparison of the total pressure along the RPV primary circuit has been presented in Figure 5.7.

5.5.2 Transient analysis

A total of 50000 s has been simulated, considering the SOT at t = 0 s with the PIE occurrence. In general, according to discussed in 5.3, the transient can be divided into three PhWs [145]:

I. **Blowdown phase** - PhW 1: it starts with the SOT and ends with the pressure equalization between the PCS and DW. It is characterized by the SCRAM, pumps-coast down, PCS depressurization, TAF uncover, DW pressurization, injection from EBTs and the activation of the EHRS system, opening of ADS Stage 1.

II. **Reflood phase** - PhW 2: it evolves from the pressure equalization between PCS and DW up to the recovery of the TAF. It is characterized by the injection from LGMS tanks.

III. **Long-term cooling phase** - PhW 3: it starts from the coverage of the TAF and includes the remaining part of the transient.

After the break, the transient is initially driven by the blowdown of the RPV. In Figure 5.8, the mass flow rate through the break and the cumulative mass discharged by the break

are shown for both codes. The initial peak of mass flow rate predicted is about 110 kg/s for both codes. However, the codes predict a different total mass of primary coolant discharged into the containment: ASTEC predicts about 50 t and MELCOR about 30 t.

The trend of primary pressure, shown in Figure 5.9, is qualitatively and quantitatively similar for both the codes during the initial 1000 s of the transient; thereafter, it is possible to notice that in ASTEC the primary pressure tends to drop faster. During the blowdown phase, both the codes well predict the pressurization of the DW and the pressurization of the secondary system from a qualitative and quantitative point of view, as presented in Figure 5.9.

Following the DW, the PSS pressure increases as well as the pressure of the LGMS tanks. Once the high containment pressure set-point is reached, the S-signal is triggered, activating the SCRAM, the isolation of the secondary side of SGs and the opening of EHRS loops. Due to the SGs' secondary side isolation, the secondary pressure increase is predicted in both codes as shown in Figure 5.9. After the peak, predicted by the codes with similar timing, the secondary pressure trends are qualitatively similar. From a quantitative point, the secondary pressure in ASTEC is slightly lower than in MELCOR after about 1000 s after the SOT. The activation of the EHRS system allows the cooling of the core by natural circulation, predicted in both codes. The decay power and the power transmitted to the primary coolant from the core are shown in Figure 5.10 and the power transmitted to the EHRS system from the SGs and to the RWST from the EHRS HXs in Figure 5.11. During the initial 1000 s, the power transmitted to RWST is higher in ASTEC than in MELCOR, with a peak of about 140 MW in ASTEC and 100 MW in MELCOR. Afterwards, it is qualitatively and quantitatively similar. The EHRS flow rates predicted by the codes are qualitatively and quantitatively similar, as presented in Figure 5.12. Approximately 122 s after the SOT in MELCOR and 65 seconds in ASTEC, the low PRZ level signal is triggered, with the following primary pumps coast down and the opening of RI-DC valves. The mass flow rate is now sustained only by natural circulation inside the RPV. The low PRZ pressure determines the activation of the LM-Signal at around 148 s after the SOT in MELCOR and 158 s in ASTEC, triggering the opening of the ADS Stage-1 and EBTs. In Figure 5.13 the mass flow rate and cumulative mass discharged by the ADS Stage-1 in both codes are presented.

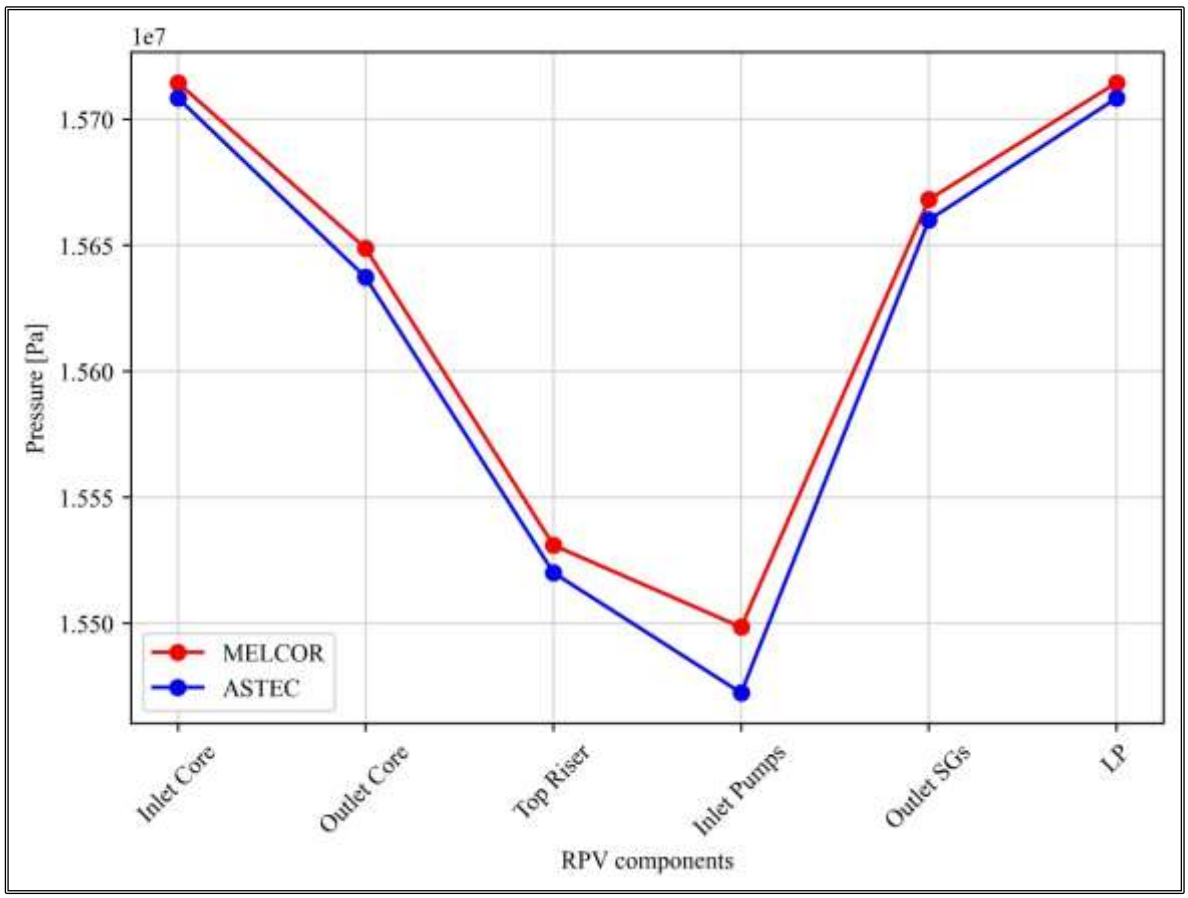

Figure 5.7 Pressure profile along the RPV primary circuit along the steady-state.

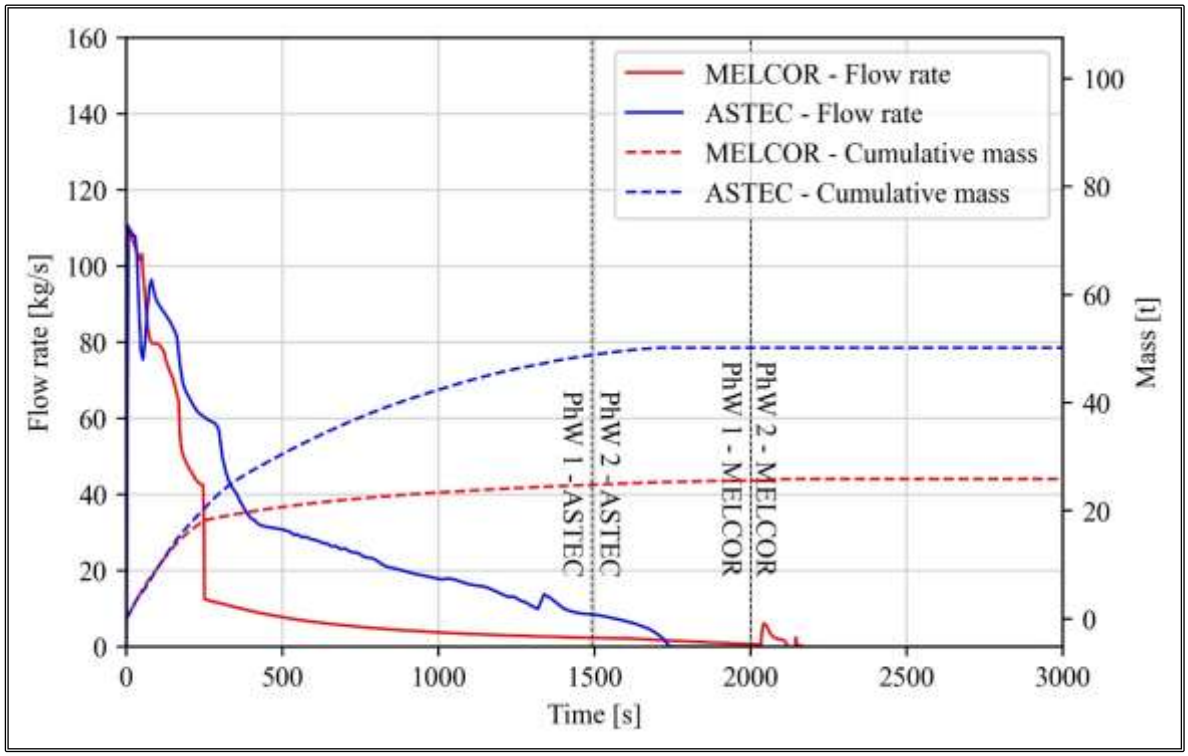

Figure 5.8 Break mass flow rate and cumulative discharged mass.

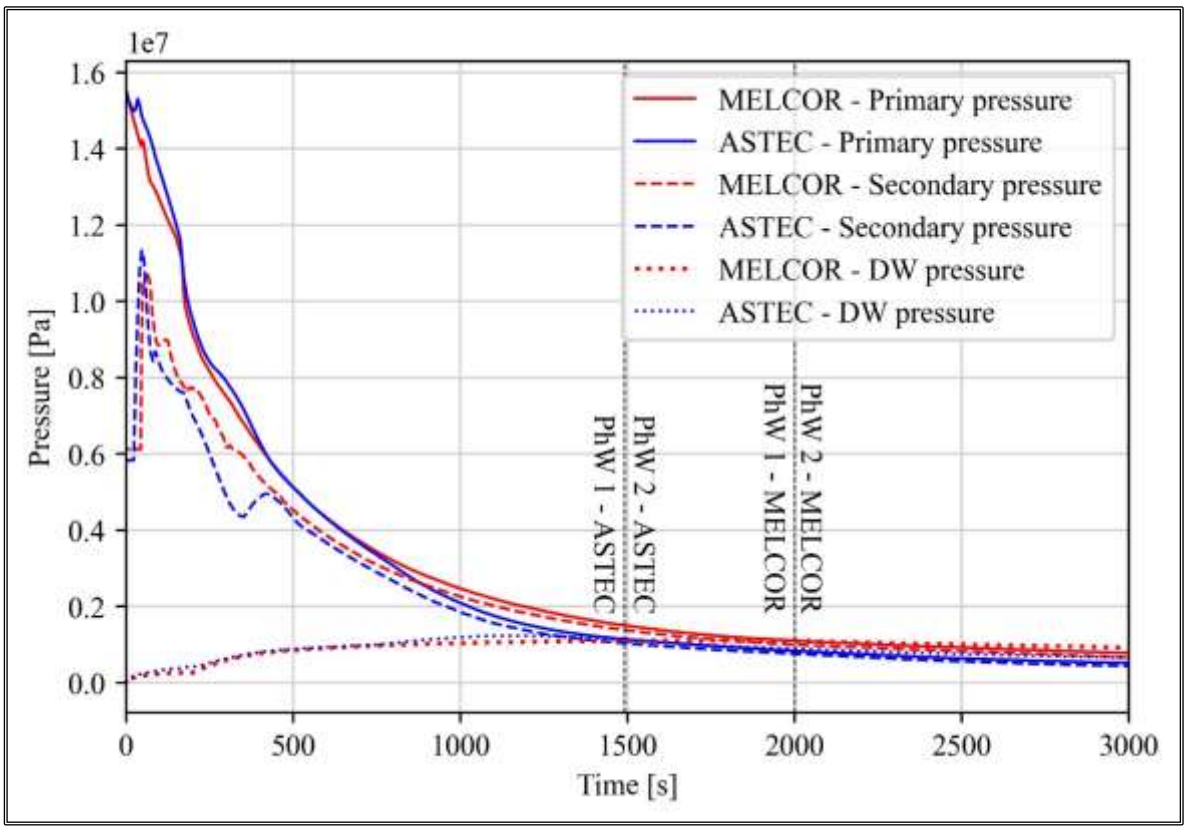

Figure 5.9 Primary, secondary and DW pressure.

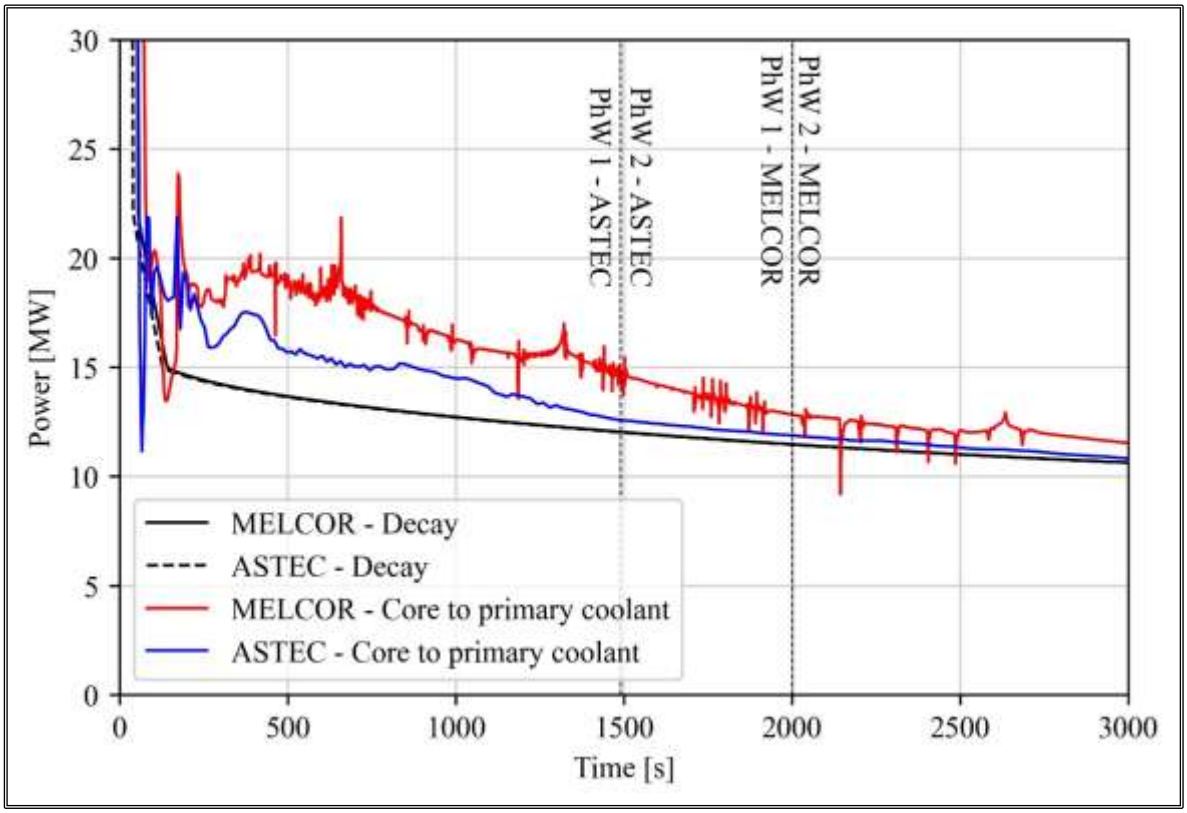

Figure 5.10 Decay power – Power to the primary coolant.

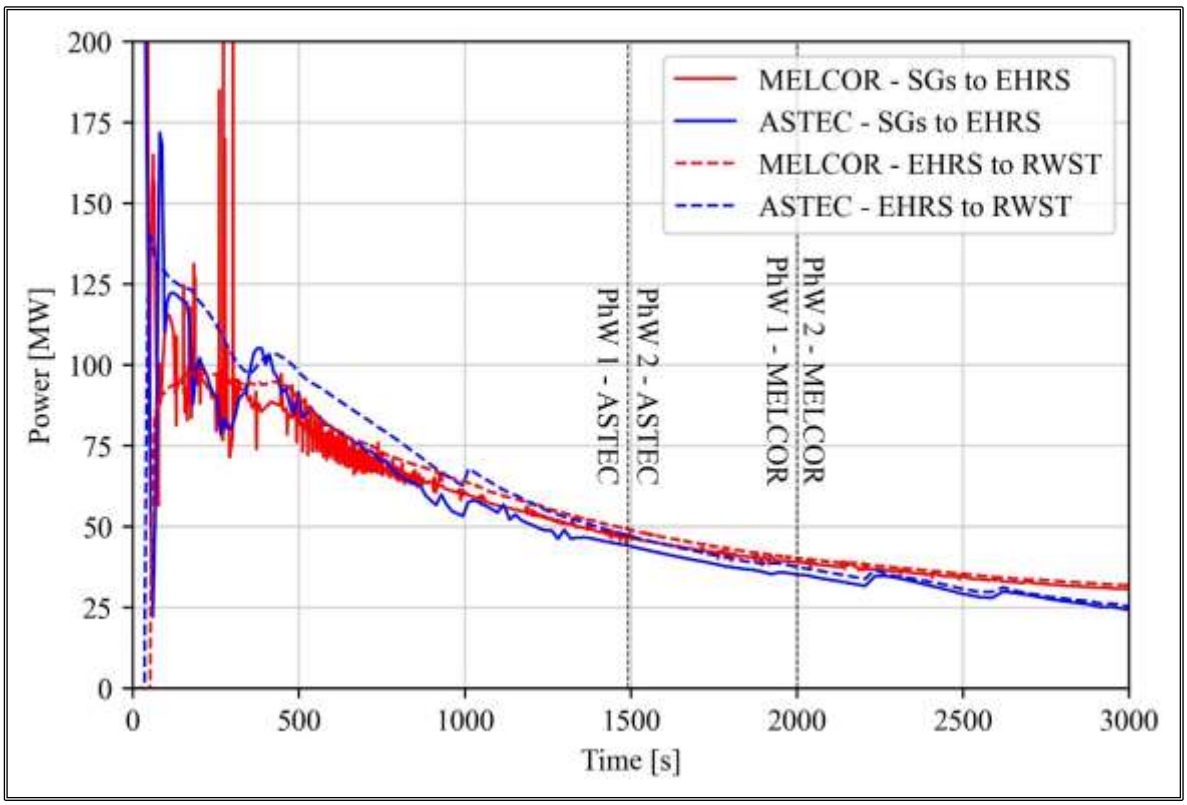

Figure 5.11 Power to EHRS – Power to RWST.

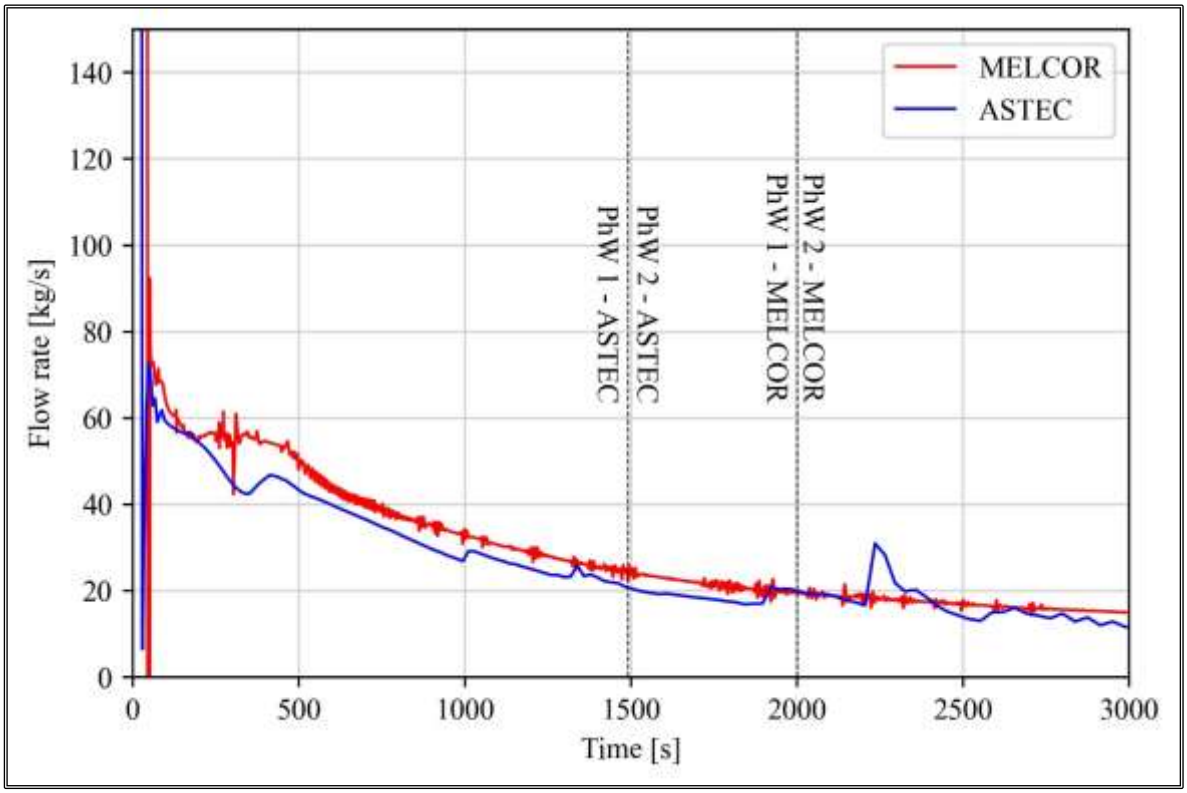

Figure 5.12 EHRS system mass flow rate.

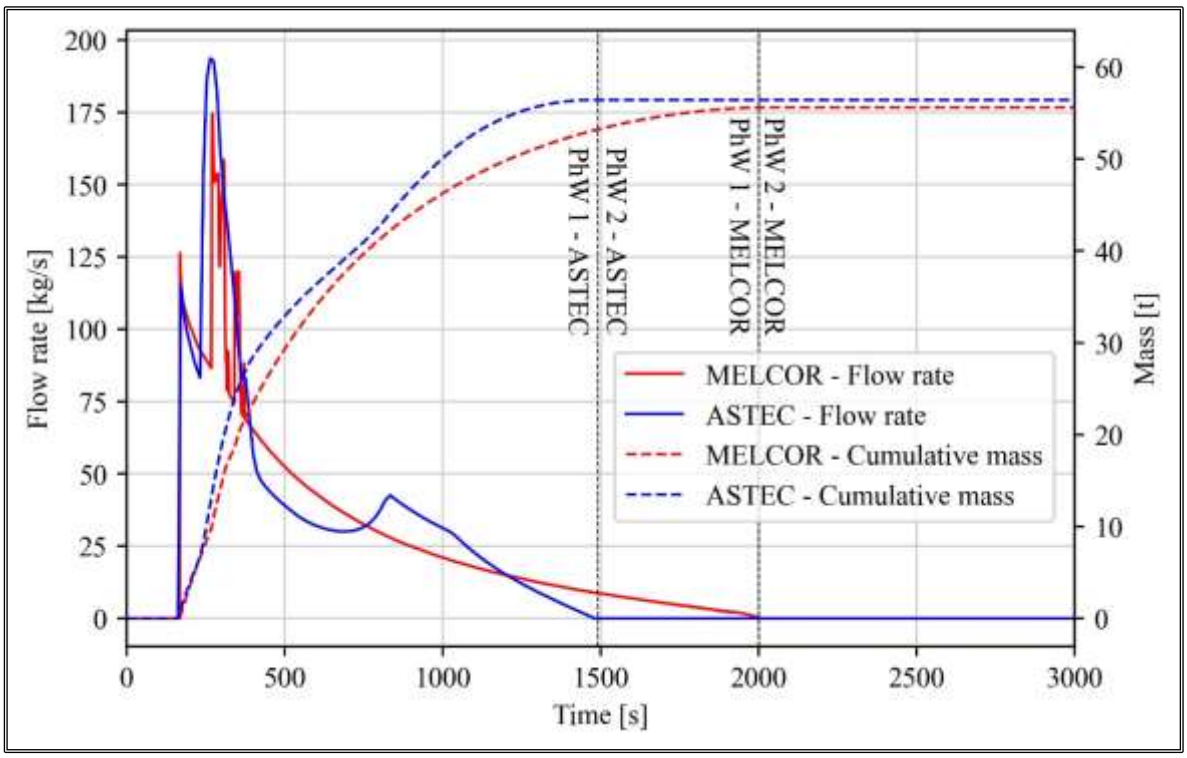

Figure 5.13 ADS Stage-1 mass flow rate and cumulative discharged mass.

A first peak of about 120 kg/s is predicted in MELCOR and ASTEC at the ADS Stage-1 opening. The second peak, given by the liquid water in PRZ reaching the ADS Stage-1 level, is foreseen at almost 190 kg/s in ASTEC and 175 kg/s in MELCOR. A total of 55 t of primary coolant is discharged in the prediction of both codes.

The reactor core uncover and core heat-up are prevented by the discharge through the undamaged DVI line by the injection of EBT and LGMS. This latter injects subsequently the pressure equalization between the RPV and DW, predicted at 1884 s after the SOT in MELCOR and 1398 s in ASTEC. In this regard, the normalized level of EBTs and LGMSs is shown in Figure 5.14. The trends of the levels in both codes are qualitatively similar except for the LGMS in the intact line in MELCOR which does not empty completely but remains about 20% filled. The normalized collapsed levels in the reactor core and the cavity are presented in Figure 5.15. It is underlined that the TAF is uncovered at about 175 s in both codes.

The pressure inversion between the DW and the PSSs determines the rise of the water level within the PSSs vent pipes and the subsequent injection of water into the containment, as shown in Figure 5.16 where the mass flow rate and the cumulative mass discharged from the PSSs vent pipes to DW are presented. Both codes predict this phenomenon, expected for the selected iPWR design as previously studied in [129] [146].

Some differences between the two codes are highlighted: a first injection of about 2700 s from the SOT with a peak of about 300 kg/s and a second peak of about 100 kg/s at about 6000 s are predicted in MELCOR. Instead, ASTEC predicts a first injection at 6000 s after the SOT with a peak of about 200 kg/s and a second injection at about 6500 s after the SOT with a peak of about 180 kg/s. Moreover, in the first 2000 seconds of the transient, the steam and gas flow rate from DW to PSSs vent pipes is higher in MELCOR than in ASTEC as can be noted in Figure 5.16. MELCOR predicts a major amount of cumulative mass discharged from the PSS vents to DW than ASTEC. It determines the different trends in the refill of the cavity, as shown in the previous Figure 5.15.

The PSS vent pipes injection to DW allows to completion of the core refill phase and coupled with the LGMS injection, the reactor core long-term cooling. In Figure 5.17 the maximum cladding temperature trend and the trend of RWST tank temperature are presented for both codes. In particular, the maximum cladding temperature is kept constant at about 400 K after about 10000 s after the SOT in both codes, ensuring the long-term cooling of the reactor core. In Table 5.4 the main timings of the event characterizing the DBA sequences for both codes are presented.

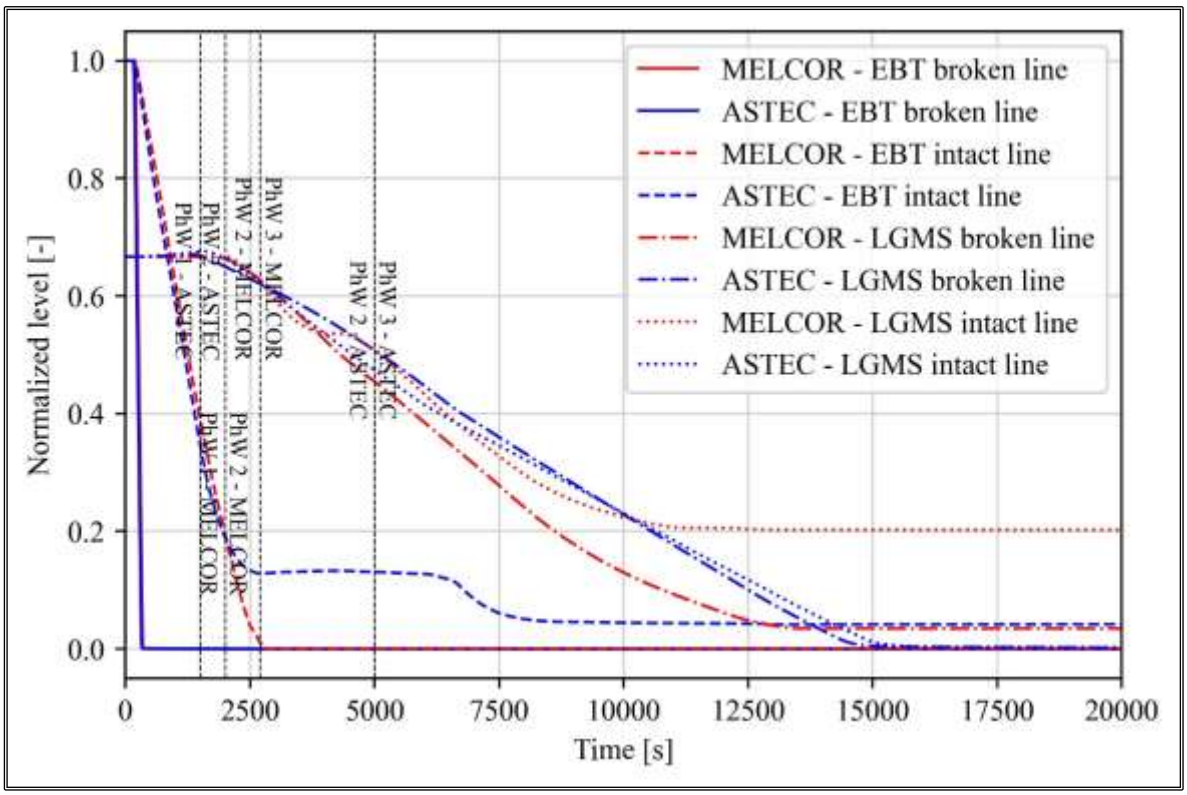

Figure 5.14 Normalized level of EBTs and LGMSs.

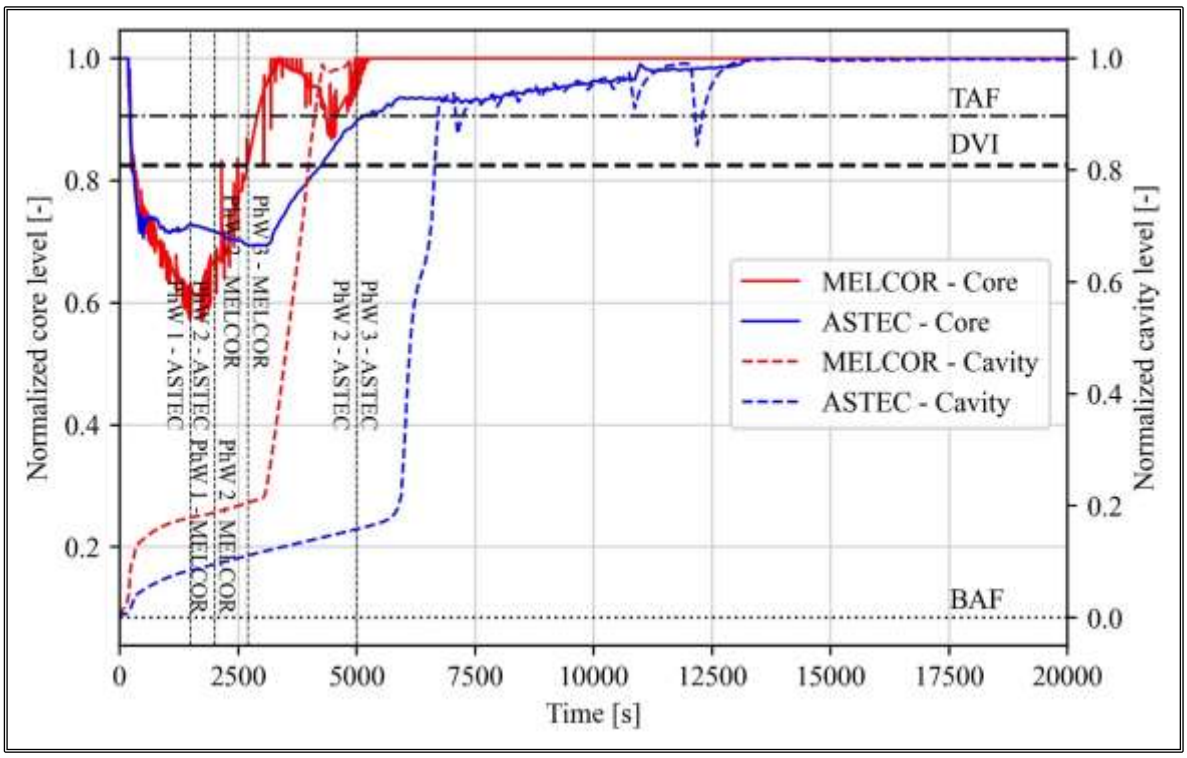

Figure 5.15 Reactor core and cavity normalized level.

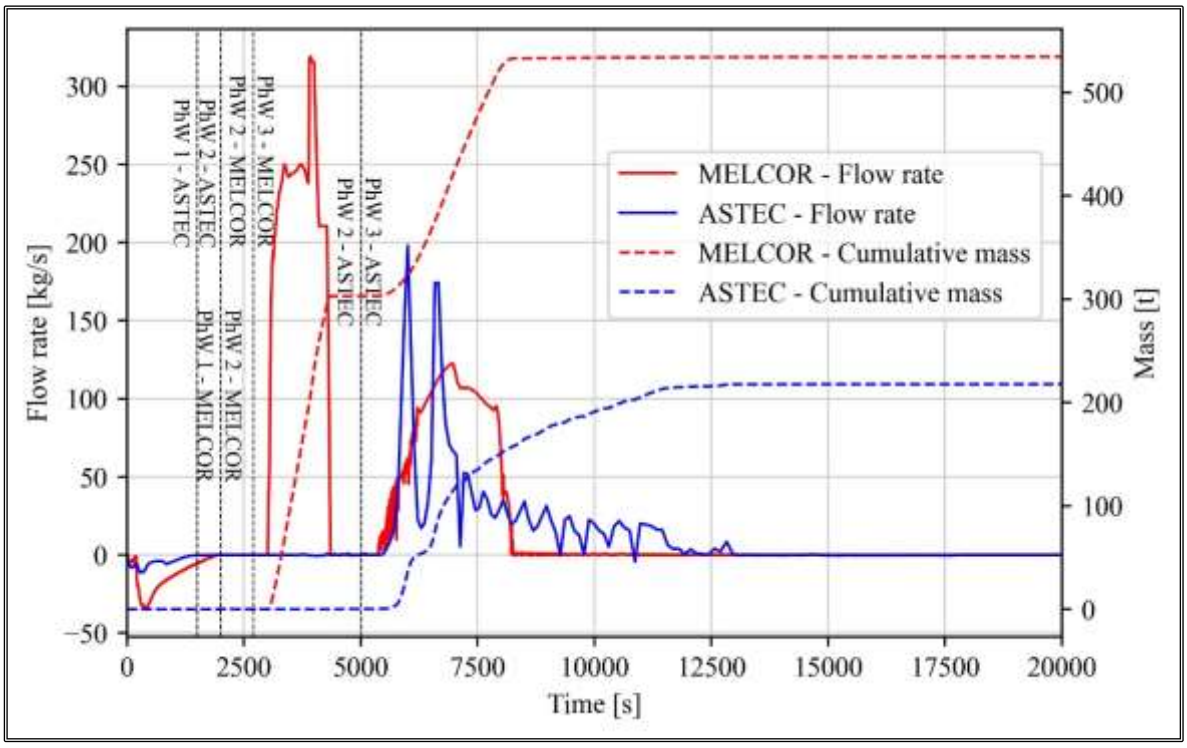

Figure 5.16 Mass flow rate from PSSs vent pipes to DW.

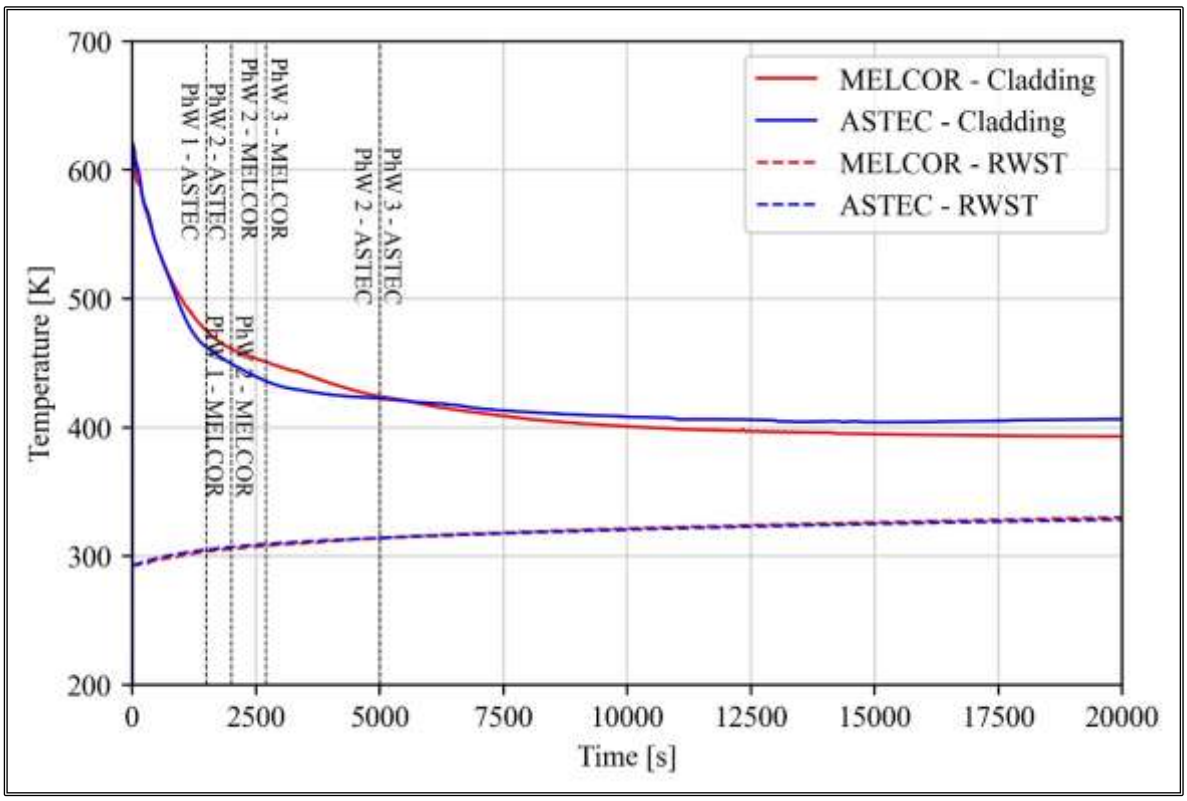

Figure 5.17 Maximum cladding temperature and RWST temperature.

Table 5.4 Table of the main events.

Event	MELCOR [s]	ASTEC [s]
Break	0	0
High containment pressure signal	41	20
SCRAM	41	25
EHRS loops opening	50	28
Low PRZ water level signal	122	65
RCP coast-down starts	122	80
Natural circulation begins through RI-DC valves	127	84
Low PRZ pressure signal	148	158
ADS Stage-1 opening	168	166
EBTs opening	152	160
Low DP RV-Containment	1884	1398
LGMSs opening	1888	1401
Low LGMS mass	12265	12902

5.6 Uncertainty analysis of the Design Basis Accident sequence

To investigate the uncertainties of the code on the main thermal-hydraulic phenomena during the DBA scenario described in 5.3 and simulated in 5.5.2, the uncertainty analysis adopting the methodology described in the previous chapters has been carried out. In addition, this analysis is a key step in assessing the applicability of the uncertainty methodology in view of its use in SA scenarios. The uncertainty analysis has been carried out using the in-house tool developed in Python and described previously in 2.4.2.

5.6.1 Hypotheses of the uncertainty analysis

This study aims to develop a comprehensive uncertainty analysis on a generic iPWR design, rather than conducting a detailed uncertainty assessment, and to give preliminary information about the statistical correlation between the most relevant FOMs in terms of safety and uncertain input parameters, in particular the ones related to the passive safety system. Following as done in [44], the FOMs selected for the present analysis are the peak of maximum cladding temperature (referred to as FOM_1)[9], the minimum collapsed coolant level in the core region (referred to as FOM_2) and the maximum containment pressure (referred to as FOM_3).

These FOMs are of high importance from the point of view of the safety of SMR nuclear reactors, particularly iPWRs. Then, fourteen uncertain input parameters associated with thermal-hydraulics as well as passive safety systems have been chosen for this analysis. Table 5.5 presents the uncertain input parameters used. In this regard, they have been selected and extrapolated from [37] [67] [143] and based on engineering judgment.

Considering Wald's Formula (see 1.5.2.1) for three FOMs and the one-sided tolerance level, 129 code runs are needed considering a probability γ and confidence level β of 0.95. For the present application, possible failed runs are not considered and replaced with new ones with a different combination of the uncertain input parameters (see 2.3.3).

5.6.2 Results

Table 5.6 presents the main statistical parameters which characterize the FOMs. It underlined an uncertainty band width of 42.77 K for FOM_1, 0.7 m for FOM_2 and then, 3.76E5 Pa for FOM_3. From Figure 5.18 to Figure 5.23 the empirical CDF and PDF of the

[9] In relation to the FOM_1, the maximum cladding temperature after 1000 seconds has been chosen to better analyse the causes that lead, as will be seen in Figure 5.42, to the widening of the uncertainty band before the start of the second PhW.

FOMs are presented. These figures also show the comparison between the reference value and the calculated statistical parameters such as the mean, median, lower and upper bound.

Table 5.5 Uncertain input parameters [37] [67] [143].

Uncertain input parameter	Unit	Distribution Type	Reference value	Lower and Upper bound	
Decay Power	[-] (multiplier)	Normal	1.0	min	0.98
				max	1.02
PRZ initial pressure	[Pa]	Normal	1.55E7	min	1.54E7
				max	1.56E7
EBT initial temperature	[K]	Normal	321.9	min	311.9
				max	331.9
LGMS initial temperature	[K]	Normal	321.9	min	311.9
				max	331.9
Initial DW pressure	[Pa]	Uniform	1.013E5	min	0.85E5
				max	1.15E5
RWST initial liquid level	[m]	Normal	9.0	min	8.9390
				max	9.0610
RWST and environment initial temperature	[K]	Uniform	293.0	min	283.0
				max	303.0
Heat Transfer Surface EHRS HXs	[-] (multiplier)	Uniform	1.0	min	0.75
				max	1.25
Break flow discharge coefficient	[-]	Uniform	0.7	min	0.7
				max	1.0
EHRS valves loss coefficient	[%]	Uniform	0	min	-100
				max	+100
EBT valves loss coefficient	[%]	Uniform	0	min	-100
				max	+100
LGMS valve loss coefficient	[%]	Uniform	0	min	-100
				max	+100
ADS Stage-1 loss coefficient	[%]	Uniform	0	min	-100
				max	+100
ADS Stage-2 loss coefficient	[%]	Uniform	0	min	-100
				max	+100

Table 5.6 Statistical parameters of the FOMs.

Statistical parameter	FOM_1		FOM_2		FOM_3	
	Value	Unit	Value	Unit	Value	Unit
Mean	504.74	[K]	4.46	[m]	11.37E5	[Pa]
Median	505.53	[K]	4.47	[m]	11.32E5	[Pa]
Lower Bound	483.66	[K]	4.05	[m]	9.73E5	[Pa]
Upper Bound	526.43	[K]	4.75	[m]	13.49E5	[Pa]
Standard deviation	8.23	[K]	0.16	[m]	0.82E5	[Pa]
Coefficient of variation	0.016	[-]	0.037	[-]	0.072	[-]

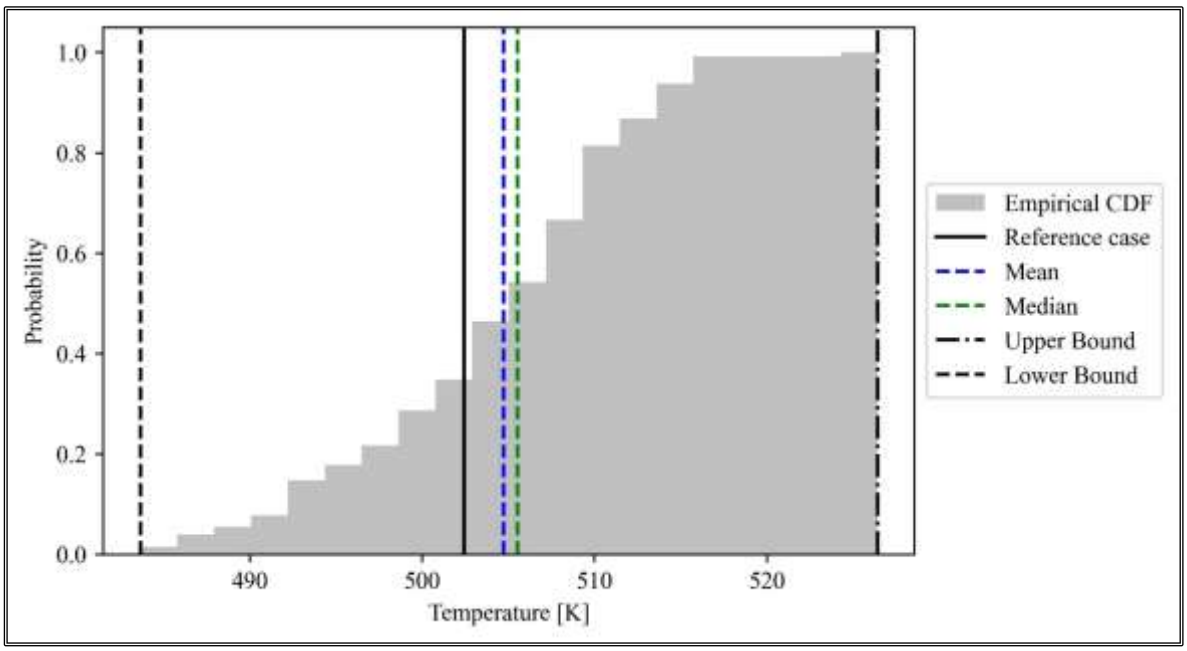

Figure 5.18 Empirical CDF of the FOM_1.

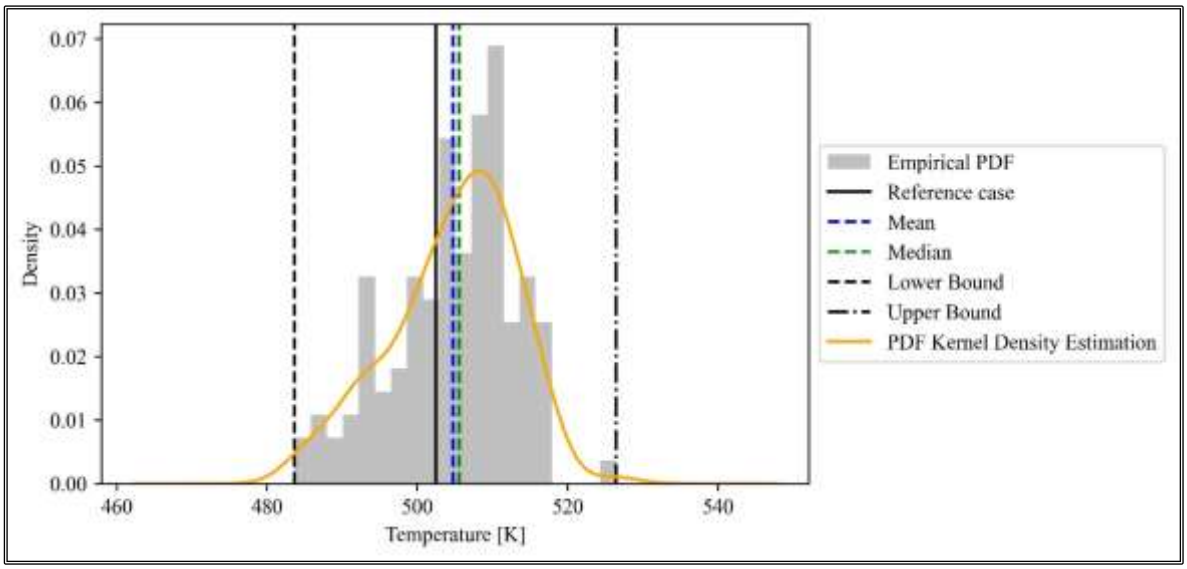

Figure 5.19 Empirical PDF of the FOM_1.

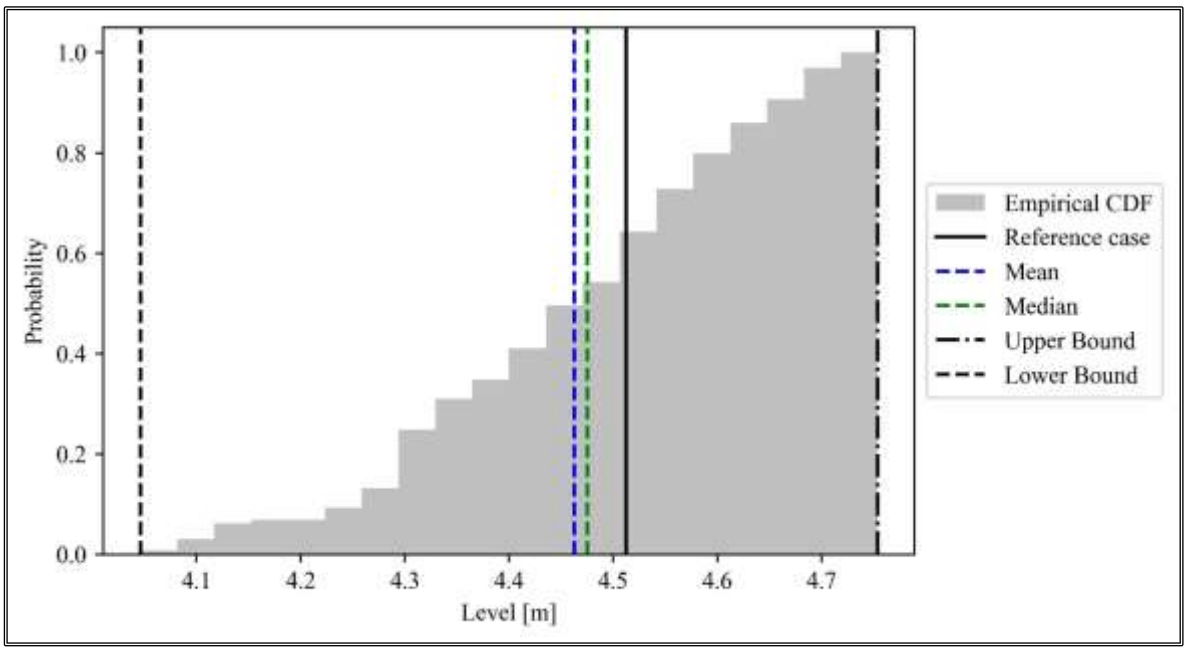

Figure 5.20 Empirical CDF of the FOM_2.

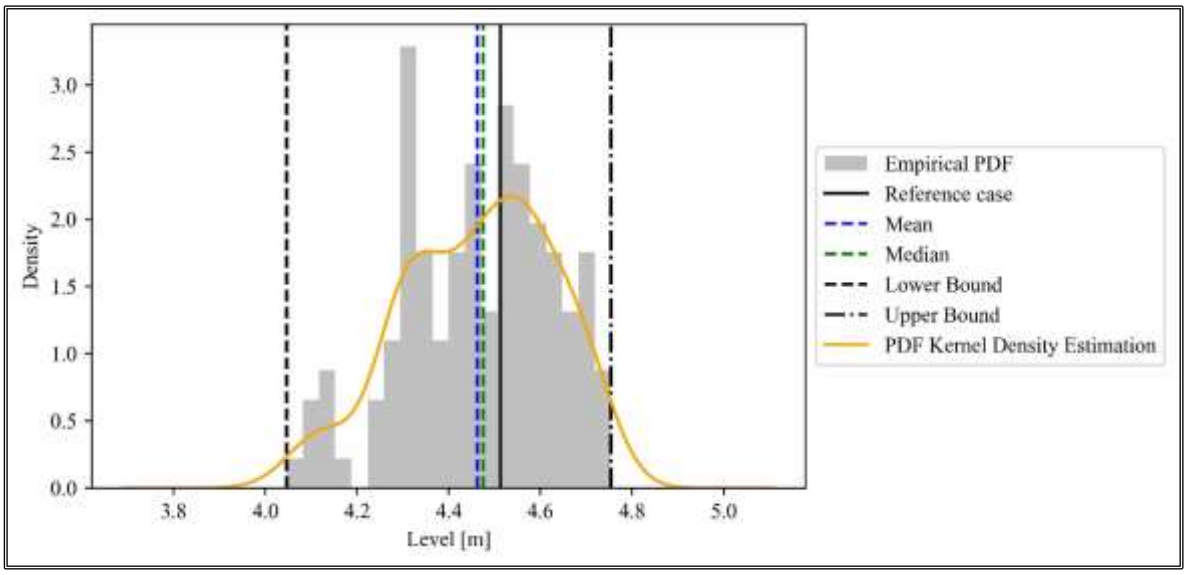

Figure 5.21 Empirical PDF of the FOM_2.

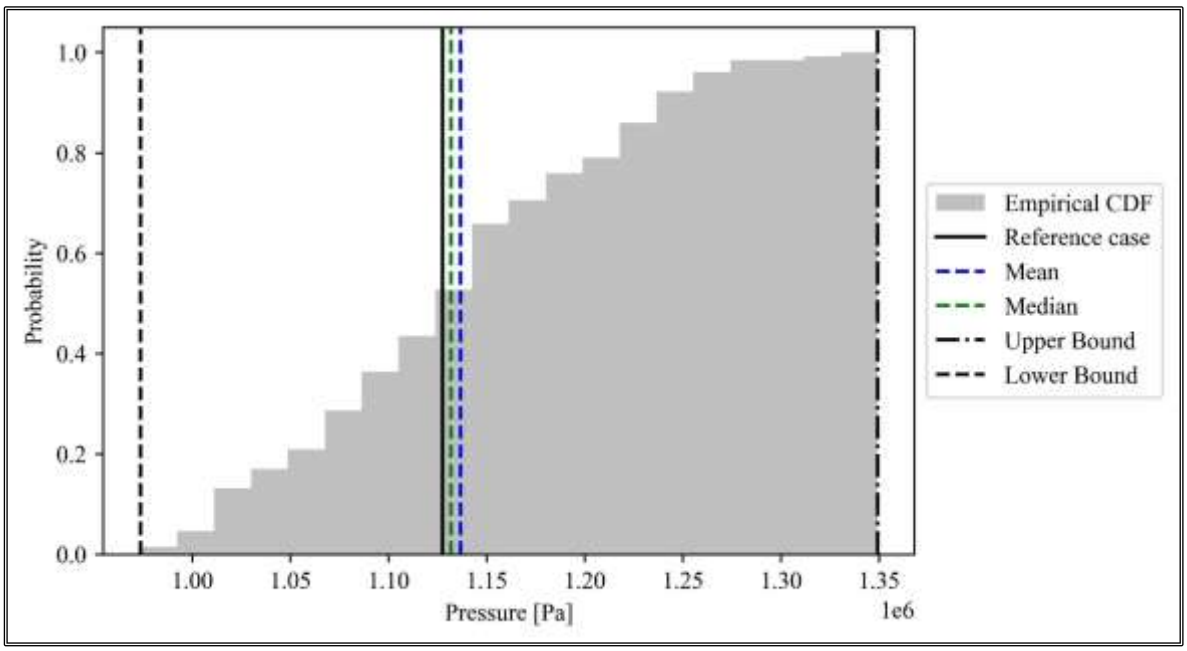

Figure 5.22 Empirical CDF of the FOM_3.

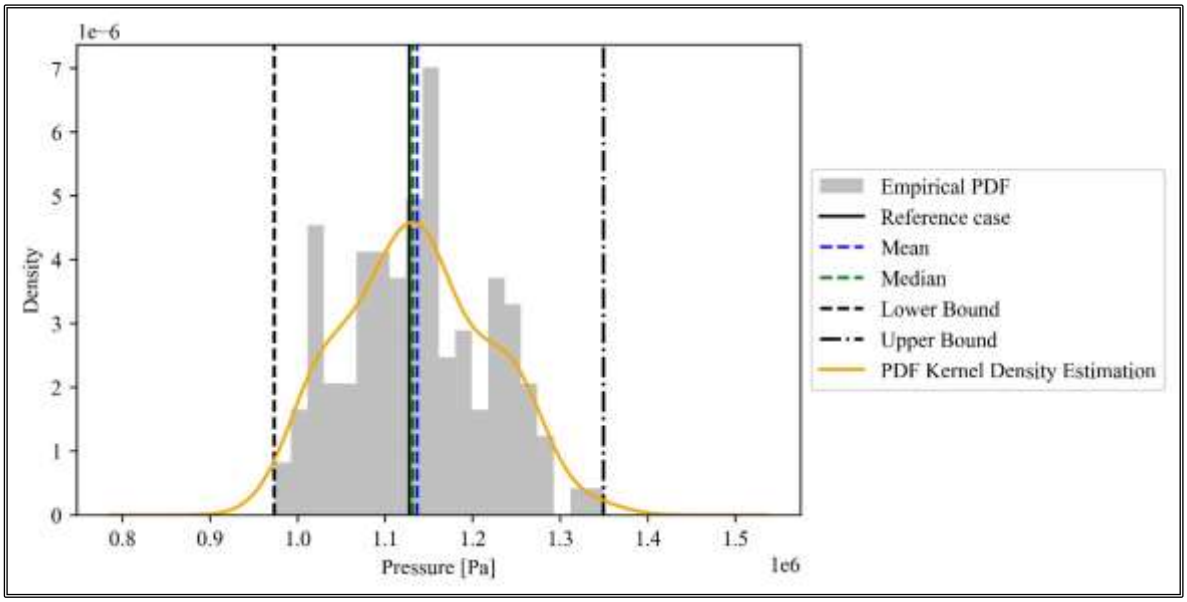

Figure 5.23 Empirical PDF of the FOM_3.

The simple and simple rank correlation coefficients have been calculated by Pearson and Spearman's correlations for each FOM and each uncertain input parameter. From the statistical correlation analysis, it emerges that the FOM_1 presents a significant statistical correlation with the heat transfer surface of the EHRS HXs (negative correlation) and the ADS Stage-1 loss coefficient (positive correlation). Instead, the other uncertain input parameters have a low statistical correlation with the FOM_1, as shown by the simple and simple rank coefficients listed in Figure 5.24 to Figure 5.27. The previously discussed

significant statistical correlations can be visualized by scatter plots and the trend curves obtained through linear regression techniques in Figure 5.28 and Figure 5.29.

The FOM_2 presents a moderate statistical correlation with the initial DW pressure (positive correlation), the heat transfer surface of EHRS HXs (negative correlation) and a significant correlation with the ADS Stage-1 loss coefficient (positive correlation). From Figure 5.30 to Figure 5.33, the simple and simple rank correlation coefficients referred to FOM_2 are presented. Then, Figure 5.34, Figure 5.35 and Figure 5.36 show the scatter plots of FOM_2 values and the values of the uncertain input parameters with a moderate or significant correlation.

Finally, FOM_3 presents, as expected, a moderate statistical correlation with the initial DW pressure (positive correlation) and a significant statistical correlation with the ADS Stage-1 loss coefficient (negative correlation). From Figure 5.37 to Figure 5.40, the simple and simple rank coefficients related to FOM_3 are presented.

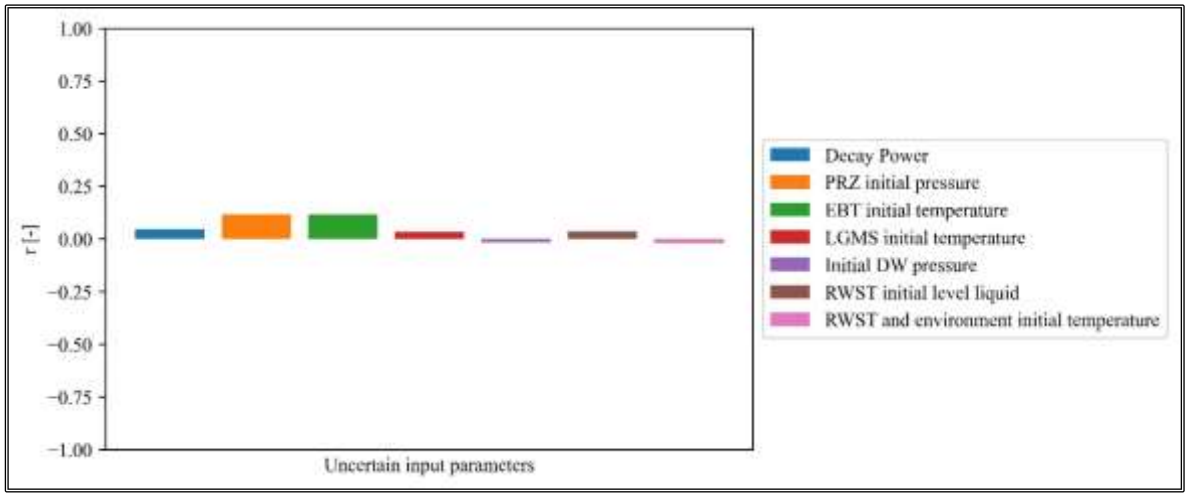

Figure 5.24 Simple correlation coefficient – FOM_1 (a).

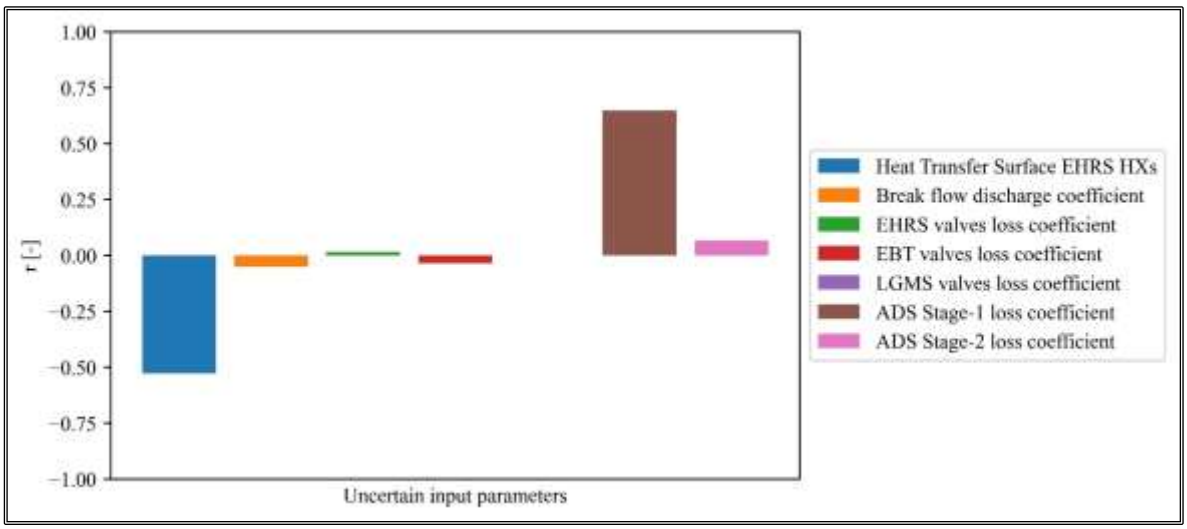

Figure 5.25 Simple correlation coefficient – FOM_1 (b).

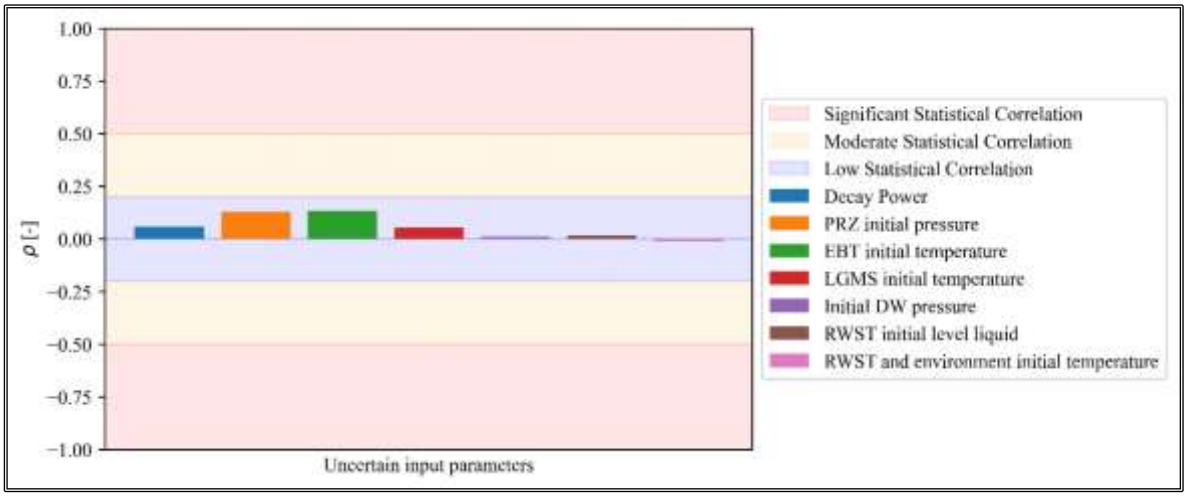

Figure 5.26 Simple rank correlation coefficient – FOM_1 (a).

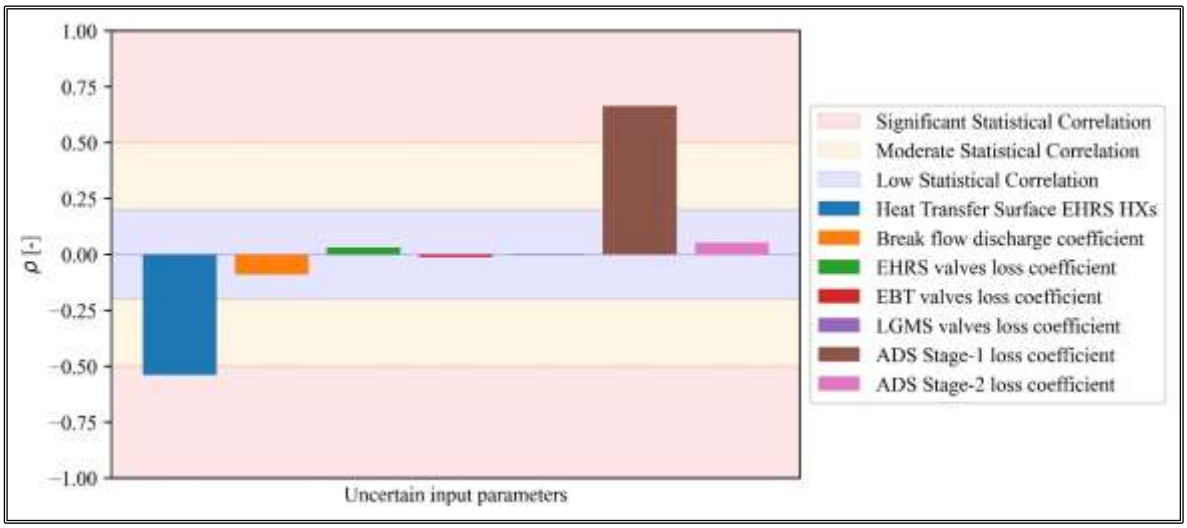

Figure 5.27 Simple rank correlation coefficient – FOM_1 (b).

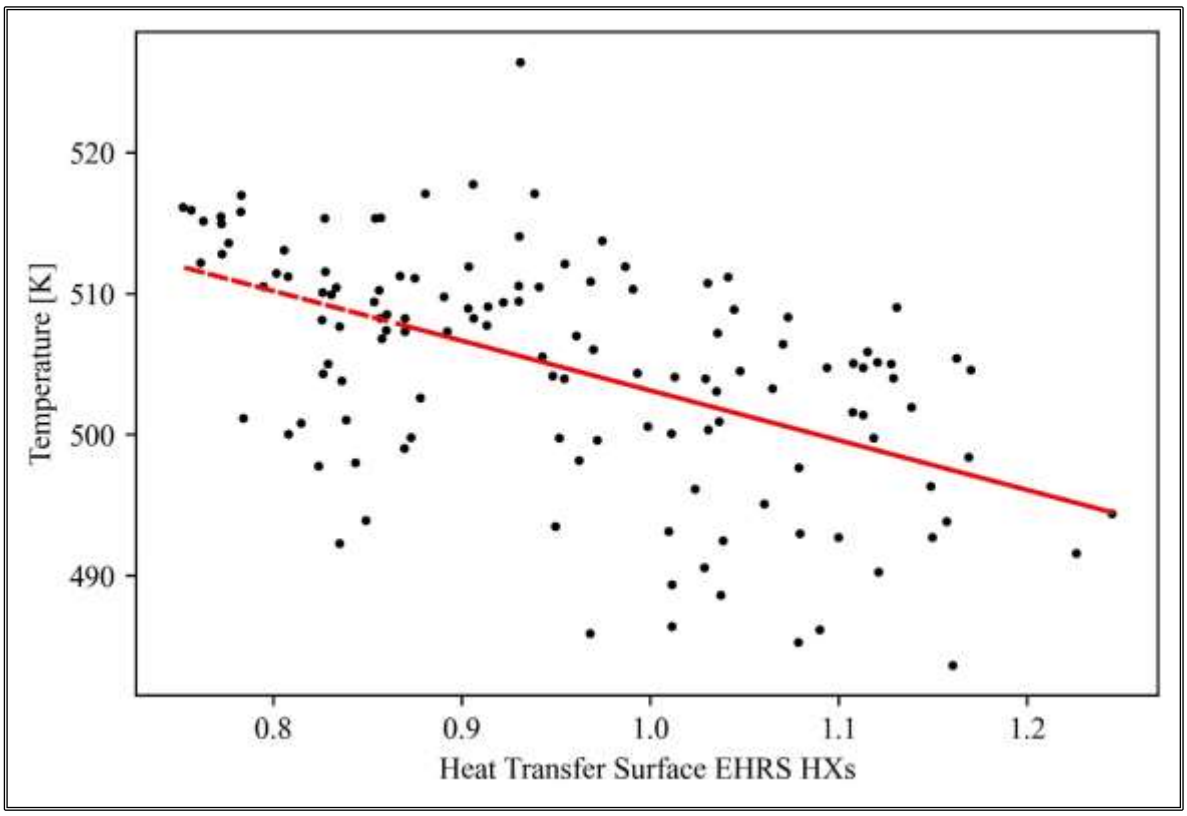

Figure 5.28 Scatter plot of FOM_1 and Heat Transfer Surface EHRS HXs values.

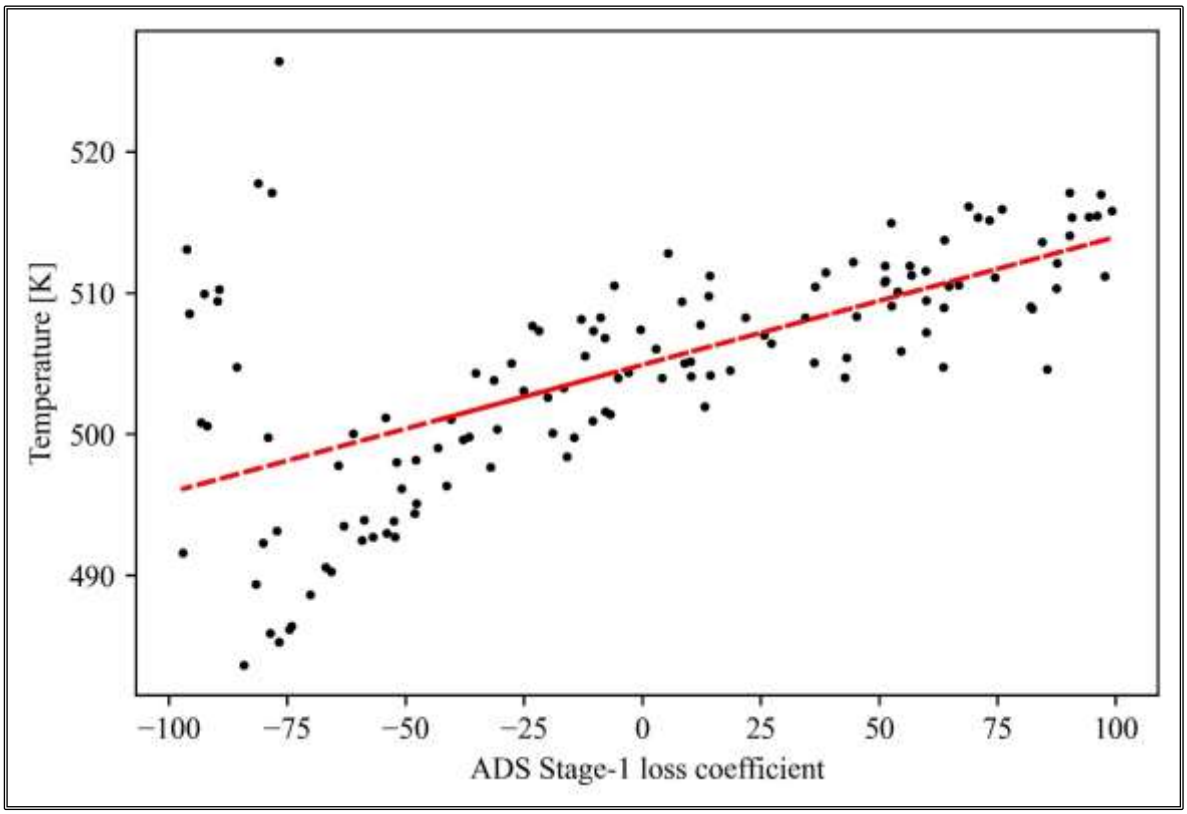

Figure 5.29 Scatter plot of FOM_1 and ADS Stage-1 loss coefficient values.

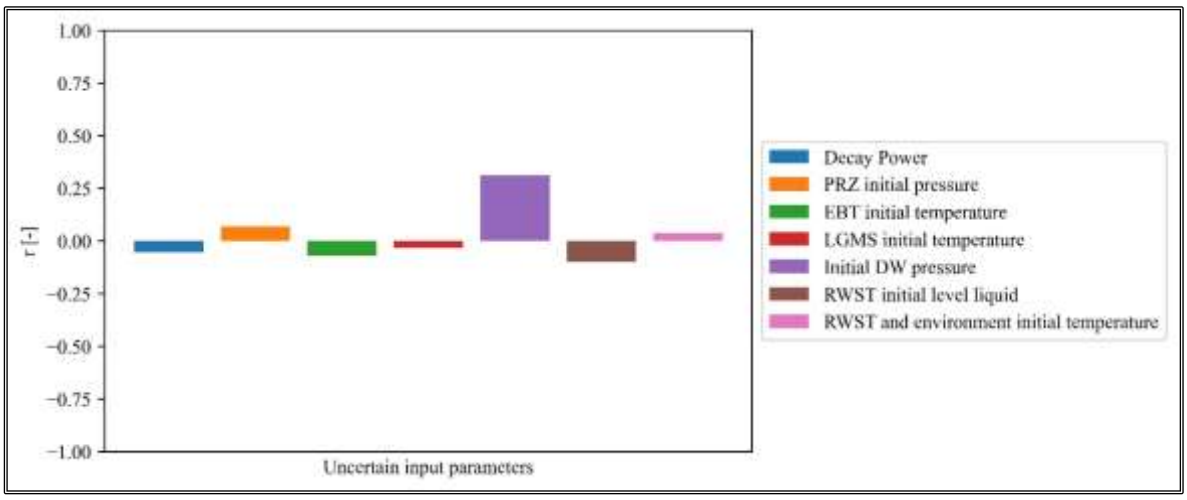

Figure 5.30 Simple correlation coefficient – FOM_2 (a).

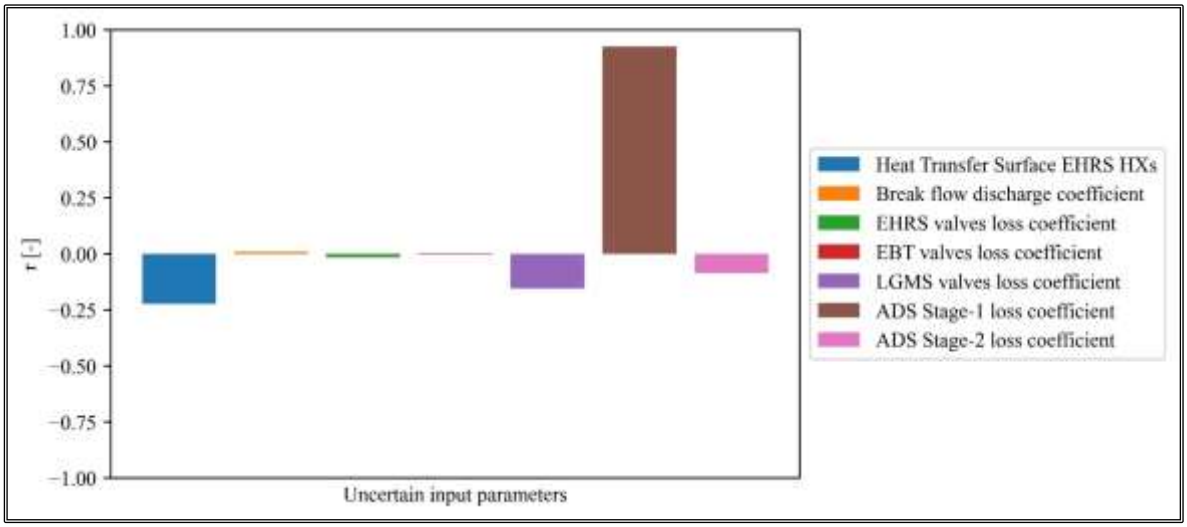

Figure 5.31 Simple correlation coefficient – FOM_2 (b).

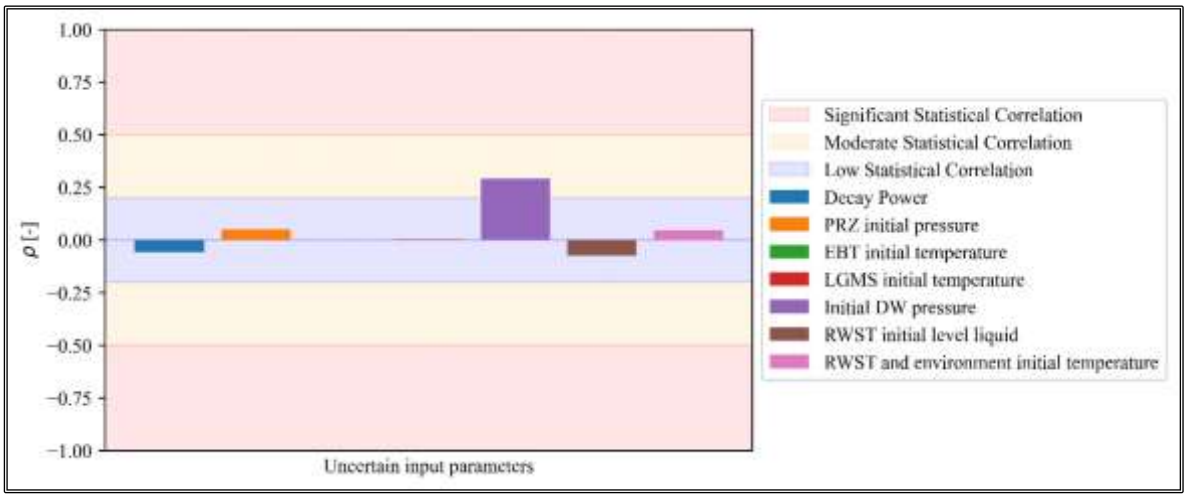

Figure 5.32 Simple rank correlation coefficient – FOM_2 (b).

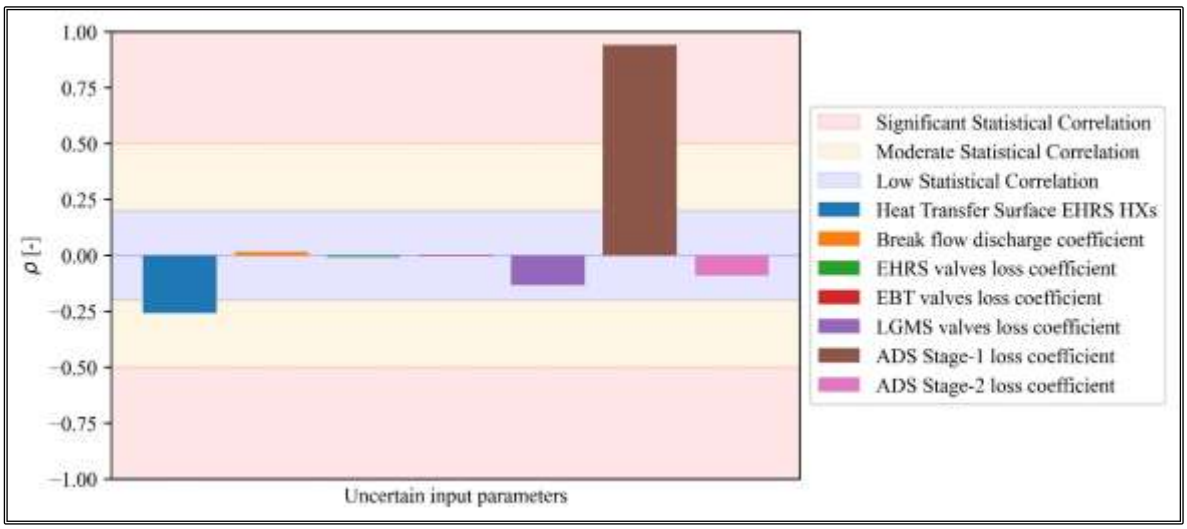

Figure 5.33 Simple rank correlation coefficient – FOM_2 (b).

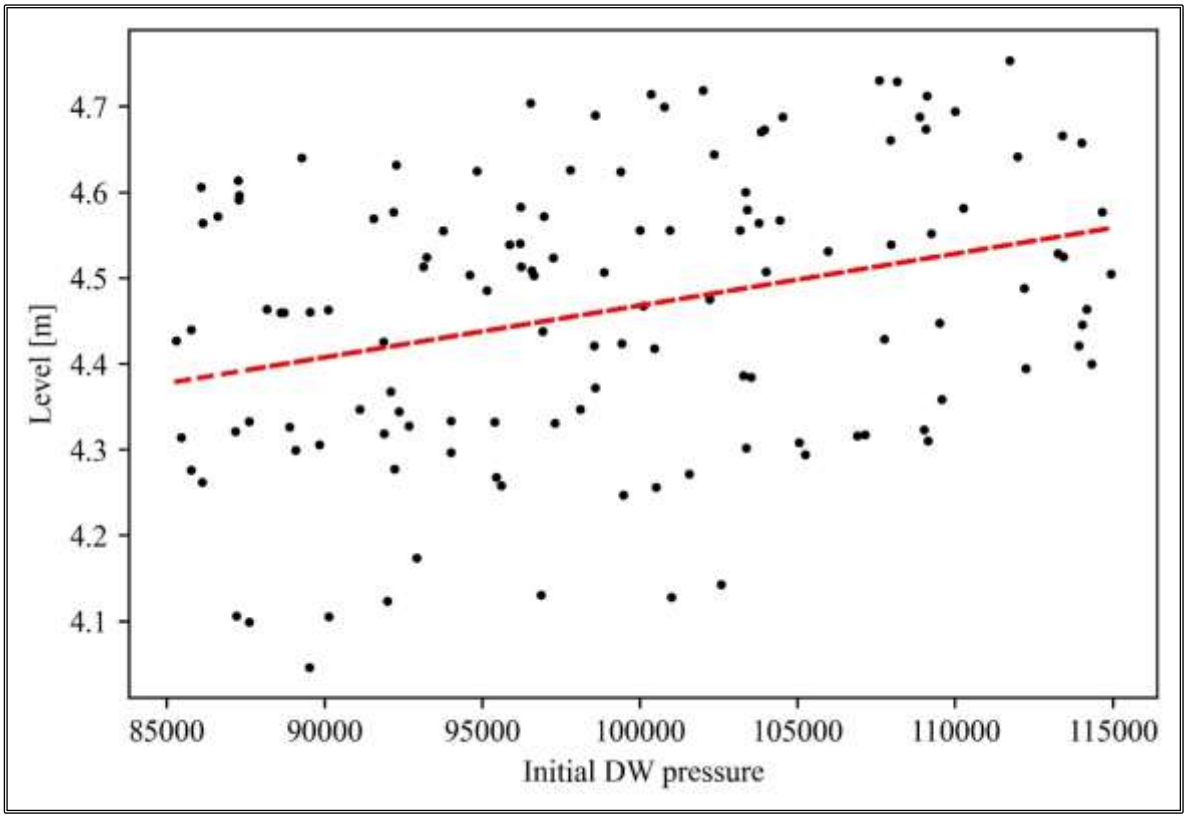

Figure 5.34 Scatter plot of FOM_2 and initial DW pressure values.

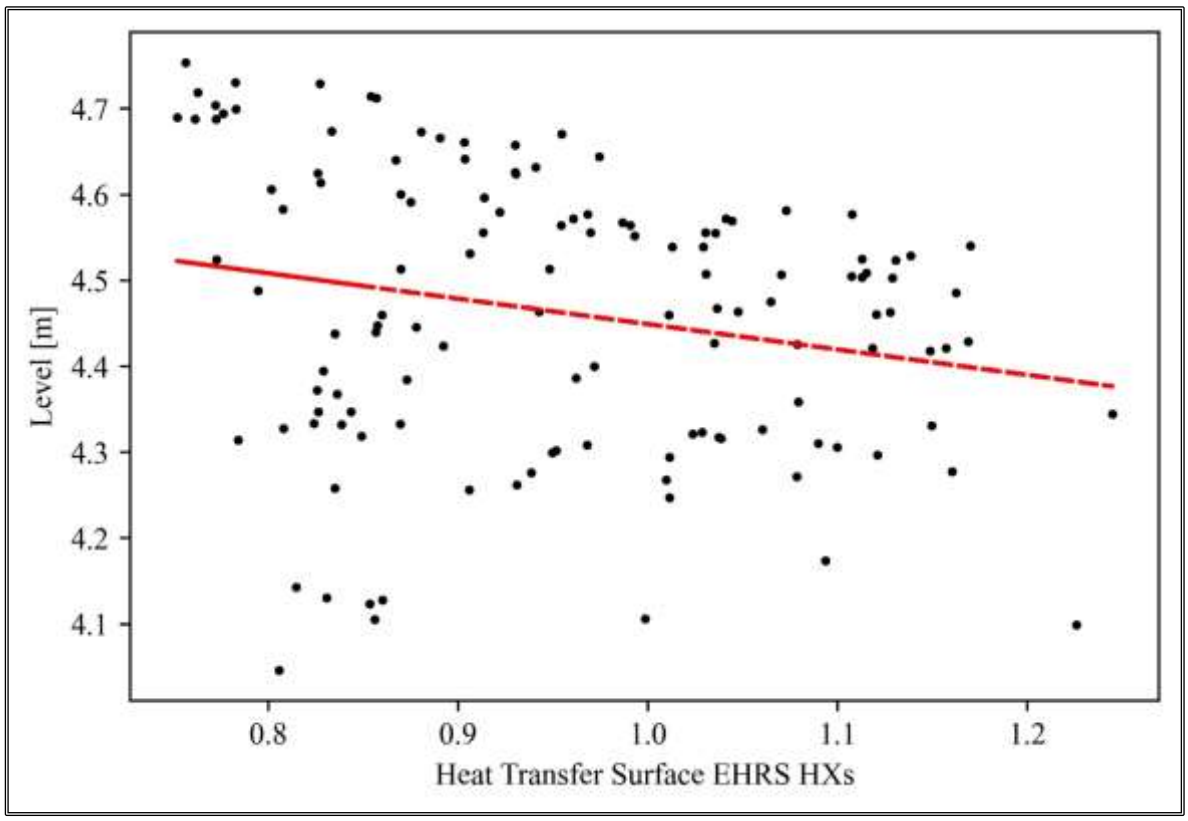

Figure 5.35 Scatter plot of FOM_2 and Heat Transfer Surface EHRS HXs values.

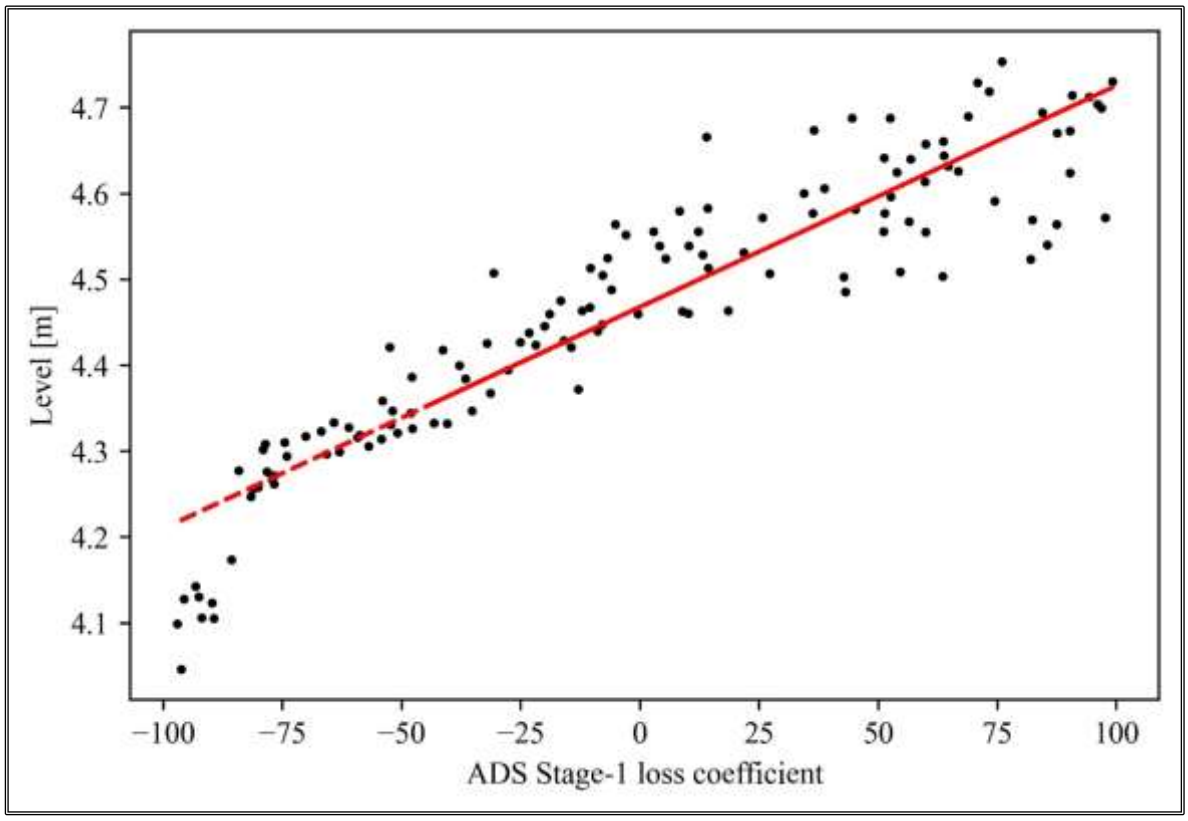

Figure 5.36 Scatter plot of FOM_2 and ADS Stage-1 loss coefficient values.

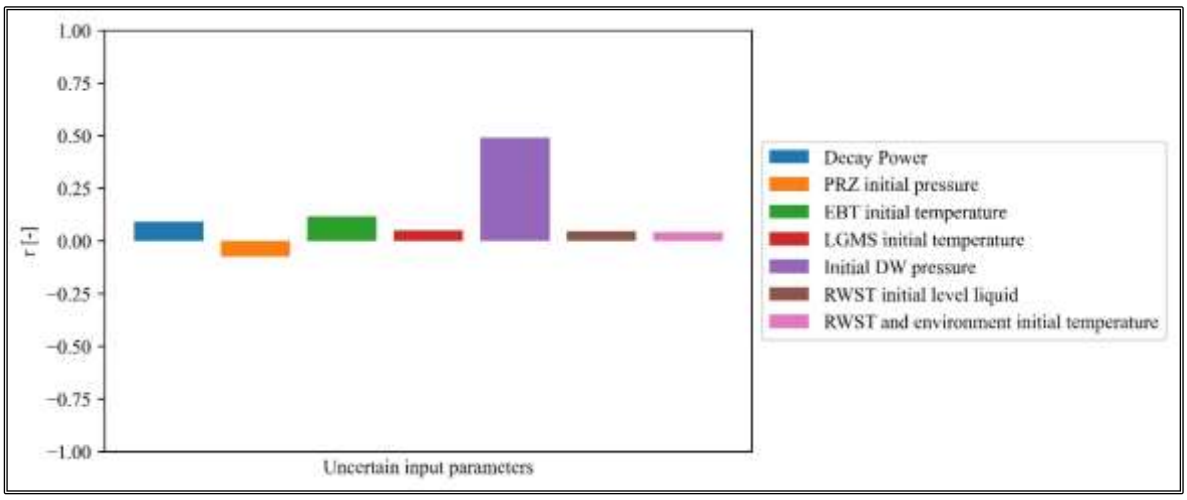

Figure 5.37 Simple correlation coefficient – FOM_3 (a).

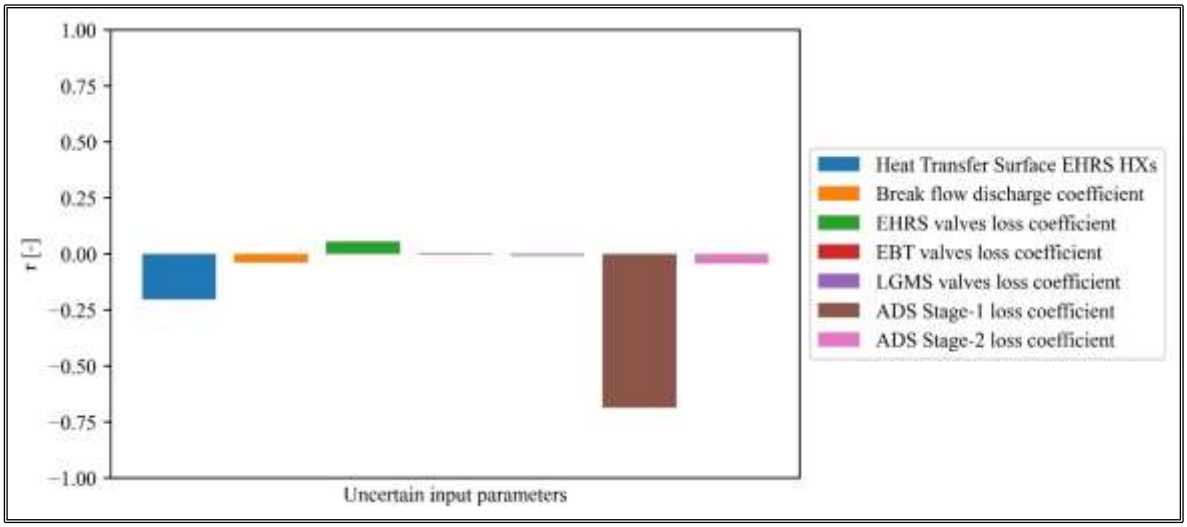

Figure 5.38 Simple correlation coefficient – FOM_3 (b).

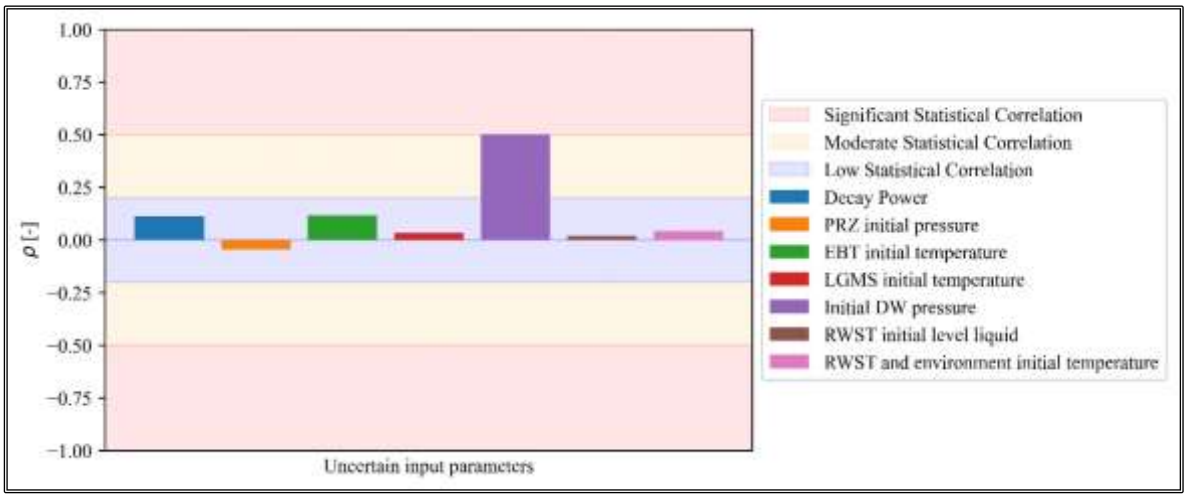

Figure 5.39 Simple rank correlation coefficient – FOM_3 (a).

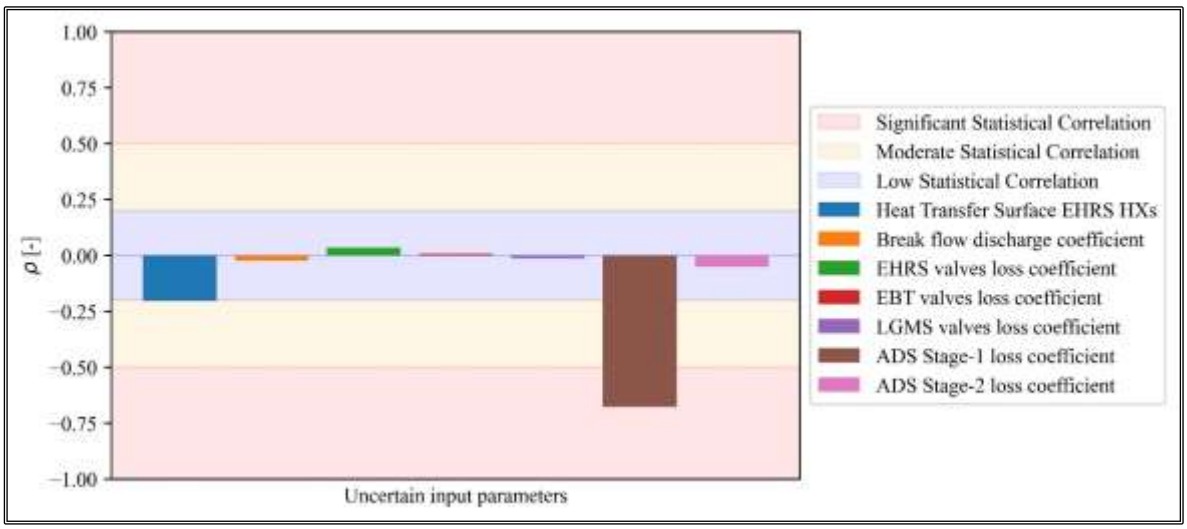

Figure 5.40 Simple rank correlation coefficient – FOM_3 (b).

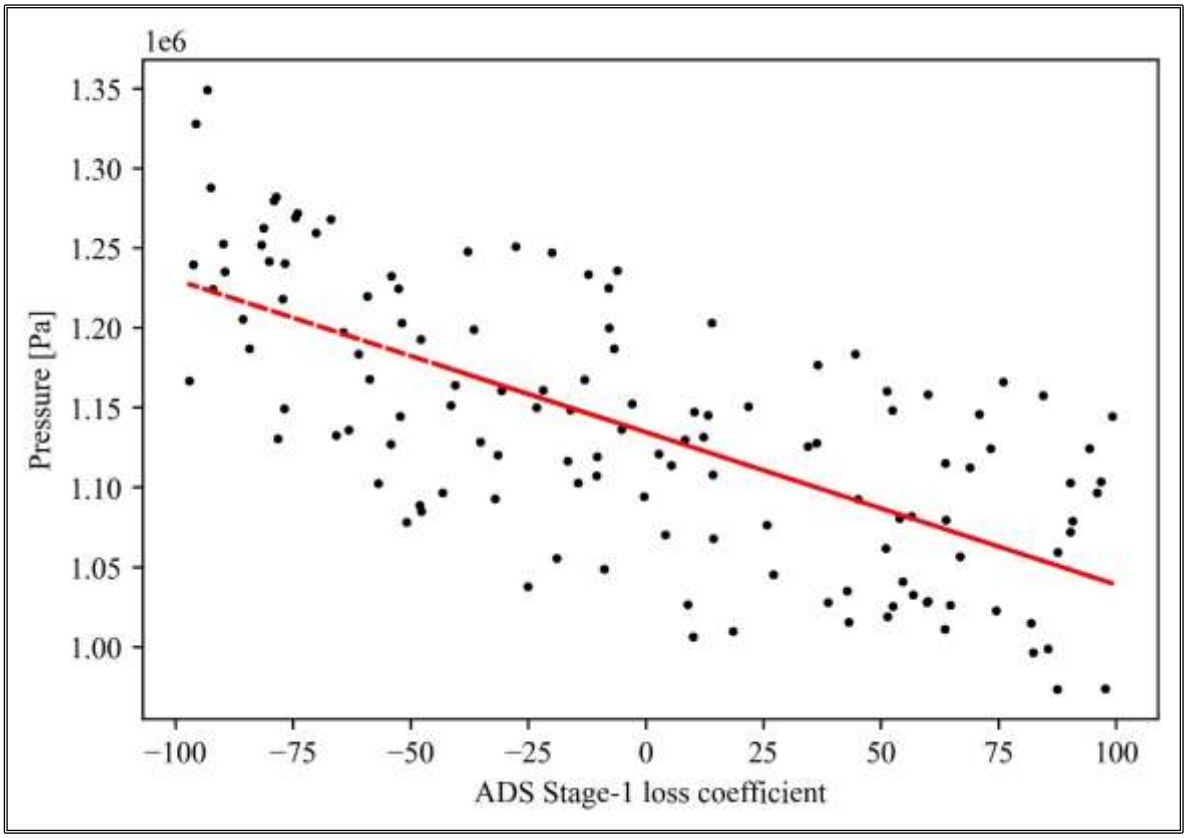

Figure 5.41 Scatter plot of FOM_3 and ADS Stage-1 loss coefficient.

To characterize the uncertainty band, the values of the N cases referred to the maximum cladding temperature, core collapsed coolant level and DW pressure have been compared at each time-step to the reference case and the upper and lower bound, mean and median.

The maximum cladding temperature presents a quantifiable uncertainty band of about 25 K for the first 1000 s of the transient, after which it increases, reaching the greatest amplitude

of about 50 K, between 1000 and 2000 s after the SOT, as shown in Figure 5.42. In this time region of the transient, the code predicts some local peaks of the maximum cladding temperature up to 525 K.

After 2000 s, the uncertainty band remains almost constant and equal to about 25 K. The mean and median, in agreement with the previous analyses, have been calculated at each time step. Concerning the maximum cladding temperature, the mean and the median are qualitatively and quantitatively in agreement with the reference case for the first 3000 s of the transient, after which they have a lower value than the reference case. The trend of the uncertainty band is reflected in the trend of the standard deviation, which is presented in Figure 5.43 together with the coefficient of variation.

Figure 5.44[10] shows the uncertainty band related to the core collapsed coolant level. It increases its amplitude 200 s after the SOT to a value of 1.20 m and reaches its maximum value at about 3000 s after the SOT. Furthermore, the uncovering of the TAF during the transient presents a high uncertainty band in time terms, quantifiable on 4000 s.

The mean and median are characterized by a qualitative and quantitative similarity of their time-trend with the reference case during the first 2000 s of the transient. After this time point, a qualitatively and quantitatively slightly different trend is highlighted. The standard deviation and coefficient of variation at each time step for the core collapsed coolant level are presented in Figure 5.45.

Concerning DW pressure, the uncertainty band presents a maximum value at about 3000 s after the SOT equal to about 7E5 Pa. Moreover, the trend of the mean and the median is in qualitative and quantitative agreement with the reference case. Finally, the standard deviation and coefficient of variation are presented in Figure 5.45.

[10] With reference to Figure 5.44, the uncertainty band is cut just above the TAF as only the volume representative of the core region has been considered for the collapsed level.

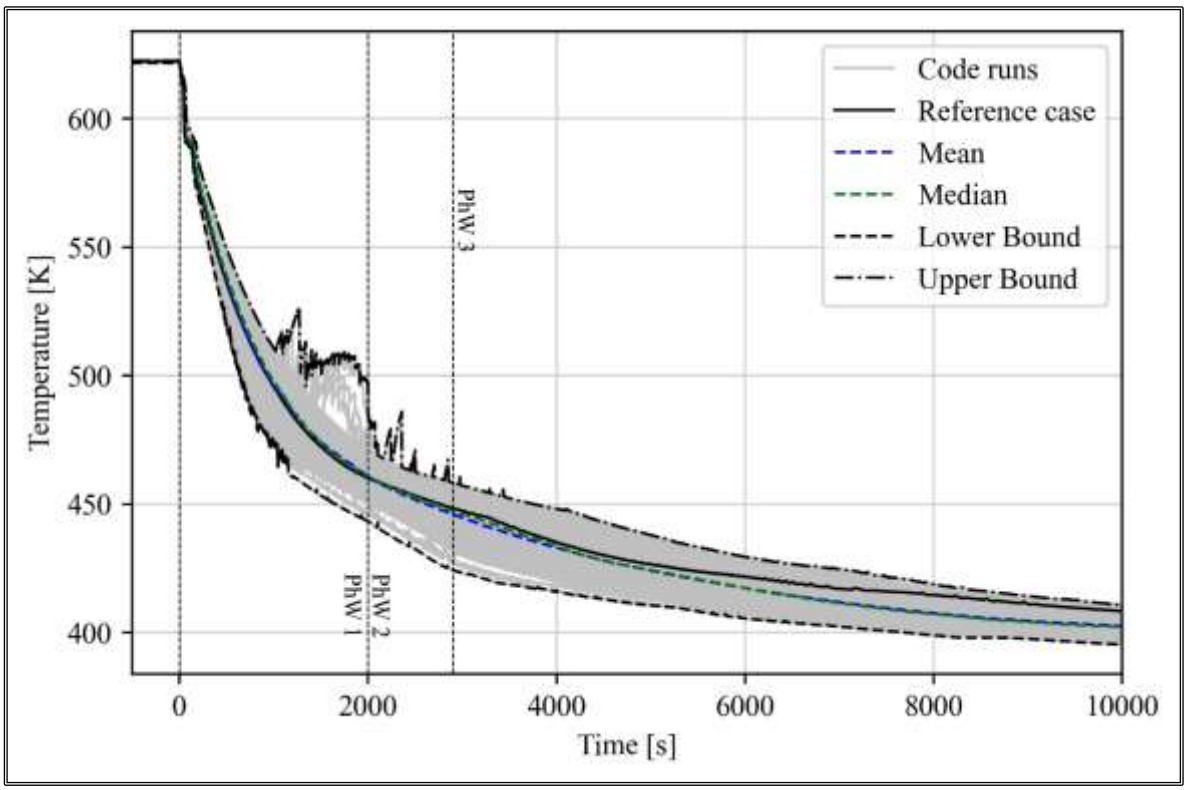

Figure 5.42 Maximum cladding temperature uncertainty band.

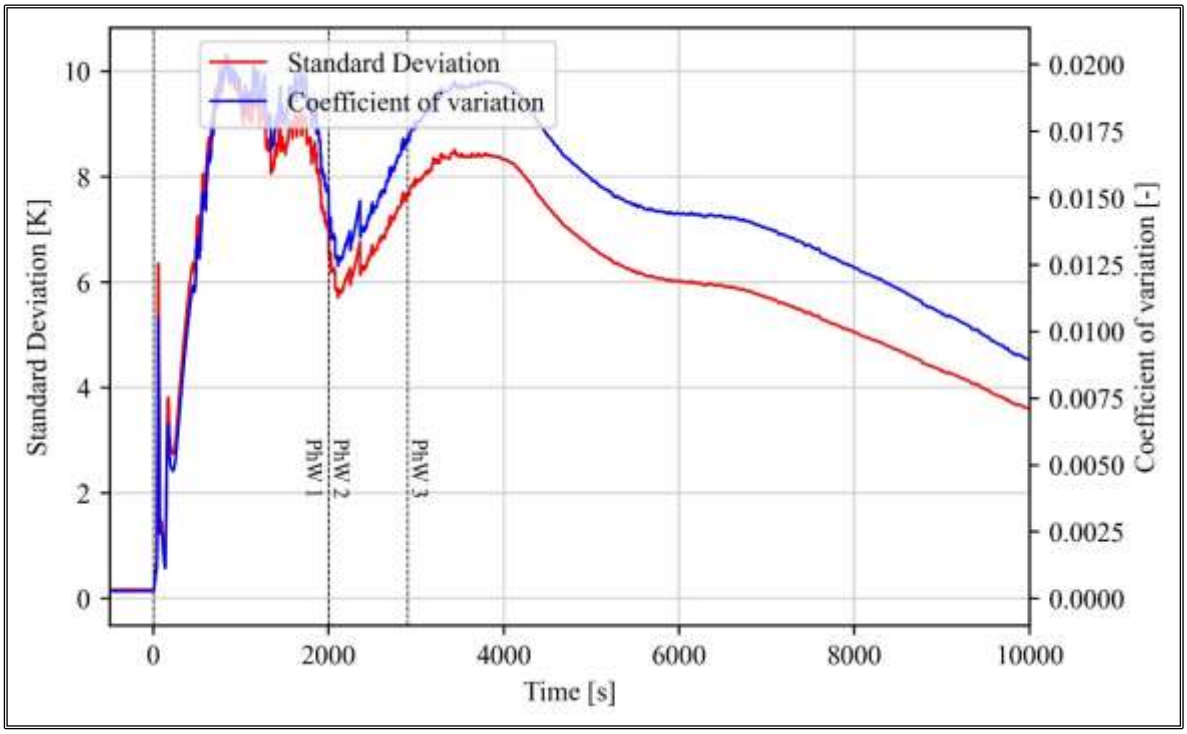

Figure 5.43 Standard deviation and coefficient of variation of maximum cladding temperature.

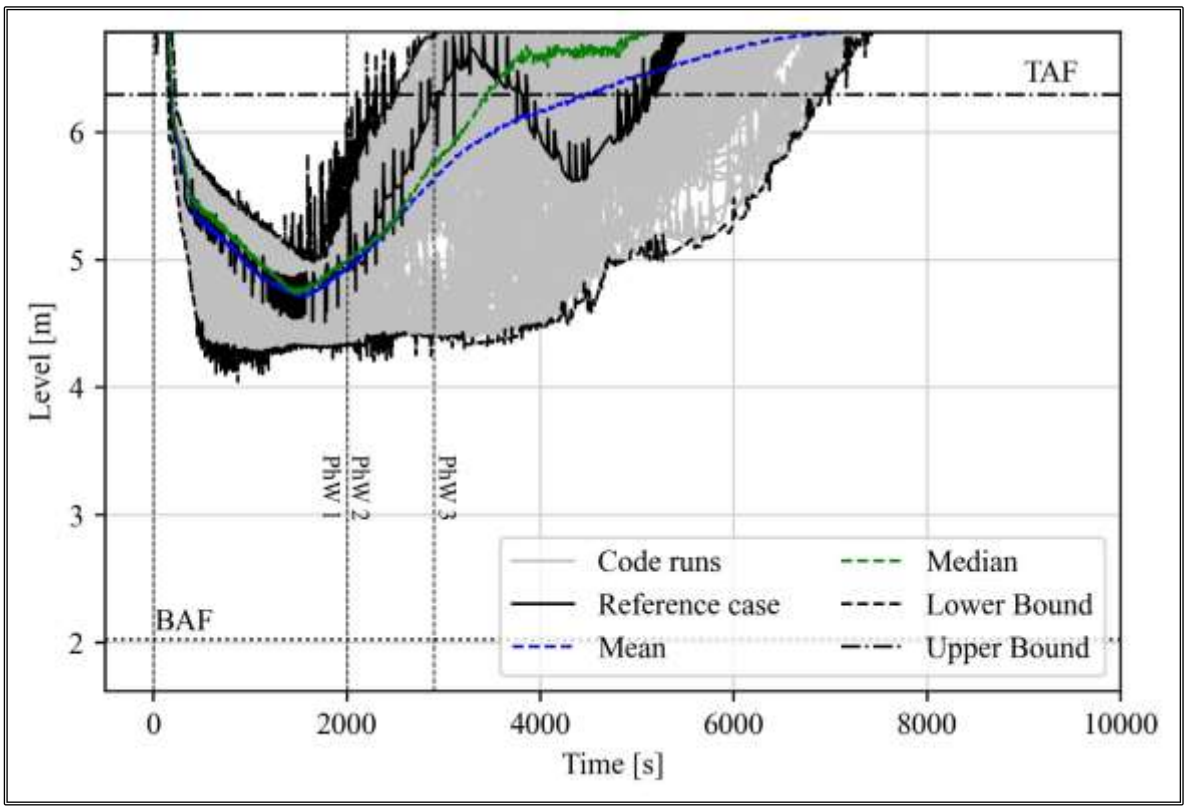

Figure 5.44 Collapsed coolant level in the core region uncertainty band.

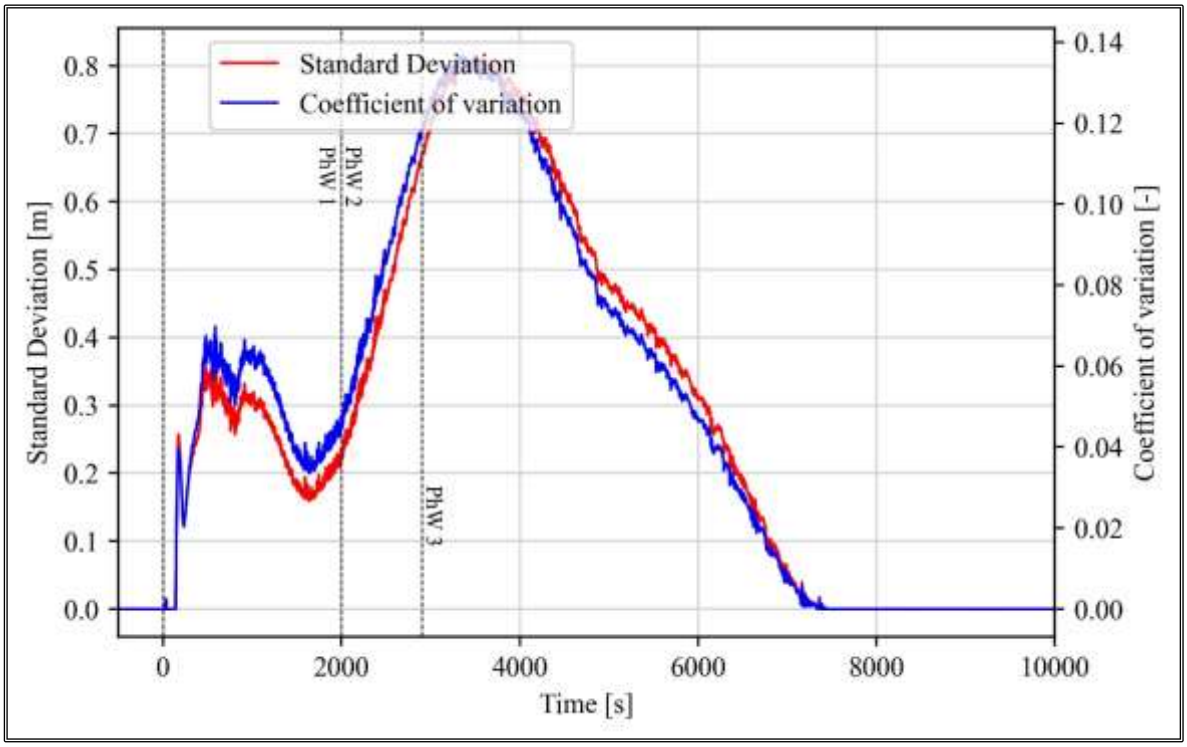

Figure 5.45 Standard deviation and coefficient of variation of the collapsed level in the core region.

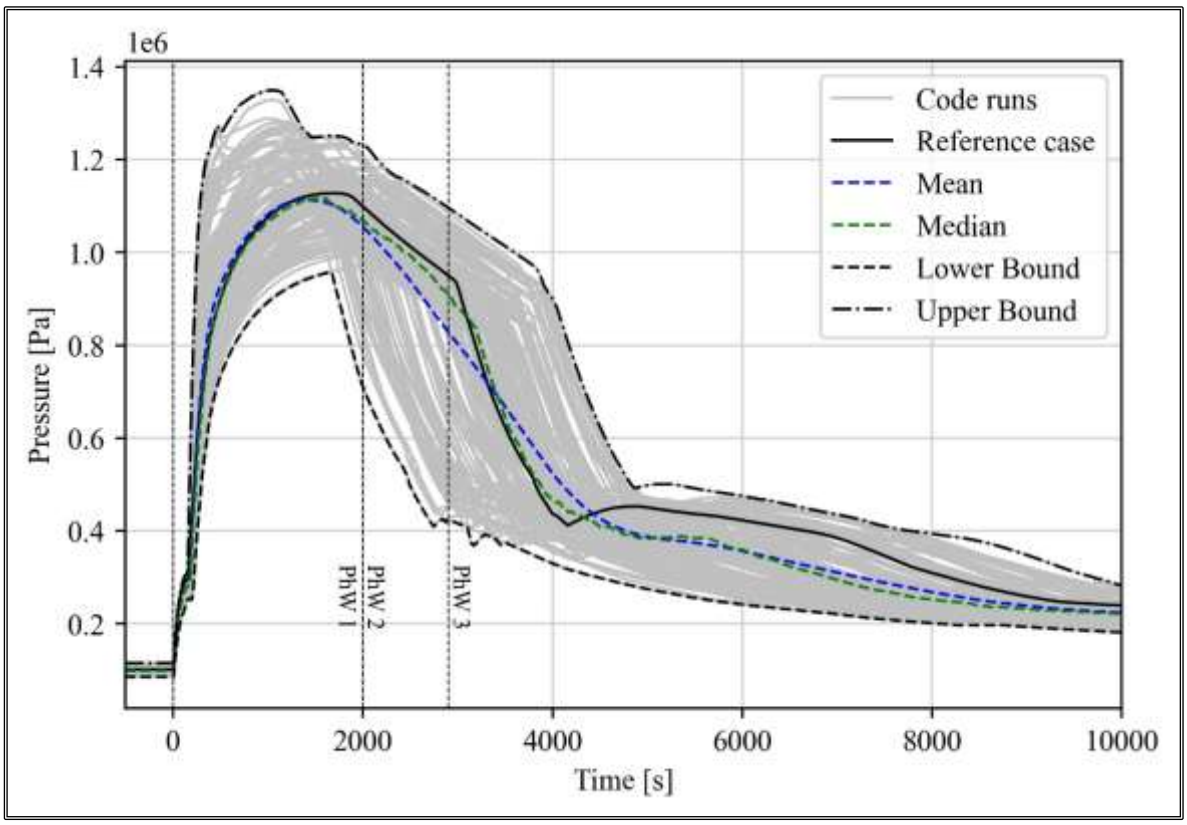

Figure 5.46 DW pressure uncertainty band.

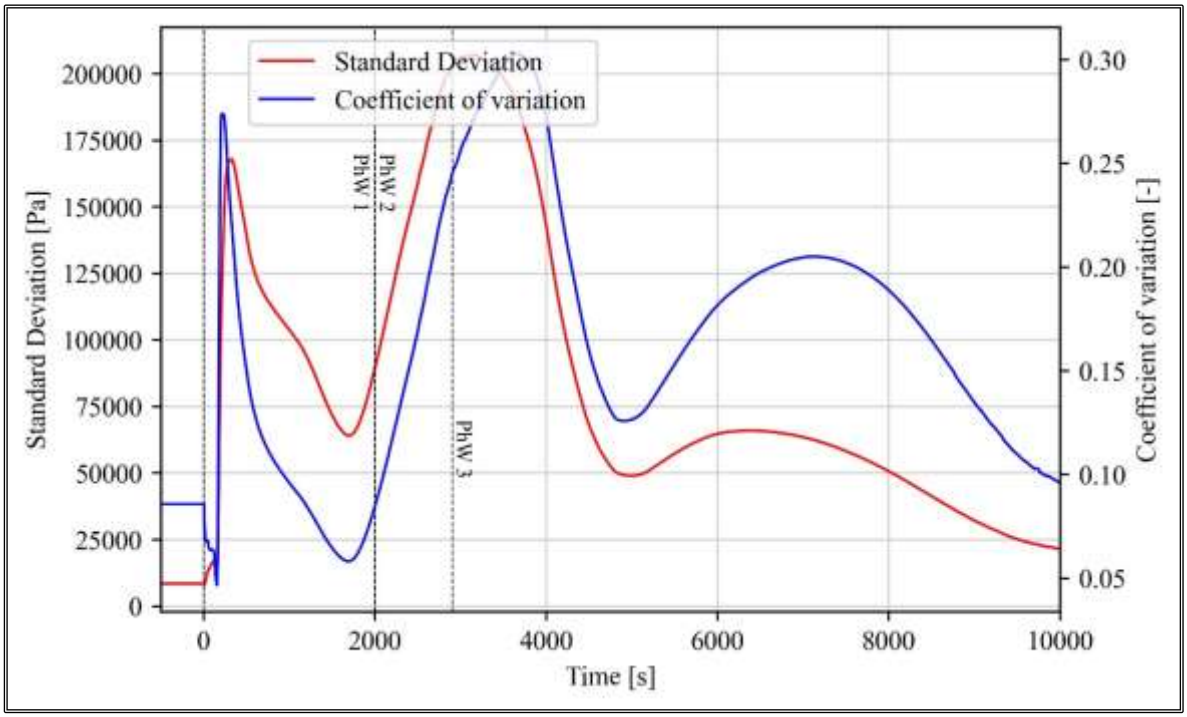

Figure 5.47 Standard deviation and coefficient of variation of the DW pressure.

The statistical correlation analysis, using the simple and simple rank correlation coefficients, has been also carried out during the investigated time of the transient, in view to analyse the trend of the statistical correlation coefficients.

Concerning the maximum cladding temperature, for about the first 300 s, a significant statistical correlation with the decay power (positive correlation), the initial pressure of the DW (negative correlation) and the pressure at the PRZ (positive correlation) is underlined. In addition, in this initial phase of the transient, a significant correlation is underlined for the break coefficient. Regarding the correlation with the break coefficient, the trend is characterized by a rapid change from negative to positive correlation and then, negative. A significant statistical correlation is underlined for the ADS Stage-1 loss coefficient (positive correlation) and the heat transfer surface of EHRS HXs (negative correlation) during the entire analysed transient. The simple and simple rank coefficients related to the maximum cladding temperature are reported from Figure 5.48 to Figure 5.51.

The collapsed level in the core region presents a significant statistical correlation with the ADS Stage-1 loss coefficient (positive correlation) for the first 4000 s and after this time point with the heat transfer surface of the EHRS HXs. The initial pressure of the DW presents a moderate statistical correlation (positive correlation) after about 1000 s. On the other hand, at about 3000 s after the SOT, the LGMS loss coefficient parameter presents a moderate statistical correlation (negative correlation), while the EBT initial temperature has a moderate statistical correlation during PhW 2 (negative correlation). The simple and simple rank correlation coefficients related to the collapsed coolant level in the core region are shown in Figure 5.52 to Figure 5.55.

The pressure of the DW presents, as expected, a significant statistical correlation with its initial value (positive correlation) along the first instants of the transient. Moreover, a significant statistical correlation with the break coefficient during the first 300 s of the transient has been underlined (positive correlation). The ADS Stage-1 loss coefficient presents a significant statistical correlation with the DW pressure. In this regard, during the first 1000 s, it is characterized by a negative significant statistical correlation and then, a positive significant statistical correlation. After PhW 2, the heat transfer surface of the EHRS HXs shows a significant statistical correlation (negative correlation).

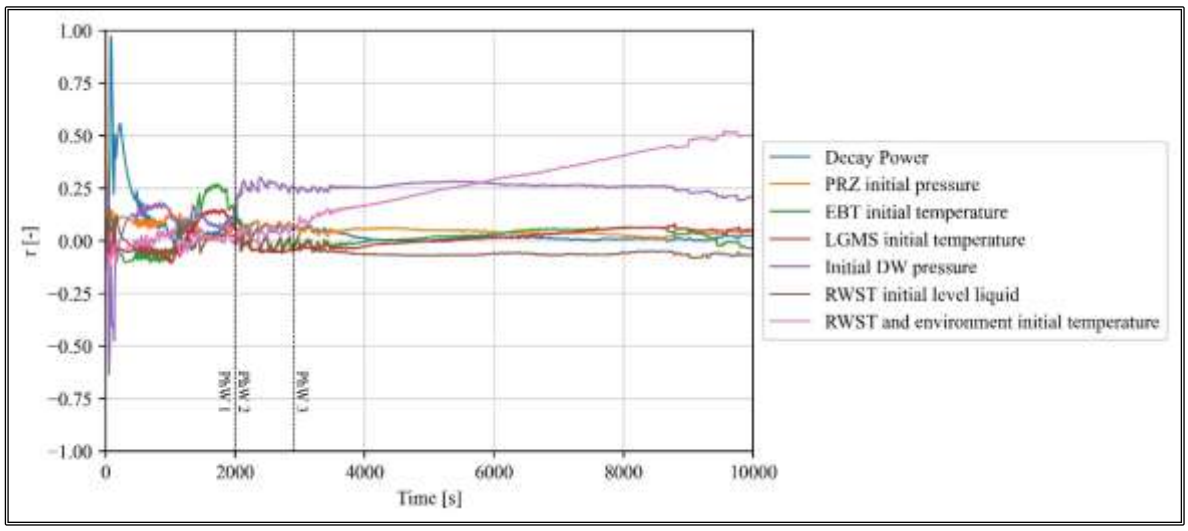

Figure 5.48 Simple correlation coefficient calculated along the transient – Maximum cladding temperature (a).

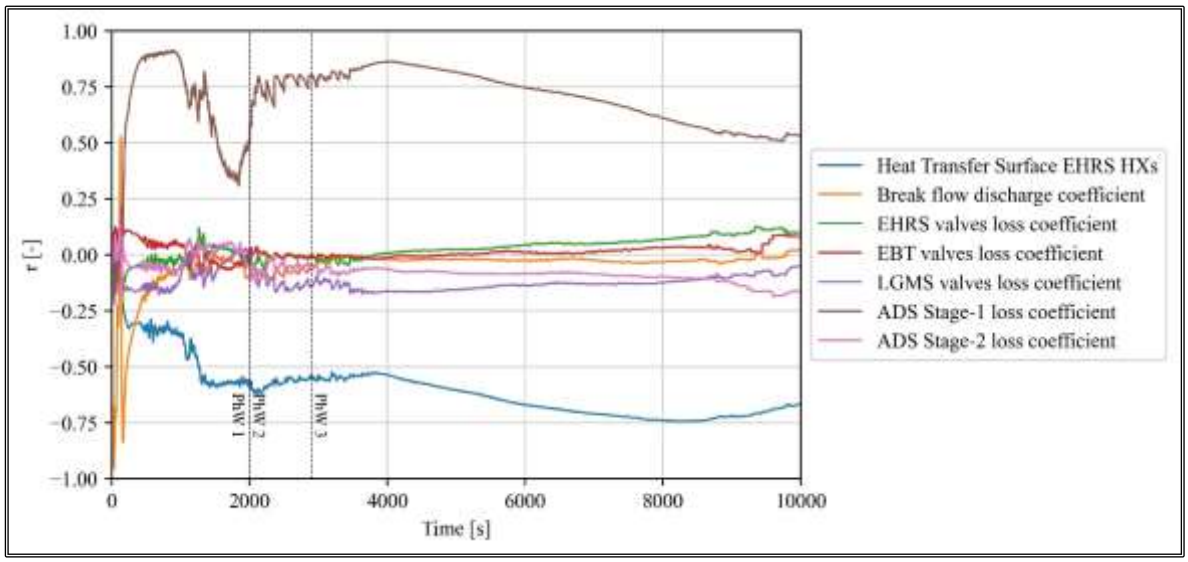

Figure 5.49 Simple correlation coefficient calculated along the transient – Maximum cladding temperature (b).

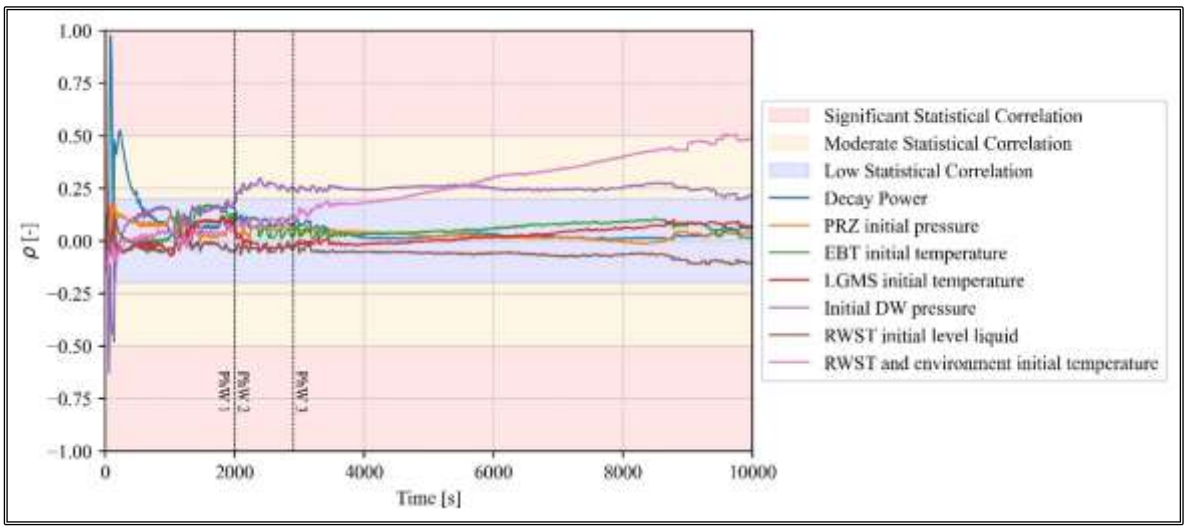

Figure 5.50 Simple rank correlation coefficient calculated along the transient – Maximum cladding temperature (a).

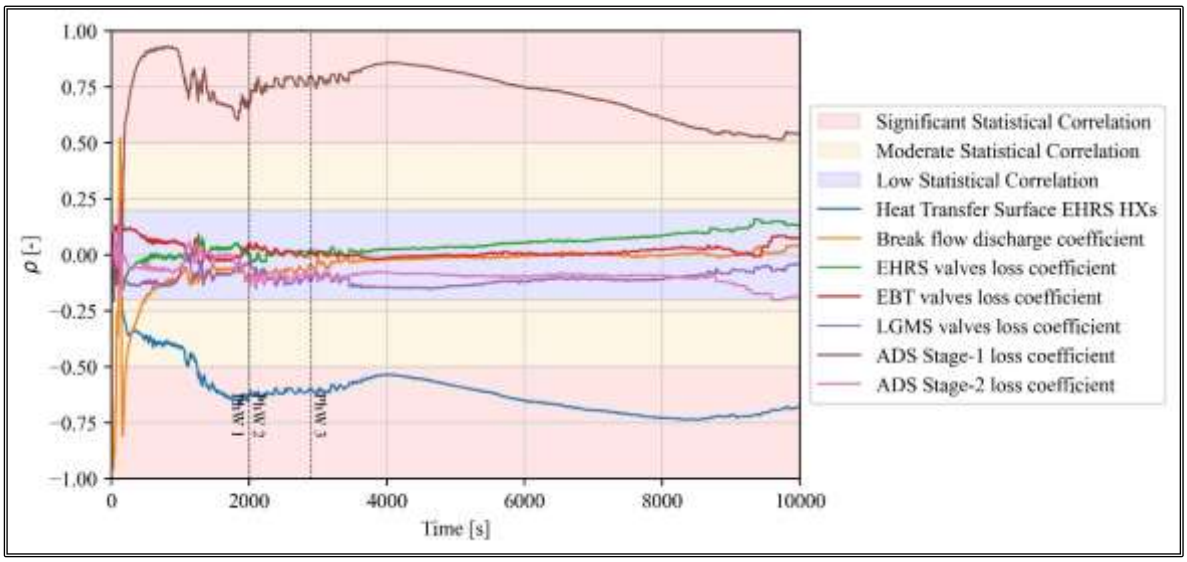

Figure 5.51 Simple rank correlation coefficient calculated along the transient – Maximum cladding temperature (b).

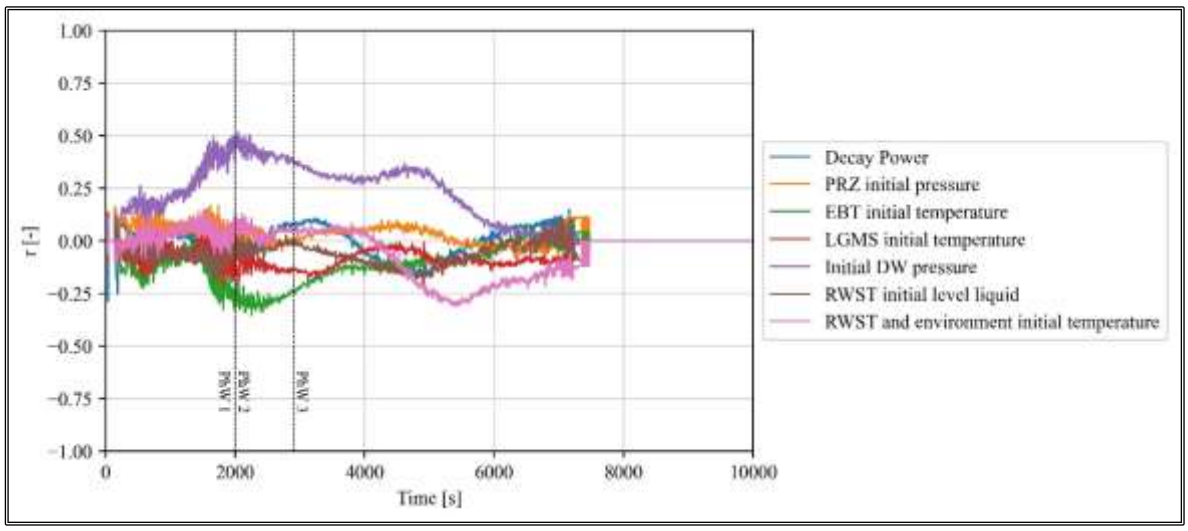

Figure 5.52 Simple correlation coefficient calculated along the transient – Collapsed coolant level in the core region (a).

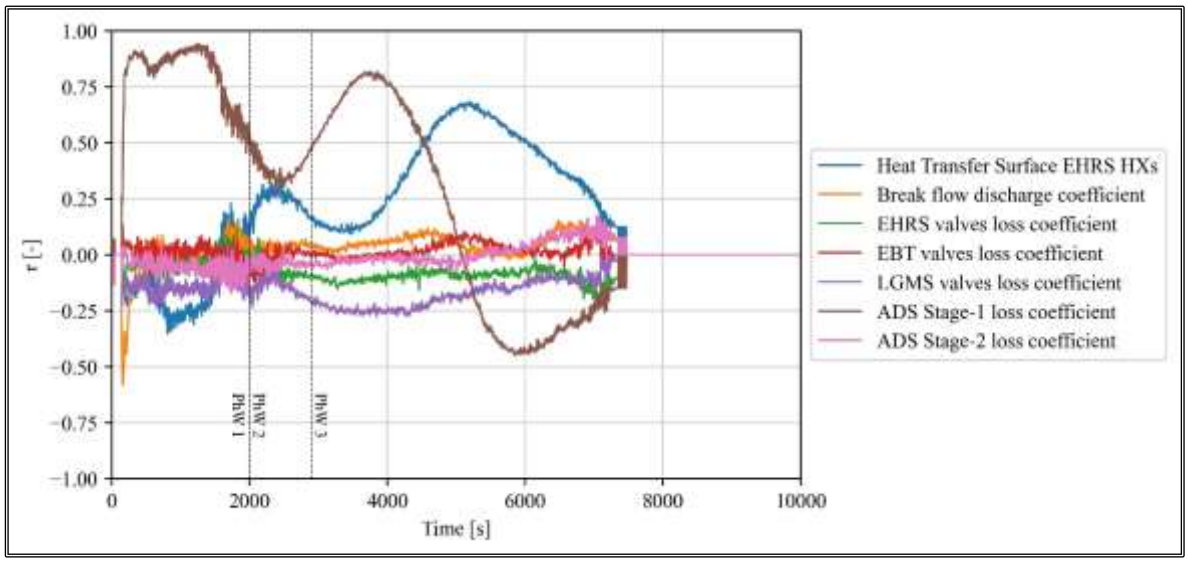

Figure 5.53 Simple correlation coefficient calculated along the transient – Collapsed coolant level in the core region (b).

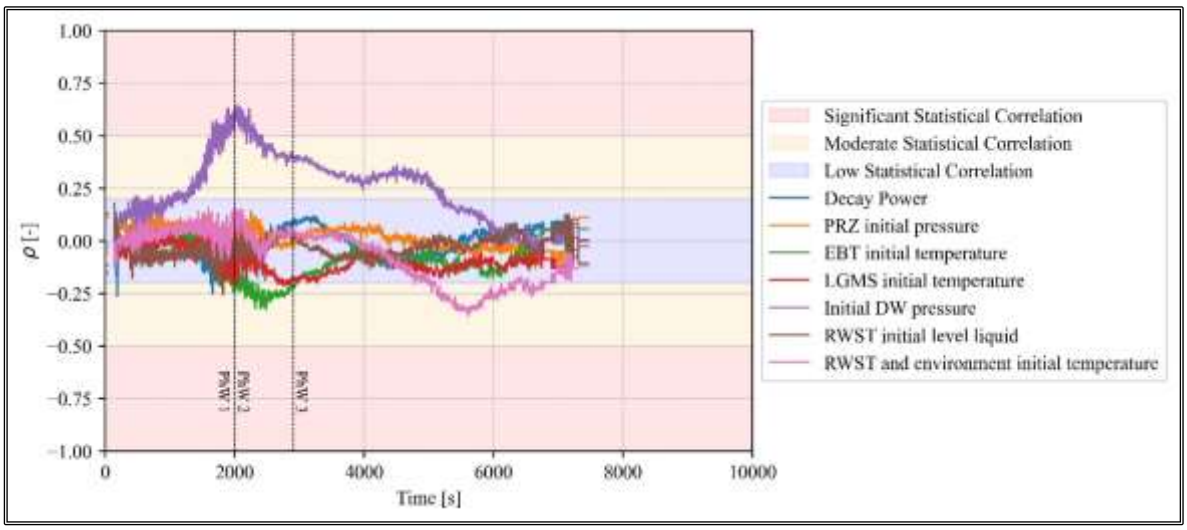

Figure 5.54 Simple rank correlation coefficient calculated along the transient – Collapsed coolant level in the core region (a).

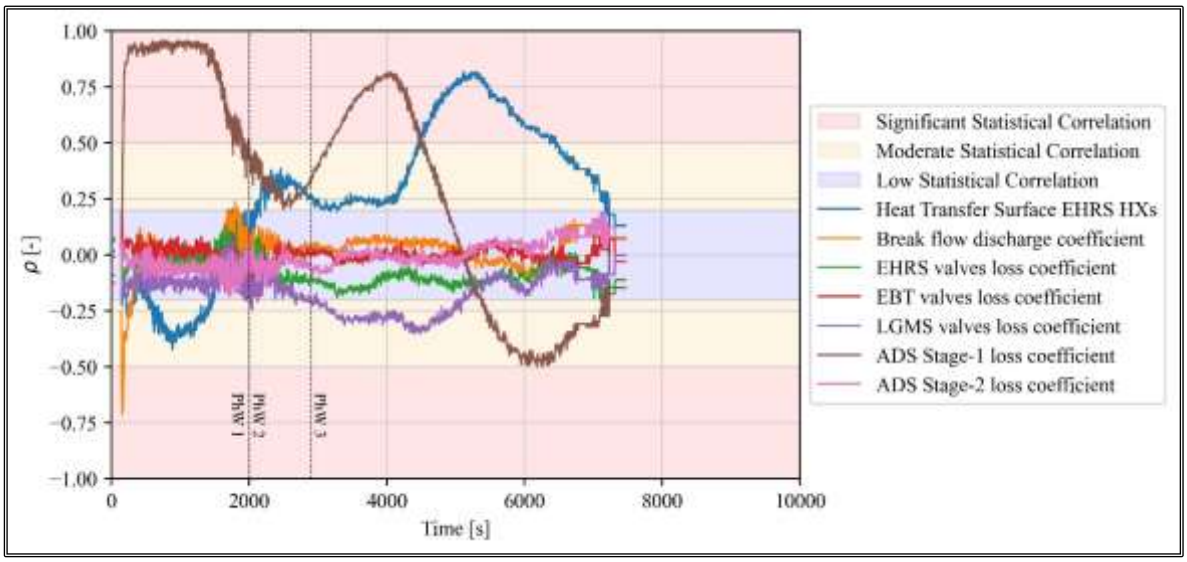

Figure 5.55 Simple rank correlation coefficient calculated along the transient – Collapsed coolant level in the core region (b).

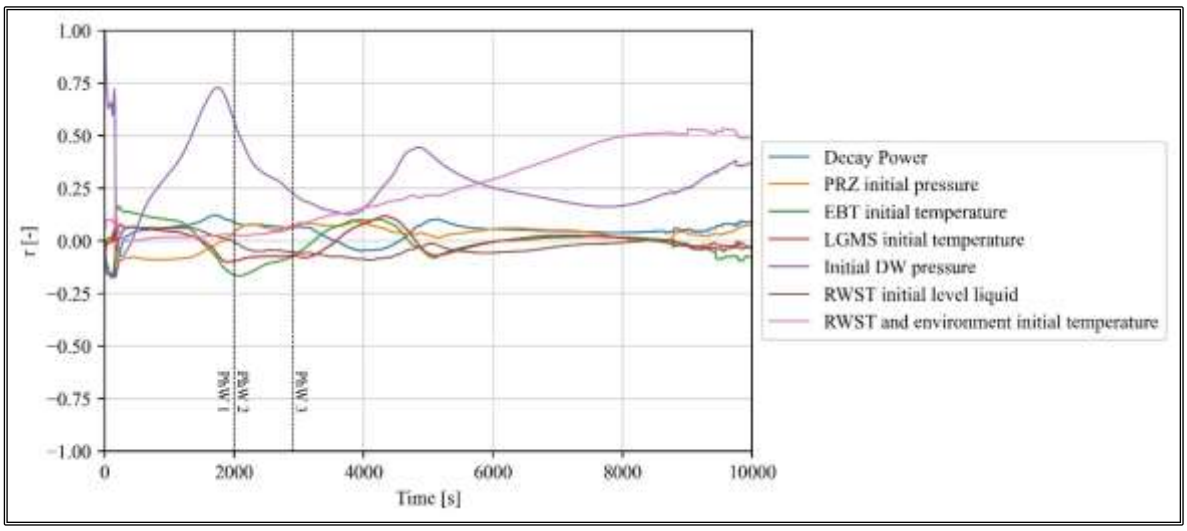

Figure 5.56 Simple correlation coefficient calculated along the transient – DW pressure (a).

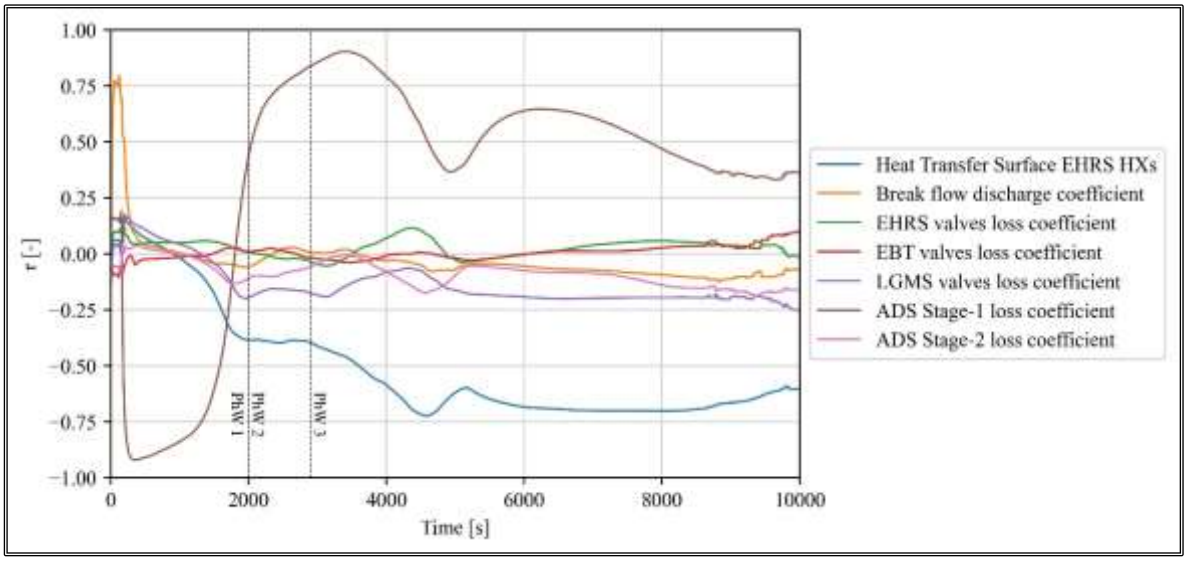

Figure 5.57 Simple correlation coefficient calculated along the transient – DW pressure (b).

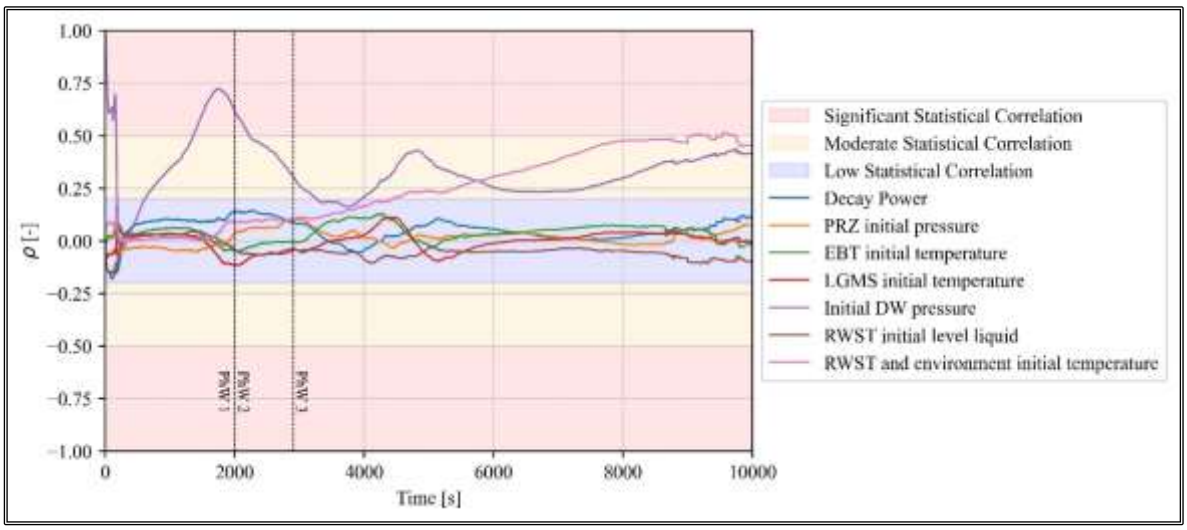

Figure 5.58 Simple rank correlation coefficient calculated along the transient – DW pressure (a).

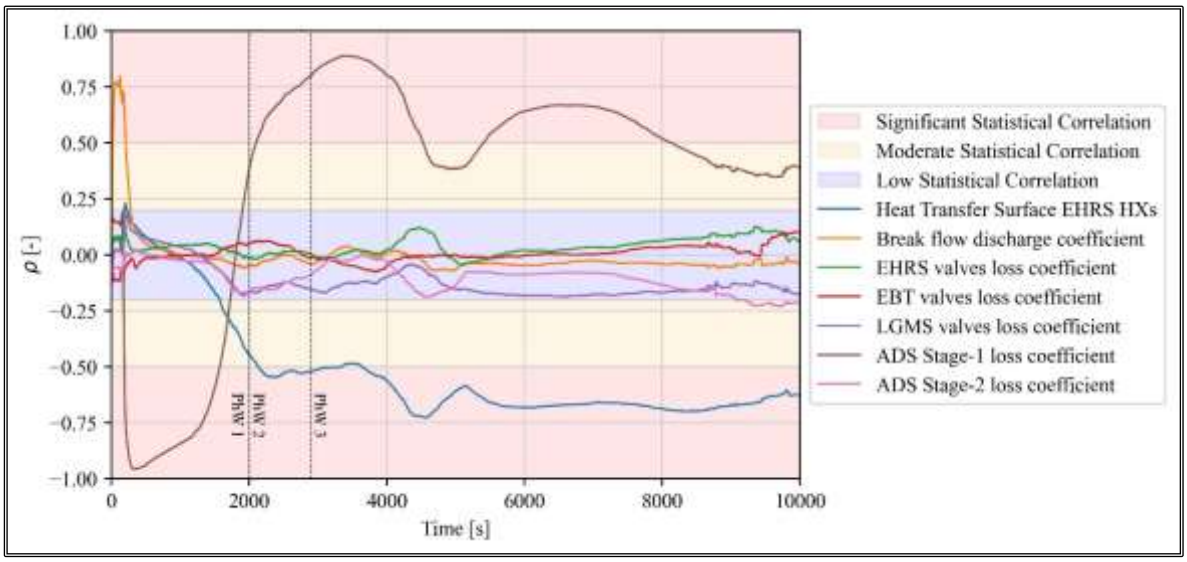

Figure 5.59 Simple rank correlation coefficient calculated along the transient – DW pressure (b).

5.7 Uncertainty analysis of the Severe Accident sequence

After the application of the uncertainty methodology to the DBA sequence, it has been applied to the SA sequence, which is characterized by the postulated failure of all passive systems. In addition, to test the applicability of the methodology in the SA domain to an iPWR design, this analysis aims to give preliminary insights on the uncertainty of the code on the total production of hydrogen, representing a key FOM for the nuclear safety (see 1.3.2) in ad advanced nuclear reactor. For that reason, the total hydrogen production in the core has been chosen as FOM. Uncertain input parameters related to the main processes leading to hydrogen production during an SA sequence in LWRs described in [66] [147] have been selected. The application of the uncertainty analysis has been carried out using the in-house tool in Python described in 2.4.2.

5.7.1 Description of the reference case

The transient is characterized by the same PIE and described in 5.3. Despite the previously discussed transient, for this sequence, the postulated failure of all the passive systems as well as the failure of ADS Stage-1 and ADS Stage-2 have been considered. Following the scheme presented in 1.3.2.2, in general, the transient can be divided into the following PhWs:

I. **Thermal-hydraulic phase** - PhW 1: it evolves from the SOT to the core heat-up. It includes the reactor SCRAM, the pumps coast-down, the TAF uncover, the PCS depressurization and DW pressurization.
II. **Heat-up phase** - PhW 2: it starts with the fuel heat-up and ends when the core temperature reaches 1500 K. It is characterized by the DW rupture, the onset of zircalloy oxidation reactions.
III. **Oxidation, melting, relocation and slumping phase** - PhW 3: it begins when the fuel temperature reaches 1500 K and ends with the core slumping. It is characterized by the BAF uncover, the runaway of zircalloy oxidation reactions and the massive production of hydrogen.
IV. **LH heating** - PhW 4: it starts with the slumping and includes the remaining part of the transient.

Following the break, the transient is driven by the blowdown of the RPV and, in this regard, Figure 5.60 shows the mass flow rate from the break. Due to the loss of coolant from the PCS, the DW pressure increases and, at about 41 s after the SOT, the high containment

pressure set-point triggers the S-signal, causing the switch from fission power to decay power. After the S-signal, the SCS pressure increases. The code predicts a pressure peak of about 1.2E7 Pa. Figure 5.61 shows the primary, secondary and DW pressures.

Due to the loss of primary coolant, the inventory of primary mass decreases, as shown in Figure 5.62, as well as the collapsed coolant level in the core region. As shown in Figure 5.63, the code predicts the uncover of the TAF at about 2520 seconds after the SOT. During the PhW 1, the primary pressure tends to increase from about 1.0E7 to 1.2E7 Pa, followed by the SCS pressure. The decay power is removed only by the flow rate coming out of the break and by the water present in the SGs acting as a heat sink (considering negligible heat losses to the DW). Considering the heat capacity of the secondary coolant in the SGs, the primary pressure begins to increase followed by secondary pressure, as shown in Figure 5.61. The increase of the primary and, consequently, secondary pressure is stopped at about 3200 s after the SOT, when the collapsed level in the downcomer reaches the DVI elevation, as shown in Figure 5.63. Then, the primary pressure decreases as well as the secondary pressure.

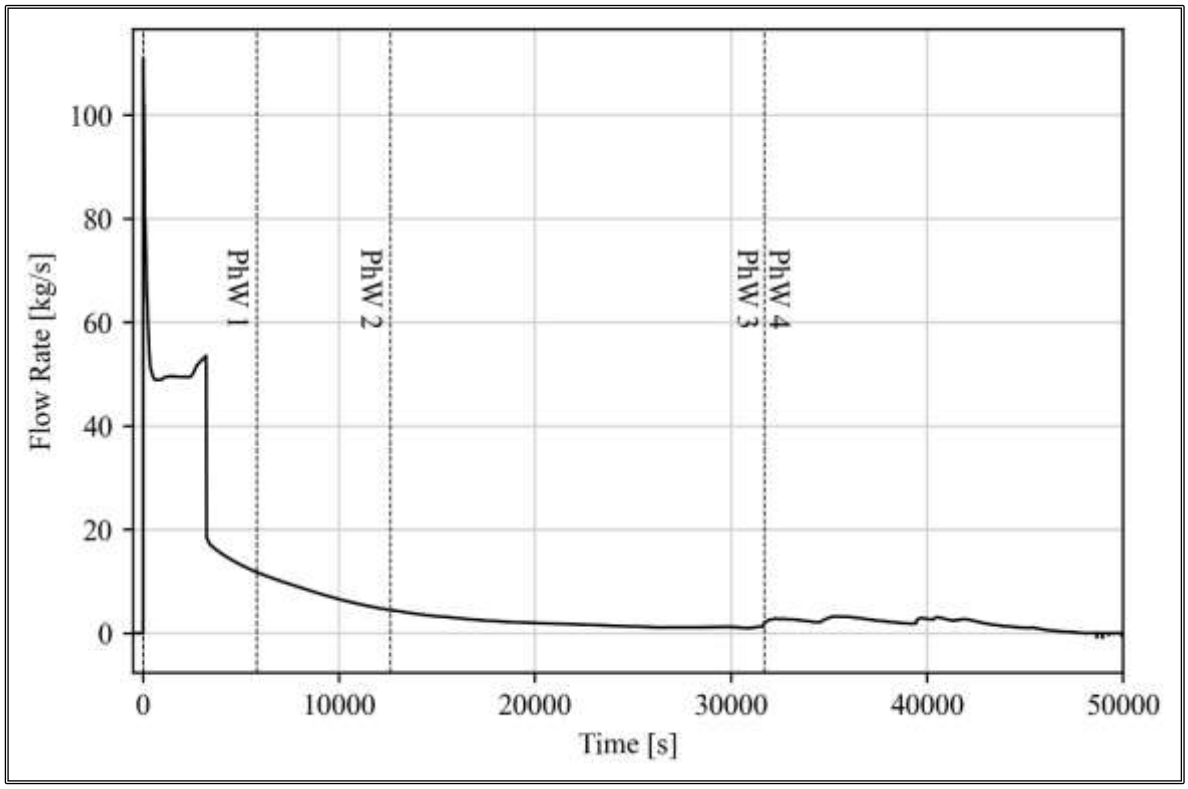

Figure 5.60 Mass flow rate through the break.

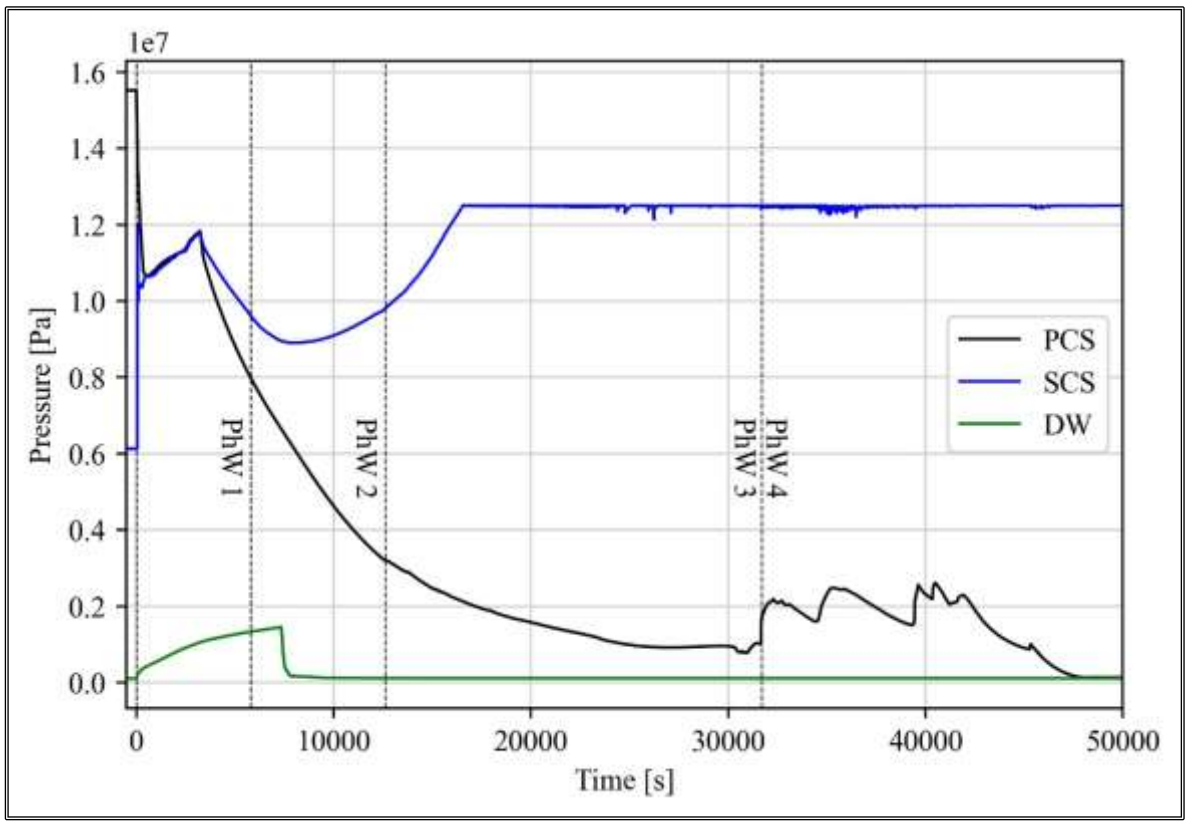

Figure 5.61 Primary, secondary and DW pressure.

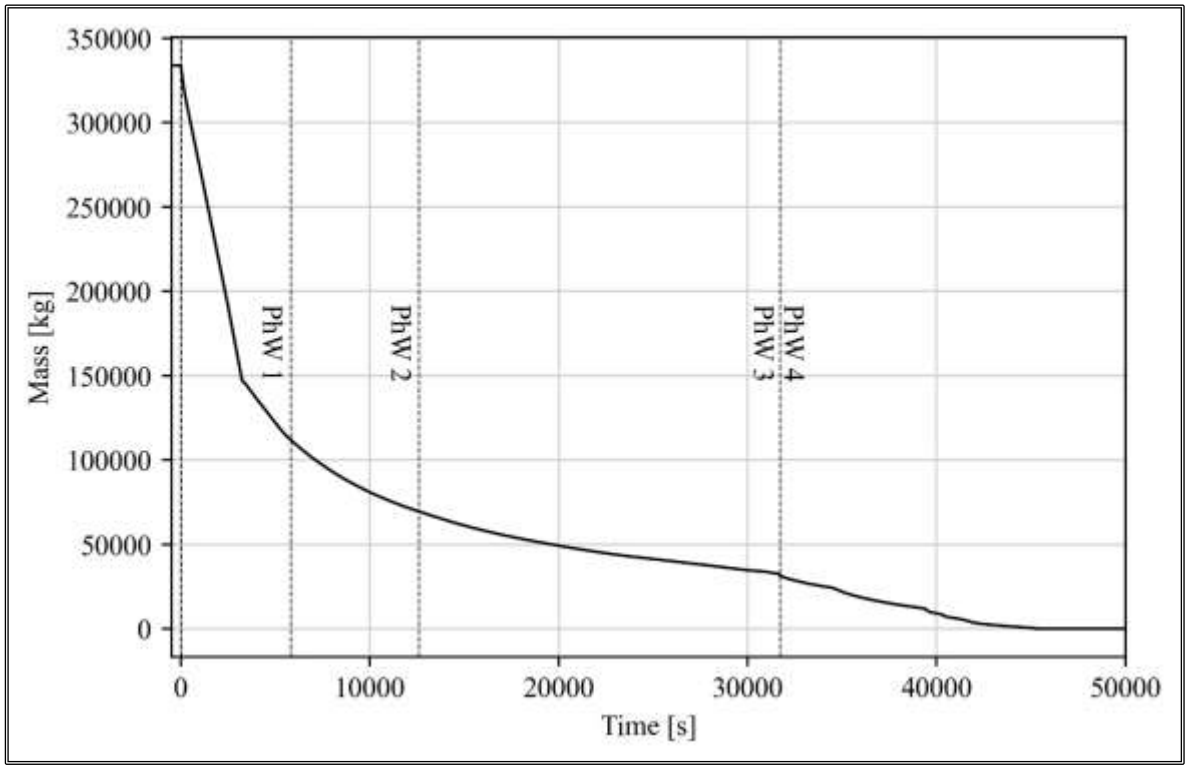

Figure 5.62 PCS water inventory.

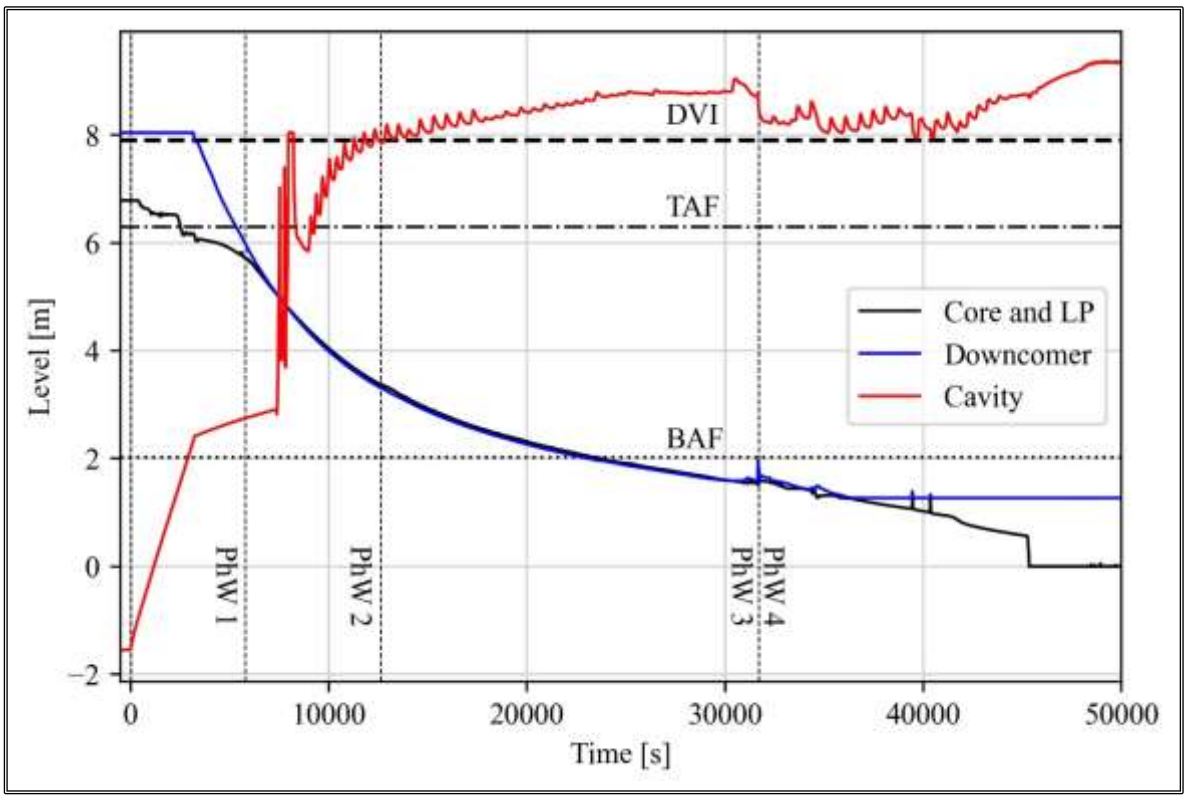

Figure 5.63 Core, downcomer and cavity collapsed coolant level.

At about 7300 s after the SOT, the DW pressure reaches the rupture set-point. In this regard, it has been assumed that opening a large breach in the DW is directly connected to the environment when the internal pressure is greater than 13.5E5 Pa, as hypothesized in [130]. It determines a fast depressurization of the containment to the atmospheric pressure, as shown in Figure 5.61.

Due to the fast depressurization of the DW, the code predicts the fast rise of the water inside the PSSs through the PSS vent pipes and the injection into the DW. It causes a rapid increase in the collapsed coolant level in the reactor cavity, as shown in Figure 5.63. Although the collapsed level of coolant in the cavity reaches a level higher than the DVI level, no coolant is injected into the RPV because the primary pressure at this stage is still higher than the pressure prevailing in the DW (atmospheric pressure).

At this stage of the transient, the core is uncovered, and the collapsed level continues to decrease. The secondary pressure increases again, considering the role of the heat sink of the secondary system, and the rise of the pressure is stopped by the start of the cycling of the safety valves of the SGs, as shown in Figure 5.61. The core uncover causes the fuel heat-up and the increase of the cladding temperature as shown in Figure 5.64. At about 12270 s after the SOT, the cladding temperature reaches the onset value for the zircalloy oxidation reaction and the beginning of hydrogen generation, as shown in Figure 5.65. As a

consequence of zircalloy oxidation, the ZrO_2 mass in the core increases and the Zr mass decreases, as also presented in Figure 5.66.

At about 23000 s after the SOT, the collapsed level in the RPV reaches the BAF, leaving the core uncovered. Then, the core degradation mechanisms continue, and the slumping begins at about 31700 s, as underlined in Figure 5.61 by the primary pressure peaks. In Figure 5.67 the main phases of the core degradation are presented with the SNAP animation, reporting the core material composition and the LH thermal field calculated by the code. The adopted colour maps are the same as reported in Table 4.2 and Table 4.3. Concerning the last core degradation phase, unlike what has been done in Figure 4.15, it has been chosen to report the core composition and the thermal loads on the LH at the end of the calculation. In Table 5.7 the main events characterizing the SA sequence have been reported.

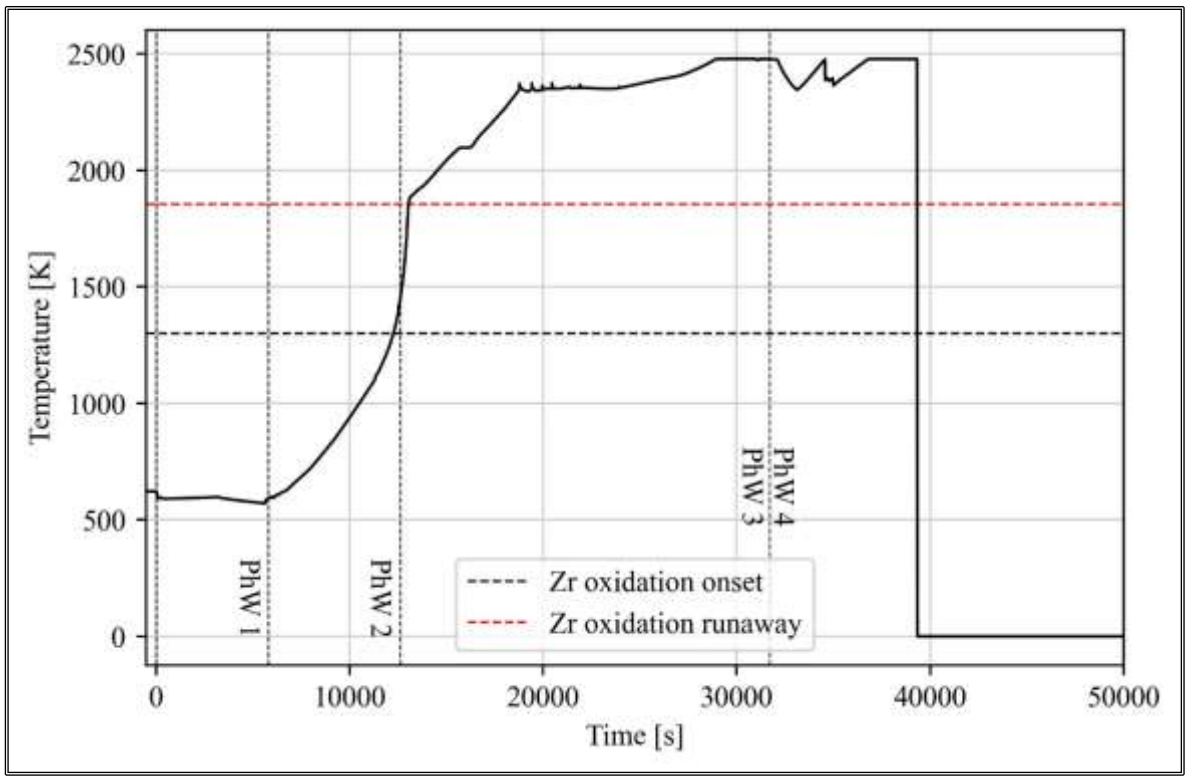

Figure 5.64 Maximum cladding temperature.

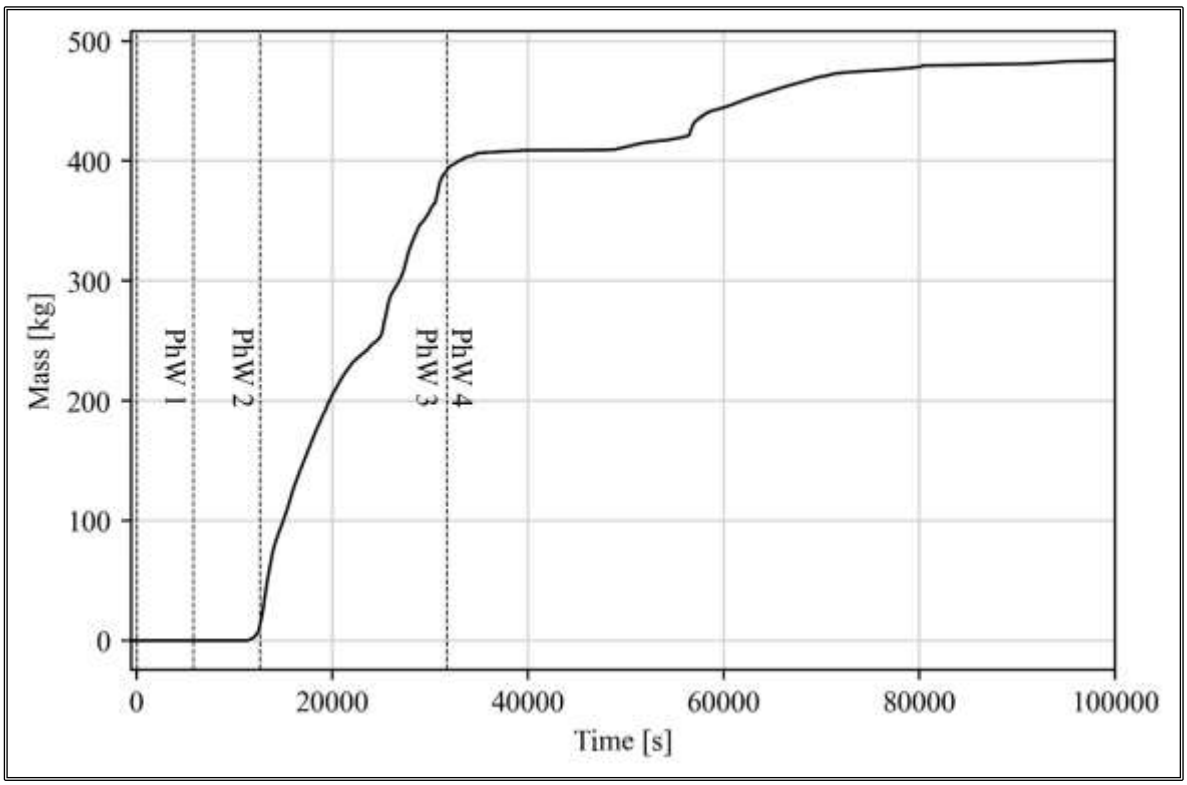

Figure 5.65 Cumulative hydrogen production.

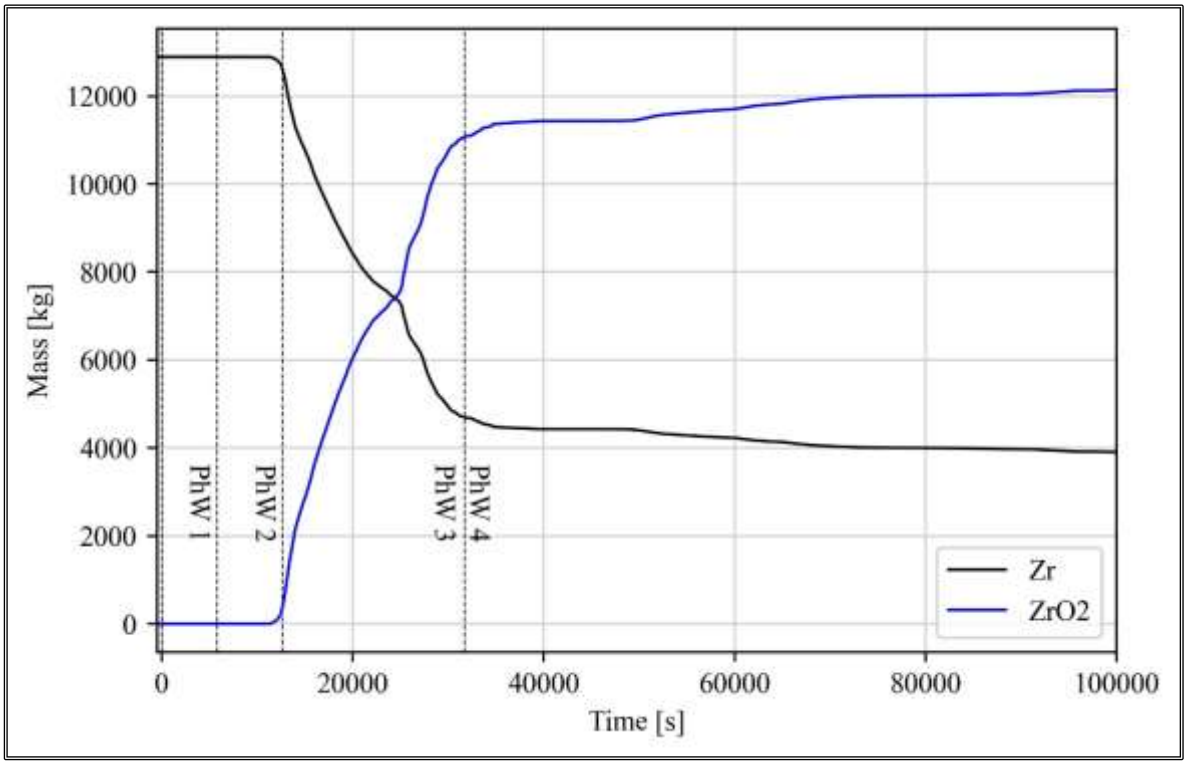

Figure 5.66 Mass of Zr and ZrO_2.

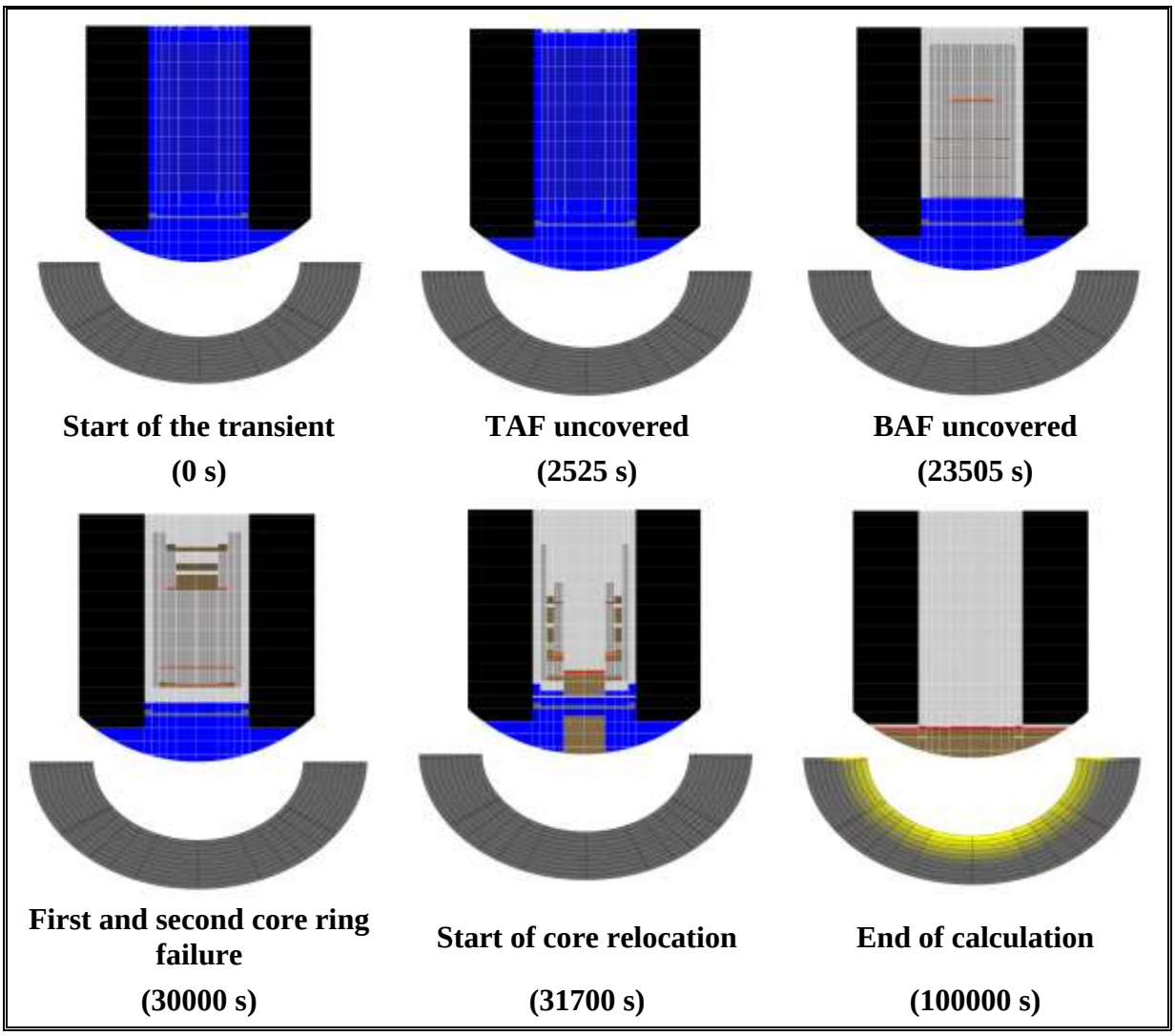

Figure 5.67 SNAP animation of core degradation and thermal field of LH.

Table 5.7 Table of the main events.

Event	Time [s]
SOT	0
S-Signal	41
Low PRZ level Signal	186
LM-Signal	237
TAF uncovered	2525
DW rupture	7345
Start of H2 generation	11300
Start of the core relocation	31700
End of the core relocation	45000

5.7.2 Hypotheses of the uncertainty analysis

The goal of this uncertainty analysis is to apply the uncertainty methodology, investigated and analysed in the applications discussed so far, to a postulated SA sequence in an advanced reactor design, such as the iPWR design. Furthermore, a key point is to investigate and

characterize the uncertainties of the code about the production of hydrogen during the in-vessel phase.

Five of the main uncertain input parameters influencing the in-vessel production of hydrogen have been considered. These parameters, as evidenced in the literature [66] [147], are among the most influential ones on hydrogen production in LWRs:

- *Zircalloy oxidation reaction kinetics*: a detailed description of these parameters has been presented in 3.3.4.
- *Zircalloy Melt Breakout Temperature*: the oxidation of the fuel cladding forms a shell of ZrO_2 which can contain molten clad materials until the thickness of ZrO_2 or the temperature limit is crossed. For this reason, the molten mass candles and relocates. This parameter influences flow obstructions, steam interaction with zirconium and, consequently, hydrogen generation. In the MELCOR oxidation model, the breakout temperature for the cladding component is editable as a sensitivity coefficient.
- *Debris Porosity*: the porosity of core debris has an impact on oxidation processes because influences heat transfer and surface area.
- *Eutectic temperature of ZrO_2/UO_2 mixture*: the melting point of the binary eutectic mixture of ZrO_2 and UO_2 can affect the dynamics of blockage by candling materials and, consequently, oxidation processes.

Table 5.8 shows the uncertain input parameters with their distribution type and range of variation.

Table 5.8 Uncertain input parameters [66] [147].

Uncertain input parameter	Unit	Distribution Type	Reference value	Lower and Upper bound	
K1	[$kg^2(Zr)/m^4$-s]	Normal	294.2	min	256.54
				max	331.85
K2	[K]	Normal	20100	min	19768.35
				max	20431.65
Zircalloy Melt Breakout Temperature	[K]	Normal	2400.0	min	2250
				max	2550
Debris Porosity	[-]	Normal (truncated)	0.38	min	0.1
				max	0.5
UO_2/ZrO_2 eutectic temperature	[K]	Normal	2479.0	min	2230
				max	2728

The FOM considered for this uncertainty application is the final cumulative hydrogen mass. Then, following the Wilks formula for one FOM and the one-sided tolerance interval considering a probability content γ and a confidence level β of 0.95, 59 code runs are needed.

5.7.3 Results

The uncertainty band of the FOM has been estimated as well as the mean, median and standard deviation. The statistical parameters of the FOM are reported in Table 5.9.

Table 5.9 Statistical parameters of the FOM.

Statistical parameter	Unit	Value
Mean	[kg]	473.06
Median [kg]	[kg]	473.63
Lower Bound [kg]	[kg]	401.86
Upper Bound [kg]	[kg]	547.51
Standard deviation [kg]	[kg]	32.18
Coefficient of variation [-]	[-]	0.07

The estimated uncertainty band is about 146 kg and the mean and median have a value of 473 kg. In Figure 5.68 and Figure 5.69, the empirical CDF and PDF of the FOM are reported. The simple and simple rank correlation coefficients, shown in Figure 5.70 and Figure 5.71, highlight a moderate statistical correlation (positive correlation) with the zircalloy breakout temperature, the fuel rod collapse temperature and the melting temperature of the eutectic mixture UO_2/ZrO_2. In addition, a moderate statistical correlation with the zircalloy oxidation kinetics parameter K2 is highlighted (negative correlation). The statistical correlation is presented considering the scatter plots and the trend curves obtained by linear regression, shown from Figure 5.72 to Figure 5.74.

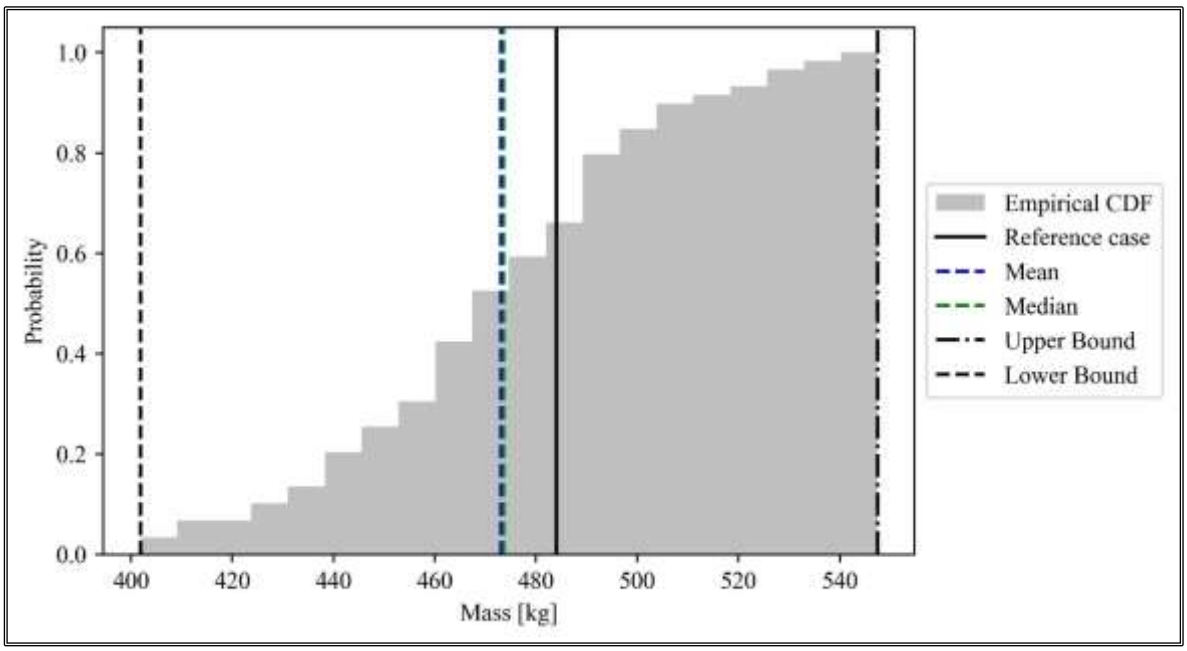

Figure 5.68 Empirical CDF of the FOM.

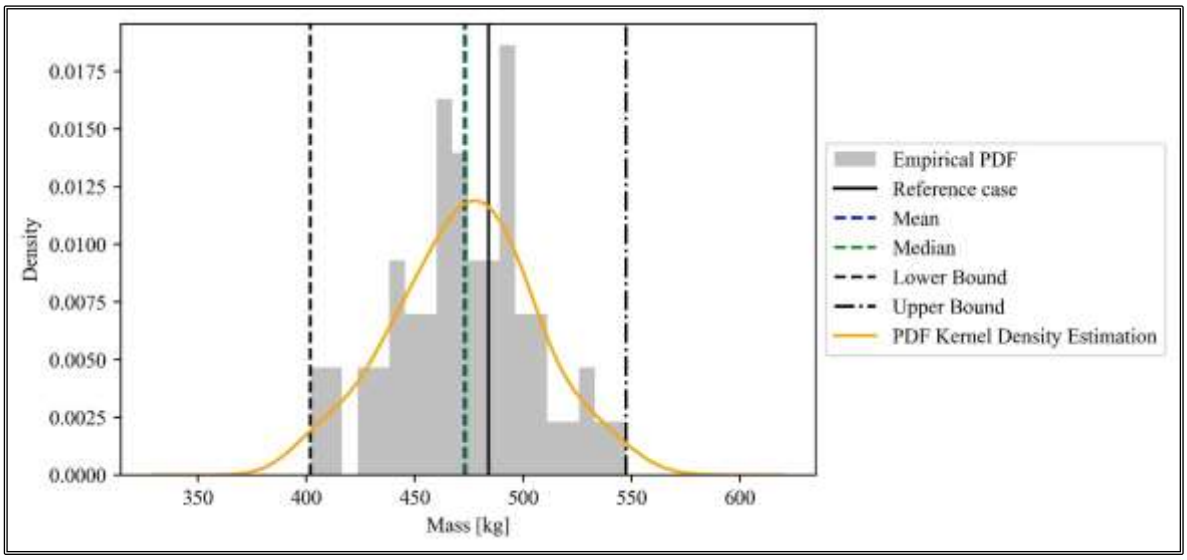

Figure 5.69 Empirical PDF of the FOM.

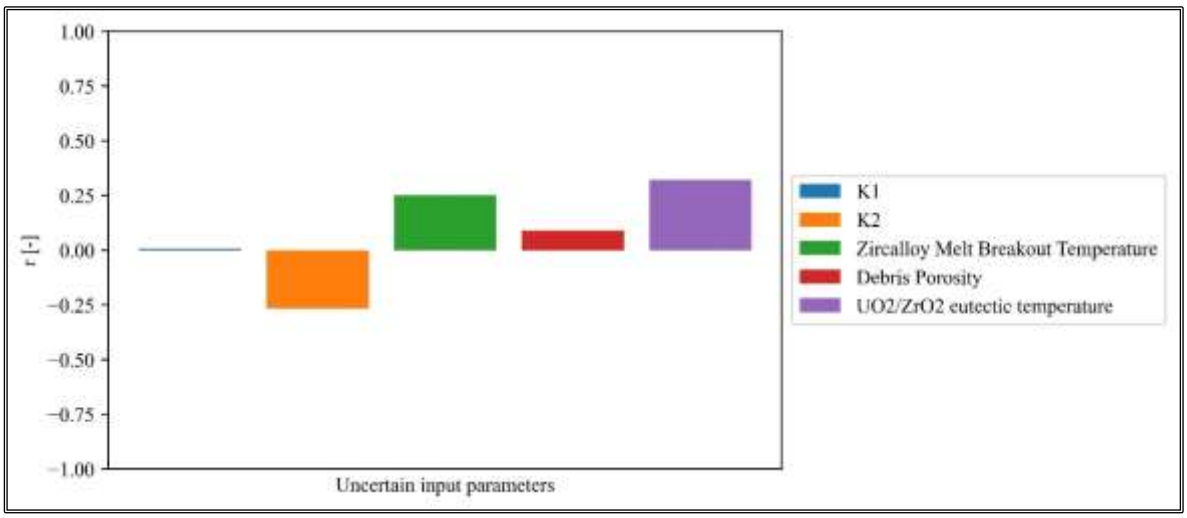

Figure 5.70 Simple correlation coefficient.

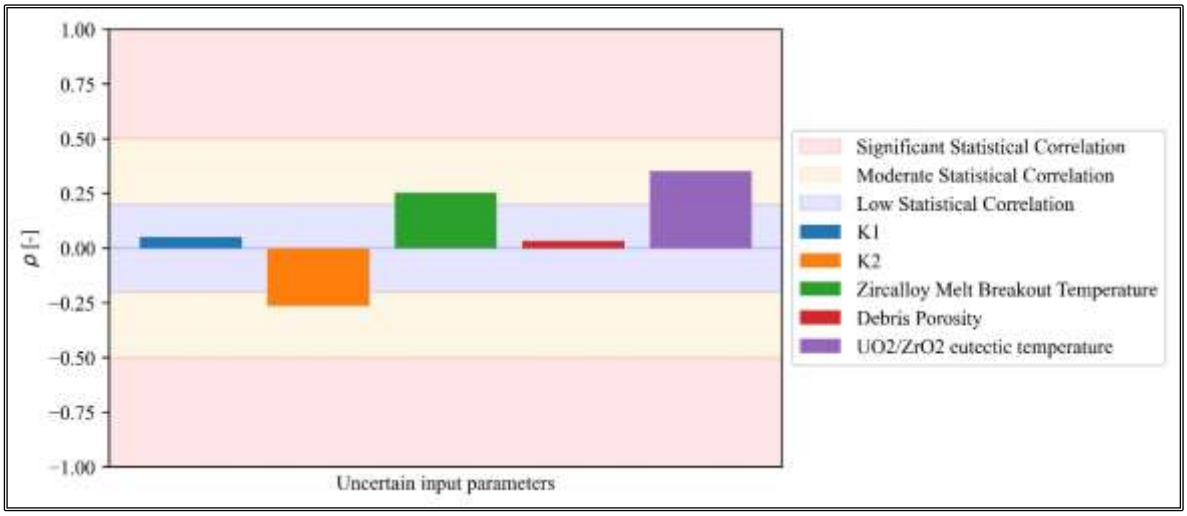

Figure 5.71 Simple rank correlation coefficient.

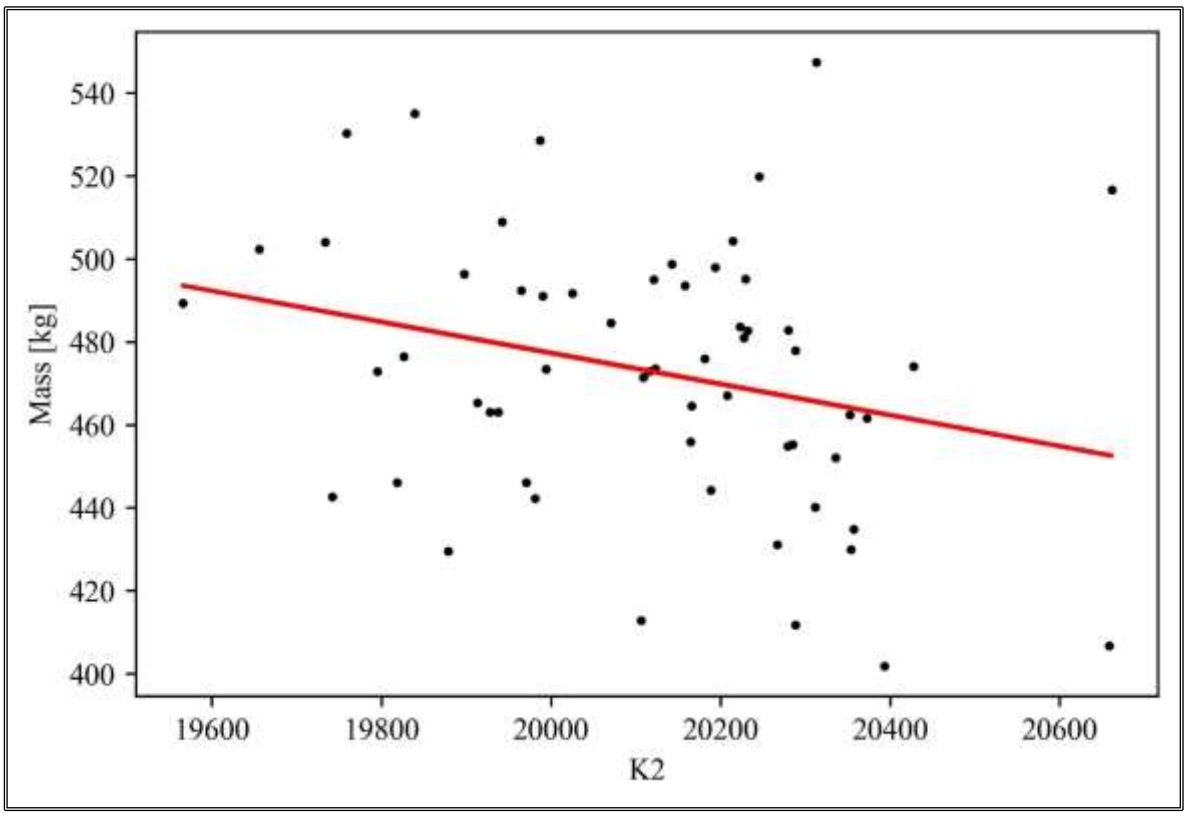

Figure 5.72 Scatter plot of FOM and K2 values.

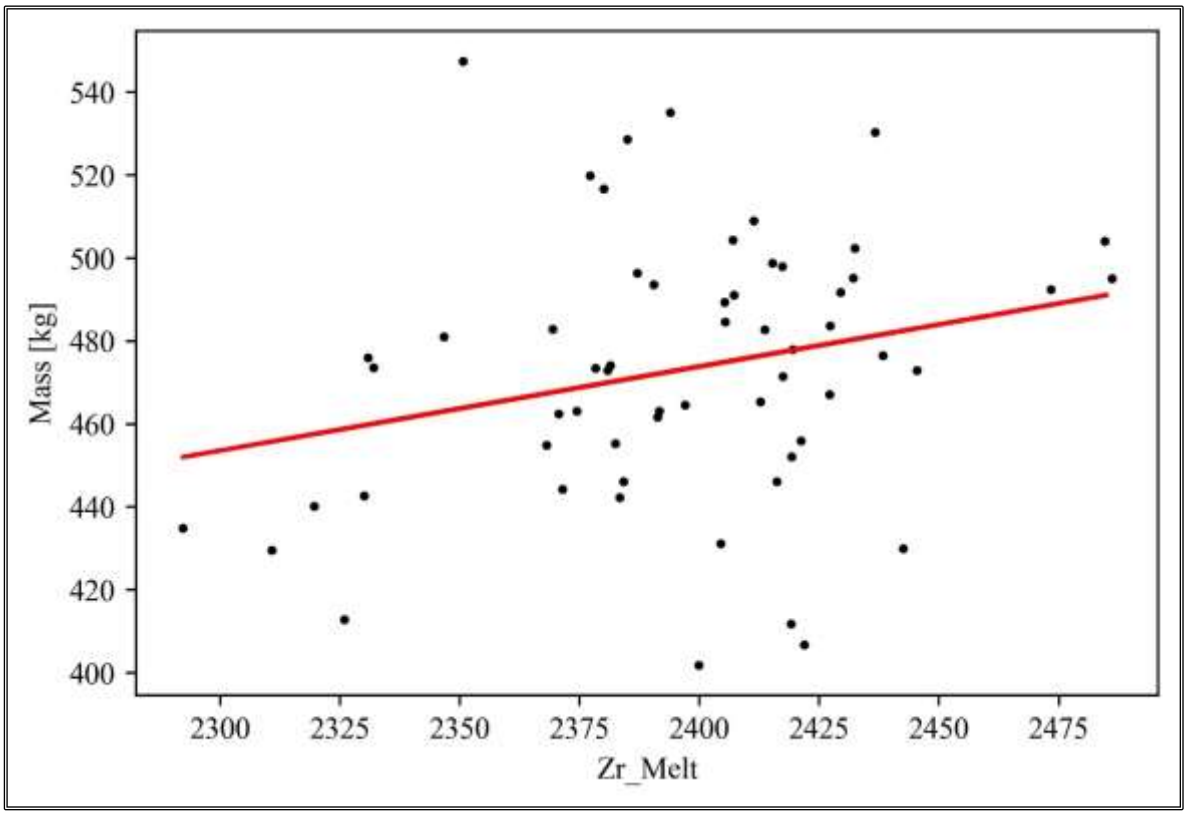

Figure 5.73 Scatter plot of FOM and Zircalloy Melt Breakout Temperature values.

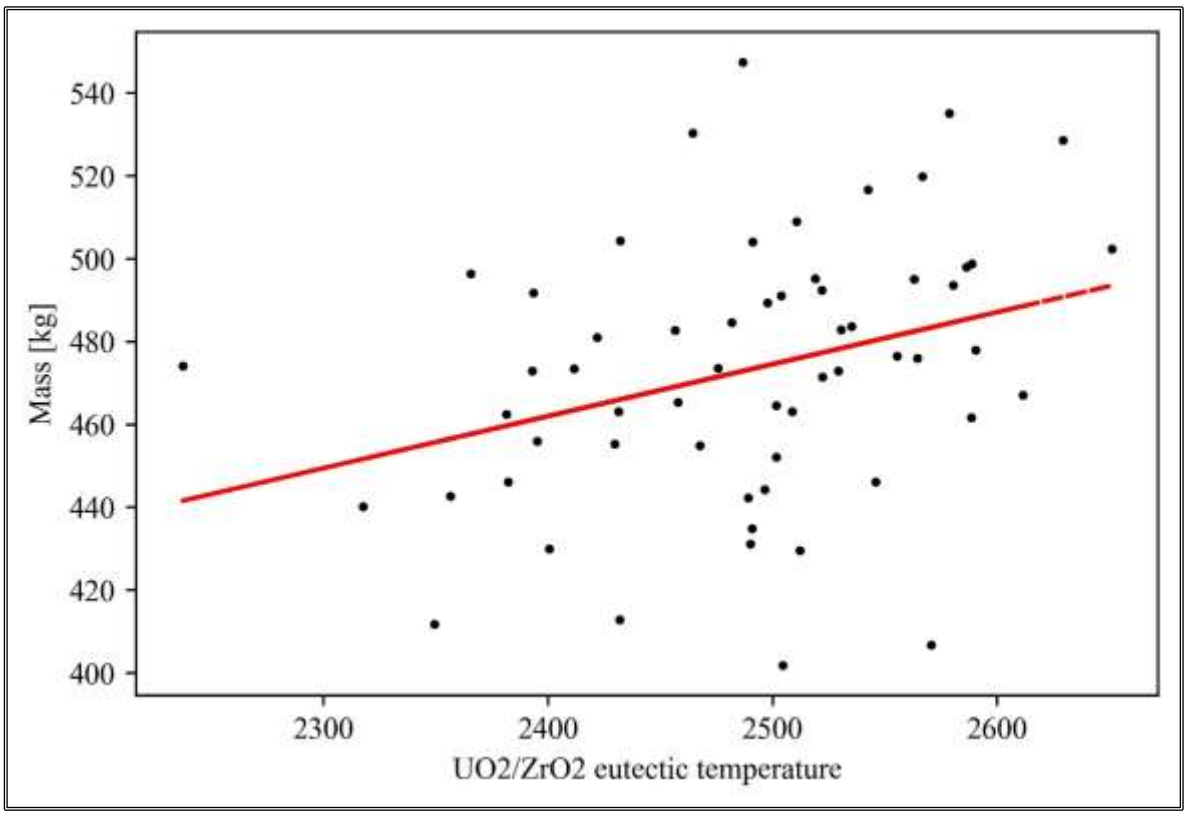

Figure 5.74 Scatter plot of FOM and UO_2/ZrO_2 eutectic temperature.

The uncertainty band of the hydrogen cumulative mass during the entire SA sequence has been analysed and presented in Figure 5.75. The uncertainty band increases after the zircalloy oxidation runaway, reaching a value of about 100 kg at the slumping. It increases subsequently until it reaches a final value of 146 kg. The trend of the code uncertainty band can be visualized through the analysis of the standard deviation and the coefficient of variation which is shown in Figure 5.76. By calculating the simple and simple rank correlation coefficients, it is possible to investigate along the entire incident sequence how the uncertainty parameters affect the cumulative hydrogen production from a statistical correlation point of view. In Figure 5.77 and Figure 5.78 the temporal trend of the correlation coefficients was represented. Before the slumping of the molten core into the LP, hydrogen production has a statistically significant correlation with K1 (positive correlation), K2 (negative correlation) and the debris porosity parameter (negative correlation). The importance of the K1 and K2 parameters from a correlation point of view was also highlighted during the uncertainty application of the QUENCH-06 test, discussed in 3.3.5. After the slumping, the statistical correlation of the coefficients characterizing the oxidation kinetics of zircalloy changes from significant to moderate in the case of K2 and from significant to low in the case of K1. On the other hand, the statistical correlation of UO_2/ZrO_2

eutectic temperature goes from low to moderate and at around 55000 seconds it becomes significant.

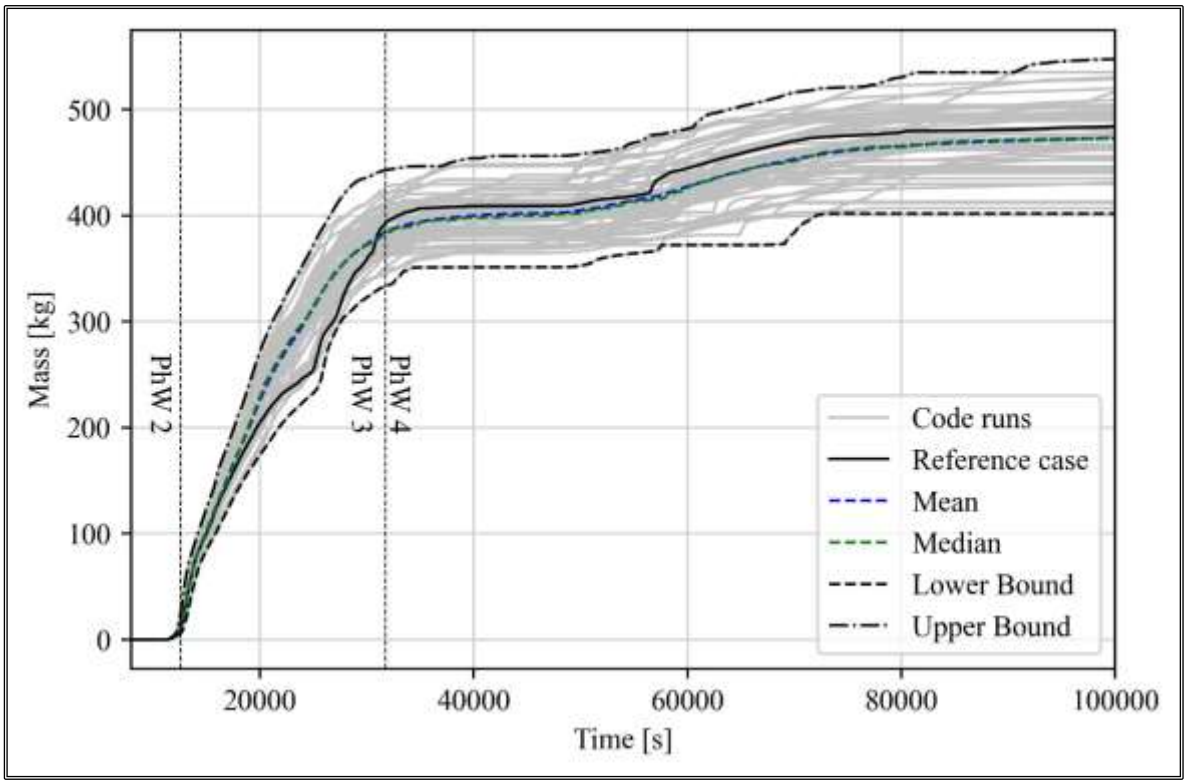

Figure 5.75 Hydrogen cumulative mass uncertainty band.

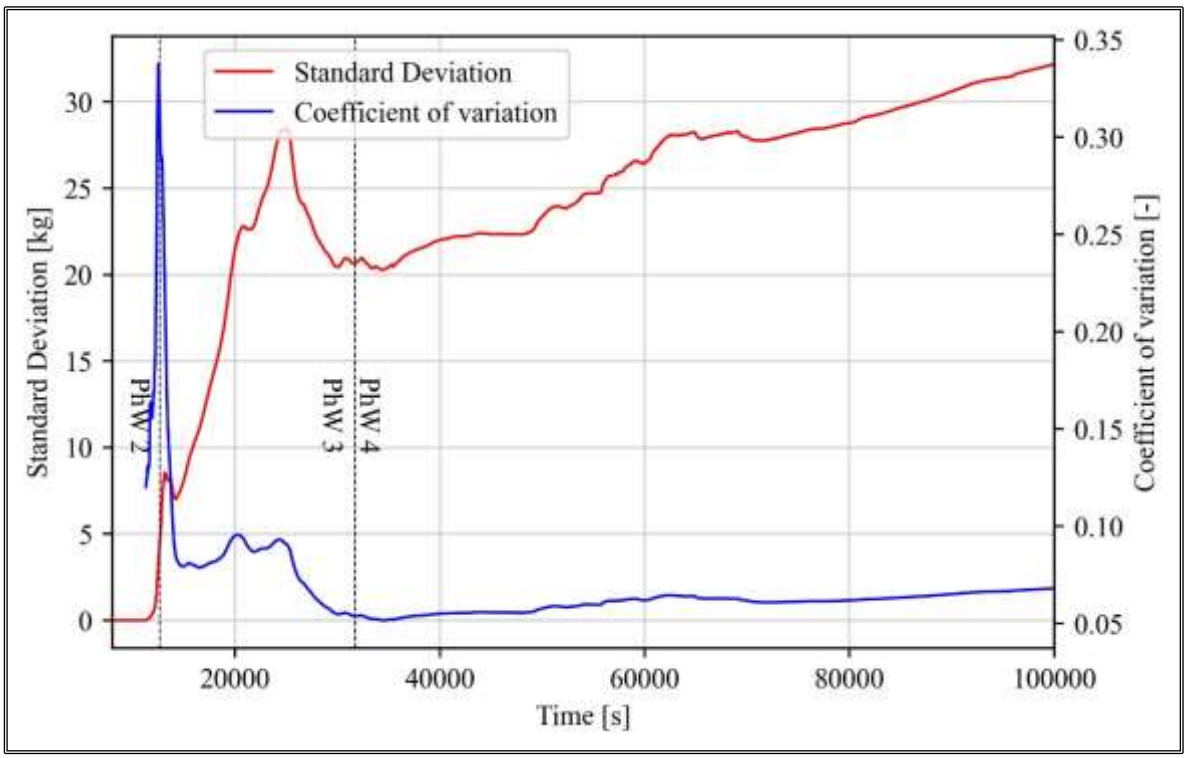

Figure 5.76 Standard deviation and coefficient of variation of the hydrogen cumulative mass.

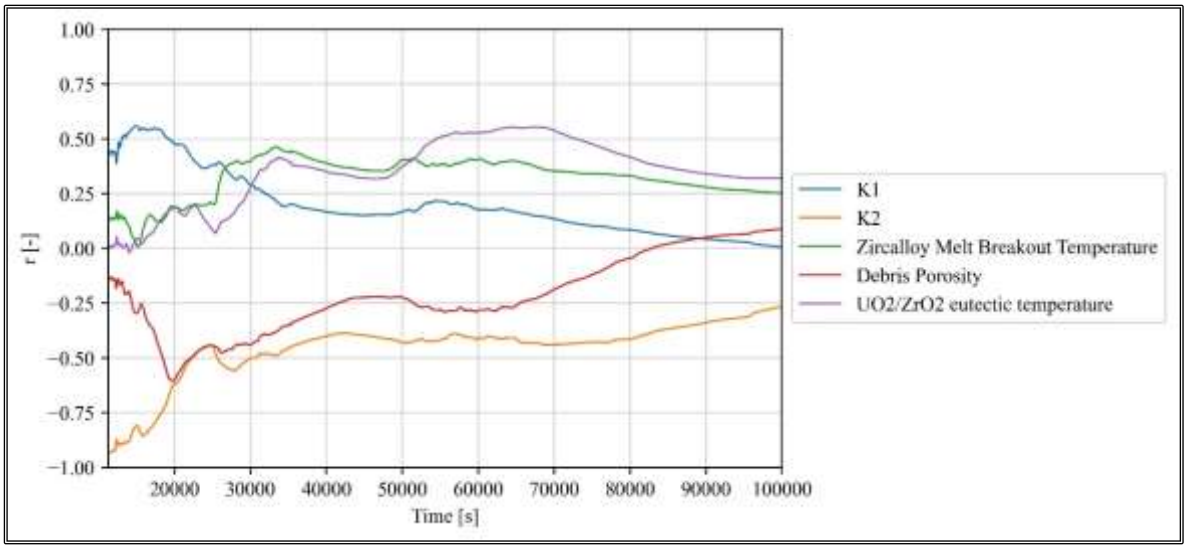

Figure 5.77 Simple correlation coefficient calculated along the transient.

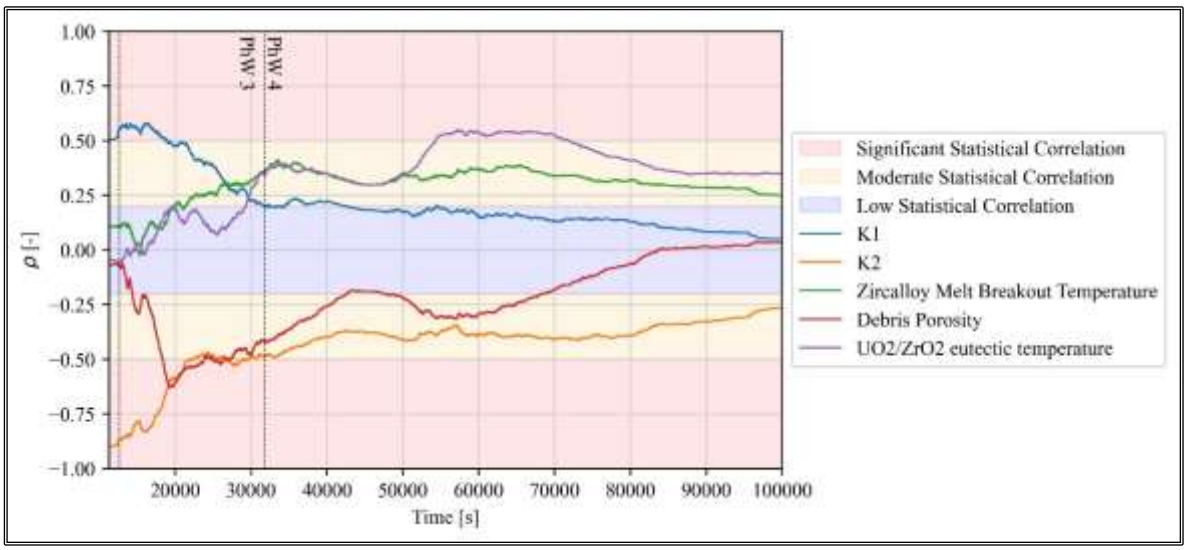

Figure 5.78 Simple rank correlation coefficient calculated along the transient.

Conclusions

The research campaign discussed in this work is framed within the scope of the ongoing R&D activities conducted by the international nuclear scientific community dealing with SAs and aimed, at first, to explore and investigate know-how and methodologies established in the past about uncertainty quantification of thermal-hydraulic system codes results and, considering the need to define and consolidate the state-of-the-art for the uncertainty methodology in the SA domain using SA integral codes, to investigate the applicability of such methodologies in SA domain.

In this view, the uncertainty methodology based on the adoption of the "probabilistic method to propagate input uncertainty" has been tested against two experimental tests: the Phebus FPT1 and the QUENCH-06 tests. These activities have been carried out respectively within the framework of the HORIZON 2020 MUSA and the IAEA CRP projects and their pivotal objective regards gaining insights about the uncertainties of the MELCOR code on aerosol physics and hydrogen production mechanisms and the statistical correlations between the FOMs and uncertain input parameters. On the other hand, these applications have been pivotal for the PhD program since they allowed for the creation and the assessment of computational environments employed for the uncertainty quantification studies here presented. In this regard, it has been highlighted that a computational environment involving the use of an external UT allows the user to fully exploit its potential and the use of complex models. The uncertainty analysis of the Phebus FPT1, conducted by using the coupling between MELCOR and DAKOTA in Python, highlighted that the set-up of a coupling between a SA integral code and an UT could be not particularly user-friendly, requiring a scripting-based approach. Starting from the expertise gained during the first application of the uncertainty methodology, the research campaign discussed in this work focused on the development of an independent tool, totally written in Python language. It has been highlighted that using a full scripting approach requires not basic programming knowledge and an initial time for the development of the scripts, but it allows one to obtain a tool that is highly customizable according to the user's needs and easily updated over time.

Then, the methodology and the computational environments have been applied to two different full plant applications. Within the framework of the MUSA project, uncertainties of the MELCOR code on aerosol physics have been evaluated during an unmitigated SBO in a generic PWR-900 and compared with ones obtained in the previous Phebus FPT1 uncertainty application. From the comparison, based on normalized values on mean, of the empirical PDFs of the FOM, the uncertainty band, as well as the form of the PDFs obtained,

are qualitatively similar. On the other hand, in both applications, the GAMMA parameter, representing the aerosol agglomeration shape factor, presents a statistically significant correlation with FOM and is quantitatively comparable.

Subsequently, the uncertainty methodology has been applied to an innovative SMR based on the iPWR concept. In this regard, during the last year of the PhD program, a generic iPWR MELCOR nodalization has been developed in the framework of the Horizon Euratom SASPAM-SA project. The thermal-hydraulic response of the code throughout a DBA sequence has been compared with the results of the integral SA code ASTEC in a code-to-code benchmark activity. It shows a quantitative and qualitative good prediction of the main phenomena characterizing the iPWR design concept, based on the adoption of passive safety systems. Afterwards, to investigate the uncertainties of the code on thermal-hydraulics phenomena in view of the SA uncertainty application, the uncertainty analysis of the DBA sequence has been carried out, adopting the full UT developed in Python, considering uncertain input parameters related to boundary conditions and passive safety systems. The uncertainties of the code have been analysed by assessing three relevant FOMs for the safety of such plant conceptual design such as the peak of the maximum cladding temperature, the minimum collapsed level in the core region and the maximum containment pressure. A moderate and significant statistical correlation has been underlined between the FOMs and the Heat Transfer Surface of EHRS HXs, the initial DW pressure and the ADS Stage-1 loss coefficient. Then, the uncertainty analysis in the SA domain has been carried out to have first insights about the uncertainty of the code on hydrogen production on a potential SA sequence in the iPWR design, considering some of the main uncertainty parameters influencing the production of in-vessel hydrogen described in the literature. These applications have made it possible not only to test and apply the methodologies previously discussed but, on the other hand, to obtain preliminary feedback on the uncertainties that the code returns when applied to an innovative system and based on the use of passive systems, providing key information to the community about the applicability of integral SA system codes to light water SMRs.

During the three years of the PhD program in Energy, the research activity discussed has allowed to apply the methodology already used and consolidated in the field of thermal-hydraulics and to adapt it, trying to cope with the main difficulties encountered by the international scientific community in the SA domain. In future developments, the methodology can be further enriched, considering mixed approaches with the use of artificial intelligence and/or machine learning methods.

APPENDIX A

MELCOR CODE DESCRIPTION

MELCOR [29] [30] is a fully integrated, engineering-level SA integral code, developed by SNL for the USNRC to model the progression of SA in LWRs, Spent Fuel Pools (SFPs) and gas reactors. The code is based on a finite-difference resolution method for the conservation equations of the Control Volumes (CVs) and can be used with SNAP.

In general, MELCOR is designed to model:

- Thermal-hydraulic phenomena typical of the PCS of a reactor, the reactor cavity and the containment.
- Core degradation phenomena.
- Thermo-mechanical behaviour of the LH and its possible failure.
- Interactions between corium and the concrete composing the reactor cavity (MCCI).
- Release, transport and deposition phenomena of FPs.
- Aerosol and vapour physics.

MELCOR is characterized by a modular structure with multiple packages. The packages permit the simulation of typical SA phenomena. In Table A-1 a list of the packages composing the MELCOR code is presented. In the following paragraphs, the CVH, FL, HS, COR and RN packages are described in more detail.

A.2 CVH package

The Control Volume Hydrodynamic (CVH) package permits to model of the hydrodynamic material, composed of liquid phase, vapor phase, non-condensable gases, and fog. CVH package describes the state of the fluid in each CV in terms of temperature, pressure, etc. Instead, the connections between CVs are modelled by the FL package, described in the next section.

The geometry of a CV is defined by the user in a volume/height tabular function. Each row of the table corresponds to the cumulative volume available to the hydrodynamic fluid, defined as *hydro volume*, at the specified altitude, as schematically shown in Figure A-1. The hydro volume does not consider the volume occupied by the intact core structures or by the ice condenser. These components occupy a volume, named *virtual volume*, defined in

different packages. The virtual volume may change along the transient and, in turn, may cause the variation of hydro volume.

Table A-1 MELCOR code packages [29] [30].

Package name	Extended package name
EXEC	Executive
ACC	Accumulator
BUR	Burn
CAV	Cavity
CND	Condenser
CF	Control Function
COR	Core
CVH	Control Volume Hydrodynamic
DCH	Decay Heat
EDF	External Data File
FCL	Fan Cooler
FDI	Fuel Dispersal
FL	Flow Path
HS	Heat Structure
MP	Material Properties
NCG	NonCondensable
PAR	Passive Autocatalytic Hydrogen Recombiner
RN	RadioNuclide
SPR	Containment Sprays
TF	Tabular Function
TP	Transfer Process

Therefore, the volume available to hydrodynamic material varies as a function of time. Figure A-2 shows a diagram referencing the hydro volume and the virtual volume associated. The hydro volume is divided into *pool* and *atmosphere*, as shown in Figure A-3. The pool consists of single-phase or two-phase liquid water, and the atmosphere contains water vapour and/or non-condensable gases. The atmosphere may also contain suspended water droplets called fog.

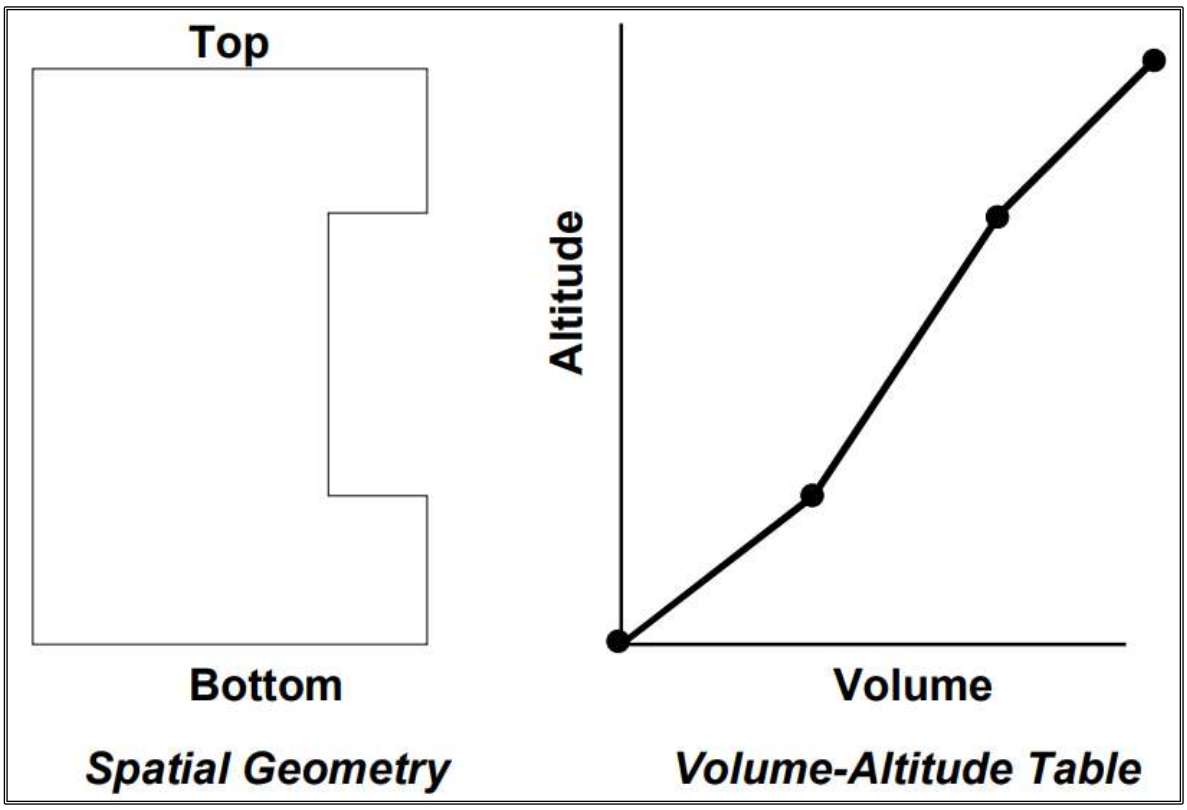

Figure A-1 Definition of the geometry of a CVH CV [30].

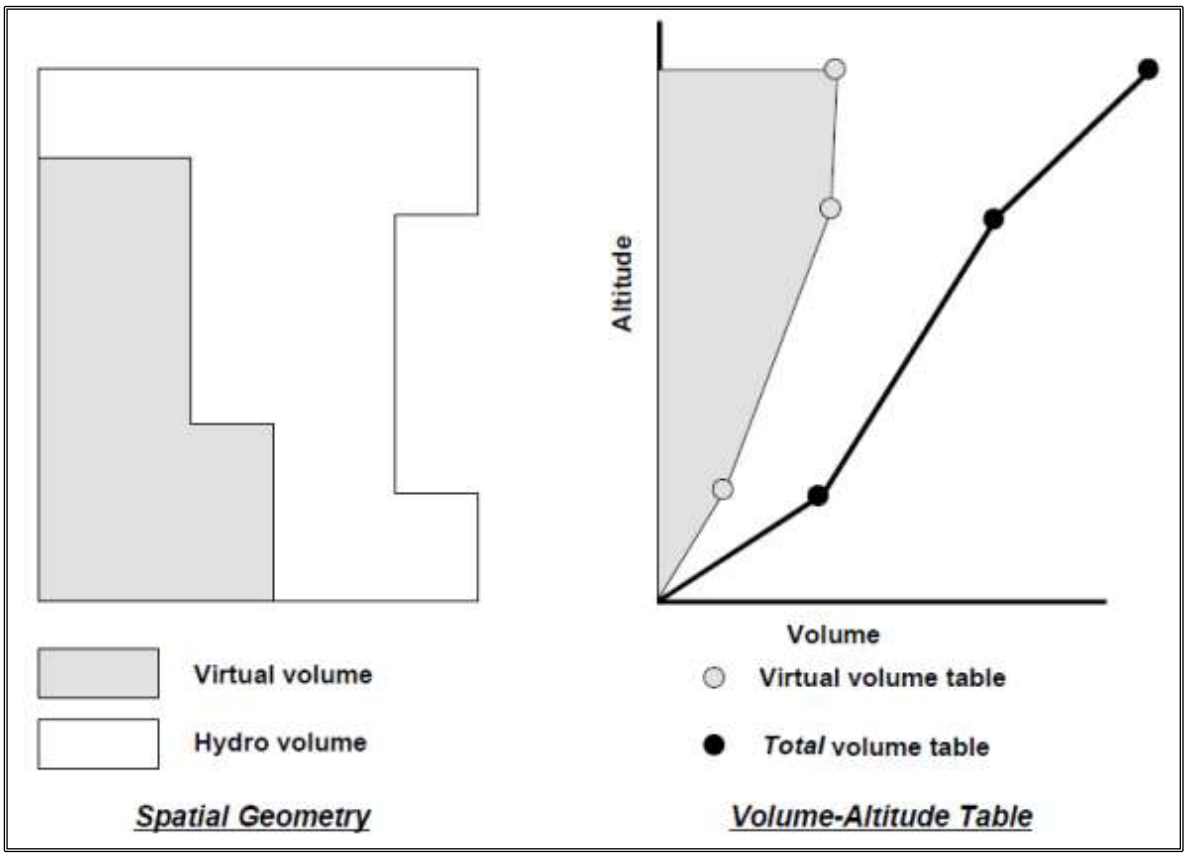

Figure A-2 Hydro-volume and virtual-volume [30].

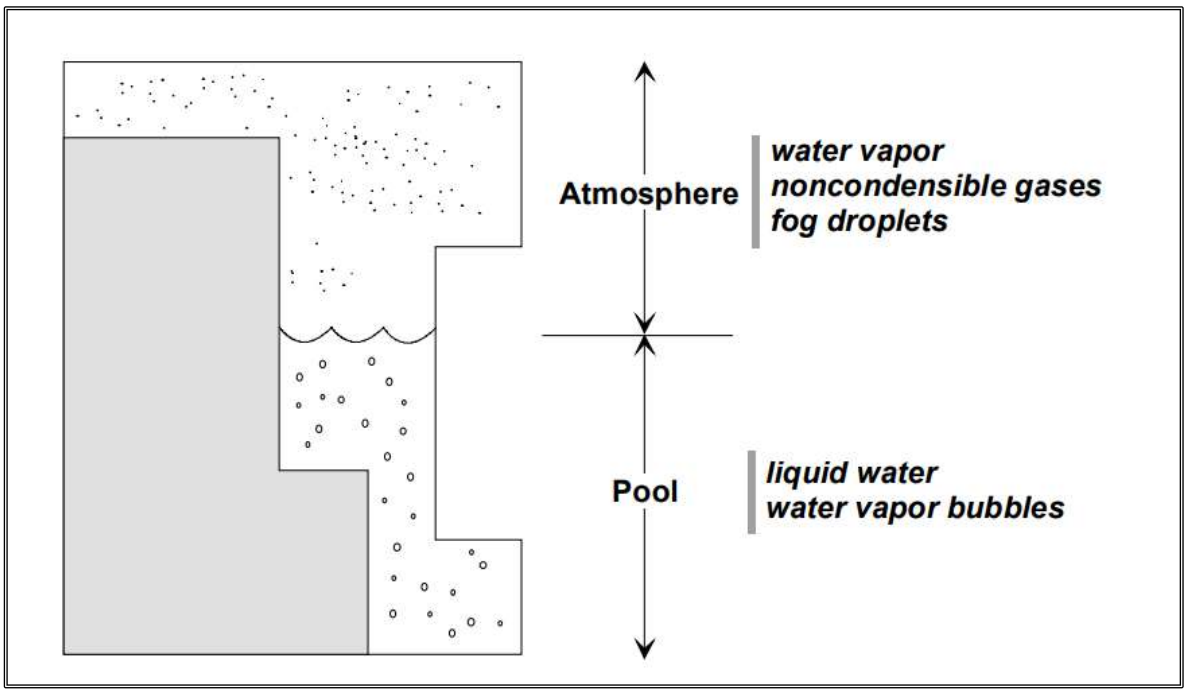

Figure A-3 Definition of pool and atmosphere [30].

A.3 FL package

The Flow Path (FL) package allows to model of the geometry and main characteristics of the connections between the CVs and permits the flow of hydrodynamic material, as shown in Figure A-4. Therefore, the FL package permits to modelling of distributed and concentrated pressure drops, and the presence of valves and pumps. No fluid mass or energy is associated with each flow path. Instead, they are associated with CVs modelled with the CVH package.

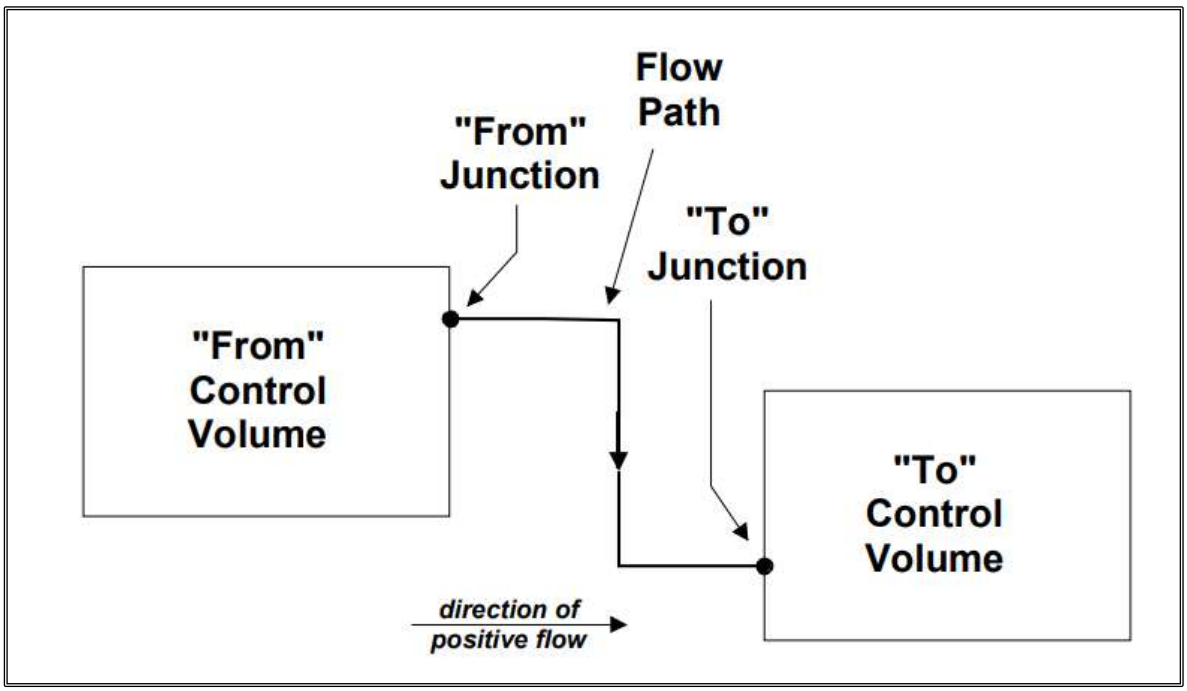

Figure A-4 Definition of a flow path [30].

A.4 HS package

The package Heat Structure (HS) is responsible for calculating heat transfer between structures and the hydrodynamic material contained in the CVs, as shown in Figure A-5. In general, an HS is defined as an intact solid structure, characterized by one-dimensional thermal conduction heat transfer, with specific boundary conditions for each of the two surfaces. It can be characterized by a rectangular, cylindrical, spherical, or hemispherical geometry.

As shown in Figure A-5, an HS is modelled using nodes, where the first is relative to the left boundary surface and the last is relative to the right boundary surface regarding rectangular geometry; on the other hand, it is relative to the inner and outer surface respectively in the case of cylindrical, spherical and hemispherical geometry. Each region between two adjacent nodes can contain different materials, the properties of which are provided by the Material Properties (MP) package. On each of the two boundary surfaces, a boundary condition can be imposed between adiabatic conditions, convective conditions, imposition of surface temperature, or imposition of surface heat flux.

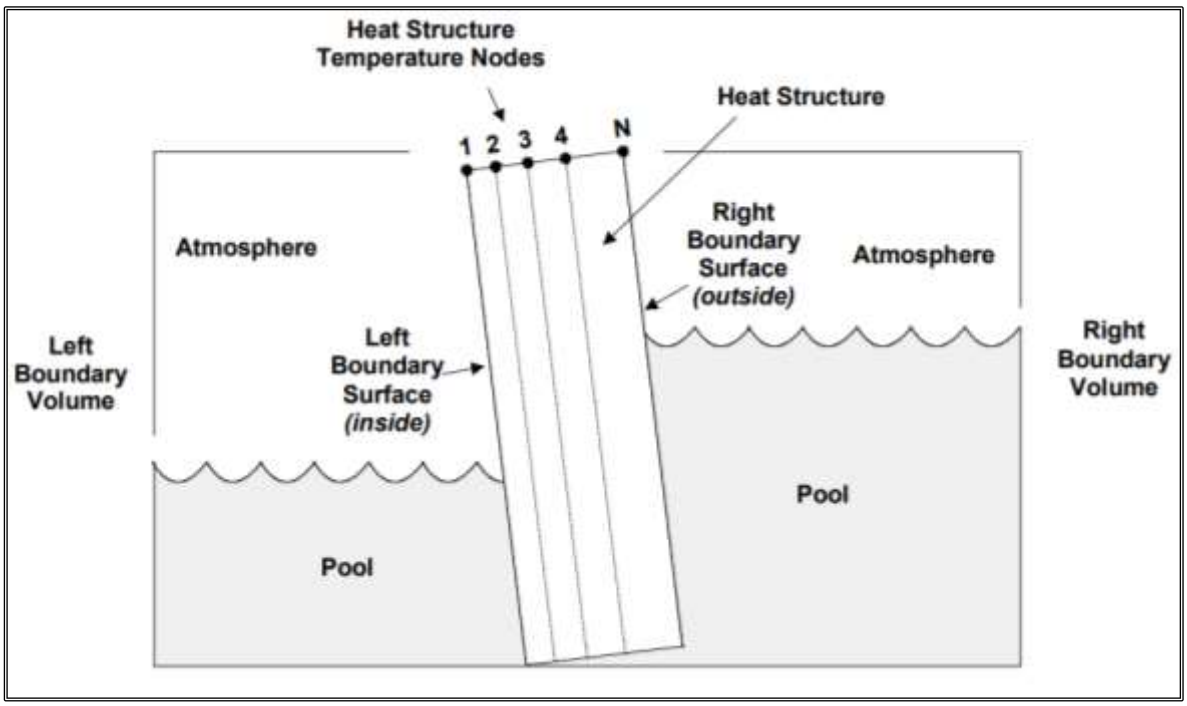

Figure A-5 Scheme of a generic HS [30].

To calculate the evolution of the thermal field in an HS, MELCOR uses finite difference equations, obtained from the integral form of the one-dimensional equation of thermal conduction by an implicit numerical method. Using the finite difference approximation, a tridiagonal system of equations, equal to the number of nodes, is obtained which is solved by the algorithm for tridiagonal systems of linear equations. This provides for an iterative solving, with the updating of the coefficients, a function of the temperature, at each timestep of the calculation.

A.5 COR package

The CORe (COR) package allows the calculation of the response of the reactor core and the structures associated with it, as well as the structures located within the LP. It permits obtaining the transient response of these structures, modelling their relocation in the LP during an unmitigated transient sequence. Therefore, it allows to simulation of the formation of debris, the failure of LH and the consequent relocation of the corium within the reactor cavity.

The reactor core and LP region are modelled subdividing it into radial rings and axial levels. Then, a certain number of cells are defined, as shown in Figure A-6. Each cell contains different components, including fuel, cladding, canisters, particulate debris, molten pool, etc. The materials of which each component is composed (e.g. UO_2, zircalloy, steel, etc.) can melt, relocate, solidify, etc. The LH is modelled using different geometries (e.g.

hemispheric shell, truncated hemispheric shell or plate) as shown in Figure A-7. It is divided into nodes and segments. Each segment interfaces with one or more core cells. The code assumes that the failure of the LH occurs based on several criteria, such as the achievement of a critical temperature of one of the LH nodes.

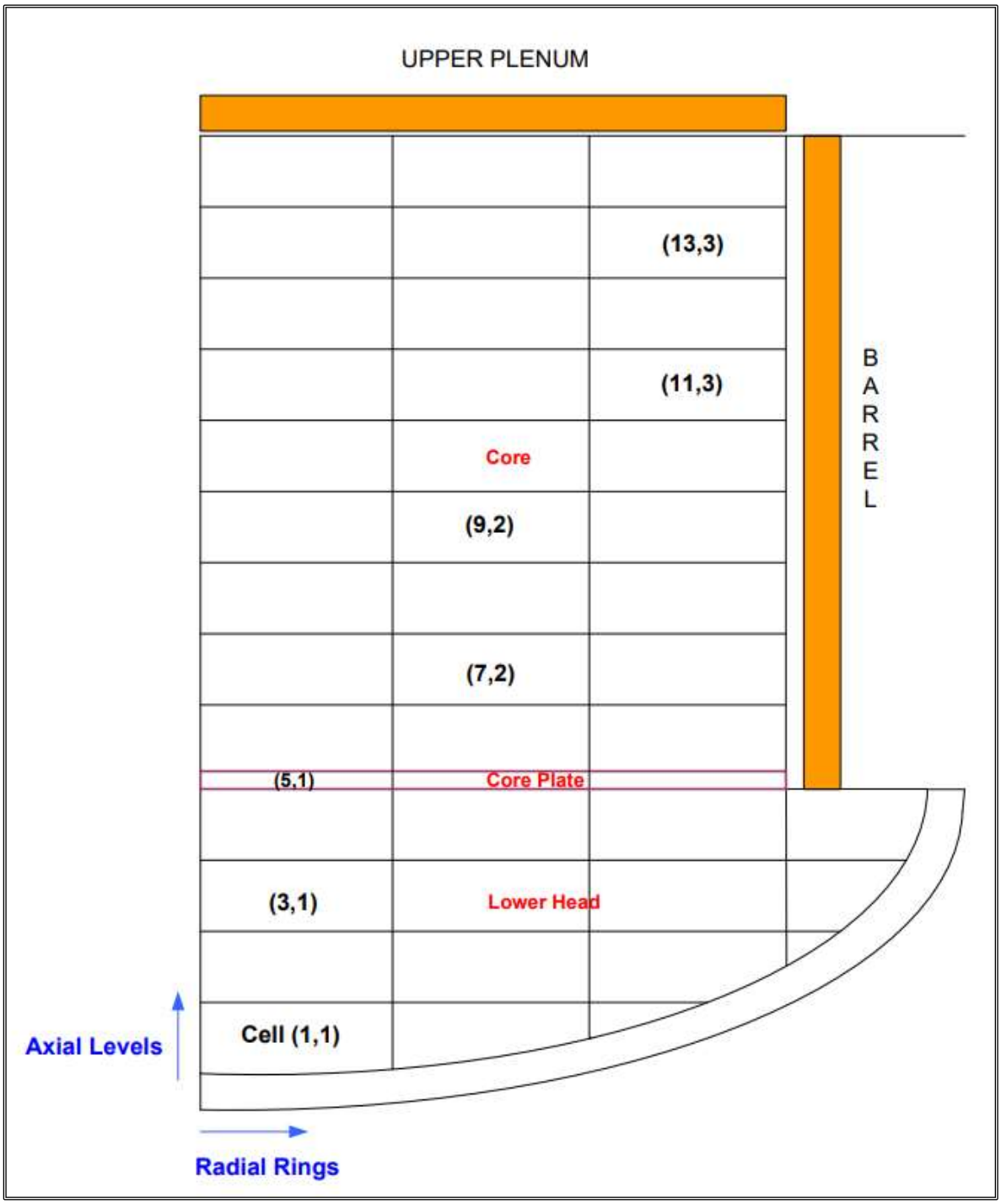

Figure A-6 Generic scheme of the COR package nodalization [30].

The materials composing the core can be relocated by melting, candling, or due to mechanical failure. In the latter case, they are converted to particulate debris. Such relocation

processes often involve interactions between the various materials, through the formation of eutectic mixtures, for which the code has specific models. When the materials composing the core begin the melting process, it is assumed that they begin the candling process, except for molten metals which are supported by oxide shells. Intact components in cells are reduced to particulate debris when the residual thickness of non-oxidized metals is reduced below a user-defined threshold or when they lose the associated support structure. An exception is made for fuel rods. It is assumed that the fuel rods do not fail until the temperature reaches the eutectic temperature value of the UO_2/ZrO_2 eutectic mixture.

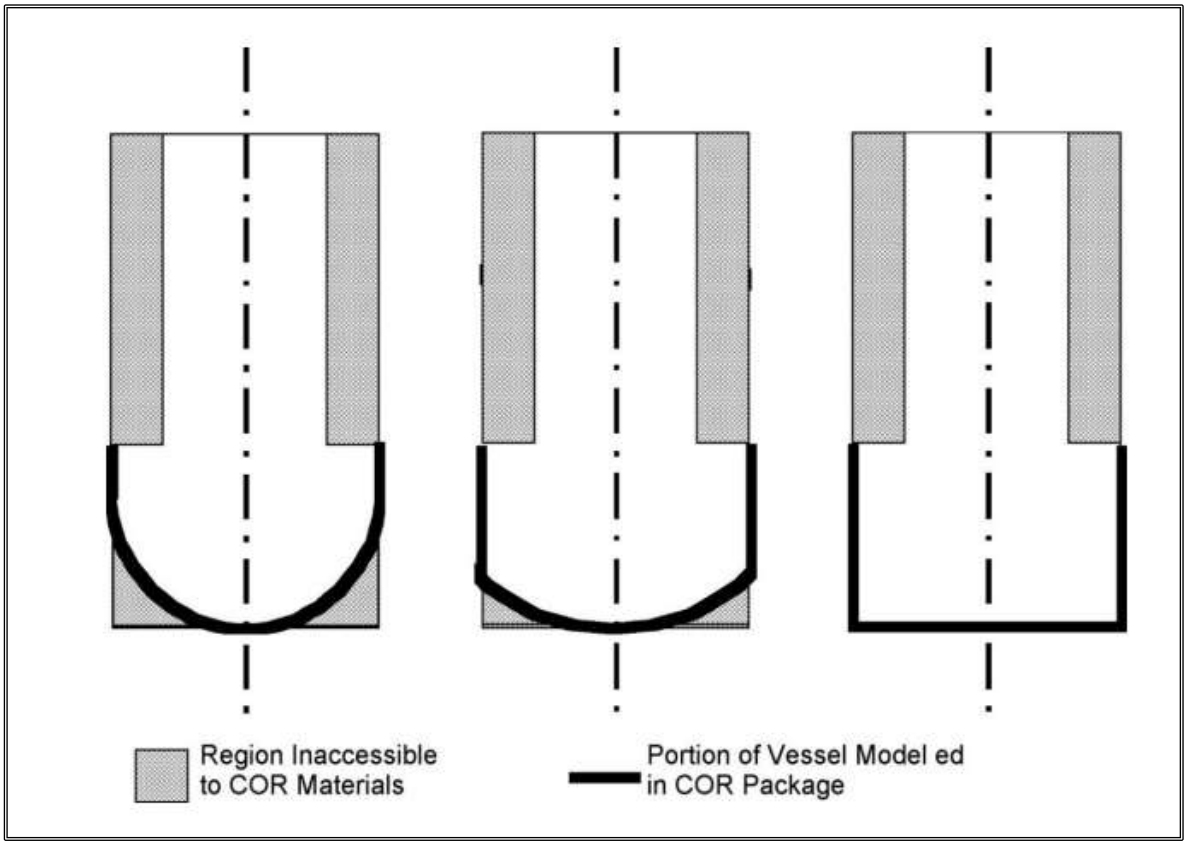

Figure A-7 Different modelling approaches for the LH in the COR package [30].

A.6 RN package

The RadioNuclide (RN) package models FPs in the form of aerosols and vapours. It is based on the definition of classes. They are defined as groups of elements with similar chemical properties. By default, MELCOR considers 17 classes. The radionuclides which are contained in the fuel, modelled in the COR package, are hypothesized in elemental form and are converted into compounds after the release. The code considers four specific models used to calculate the release of radionuclides from the fuel of the core. On the other hand, concerning the release in the cavity, the RN package uses the VANESA model coupled with

CORCON, a specific code part of the package modelling the reactor cavity and able to simulate MCCIs.

The modelling of aerosol physics is based on the MAEROS (Multi-Component Aerosol Module for CONTAIN) code. Aerosols can be deposited on the surfaces of HSs or pools through several processes, including gravity deposition, diffusion, thermophoresis, and diffusiophoresis. In addition, it is considered that aerosols can also migrate from one CV to another through available flow paths. Finally, aerosols can also be subject to agglomeration, reaching larger diameters than a minimum diameter, which is set by the user.

A.7 Validation of MELCOR code

MELCOR is validated against numerous experiments simulating SA sequences carried out by the USNRC, the EPRI, DOE and numerous other international research programs such as the OECD through the ISPs.

More than 50 tests were selected for the validation of MELCOR. Figure A-8 provides a summary of the experiments used for the validation of the code.

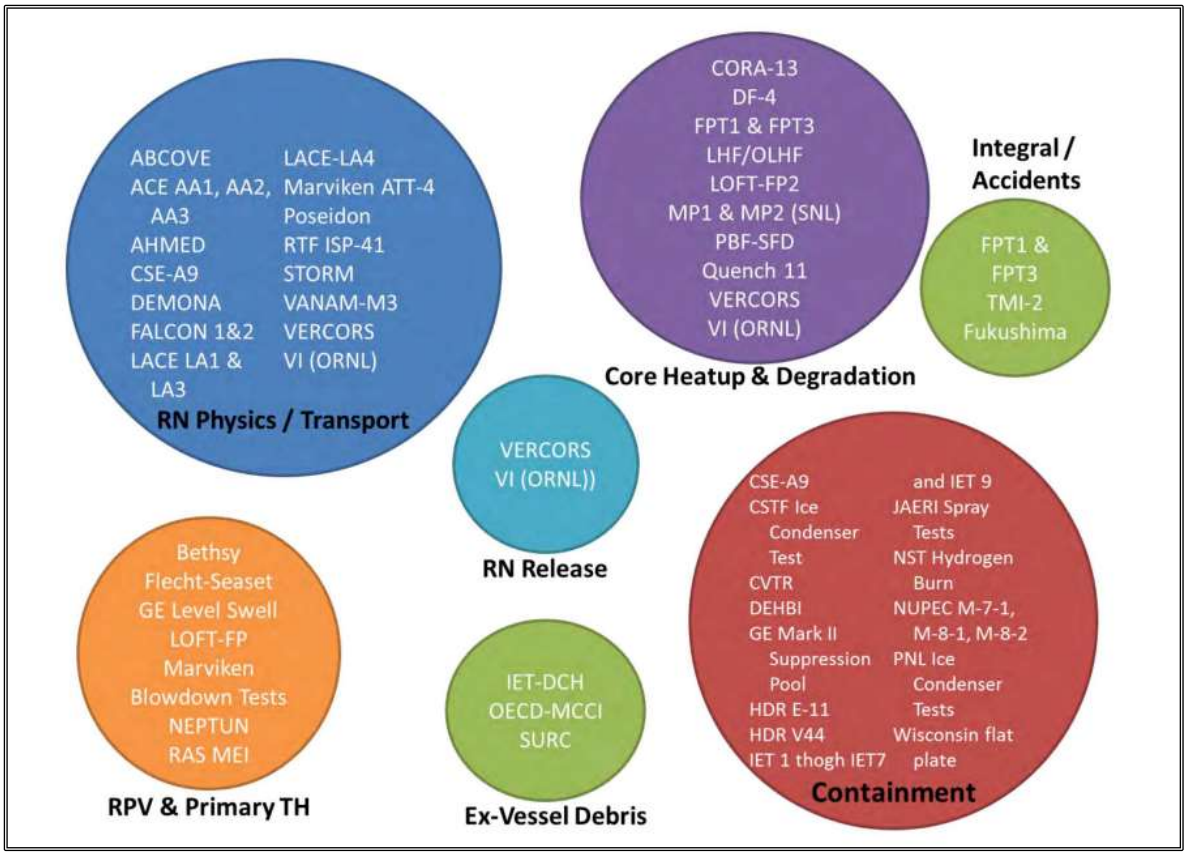

Figure A-8 Tests used for the MELCOR code validation [99].

They were categorized according to the type of phenomena examined: physics and radionuclide transport (RN Physics/Transport), radionuclide release (RN Release), heat up

and degradation of the core (Core), thermal-hydraulics of RPV and PCS (RPV & Primary TH), reactor containment behaviour (Containment), behaviour of the corium during ex-vessel phase (Ex-vessel Debris) and integral experiment (Integral/Accidents). These tests allowed the validation of numerous phenomena including heat transfer, material oxidation, reflooding refrigeration, core degradation, modelling of melt pools, FPs release, LH failure, critical flow, MCCI phenomena, DCH, condensation processes, thermal stratification of containment, hydrogen combustion, hygroscopic effect, aerosol deposition, radionuclide transport, iodine chemistry, pool scrubbing and vent cleaning.

Most of the packages of the code have been validated against these tests except for the Condenser, Fan Cooler and Passive Autocatalytic Recombiner packages. Additionally, some models are included in the code but not validated against the examined validation tests. These models are the point kinetics model, High-Temperature Gas Reactor model, SFP model, LH penetration model, mechanical model, integral heat exchanger model, flashing model and the counter-current stratified model.

APPENDIX B

THE MUSA PROJECT

Funded in the HORIZON 2020, the MUSA project was aimed at determining a harmonized approach for uncertainty analysis during SA scenarios. It was coordinated by CIEMAT (Spain) and involved European and non-European organizations. In general, the goal of the project is to assess the SA integral codes capabilities in modelling NPP and SFPs. It is reached by identifying the uncertainty methodologies to be used. Furthermore, specific innovative SAM related to the mitigation of source terms has been identified. Then, state-of-the-art SA integral codes have been used to determine source term prediction and the uncertainties related have been quantified.

The project was divided into seven different WPs. WP1 and WP7 were dedicated to the coordination and dissemination respectively. The other five WPs were divided as follows:

- Identification and Quantification of Uncertainty Sources (WP2).
- Review of Uncertainty Methodologies (WP3).
- Application of Uncertainty Quantification Methods against Integral Experiments (WP4).
- Uncertainty Quantification in Analysis and Management of Reactor Accidents (WP5).
- Innovative Management of SFP Accidents (WP6).

Further detailed information can be found in [72].

APPENDIX C

THE IAEA CRP ON ADVANCING THE STATE-OF-PRACTICE IN UNCERTAINTY AND SENSITIVITY METHODOLOGIES FOR SEVERE ACCIDENT ANALYSIS IN WATER-COOLED REACTORS

Started in 2019, the IAEA's CRP titled "Advancing the State-of-Practice in Uncertainty and Sensitivity Methodologies for Severe Accident Analysis in Water-Cooled Reactors" aims to advance the state-of-the-art uncertainty analysis of the results obtained with SA integral codes on SA sequences.

The project involves 22 organizations from 18 different countries and has a duration of 5 years. It focuses on the study of water-cooled reactors. The purpose of the project is to achieve a substantial advancement regarding the studies of accidental sequences with core degradation conducted by the project participants. In addition, the project aims to support and encourage collaboration among different international organizations to improve the competence and experience of using SA integral codes by organizing benchmarking activities. Finally, the purpose of the project is to disseminate the uncertainty results obtained from the research campaign conducted through the different tools employed.

To fulfil these goals, the CRP has been divided into four tasks described below:

- QUENCH-06 test application uncertainty exercise (Task 1).
- Plant application uncertainty exercise (Task 2).
- Develop reports on uncertainty and sensitivity in SA analysis (Task 3).
- Development of PhD training programme (Task 4).

Further detailed information can be found in [73] [75] and [76].

APPENDIX D

THE SASPAM-SA PROJECT

Currently, SMRs are one of the main options for the near-term realization of new nuclear reactors. Currently, there is a growing interest in Europe in the realization of SMRs, and in many countries, several activities are underway to prepare for eventual licensing.

Among the different SMR concepts, iPWRs build on the proven and well-established technology of LWRs and incorporate the plant's operational experience, including evolutionary modifications to increase its intrinsic safety.

Despite the reinforcement of the first three levels that characterize the DiD (e.g. design characterized by the use of passive systems), the demonstration of the ability of these systems to withstand possible SA sequences (levels four and five of the DiD) is required. Through the analysis of the already completed initiatives on iPWRs, the investigation of possible SA sequences in iPWRs is very limited and for this reason, an assessment of the safety in such plants during postulated SA sequences is necessary. For this reason, the analysis of the applicability and transfer of the current experimental database developed for the already operational LWRs to advanced iPWRs to assess their safety is a topic of great technical and scientific interest.

In this framework, the SASPAM-SA project, coordinated by ENEA (Italy) and funded in Horizon-Euratom, aims to investigate the applicability and transfer of the knowledge and know-how related to large LWR to the near-term deployment of iPWR, given SA and Emergency Planning Zone (EPZ) European licensing needs.

The project aims to identify plausible SA sequences in iPWRs and to evaluate possible conditions of the RPV and containment under these sequences which differ from those in LWRs. Furthermore, the project is focused on evaluating the applicability of the existing experimental database (related to LWR) to iPWRs and assessing the capabilities of European and Non-European SA integral code in predicting the response of iPWR under postulated SA scenarios to assess the radiological impact on- and off-site, considering special SA mitigation and management strategies.

The structure of the project is characterized by seven WPs (including one for coordination and one for dissemination). They are divided into:

- Development of generic but representative iPWR SA code input decks and the analysis of the iPWR behaviour under hypothetical postulated SA conditions (WP2).

- Study the relevance and applicability of the existing experimental database to iPWR, develop methods to extend the applicability of existing data, and identify the need for new experiments (WP3).
- Investigate the IVMR strategy in a postulated SA scenario in iPWR, assess the capability to simulate the main phenomena characterizing the IVMR in iPWR, and characterize its feasibility by guided calculations (WP4).
- Study the containment behaviour during a SA in an iPWR (WP5).
- Provide evaluations of size and extension of EPZ for selected SA scenarios coupling the results of best estimate ST codes to radiological consequences tools (WP6).

To maximize the project's results, two generic iPWR designs were considered. The two designs include the main iPWR evolutionary features compared to large LWR and, therefore, allow to study in a wider way the capabilities of the tools to simulate the main SA phenomena. It is not the project’s objective to assess the generic reactor designs selected. Instead, it aims to make broader statements on the code's applicability to iPWR under postulated SA conditions. No PSA considerations will be made due to the generic nature of the reactor concept considered. The scenarios identified will be characterized by their severity, not probability. The proposed project outcomes are intended to support the iPWR licensing process by highlighting key elements of the necessary safety demonstration, thereby helping to expedite the licensing process.

Further detailed information can be found in [125] [126] and [148].

Acknowledgements

The development of the research activity discussed in this thesis has been something extremely challenging, representing a long, extremely complex, but incredibly rewarding journey. During these three years of my PhD in Energy at the University of Palermo, I have been presented with various challenges, professional but also personal, that have allowed me to grow, enrich my knowledge and skills and prepared me to face new challenges that life will put in front of me with confidence and determination.

I would like to express my sincere gratitude to my Supervisor, Prof Pietro Alessandro Di Maio, for his guidance and ever-present support throughout my career. His experience and passion for research have been and will be a constant source of inspiration for me. In addition to his professional support, I am grateful for his support and for believing in my abilities even in times of doubt.

A special thanks go to my co-supervisor, Dr Fulvio Mascari, for his constant presence and assistance during these three years. His willingness to discuss ideas, his ability to provide constructive feedback and his encouragement helped me to overcome obstacles along the way and to grow as a young researcher.

I deserve special thanks to my UNIPA colleagues of the LAMNE group: Francesca, Salvatore, Silvia, Alberto, Andrea, Ilenia, Eugenio, Gaetano, and Prof Pierluigi Chiovaro. They were fundamental during this PhD journey, considering their constant support.

A sincere thanks go to the colleagues of the ENEA team: Gianmarco, Pietro, Andrea, Stefano, Antonio, Mattia and the head of the ENEA laboratory Dr Federico Rocchi. They supported me during my research activity, always demonstrating availability and competence.

Finally, I would like to thank my friends who have always supported and blindly believed in me and my abilities since the first day I started this journey. A thousand thanks to my family for their infinite support, even during times when I was away from home.

UNIPA carried out the research activity with MELCOR code and SNAP, obtained in the framework of the UNIPA-ISIN agreement signed on March 26th 2021 as part of the General Arrangement between the United States Nuclear Regulatory Commission (US-NRC) and the Italian National Inspectorate for Nuclear Safety and Radiation Protection (ISIN).

ENEA carried out the research activity with MELCOR code and SNAP, obtained in the framework of the ENEA-ISIN agreement signed on March 23rd 2020 as part of the General Arrangement between the United States Nuclear Regulatory Commission (US-NRC) and the Italian National Inspectorate for Nuclear Safety and Radiation Protection (ISIN).

Bibliography

[1] IAEA, “Format and Content of the Safety Analysis Report for Nuclear Power Plants,” Vienna, 2004.

[2] IAEA, “Safety Assessment of Research Reactors and Preparation of the Safety Analysis Report,” Vienna, 1994.

[3] IAEA, “IAEA Safety Glossary: Terminology Used in Nuclear Safety and Radiation Protection,” Vienna, 2018.

[4] International Nuclear Safety Advisory Group, “Defence in Depth in Nuclear Safety, INSAG-10,” IAEA, 1996.

[5] IAEA, “Deterministic Safety Analysis for Nuclear Power Plants,” Vienna, 2019.

[6] IAEA, “Safety of Nuclear Power Plants: Design,” Vienna (Austria), 2016.

[7] ETSON, “TECHNICAL SAFETY ASSESSMENT GUIDE DETERMINISTIC SEVERE ACCIDENTS ANALYSIS,” January 2013.

[8] D. Jacquemain, Nuclear power reactor core melt accidents, Current State of Knowledge, edp sciences, 2015.

[9] IAEA, “Status and Evaluation of Severe Accident Simulation Codes for Water Cooled Reactors,” IAEA-TECDOC-1872, 2019.

[10] J.P. Van Dorsselaere, T. Albiol, J.C. Micaelli, “Research on Severe Accidents in Nuclear Power Plants,” in *Nuclear Power - Operation, Safety and Environment*, IntechOpen, 2011.

[11] NEA/CSNI, “In-Vessel Core Degradation Code Validation Matrix Update 1996-1999,” NEA/CSNI/R(2000)21, 2001.

[12] NEA/CSNI, “CSNI Integral Test Facility Validation Matrix For The Assessment Of Thermal-Hydraulic Codes For LWR LOCA and Transients,” NEA/CSNI/R(96)17.

[13] NEA/CSNI, “Separate Effects Test Matrix for Thermal-Hydraulic Code Validation,” NEA/CSNI/R(93)14.

[14] NEA/CSNI, “Evaluation of the Separate Effects Tests (SET) Validation Matrix,” NEA/CSNI/R(96)16.

[15] NEA/CSNI, “Relevant Thermal Hydraulic Aspects of Advanced Reactor Design, Status Report,” ODE/GD(97)8, NEA/CSNI/R(1996)22.

[16] IAEA, “Natural circulation in water cooled nuclear power plants: Phenomena, models, and methodology for system reliability assessment,” IAEA-TECDOC-1474, 2005.

[17] IAEA, “Passive Safety Systems and Natural Circulation in Water Cooled Nuclear Power Plants,” IAEA-TECDOC-1624, 2009.

[18] IAEA, “Natural Circulation Phenomena and Modelling for Advanced Water Cooled Reactors,” IAEA-TECDOC-1677, 2012.

[19] L. Soffer, S.B. Burson, C.M. Ferrel, R.Y. Lee, J.N. Ridgely, “Accident Source Terms for Light-Water Nuclear Power Plants,” NUREG-1465, 1995.

[20] IAEA, “Approaches and Tools for Severe Accident Analysis for Nuclear Power Plants,” Safety Report Series 56, 2008.

[21] OECD/NEA/CSNI, “State-of-the-Art Report on Molten-Corium-Concrete interaction and Ex-Vessel Molten-Core Coolability,” Report NEA/CSNI/R(2016)15, 2016.

[22] OECD/NEA/CSNI, “State-Of-The-Art Report On Nuclear Aerosols,” NEA/CSNI/R(2009), 2009.

[23] B.R. Sehgal, Nuclear Safety in Light Water Reactors, Severe Accident Phenomenology, Boston: Academic Press, 2012.

[24] F. Mascari, H. Nakamura, K. Umminger, F. De Rosa, F. D'Auria, “Scaling issues for the experimental characterization of reactor coolant system in integral test facilities and role of system code as extrapolation tool,” Vols. NURETH-16, August 30 - September 4, 2015.

[25] F. Mascari, “Circolazione naturale e fenomenologie di boron dilution in reattori nucleari ad acqua in pressione,” Tesi di dottorato, Università degli Studi di Palermo, 2010.

[26] IAEA, “Safety Reports Series No. 56: Approaches and Tools for Severe Accident Analysis for Nuclear Power Plants,” IAEA, 2008.

[27] P. Chatelard, S. Belon, L. Bosland, L. Carénini, O. Coindreau, F. Cousin, C. Marchetto, H. Nowack, L. Piar, L. Chailan, “Main modelling features of the ASTEC V2.1 major version,” *Annals of Nuclear Energy*, vol. 93, pp. 83-93, 2016.

[28] EPRI, “Modular Accident Analysis Program Version 5.04,” EPRI Product ID 3002007340, Vol. 1-4, 2016.

[29] L.L. Humphries, B.A. Beeny, F. Gelbard, T. Haskin, J. Phillips, J. Reynolds, R.C. Schmidt, “MELCOR Computer Code Manuals: Vol. 1: Primer and User's Guide Version 2.2 r2023.0,” Sandia National Laboratories, Albuquerque (USA), 2023.

[30] L.L. Humphries, B.A. Beeny, F. Gelbard, T. Haskin, D. Louie, J. Phillips, J. Reynolds, R.C. Schmidt, “MELCOR Computer Code Manuals: Vol.2: Reference Manual Version 2.2 r2023.0,” Sandia National Laboratories, Albuquerque (USA), 2023.

[31] A. Wielenberg, L. Lovasz, P. Pandazis, A. Papukchiev, L. Tiborcz, P. Schöffel, C. Spengler, M. Sonnenkalb, A. Schaffrath, "Recent improvements in the system code package AC2 2019 for the safety analysis of nuclear reactors," *Nuclear Engineering and Design,* vol. 354, no. 110211, 2019.

[32] RELAP5 Code Development Team, "RELAP5/MOD 3.3 Code Manual," Vol 1–8, NUREG/CR-5535/Rev1, 2010.

[33] SCDAP/RELAP5 Development Team, "SCDAP/RELAP5/MOD3.2 Code Manual, Vol. 1–5," NUREG/CR-6150, INEL-96/0422, 1998.

[34] IAEA, Safety Reports Series No.52: Best Estimate Safety Analysis for Nuclear Power Plants: Uncertainty Evaluation, Vienna, 2008.

[35] F. D'Auria, "Best Estimate Plus Uncertainty (BEPU): Status and perspectives," *Nuclear Engineering and Design,* vol. 352, no. 110190, 2019.

[36] H. Glaeser, "GRS Method for Uncertainty and Sensitivity Evaluation of Code Results and Applications," *Science and Technology of Nuclear Installations,* vol. Volume 2008, no. 798901, 2008.

[37] F. Alcaro, A. Bersano, C. Bertani, F. Mascari, "BEPU analysis of a passive decay heat removal system with RELAP5/MOD3.3 and RELAP5-3D," *Progress in Nuclear Energy,* vol. 136, no. 103724, 2021.

[38] M.E. Stephens, B.W. Goodwin, T.H. Andres, "Deriving parameter probability density funtions," *Reliability Engineering and System Safety,* vol. 42, pp. 271-291, 1993.

[39] G. Roma, F. Di Maio, A. Bersano, N. Pedroni, C. Bertani, F. Mascari, E. Zio, "A Bayesian framework of inverse uncertainty quantification with principal component analysis and Kriging for the reliability analysis of passive safety systems," *Nuclear Engineering and Design,* vol. 379, no. 111230, 2021.

[40] A. Guba, M. Makai, L. Pal, "Statistical aspects of best estimate method-I," *Reliability Engineering and System Safety,* vol. 80, pp. 217-232, 2003.

[41] S.S. Wilks, "Determination of sample size for setting tolerance limits," *The Annals of Mathematical Statistics,* vol. 12, pp. 91-96, 1941.

[42] S.S. Wilks, "Statistical prediction with special reference to the problem of tolerance limits," *The Annals of Mathematical Statistics,* vol. 13, pp. 400-409, 1942.

[43] A. Wald, "An extension of Wilks' method for setting tolerance limits," *Annals of Mathematical Statistics,* vol. 14, pp. 45-55, 1943.

[44] G. Agnello, P.A. Di Maio, A. Bersano, F. Mascari, "Cold Leg LBLOCA uncertainty analysis using TRACE/DAKOTA coupling," *Journal of Physics: Conference Series,* vol. 2177, no. 012023, 2022.

[45] A. Bersano, F. Mascari, M.T. Porfiri, P. Maccari, C. Bertani, “Ingress of Coolant Event simulation with TRACE code with accuracy evaluation and coupled DAKOTA Uncertainty Analysis,” *Fusion Engineering and Design,* vol. 159, no. 111944, 2020.

[46] K.A. Gamble, L.P. Swiler, “Uncertainty Quantification and Sensitivity Analysis Applications to Fuel Performance Modeling,” SAND2016-4597C, 2016.

[47] J.L. Rodgers, A. Nicewander, “Thirteen Ways to Look at the Correlation Coefficient,” *The American Statistician,* vol. 42, pp. 59-66, 1987.

[48] United States Nuclear Regulatory Commission, “TRACE v5.0 Patch 6 Theory Manual,” 2020.

[49] United States Nuclear Regulatory Commission, “TRACE v5.0 Patch 6 User's Manual Volume 1: Input Specification,” 2020.

[50] United States Nuclear Regulatory Commission, “TRACE v5.0 Patch 6 User's Manual Volume 2: Modeling Guidelines,” 2020.

[51] USNRC, “RELAP5/MOD3.3 Code Manual Volume I: Code Structure, System Models, and Solution Methods,” NUREG/CR-5535.

[52] INL, “The RELAP5-3D Code Development Team, RELAP5-3D Code Manual Volume I: Code Structure, System Models and Solution Methods,” INL/MIS-15-36723. Revision 4.3, 2015.

[53] A. Bersano, G. Agnello, P.A. Di Maio, G. Grippo, F. Mascari, “BEPU analysis of an Upgraded ICE facility test by TRACE/DAKOTA coupling,” *Journal of Physics: Conference Series,* vol. 2685, no. 012055, 2024.

[54] F. D'Auria, N. Debrecin, G.M. Galassi, “Outline of the Uncertainty Methodology Based on Accuracy Extrapolation,” *Nuclear Technology,* vol. 109, 1995.

[55] W. Ambrosini, R. Bovalini, F. D'Auria, “Evaluation of accuracy of thermalhydraulic code calculation,” *Energia Nucleare,* vol. 7, pp. 5-16, 1990.

[56] F. D'Auria, G. Fruttuoso, G.M. Galassi, S. Galeazzi, F. Oriolo, “Application of the UMAE uncertainty method in assessing the design and the safety of new generation reactors,” in *Progress in design, research and development and testing of safety systems for advanced water cooled reactors*, Piacenza, Italy, IAEA-TECDOC-872, 16-19 May 1995.

[57] NEA/CSNI, “Containment Code Validation Matrix,” NEA/CSNI/R(2014)3.

[58] OECD/NEA/CSNI, “Source term uncertainty, recent development in understanding fission product behavior,” NEA/CSNI/R(92)2, 1992.

[59] OECD/NEA/CSNI, “SOAR on Containment Thermalhydraulics and Hydrogen Distribution,” NEA/CSNI/R(1999)16, 1996.

[60] F. Mascari, J.C. De La Rosa Blul, M. Sangiorgi, G. Bandini, "Analyses of an Unmitigated Station Blackout Transient in a Generic PWR-900 with ASTEC, MAAP and MELCOR Codes," NUREG/IA-0515, 2019.

[61] F. Mascari, F. Rocchi, P. Carny, L. Liptak, M. Adorni, J. Fontanet, L.E. Herranz, "FASTNET SCENARIOS DATABASE DEVELOPMENT AND STATUS," The 9th European Review Meeting on Severe Accident Research (ERMSAR2019), Prague, Czech Republic, March 18-20, 2019.

[62] J.P. Van Dorsselaere, J. Mustoe, S. Power, M. Adorni, A. Schaffrath, A. Nieminen, "ETSON views on R&D priorities for implementation of the 2014 Euratom Directive on safety of nuclear installations," *Kerntechnik,* vol. 81(5), pp. 527-534, 2016.

[63] N. Bixler, R. Gauntt, J. Jones, M. Leonard, "State-of-the-Art Reactor Consequence Analyses Project, Volume 1: Peach Bottom Integrated Analysis," NUREG/CR-1710, Albuquerque, New Mexico, 2013.

[64] USNRC, "State-of-the-Art Reactor Consequence Analyses Project, Volume 2: Surry Integrated Analysis," NUREG/CR-7110, Albuquerque, New Mexico, 2013.

[65] N.E. Bixler, M. Dennis, K. Ross, D.M. Osborn, R.O. Gauntt, K.C. Wagner, S.T. Ghosh, A.G. Hathaway, H. Esmaili, "SOARCA uncertainty analysis of a short-term station blackout accident at the Sequoyah nuclear power plant," *Annals of Nuclear Energy,* vol. 145, no. 107495, 2020.

[66] R.O. Gauntt, N.E. Bixler, K. Wagner, "An Uncertainty Analysis of the Hydrogen Source Term for a Station Blackout Accident in Sequoyah Using MELCOR 1.8.5," SAND2014-2210, Albuquerque, New Mexico, 2003.

[67] M. Perez, et al., "Uncertainty and sensitivity analysis of a LBLOCA in a PWR Nuclear Power Plant: Results of the Phase V of the BEMUSE programme," *Nuclear Engineering and Design,* vol. 241, pp. 4206-4222, 2011.

[68] OECD/NEA/CSNI, "BEMUSE Phase III Report: Uncertainty and Sensitivity Analysis of the LOFT L2-5 Test," NEA/CSNI/R(2007)4, 2007.

[69] OECD/NEA/CSNI, "BEMUSE Phase VI Report: Status Report on the Area, Classification of the Methods. Conclusion and Recommendations," NEA/CSNI/R(2011)4, 2011.

[70] OECD/NEA/CSNI, "PREMIUM: A Benchmark on the Quantification of the Uncertainty of the Physical Models in the System Thermal-hydraulic Codes. Methodologies and Data Review," NEA/CSNI/R(2016)9, 2016.

[71] OECD/NEA/CSNI, "Post-BEMUSE Reflood Model Input Uncertainty Methods (PREMIUM) Benchmark - Final Report," NEA/CSNI/R(2016)18, 2017.

[72] L.H. Herranz, S. Beck, V.H. Sánchez-Espinoza, F. Mascari, S. Brumm, O. Coindreau, S. Paci, "The EC MUSA Project on Management and Uncertainty of Severe Accidents: Main Pillars and Status," *energies,* vol. 14, no. 4473, 2021.

[73] IAEA, “Advancing the State of the Practice in Uncertainty and Sensitivity Methodologies for Severe Accident Analysis in Water Cooled Reactors of PWR and SMR Types,” IAEA-TECDOC-2031, 2023.

[74] IAEA, [Online]. Available: https://www.iaea.org/projects/crp/i31033.

[75] IAEA, “Advancing the State of the Practice in Uncertainty and Sensitivity Methodologies for Severe Accident Analysis in Water Cooled Reactors in the QUENCH-06 Experiment,” IAEA-TECDOC-2045, 2024.

[76] F. Mascari, A. Bersano, F. Gabrielli, D. Luxat, L. Albright, T. Jevremovic, H.U. Rehman, J. Ortiz-Villafuerte, K. Ahn, J.M. Garcia, S.M. Petoukhov, “Overview of IAEA CRP I31033 "Advancing the state-of-practice in uncertainty and sensitivity methodologies for severe accident analysis in water cooled reactors,” *Proceedings of the 10th European Review Meeting on Severe Accidents Research (ERMSAR2022),* no. 1000151444, Karlsruhe, Deutschland, 16.05.2022 – 19.05.2022.

[77] F. Mascari et al., “Main outcomes of the Phebus FPT1 uncertainty and sensitivity analysis in the EU-MUSA project,” *Annals of Nuclear Energy,* vol. 196, no. 110205, 2024.

[78] K.R. Dalbey, M.S. Eldred, G.Geraci, J.D. Jakeman, K.A. Maupin, J.A. Monschke, D.T. Seidl, L.P. Swiler, A. Tran, F. Menhorn, X. Zeng , “Dakota, A Multilevel Parallel Object-Oriented Framework for Design Optimization, Parameter Estimation, Uncertainty Quantification, and Sensitivity Analysis: Version 6.13 Theory Manual,” 2020.

[79] B.M. Adams, W.J. Bohnhoff, K.R. Dalbey, M.S. Ebeida, J.P. Eddy, M.S. Eldred, R.W. Hooper, P.D. Hough, K.T. Hu, J.D. Jakeman, M. Khalil, K.A. Maupin, J.A. Monschke, E.M. Ridgway, A.A. Rushdi, D.T. Seidl, J.A. Stephens, L.P. Swiler, J.G. Winokur, “Dakota, A Multilevel Parallel Object-Oriented Framework for Design Optimization, Parameters Estimation, Uncertainty Quantification, and Sensitivity Analysis: Version 6.13 User's Manual,” 2020.

[80] A. Alfonsi, C. Rabiti, D. Mandelli, J. Cogliati, C. Wang, P.W. Talbot, D.P. Maljovec, C. Smith, “RAVEN Theory Manual,” Idaho National Lab, Idaho Falls, USA, 2016.

[81] Applied Programming Technology Inc., “Symbolic Nuclear Analysis Package (SNAP) User's Manual,” 2021.

[82] Applied Programming Technology, Inc., “Uncertainty analysis User Manual, Symbolic Nuclear Analyses Package (SNAP),” 2012.

[83] F. Mascari, A. Bersano, G. Agnello, M. Angelucci, J. Phillips, D. Luxat, “MELCOR - DAKOTA coupling for uncertainty analyses in the SNAP environment/architecture,” *Nuclear Engineering and Design,* vol. 421, no. 113078, 2024.

[84] F. Mascari, A. Bersano, G. Agnello, M. Angelucci, J. Phillips, D. Luxat, "MELCOR-DAKOTA Coupling for Uncertainty Analyses, in a SNAP Environment/Architecture," NUREG/IA-0532, 2023.

[85] A. Bersano, G. Grippo, G. Agnello, E. Zio, F. Mascari, , "Application of REPAS to analyze the sump clogging issue following a LOCA and its impact on the reliability of the ECCS long-term core cooling function," *Nuclear Engineering and Design,* vol. 417, no. 112877, 2024.

[86] Applied Programming Technology, Inc., *AptPlot User's Manual,* 2021.

[87] D. Jaquemain, S. Bourdon, A. de Braemaeker, M. Barrachin, "PHEBUS FPT1 Final Report," IPSN/DRS/SEA/PEPF Report SEA1/00,IP/00/479, Cadarache, France, 2000.

[88] B. Clément, R. Zeyen, "The objectives of the Phebus FP experimental programme and main findings," *Annals of Nuclear Energy,* vol. 61, pp. 4-10, 2013.

[89] M. Schwarz, G. Hache, P. von der Hardt, "PHEBUS FP: a severe accident research programme for current and advanced light water reactors," *Nuclear Engineering and Design,* vol. 187, pp. 47-69, 1999.

[90] O. de Luze, T. Haste, M. Barrachin, G. Repetto, "Early phase fuel degradation in Phébus FP: Initiating phenomena of degradation in fuel bundle tests," *Annals of Nuclear Energy,* vol. 61, pp. 23-35, 2013.

[91] M. P. Kissane, I. Drosik, "Interpretation of fission-product transport behavior in the Phebus FPT0 and FPT1 tests," *Nuclear Engineering and Design,* vol. 236, pp. 1210-1223, 2006.

[92] B. Simondi-Teisseire, N. Girault, F. Payot, B. Clément, "Iodine behavior in the containment in Phébus FP tests," *Annals of Nuclear Energy,* vol. 61, pp. 157-169, 2013.

[93] B. Clément, T. Haste, E. Krausmann, S. Dickinson, G. Gyenes, J. Duspiva, F. De Rosa, S. Paci, F. Martin-Fuertes, W. Scholytssek, H.J. Allelein, S. Güntay, B. Arien, S. Marguet, M. Leskovar, A. Sartmadjiev, "Thematic network for a Phebus FPT1 international standard problem (THENPEBISP)," *Nuclear Engineering and Design,* vol. 235, pp. 347-357, 2005.

[94] OECD/NEA/CSNI, "ISP-46 - PHEBUS FPT-1 Integral Experiment on Reactor Severe Accidents," NEA/CSNI/R(2004)18, 2004.

[95] B. Clément, T. Haste, "Comparison Report on International Standard Problem ISP-46 (PHEBUS FPT1)," Note Technique Semar 03/021, Cadarache, France, 2003.

[96] J. Wang, C. Wang, M. Corradini, T. Haskin, W. Tian, G. Su, S. Qiu, "PHEBUS FPT-1 simulation by using MELCOR and primary blockage model exploration," *Nuclear Engineering and Design,* vol. 307, pp. 119-129, 2016.

[97] J. Wang, M. Corradini, W. Fu, T. Haskin, Y. Zhang, W. Tian, G. Su, S. Qiu, "Simulation of the PHEBUS FPT-1 experiment using MELCOR and exploaration of the primary core degradation mechanism," *Annals of Nuclear Energy,* vol. 85, pp. 193-204, 2015.

[98] P. Darnowski, M. Włostowski, M. Stepien, G. Niewinski, "Study of the material release during PHÉBUS FPT-1 bundle phase with MELCOR 2.2," *Annals of Nuclear Energy,* vol. 148, no. 107700, 148.

[99] L.L. Humphries, L. Louie, V. Figueroa, M. Young, S. Weber, K. Ross, J. Phillips, R. Jun, "MELCOR Computer Code Manuals Vol.3: MELCOR Assessment Problems Version 2.1.7347," SAND 2015-6693 R, Albuquerque (USA), 2015.

[100] USNRC, "Cooperative Severe Accident Research Program (CSARP)," NUREG/BR-0524, Washington, DC 20555-0001, 2015.

[101] L.E. Herranz, M. Garcia, S. Morandi, "Benchmarking LWR codes capability to model radionuclide deposition within SFR containments: An analysis of the Na ABCOVE tests," *Nuclear Engineering and Design,* vol. 265, pp. 772-784, 2013.

[102] R.O. Gauntt, T. Radel, M.A. Salay, D.A. Kalinich, "Analysis of Main Steam Isolation Valve Leakage in Design Basis Accidents Using MELCOR 1.8.6 and RADTRAD," SAND2088-6601, 2008.

[103] L. Sepold, W. Hering, C. Homann, A. Miassedov, G. Schanz, U. Stegmaier, M. Streinbruck, H. Steiner, J. Stucker, "Experimental and Computational Results of the QUENCH-06 Test (OECD ISP-45)," Forschungszentrum Karlsruhe GmbH, Karlsruhe (DEU), 2004.

[104] W. Hering, Ch. Homann, J.S. Lamy, A. Miassoedov, G. Schanz, L. Sepold, M. Steinbrück, "Comparison and Interpretation Report of the OECD International Standard problem No.45 Exercise (QUENCH-06)," Programm Nuk eare S cherhe tsforschung, October 2002.

[105] M. Stanojević, M. Leskovar, "Simulation of the QUENCH-06 experiment with MELCOR 1.8.5," *Proceedings of International Conference Nuclear Energy in Central Europe,* September 10-13, 2001.

[106] P. Maccari, A. Bersano, S. Ederli, F. Gabrielli, F. Mascari, "Validation and uncertainty analysis of ASTEC in early degradation phase against QUENCH-06 experiment," *Nuclear Engineering and Design,* vol. 414, no. 112600, 2023.

[107] M. Garbarini, G. Agnello, A. Bersano, F. Gabrielli, L. Luzzi, F. Mascari, "Simulation of QUENCH-06 experiment by MELCOR v2.2 with Uncertainty Analysis," *Paper presented at the 20th International Topical Meeting on Nuclear Reactor Thermal Hydraulics (NURETH-20),* 2023.

[108] M. Garbarini, "Development of MELCOR v2.2 Input for the simulation of QUENCH-06 experiment," Master Thesis in Nuclear Engineering (Politecnico di Milano), 2022.

[109] J.V. Cathcart, R.E. Pawel, R.A. McKee, R.E. Druschel, G.J. Yurek, J.J. Campbell, S.H. Jury, "Zirconium Metal-Water Oxidation Kinetics IV. Reaction Rate Studies," ORNL/NUREG-17, 1977.

[110] A. Volchek, Yu. Zvonarev, G. Schanz, "Advanced treatment of zircaloy cladding high-temperature oxidation in severe accident code calculations PART II. Best-fitted parabolic correlations," *Nuclear Engineering and Design,* vol. 232, pp. 85-96, 2004.

[111] S. Brumm, F. Gabrielli, V. Sanchez-Espinoza, A. Stakhanova, M. Nudi, P. Groudev, P. Ou, L.E. Herranz, "Uncertainty quantification for severe-accident reactor modelling: Set-up and first results of the Horizon project MUSA," *Annals of Nuclear Energy,* vol. 191, no. 109919, 2023.

[112] USNRC, "Pressurized Water Reactor (PWR) Systems," USNRC Technical Training Center 0603.

[113] L. Foucher, "ASTEC V20R3 PWR900 Like ASTEC Input Deck," Rapport n° PSNRES/SAG/2013-451.

[114] L. Foucher, "ASTEC V20R3, PWR900 Like ASTEC Steady State Calculation," Rapport n° PSN-RES/SAG/2013-466.

[115] H. Nowack, P. Chatelard, L. Chailan, St. Hermsmeyer, V. Sanchez, L. Herranz, "CESAM - Code for European severe accident management, EURATOM project on ASTEC improvement," *Annals of Nuclear Energy,* vol. Volume 116, pp. 128-136, 2018.

[116] F. Mascari et al., "FASTNET scenarios database development and status," *Proceedings of the 9th European Review Meeting on Severe Accident Research (EMRSAR2019),* Prague (Czech Republi), 18-20 March, 2019.

[117] F. Fichot, L. Carénini, M. Sangiorgi, S. Hermsmeyer, A. Miassoedov, S. Bechta, J. Zdarek, D. Guenadou, "Status of the IVMR Project: First steps Towards a New Methodology to Assess In-Vessel Retention Strategy for High-power Reactors," *Proceedings of the 8th European Review Meeting on Severe Accident Research (ERMSAR2017),* Warsaw (Poland), May 16-18, 2017.

[118] F. Mascari, A. Guglielmelli, J.C. de la Rosa Blul, "Analysis of a postulated 2-inch Cold Leg LOCA severe accident in a PWR-like 900 MWe with MELCOR code," *Proceedings of the International Conference Nuclear Energy for New Europe (NENE2018),* Portorož (Slovenia), September 10-13, 2018.

[119] F. Mascari, S. Ederli, "Analyses with MELCOR code of an unmitigated SBO scenario with in vessel retention strategy applied to a generic PWR-900 MWe," *Proceedings of te 18th International Topical Meeting on Nuclear Reactor Thermal Hydraulics (NURETH2019),* pp. 2497-2510, 2019.

[120] M. Pescarini, F. Mascari, D. Mostacci, F. De Rosa, C. Lombardo, F. Giannetti, "Analysis of unmitigated large break loss of coolant accidents using MELCOR code," *Journal of Physics: Conference Series,* vol. 923, no. 012009, 2017.

[121] G. Agnello, P.A. Di Maio, J.C. de la Rosa Blul, F. Mascari, “Sensitivity analyses on MELCOR accumulators modelling,” *Proceedings of the 10th European Review Meeting on Severe Accident Research (ERMSAR2022)*, May 16-19, 2022.

[122] P. Maccari, F. Mascari, S. Ederli, S. Manservisi, “SBO analysis of a generic PWR-900 with ASTEC and MELCOR codes,” *Journal of Physics: Conference Series,* vol. 1868, no. 012019, 2021.

[123] G. Agnello, S. Ederli, P. Maccari, F. Mascari, “Analysis of an unmitigated 2-inch cold leg LOCA transient with ASTEC and MELCOR codes,” *Journal of Physics: Conference Series,* vol. 2177, no. 012024, 2022.

[124] P. Darnowski, P. Mazgaj, M. Włostowski, “Uncertainty and Sensitivity Analysis of the In-Vessel Hydrogen Generation for Gen-III PWR and Phebus FPT-1 with MELCOR 2.2,” *energies,* vol. 2021, no. 4884, 2021.

[125] “European Commission, Safety Analysis of SMR with PAssive Mitigation strategies - Severe Accident - SASPAM-SA Project,” 2023. [Online]. Available: https://cordis.europa.eu/project/id/101059853.

[126] “"SAFETY ANALYSIS OF SMR WITH PASSIVE MITIGATION STRATEGIES - SEVERE ACCIDENT (SASPAM-SA),” [Online]. Available: https://www.saspam-sa.eu/.

[127] “INTERNATIONAL REACTOR INNOVATIVE AND SECURE, IRIS Plant Overview,” October 2002.

[128] F. Gabrielli, M. Di Giuli, M. Malicki, A. Bersano, P. Maccari, F. Giannetti, “Generic Data on Design 1 and Design 2,” SASPAM-SA, Milestone Version 0.3 (DRAFT), 2024.

[129] P. Maccari, F. Mascari, S. Ederli, P. Meloni, S. Manservisi, “ASTEC code DBA analysis of a passive mitigation strategy on a generic IRIS SMR,” *Annals of Nuclear Energy,* vol. 156, no. 108194, 2021.

[130] P. Maccari, G. Agnello, F. Mascari, S. Ederli, “Analysis of BDBA sequences in a generic IRIS reactor using ASTEC code,” *Annals of Nuclear Energy,* vol. 182, no. 109611, 2023.

[131] M. Carrelli, L. Conway, M. Dzodzo, A. Maioli, L. Oriani, G. Storrick, B. Petrovic, A. Achilli, G. Cattadori, C. Congiu, R. Ferri, M. Ricotti, D. Papini, F. Bianchi, P. Meloni, S. Monti, F. Berra, D. Grgic, G. Yoder, A. Alamberti, “The SPES3 experimental facility design for the IRIS reactor simulation,” *Science and Technology of Nuclear installations,* vol. vol2009, no. 579430, 2009.

[132] R. Ferri, “SPES3-IRIS facility RELAP5 sensitivity analyses on the containment system for design review,” no. SIET 01 526 RT 09 Rev.0, 2010.

[133] A. Achilli, C. Congiu, R. Ferri, F. Bianchi, P. Meloni, D. Grgić, M. Dzodzo, “Integral Test Facilities and Thermal-Hydraulic System Codes in Nuclear Safety Analysis,” *Science and Technology of Nuclear Installation,* vol. Vol. 2012, no. 173637, 2012.

[134] R. Ferri, C. Congiu, “Conceptual design of SPES3-IRIS facility,” SIET 01 334 RT 07 Rev.1., Piacenza (Italy), 2008.

[135] F. Mascari, B.G. Woods, K. Welter, F. D'Auria, A. Bersano, P. Maccari, “Small modular reactors and insights on passive mitigation strategy modeling,” *Nuclear Engineering and Design,* vol. 401, no. 112088, 2023.

[136] F. Mascari, F. D'Auria, D. Bestion, P. Lien, H. Nakamura, H. Austregesilo, S.K. Moon, F. Reventos, K. Umminger, J.N. Reyes, U.S. Rohatgi, “OECD/NEA/CSNI state-of-the-art report on scaling in system thermal-hydraulics applications to nuclear reactor safety and design (The S-SOAR),” *Nuclear Engineering and Design,* vol. 416, no. 112750, 2024.

[137] R. Ferri, A. Achilli, G. Cattadori, F. Bianchi, P. Meloni, “Design, experiments and Relap5 code calculations for the perseo facility,” *Nuclear Engineering and Design,* vol. 235, pp. 1201-1214, 2005.

[138] F. Mascari, G. Vella, B.G. Woods, F. D'Auria, “Analyses of the OSU-MASLWR Experimental Test Facility,” *Science and Technology of Nuclear Installations,* vol. vol. 2012, no. 528241, 2012.

[139] F. Mascari, G. Vella, B.G. Woods, K. Welter, J. Pottorf, E. Young, M. Adorni, F. D'Auria, “Sensitivity analysis of the MASLWR helical coil steam generator using TRACE,” *Nuclear Engineering and Design,* vol. 241, pp. 1137-1144, 2011.

[140] F. Mascari, F. De Rosa, B.G. Woods, K. Welter, G. Vella, F. D'Auria, “Analysis of the OSU-MASLWR 001 and 002 Tests by Using the TRACE Code,” NUREG/IA-0466, 2016.

[141] Y.J. Chung, S.W. Lim, K.H. Bae, “Investigation of TASS/SMR capability to predict a natural circulation in the test facility for an integral reactor,” *Science and Technology of Nuclear Installations,* vol. vol. 2014, no. 181802, 2014.

[142] J. Pottorf, F. Mascari, B.G. Woods, “TRACE, RELAP5 Mod 3.3, and RELAP5-3D Code Comparison of OSU-MASLWR-001 Test,” *2009 ANS Winter Meeting and Nuclear Technology Expo. Transactions of the ANS. ISSN: 0003-018X,* vol. Volume 101, 2009.

[143] P. Maccari, J.A. Zambaux, A. Bersano, “BEPU analysis of a 2-in DVI break in a generic IRIS SMR by ASTEC - RAVEN coupling,” *EUROSAFE Forum 2021,* Paris, France, November 22-23, 2021.

[144] F. Castiglia, P. Chiovaro, M. Ciofalo, M. Di Liberto, P.A. Di Maio, M. Giardina, G. Vella, “TRACE input model for SPES3 facility,” Rep RdS/2010/62, 2010.

[145] O.C. Jones, Nuclear Reactor Safety Heat Transfer, Hemisphere Publishing Corporation, 1981.

[146] G. Agnello, F. Mascari, A. Bersano, P. Maccari, "DBA analysis of a generic SMR IRIS-like with MELCOR 2.2 code," *Proceedings of the 4th International Conference on Nuclear Power Plants; Structure Risk, Control & Decommissioning (NUPP22),* September 19-20 2022.

[147] R.O. Gauntt, "Uncertainty Analyses Using the MELCOR Severe Accident Analysis Code," *CSNI Workshop on the Evaluation of Uncertainties in Relation to Severe Accidents and Level 2 Probabilistic Safety Analysis,* 2005.

[148] ETSON, "Safety Analysis of SMR with PAssive Mitigation strategies - Severe Accident (SASPAM-SA) Horizon Euratom Project," 2022. [Online]. Available: https://etson.eu/node/290.

[149] SMR Regulators' Forum, "Pilot Project Report: Considering the Application of a Graded Approach, Defence-in-Depth and Emergency Planning Zone Size for Small Modular Reactors," January 2018.